Transport of Brownian particles in confined geometries

Steps beyond the Fick-Jacobs approach

D I S S E R T A T I O N

zur Erlangung des akademischen Grades

doctor rerum naturalium
(Dr. rer. nat.)
im Fach Physik

eingereicht an der
Mathematisch-Naturwissenschaftlichen Fakultät I
Humboldt-Universität zu Berlin

von
Dipl.-Phys. Steffen Martens

Präsident der Humboldt-Universität zu Berlin:
Prof. Dr. Jan-Hendrik Olbertz

Dekan der Mathematisch-Naturwissenschaftlichen Fakultät I:
Prof. Stefan Hecht, Ph.D.

Gutachter:
1. Prof. Dr. Lutz Schimansky-Geier
2. Prof. Dr. Dr. h. c. mult. Peter Hänggi
3. Prof. Dr. Sabine Klapp

eingereicht am: 13.11.2012
Tag der mündlichen Prüfung: 15.04.2013

Abstract

In this work, we investigate the transport of Brownian particles in confined geometries where entropic barriers play a decisive role. The commonly used *Fick-Jacobs approach* provides a powerful tool to capture many properties of entropic particle transport. Unfortunately, its applicability is mainly limited to the overdamped motion of point-like objects in weakly corrugated channels.

We perform asymptotic perturbation analysis of the probability distribution in terms of an expansion parameter specifying the channel corrugation. With this methodology, exact solutions of the associated stationary Smoluchowski equation are derived. In particular, we demonstrate that the leading order of the series expansion is equivalent to the Fick-Jacobs approach. By means of the higher expansion orders, which become significant for strong channel corrugation, we obtain corrections to the key particle transport quantities in the diffusion dominated limit. In contrast to the commonly used Lifson-Jackson formula, these corrections can be calculated exactly for most smooth and discontinuous boundaries, and they provide even better agreements with simulation results.

Going one step further, we overcome the limitation of the Fick-Jacobs approach to curl-free forces (scalar potentials). For this purpose, we study entropic transport caused by force fields containing curl-free and divergence-free (vector potential) parts. Based on our methodology, we develop a *generalized* Fick-Jacobs approach leading to a one-dimensional, energetic description. As an exemplary application, we consider the prevailing situation in microfluidic devices, where Brownian particles are subject to external constant forces and pressure-driven flows. The analysis of particle transport leads to the interesting finding that the vanishing of the mean particle current is accompanied by a significant suppression of diffusion, yielding the effect of *hydrodynamically enforced entropic trapping*. This effect offers a unique opportunity to efficiently separate particles of the same size.

Since separation and sorting by size is a main challenge in basic research, we intend to incorporate the particle size into the Fick-Jacobs approach. Finite particle size inevitably causes additional forces, e.g., hydrodynamic particle-particle and particle-wall interactions. We identify the limits for the ratio of particle size to pore size and the mean distance between particles, for which these forces can safely be disregarded in experiments. Moreover, we demonstrate that within these limits the analytic expressions for the key transport quantities, derived for point-like particles, can be applied to extended objects, too.

We study the impact of the solvent's viscosity on entropic transport. If the time scales separate, adiabatic elimination results in an effective, kinetic description for particle transport in the presence of finite damping. The possibility of such description is intimately connected with equipartition and vanishing correlation between the particle's velocity components. Numerical simulations show that this approach is accurate for moderate to strong damping and for weak forces. For strong external forces, equipartition may break down due to reflections at the boundaries. This leads to a non-monotonic dependence of particle mobility on the force strength. Finally, we study the impact of boundary conditions on entropic transport. We show numerically that perfectly inelastic particle-wall collisions can rectify entropic transport.

In summary, this work shows how experimentally relevant issues such as strong channel corrugation, sophisticated external force fields, particle size, particle inertia, and the solvent's viscosity can be incorporated into the Fick-Jacobs approach.

Zusammenfassung

Die vorliegende Arbeit befasst sich mit dem Transport von Brownschen Teilchen in beschränkten Geometrien, in denen entropische Barrieren auftreten. Die häufig verwendete Fick-Jacobs Näherung erlaubt eine genaue Beschreibung zahlreicher Eigenschaften des entropischen Transportes, ist aber nur für die überdämpfte Bewegung von Punktteilchen in sich schwach ändernden Kanalstrukturen gültig.

Im ersten Teil der Arbeit bestimmen wir die exakte Lösung für die stationäre Wahrscheinlichkeitsdichte mittels Entwicklung in einem geometrischen Parameter, der die Kanalmodulation misst. In der führenden Ordnung, welcher dem Grenzfall sich schwach ändernden Strukturen entspricht, stimmt unsere Entwicklung mit der Fick-Jacobs Näherung überein. Insbesondere die höheren Entwicklungsterme ermöglichen die Berechnung von Korrekturen zu den Transportkoeffizienten in sich stark ändernden Geometrien. Im Unterschied zur häufig genutzten Lifson-Jackson Formel lassen sich mit dieser Methode diese Korrekturfaktoren für eine Vielzahl von Kanalstrukturen exakt berechnen und, wie der Vergleich mit numerischen Simulationen zeigt, können die Transportkoeffizienten damit genauer berechnet werden.

Die Fick-Jacobs Näherung, welche in der Literatur ausschließlich auf konservative Kräfte (skalare Potentiale) beschränkt ist, kann mit Hilfe unsere Entwicklung auf komplizierte Kraftfelder, die einen rotationsfreien und divergenzfreien (Vektorpotential) Anteil besitzen, verallgemeinert werden. Die Genauigkeit der Näherung testen wir anhand eines Beispiels, dem mikrofluidischen System. Dort wird der Teilchentransport durch externe Kräfte und Strömungen hervorgerufen. Die Analyse der Transportkoeffizienten liefert, dass das Verschwinden des Teilchenstroms, ungeachtet der wirkenden starken Kräfte, mit einer signifikanten Reduktion der Diffusion einhergeht. Dieser Effekt des *hydrodynamisch induzierten entropischen Einsperrens* ermöglicht die effiziente Trennung von Objekten gleicher Größe.

Neben der Trennung gleichgroßer Teilchen, ist das effiziente Sortieren nach Größe eine der wichtigsten Ziele in der Grundlagenforschung. Daher ist es notwendig den Einfluss der Teilchengröße in die Fick-Jacobs Näherung zu integrieren. Eine Endliche Ausdehnung beeinflusst nicht nur die entropischen Barrieren sondern führt unweigerlich zu zusätzlichen Kräften, z.B., hydrodynamische Teilchen-Teilchen und Teilchen-Wand Wechselwirkung. Deswegen bestimmen wir die Grenzen für die Teilchengröße, für welche die zusätzlichen Kräfte vernachlässigbar sind, und zeigen, dass die Ergebnisse für die Transportkoeffizienten aus der Fick-Jacobs Näherung auf solche ausgedehnte Objekte erweitert werden können.

Abschließend untersuchen wir den Einfluss der Viskosität des umgebenen Mediums auf den entropischen Teilchentransport. Wenn die Zeitskalen des Systems separieren, führt adiabatische Eliminierung auch im Falle endlicher Reibung zu einer Fick-Jacobs ähnlichen Beschreibung. Eine solche Näherung ist unweigerlich mit der Gleichverteilung der Energien und mit verschwindender Korrelation zwischen den Geschwindigkeitskomponenten verbunden. Vergleiche mit numerischen Simulationen zeigen, dass diese effektive Beschreibung für moderate bis starke Dämpfung und schwache externe Kräfte gültig ist. Für starke Kräfte wird die angenommene Gleichverteilung der Energien infolge von Teilchen-Wand Kollisionen verletzt. Dies führt zu einer nichtlinearen Abhängigkeit der Teilchengeschwindigkeit und des effektiven Diffusionskoeffizienten von der Kraftstärke.

Zusammenfassend wird in der Arbeit gezeigt, wie experimentell vorherrschende Gegebenheiten, z.B., sich stark ändernde Geometrien, komplizierte Kraftfelder, Teilchenausdehnung, Trägheit oder endliche viskose Reibung, in der Fick-Jacobs Näherung berücksichtig werden können.

Contents

1. Introduction

"Diffusion is a universal phenomenon, occurring in all states of matter on time scales that vary over many orders of magnitude, and indeed controlling the overall rates of a wide variety of physical, chemical, and biochemical processes." [Kärger and Ruthven, 1992, p. vii]. Unquestionably, effective control of mass and charge transport requires a deep understanding of the diffusion mechanism involving small objects whose size ranges from the nano- to the microscale. Thereby, diffusive transport can either be described in terms of a continuum (macroscopic) description which is given by Fick's second law [Fick, 1855] or as a stochastic process accounting for the erratic motion of suspended microscopic particles. This erratic motion was first systematically investigated by the botanist Robert Brown [Brown, 1828] almost 200 years ago. In honor of Brown's observation[1] which "has played a central role in the development of both the foundations of thermodynamics and the dynamical interpretation of statistical physics" [Hänggi and Marchesoni, 2005], diffusion of microscopic (Brownian) particles is often referred to as Brownian motion. In 1905, based on the molecular-kinetic theory of heat, Albert Einstein provided the link between the underlying microscopic dynamics in suspension and the macroscopic observable phenomena [Einstein, 1905]. In particular, he derived a relation between the fluid viscosity and the diffusion constant which was confirmed by theoretical studies made by William Sutherland [Sutherland, 1905], Marian von Smoluchowski [von Smoluchowski, 1906], and Paul Langevin [Langevin, 1908]. This connection, known as the Stokes-Einstein or Sutherland-Einstein[2] relation, was later generalized in terms of the famous fluctuation-dissipation theorem [Callen and Welton, 1951] and by linear response theory [Kubo, 1957]. Although Jean-Baptiste Perrin [Perrin, 1909] was awarded the Nobel Prize in 1926 for the experimental observation of Brownian motion, it has taken more than a century till high-resolution time measurements of Brownian motion were technically feasible. These experiments provide direct verification of the energy equipartition theorem [Li et al., 2010] and show the full transition from ballistic to diffusive Brownian motion [Huang et al., 2011]. Albeit the theory of Brownian motion has found broad application in the description of phenomena in many fields in science [Frey and Kroy, 2005], the original theory was limited to *freely* suspended Brownian particles.

[1] Nevertheless that Brown's name is associated with the microscopic phenomenon of Brownian motion, he was not the first one who observed it. In 1784, Jan Ingen-Housz had already been reported the phenomenon of irregular motion of coal dust particles immersed in a fluid [Ingen-Housz, 1784].

[2] Abraham Pais points in his Einstein biography "Subtle is the Lord: The Science and the Life of Albert Einstein" (Oxford University Press, 1982) to the coincidence that the Stokes-Einstein relation has been obtained independently in 1904 by William Sutherland [Sutherland, 1905]. Therefore, according to Pais, the relation should be properly called the Sutherland-Einstein relation.

In nature, Brownian motion in spatial confinements ranging from the nano- to the microscale is ubiquitous. Today, there exists a large variety of natural and artificial confined geometries, e.g., biological cells [Zhou et al., 2008], ion channels [Hille, 2001; Lindner et al., 2004], nanoporous materials [Beerdsen et al., 2005, 2006], zeolites [Kärger and Ruthven, 1992; Keil et al., 2000], microfluidic channels [Bruus, 2008; Squires and Quake, 2005], artificial nanopores [Firnkes et al., 2010; Pedone et al., 2011], and ion-pumps [Siwy and Fulinski, 2004; Siwy et al., 2005]. In such systems, the geometric restrictions to the particle's dynamics result in confined diffusion [Verkman, 2002] and suppressed Brownian motion [Cohen and Moerner, 2006]. Due to its relevance for the understanding of molecular biological processes [Alberts et al., 2002] like the transport of molecules across membranes [Berezhkovskii and Bezrukov, 2005, 2008; Rüdiger and Schimansky-Geier, 2009] or the binding of diffusing molecules to a reaction partner [Szabo et al., 1980], the fundamental problem of particle transport through micro-domains exhibiting small openings, also called *entropic barriers*, has been studied extensively [Burada et al., 2009, 2008b; Grigoriev et al., 2002; Zwanzig, 1992]. In particular, the shape of these confinements regulates the dynamics of Brownian particles leading to transport properties which may significantly differ from the free case [Reguera et al., 2006]. Hence, a detailed understanding of the complexities of particle transport through confined geometries is essential for the development, design, and optimization of (i) shape and size selective catalysis [Corma, 1997], (ii) particle separation techniques [Howorka and Siwy, 2009; Voldman, 2006], and (iii) artificial nano- and microchannels [Martin et al., 2005; Sven and Müller, 2003]. In what follows, we briefly address these systems and their applications:

Zeolites are three-dimensional, nanoporous, crystalline solids with well-defined structures [Kärger and Ruthven, 1992]. Based on their chemical composition, zeolites form a long, regular network of cavities (cages) with connecting pores. Especially, they combine many properties such as a type-specific uniform pore size ($\varnothing \sim 0.4 - 1.3\,\mathrm{nm}$ [Corma, 1997]), large internal surface area, ion exchange ability, high thermal stability, etc. As a result, zeolites can not only improve the efficiency of catalytic processes, including petrochemical cracking, purification, and isomerization, but they can also be used to separate particles based on size, shape, and polarity. For this reasons, zeolites are often called *molecular sieves* [Duke and Austin, 1998; Kärger, 2008].

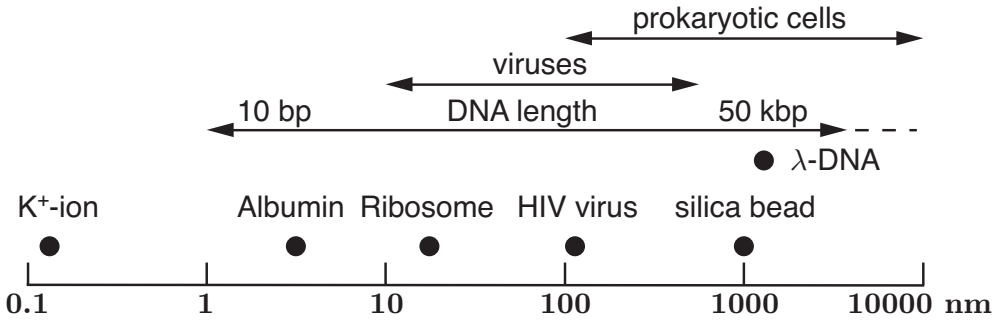

Figure 1.1.: Typical dimensions of a number of particles discussed in the introduction.

The **separation** and sorting of size-dispersed particles [Cheng et al., 2008; Di Carlo et al., 2007] is a main challenge in basic research, industrial processing, and in nanotechnology. By particles, we mean micro- or even nanosized particulate matter, including proteins, DNA, viruses, prokaryotic cells, and colloids (see Fig. 1.1). Filtering of these particles is traditionally performed by means of centrifugal fractionation [Harrison et al., 2002], external electric fields, causing electroosmotic [Mishchuk et al., 2009] or induced-charge electrokinetic flows [Bazant and Squires, 2004], and phoretic forces leading to acousto- [Petersson et al., 2007], magneto- [Pamme and Wilhelm, 2006], dielectro- [Gascoyne and Vykoukal, 2002], and electrophoresis [Dorfman, 2010]. Unquestionably, electrophoretically separating DNA by size is one of the most powerful tools in molecular biology [Slater et al., 2002; Volkmuth and Austin, 1992] which is usually performed in gel, "DNA prism" [Huang et al., 2002], or in nano- and microfluidic channels [Eijkel and van den Berg, 2005; Zhao and Yang, 2012].

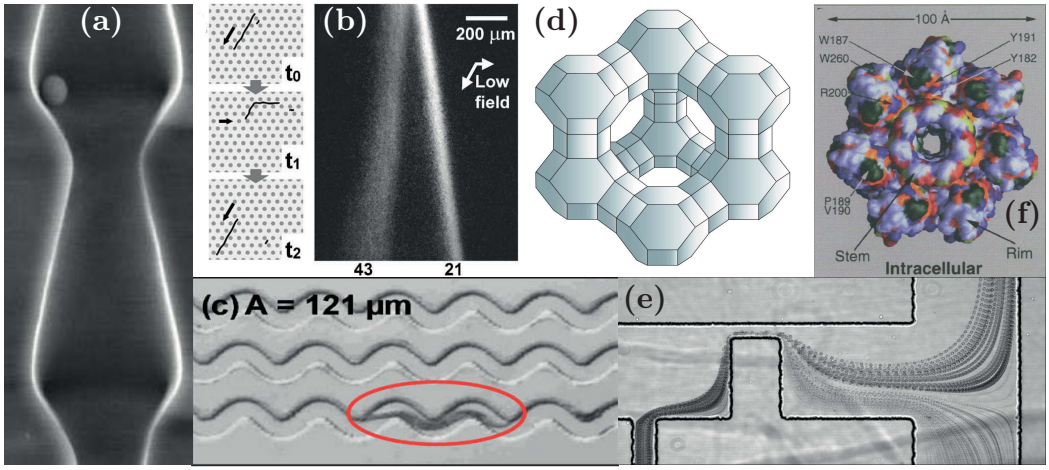

Figure 1.2.: Panel (a): Scanning electron micrograph of a cleaved modulated macroporous silicon ratchet membrane with an attached colloidal spheres. Reprinted by permission from Macmillan Publishers Ltd: *Nature* [Sven and Müller, 2003], copyright (2003). (b): Fluorescence micrographs of continuous DNA separation in a pulsed-field electrophoretic DNA prism, where DNA molecules of different lengths naturally follow different trajectories. Reprinted by permission from Macmillan Publishers Ltd: *Nature Biotechnol.* [Huang et al., 2002], copyright (2002). (c): Wild-type C. elegans (encircled) crawling in a modulated sinusoidal channel with amplitude $A = 121\mu$m. Reprinted by permission from Macmillan Publishers Ltd: *Biomicrofluidics* [Parashar et al., 2011], copyright (2011). (d): Illustration of a zeolite. By courtesy of NASA Marshall Space Flight Center. (e): Separation of white blood cells by dielectrophoresis along a rectangular hurdle. Cells below 10μm move downwards and larger ones move upwards. Reprinted with permission from Kang et al., 2008 ©Springer Science + Business Media, LLC 2007. (f): Intracellular view on the heptameric transmembrane pore Staphylococcus aureus α-hemolysin. Reprinted by permission from Macmillan Publishers Ltd: *Science* [Song et al., 1996], copyright (1996).

Nowadays, techniques to construct artificial **micro- and nanochannels** [Kang and Li, 2009; Martin et al., 2005; Squires and Quake, 2005] are established which make the development of innovative *Lab-on-chip* devices feasible [Dittrich and Manz, 2006; Srinivasan et al., 2004]. These devices perform a continuous sequence of identical separation operations, for instance, the sieving of healthy cells from deceased (cancer) or dead cells [Becker et al., 1995; Gascoyne et al., 1997]. Other devices are based on the realization of *entropic ratchets* [Chou et al., 1999; Freund and Schimansky-Geier, 1999; Hänggi et al., 2005; Lindner and Schimansky-Geier, 2002; Slater et al., 1997] which make use of the asymmetric channel profile to transport and separate particles. In addition to solely sorting objects, revealing the sequence and analysing the structure of polymers, DNA and RNA molecules via artificial nanopores [Dekker, 2007; Keyser et al., 2006] have been challenging tasks in recent years. These nanopores use the fact that each base pair (bp) in a structured polynucleotide exhibits its own distinct electronic signature which is recorded during the passage through the charged small opening [Matysiak et al., 2006; Muthukumar, 2001]. A similar mechanism applies if ions pass through a nanopore where different ionic species generate different ionic currents [Kosińska et al., 2008; Siwy et al., 2005].

A common characteristic of all these systems is that the volume accessible to a diffusing particle is restricted by confining boundaries or obstacles. Variations of the structural shape along the direction of motion imply changes in the number of accessible states of the particles or, equivalently, lead to spatial variations of entropy. Consequently, the directed motion of Brownian particles induced by the presence of external driving forces – *entropic transport* – is controlled by entropic barriers. These barriers are promoting or hindering the transfer of mass and energy to certain regions. Along with the progress of experimental techniques, theoretical methods to study the kinetics of entropic transport have received substantial attention. Clearly, solving the governing equation for the joint probability density function (PDF) for finding a Brownian particle at a given position within an arbitrarily shaped channel (boundary value problem) is a difficult task. Previous studies by Merkel H. Jacobs [Jacobs, 1967] and Robert Zwanzig [Zhou and Zwanzig, 1991; Zwanzig, 1992] ignited numerous research activities in this topic, resulting in the development of an approximate description of the diffusion problem – the *Fick-Jacobs approach*. This approach, in which the elimination of the transversal degree(s) of freedom leads to an effective one-dimensional, kinetic description for the longitudinal coordinate, provides a powerful tool to describe particle transport through corrugated channel geometries [Berezhkovskii et al., 2009; Burada et al., 2009; Grigoriev et al., 2002; Reguera et al., 2006]. In the developed *Fick-Jacobs equation*, spatial variations of the confinements are taken into account by means of the potential of mean force or the so-called effective entropic potential. The accuracy of the Fick-Jacobs (FJ) approach has been intensively studied for diffusing particles in two- [Burada et al., 2008b; Reguera and Rubí, 2001] and three-dimensional channels [Ai and Liu, 2006; Berezhkovskii et al., 2007; Dagdug et al., 2011] with smooth walls. Additionally, it has been tested in discontinuous geometries formed by circular cavities [Berezhkovskii et al., 2010; Cheng et al., 2008], obstacles [Dagdug et al., 2012; Ghosh et al., 2012a], and in channels with abruptly changing cross-sections [Borromeo and Marchesoni, 2010; Dagdug et al., 2011; Makhnovskii et al., 2010]. Nevertheless that

the FJ formalism can provide a highly accurate description, its derivation entails a tacit requirement, namely, the existence of a hierarchy of relaxation times [Wilemski, 1976]. This hierarchy guarantees the separation of time scales and supports the approximation that the particle distributions equilibrate much faster in transverse directions than in the transport (longitudinal-) direction. Since this ansatz neglects the influence of finite relaxation dynamics, large deviations were found for strongly corrugated confinements [Burada et al., 2007; Kalinay and Percus, 2008]. In order to improve the accuracy of the FJ equation, Zwanzig proposed the consideration of a spatially dependent diffusion coefficient which substitutes the constant diffusion coefficient present in the common FJ equation [Zwanzig, 1992]. This idea is equivalent to an imposed artificial separation of time scales. Later, the ansatz was supported by heuristic arguments [Reguera and Rubí, 2001] and operator projection techniques [Kalinay and Percus, 2006]. However, in the presence of external forces the time scales may not separate and thus the equilibration ansatz may get violated. By analyzing the different time scales involved in the problem, Burada et al. derived an estimate for the conditions under which equilibration is established in confined geometries. They demonstrated that the FJ approach is accurate for any external force strengths only for narrow channels. Moreover, the authors showed that the applicability diminishes with growing width, respectively, corrugation of the confinement. Even though, the Fick-Jacobs approach captures many properties of entropic particle transport its usage is limited to narrow channel geometries, so far.

With this thesis we aim at addressing two main issues:

1. The first issue concerns a methodology to derive the exact solution for the joint probability density function in an arbitrary corrugated channel. We ask the question, whether there exists a systematic treatment which reproduces the Fick-Jacobs equation for weakly modulated geometries and, more importantly, leads to an extension towards extremely corrugated boundaries. In a wider sense, we intend to derive analytic results for the key particle transport quantities which go beyond the commonly used formulas comprising the artificially introduced spatially dependent diffusion coefficient.

2. Based on our derived methodology, we give answers to the second question: "Under which conditions is a generalization of the Fick-Jacobs approach to finite-sized Brownian particles and to more sophisticated external force fields feasible?". This question is of practical interest since in micro- and even nanoscale devices neither objects with negligible (point-like) extension are separated, nor conservative forces are solely exerted on the particles. These two simplifications are state of the art in the current literature. Additionally, to gain deeper insight into the key physical assumptions behind the Fick-Jacobs approach, we investigate the impact of the viscosity of the surrounding solvent. Since finite viscous friction comprises an additional time scale, the question arises, whether the assumption of equilibration is violated.

By explicitly taking account of the channel's corrugation, we provide an analytic tool to gain new perspectives in the understanding of entropic transport. With the use of numerical simulations, we study the problem of biased Brownian motion through

spatially confined geometries and, in fact, we check the accuracy and applicability of our analytic predictions. Thereby, the sinusoidally modulated channel is our reference geometry throughout the thesis.

The outline of the thesis is as follows. Prior to calculations, in chapter 2 we briefly discuss transport processes in systems without geometrical constraints, followed by a short introduction to macrotransport theory. In the next step, we present the Fick-Jacobs approach in detail and outline how analytical expressions for the key transport quantities can be derived via the mean first passage time approach.

In chapter 3, we proceed to a systematic treatment for entropic transport. More precisely, we perform asymptotic perturbation analysis of the stationary joint probability density function in terms of an expansion parameter which specifies the corrugation of the channel walls. With this method, exact solutions of the associated stationary Smoluchowski equation are derived. In particular, we demonstrate that the leading order of our series expansion is equivalent to the Fick-Jacobs approach. Additionally, analytic expressions to calculate the particle transport quantities in strongly corrugated confinements are obtained.

Going one step further, we overcome the limitation of the FJ approach to conservative forces (scalar potentials) in chapter 4. There, based on our derived methodology, we generalize the FJ description to the most general external force field exerted on a particle which is composed of a curl-free (scalar potential) and a divergence-free component (vector potential). We put forward an effective one-dimensional description involving the generalized potential of mean force, which along with the commonly known "entropic" contribution, acquires a qualitatively novel contribution associated with the divergence-free force. To elucidate the intriguing features caused by vector potentials, we apply our approach to the experimentally relevant situation where Brownian particles are subject to both an external constant bias and to a pressure-driven flow (microfluidic device). The analysis of particle transport leads to the interesting finding that the vanishing of the mean particle current is accompanied by a significant suppression of diffusion, yielding the effect of selective *hydrodynamically enforced entropic trapping*.

Since separation and sorting by size is a main challenge in basic research, chapter 5 is devoted to the question, whether the FJ approach can be applied to extended spherical particles. Finite particle size causes additional forces exerted on the particles, e.g., hydrodynamic particle-particle and particle-wall interactions, which have been disregarded in our preceding theoretical considerations. Hence, we identify the limits for the ratio of particle size to pore size and the mean distance between the particles. Moreover, we demonstrate that within these limits the analytic expressions for the transport quantities, derived for point-like particles in the preceding chapters, can be generalized to extended colloids. Furthermore, we present simulation results for large particles in extremely corrugated channels showing a sensitive dependence of the particles' terminal speeds on their size.

In the concluding chapter 6, we study the impact of the viscous friction coefficient on entropic transport. The existence of a hierarchy of relaxation times, governed by the geometry of the channel and the viscous friction, guarantees the separation of time scales and the equipartition of energy. Supposing further a vanishing correlation

between the particle's velocity components, we derive an effective, kinetic description for entropic transport in the presence of finite damping. A comparison of the reduced description (FJ approach) with numerical results shows that the FJ approach is accurate for moderate to strong damping and for weak forces. In particular, we identify an upper limit for the external bias beyond which the FJ approach fails even in narrow, weakly modulated channels. The origin of the failure is the violation of equipartition for the transversal coordinate and velocity. The latter is caused by the transfer of the externally applied acceleration into the "fast" coordinates due to reflections at the boundaries. Lastly, we study the impact of the boundary conditions on the particle transport and show numerically that perfectly inelastic particle-wall collisions can rectify entropic transport. With these findings, we conclude the main part of the thesis. Finally, we summarize all our findings and draw conclusions for possible forthcoming studies in chapter 7.

2. Transport in confined geometries – The Fick-Jacobs approach

In order to give a short outline, we discuss briefly transport processes in systems without geometrical constraints, followed by a short introduction in macrotransport theory. In the next step, we present the Fick-Jacobs approach, which allows a reduction of the problem's dimensionality to an effective one-dimensional (1D) energetic problem. At the end of this chapter, we demonstrate how analytical expressions for the key transport quantities for Brownian motion in confined geometries can be evaluated with the use of the mean first passage time approach.

We consider first the case without any spatial constraints, which we refer to as the *free case*: A spherical Brownian particle with mass m, spatially homogeneous particle density ρ_p, and diameter d_p is subject to an external force $\mathbf{F}(\mathbf{q}^*, t)$ in a solvent with spatially homogeneous density ρ_f and dynamic viscosity η. The motion of particles that are immersed in a fluidic medium is influenced by various types of forces [Maxey and Riley, 1983]. The systematic impact of the solvent on the motion of a solid particle at position $\mathbf{q}^* = (x^*, y^*, z^*)^T$ can be approximated by the Stokes drag force

$$\mathbf{F}^{\mathrm{drag}} = -\gamma \left[\mathbf{v} - \mathbf{u}(\mathbf{q}^*, t)\right]. \tag{2.1}$$

Here, $\mathbf{u}(\mathbf{q}^*, t)$ is the instantaneous velocity of the fluid in absence of the particle, $\dot{\mathbf{q}}^*(t) = \mathbf{v}(t) = (v_x, v_y, v_z)^T$ represents the particle velocity at time t, and $\gamma = 3\pi\,\eta\,d_p$ is the viscous friction coefficient. At the same time, the "tracer" particle collides randomly with the $\sim 10^{23}$ molecules per mol of the surrounding fluid with a rate up to 10^{21} times per second. These random collisions result in the particle's Brownian motion [Brown, 1828; Perrin, 1909] and can be effectively described by a stochastic thermal force $\boldsymbol{\xi}(t) = (\xi_x, \xi_y, \xi_z)^T$. Following Langevin, 1908, the particle's equation of motion (EOM) at position $\mathbf{q}^*$ is determined by the stochastic differential equation

$$m\,\frac{\mathrm{d}\,\mathbf{v}}{\mathrm{d}\,t} \;=\; m\,\dot{\mathbf{v}} = \;-\gamma\,\mathbf{v} + \mathbf{F}(\mathbf{q}^*, t) + \boldsymbol{\xi}(t). \tag{2.2}$$

For small solid particles in laminar solvent flows, the Oseen correction [Faxen, 1922; Oseen, 1910] to the Stokes drag Eq. (2.1), effects of solvent inertia, including those described by the Basset history force, added mass force, and Saffman lift force [Saffman, 1965], and effects that can be initiated by rotation of particles (e.g., Magnus force, modified drag, and rotational Brownian diffusion [Favro, 1960]) are generally small compared to the Stokes drag, Eq. (2.1), and can be disregarded in the EOM, Eq. (2.2), [Maxey, 1990; Maxey and Riley, 1983]. As an additional simplification, if not explicitly stated otherwise, we always consider a quiescent solvent $\mathbf{u}(\mathbf{q}^*, t) = \mathbf{0}$. Throughout this thesis, each component of the stochastic force $\boldsymbol{\xi}(t)$ is assumed to be Gaussian white

noise with zero mean

$$\langle\, \xi_i(t) \,\rangle = 0, \tag{2.3a}$$

and temporal δ-correlation

$$\langle\, \xi_i(t)\, \xi_j(t') \,\rangle = 2\,\gamma\, k_B T\, \delta_{i,j}\delta(t-t'), \quad \text{for} \quad i,j = x,y, \text{ or } z, \tag{2.3b}$$

where k_B is the Boltzmann constant and T refers to the spatially homogeneous environmental temperature. Thereby $\langle\, \cdot \,\rangle$ represents the ensemble average.

Solving Eq. (2.2) under the simplification that $\mathbf{F}$ is independent of time and position, i.e., $\partial_t \mathbf{F} = 0$ and $\boldsymbol{\nabla}_{\mathbf{q}} \mathbf{F} = 0$, gives

$$\dot{\mathbf{q}}^* = \mathbf{v}(t) = \mathbf{v}(0)\, e^{-\gamma\, t/m} + \frac{\mathbf{F}}{\gamma}\left(1 - e^{-\gamma\, t/m}\right) + \int_0^t \mathrm{d}t'\, e^{-\gamma\,(t-t')/m} \boldsymbol{\xi}(t'), \tag{2.4a}$$

with $\mathbf{v}(0)$ being the particle velocity at time $t = 0$. Thereby, $\boldsymbol{\nabla}_{\mathbf{q}} = (\partial_x, \partial_y, \partial_z)^T$ represents the gradient. Integrating the last equation once more with respect to the time, yields

$$\mathbf{q}^* = \mathbf{q}^*(0) + \frac{\mathbf{F}}{\gamma} t + \left(\mathbf{v}(0) - \frac{\mathbf{F}}{\gamma}\right) \frac{1 - e^{-\gamma\, t/m}}{\gamma/m} + \int_0^t \mathrm{d}t' \int_0^{t'} \mathrm{d}t''\, e^{-\gamma\,(t'-t'')/m} \boldsymbol{\xi}(t''), \tag{2.4b}$$

where $\mathbf{q}^*(0)$ denotes the initial particle position at time $t = 0$.

The Langevin equation Eq. (2.2) provides a mathematical description of a Brownian particle dynamics that include its inertia and is applicable over the entire time domain. However, experiments showed that this description is not exact for all times [Huang et al., 2011; Weitz et al., 1989]. Deviations from the random diffusive behavior were shown to originate from the inertia of the surrounding fluid, which leads to long-living vortices caused by and in turn affecting the particle motion. These hydrodynamic memory effects [Hinch, 1975; Vladimirsky and Terletzky, 1945] introduce an intermediate regime between the purely ballistic and the diffusive regime. The characteristic time scale for the onset of this effect is given by $\tau_f = d_p^2 \rho_f / (4\,\eta)$ and it is related to the characteristic velocity correlation time $t_{\mathrm{corr}} = m/\gamma$ via $\tau_f / \tau_{\mathrm{corr}} = 9\rho_f/(2\rho_p)$. For micro-sized particles ($d_p \simeq 1\,\mu\mathrm{m}$) moving through water ($\rho_p \simeq \rho_f = 998\,\mathrm{kg/m^3}$ and $\eta = 10^{-3}\,\mathrm{kg/ms}$), both time scales are of the order $\tau_f \gtrsim \tau_{\mathrm{corr}} \approx 0.1\,\mu\mathrm{s}$ at room temperature $T = 293,15\,\mathrm{K}$. The description can be improved by incorporating effects of fluid inertia via the added mass force in Eq. (2.2). Accordingly, the particle's mass m is replaced by an effective mass m^*, where m^* is given by the sum of the mass of the particle and half the mass of the displaced fluid [Maxey and Riley, 1983]. The latter is the weight added to a system due to the fact that an accelerating or decelerating body must move some volume of surrounding fluid with it as it moves. Then, in the absence of external forces $\mathbf{F} = \mathbf{0}$, the velocity variance approaches $\langle\, \mathbf{v}^2 \,\rangle = 3\, k_B T / m^*$ as demanded by the equipartition theorem. Only on timescales shorter than $\tau_c = d_p/c \approx 0.3\,\mathrm{ns}$,

where c is the speed of sound in the fluid, the particle is able to decouple from its fluid envelope and thus $m^* \to m$.

Referring to Kramers, 1940, see also Becker, 1985, the inertial term in Eq. (2.2) is negligible if all other forces do not change much during the effective characteristic velocity correlation time $t^*_{\mathrm{corr}} = m^*/\gamma$. In detail, if the particle's velocity becomes uncorrelated during the time the particle needs to move its own size $t^*_{\mathrm{corr}} < d_p/v$, the inertial forces become negligible in comparison with the viscous forces [Purcell, 1977]. For micro-sized particles ($d_p \simeq 1\,\mu\mathrm{m}$, $\rho_p \simeq \rho_f$) moving with typical velocities of the order $v = 1\,\mathrm{mm/s}$ through water, $t^*_{\mathrm{corr}} \approx 0.1\,\mu\mathrm{s}$ is four magnitudes smaller compared to the typical drift time d_p/v at room temperature. Then the inertial term $m^*\,\dot{\mathbf{v}}(t)$ in Eq. (2.2) is negligibly small compared to the other forces and thus one can safely set $m^* = 0$ (overdamped limit or Smoluchowski approximation [von Smoluchowski, 1906]). Under this condition Eq. (2.2) reduces to the overdamped Langevin equation

$$\gamma\,\dot{\mathbf{q}}^* = \mathbf{F}\,(\mathbf{q}^*, t) + \boldsymbol{\xi}(t). \tag{2.5}$$

Obviously, the fluid envelope carried by the particle does not affect its dynamics in the high friction limit. If not explicitly stated otherwise, we always consider the overdamped limit in the following.

However, the detailed solution of the individual dynamics is in most cases not of practical interest. Instead, one is interested in the behavior of the long-time moments of the joint probability density function $P(\mathbf{q}^*, t)$ of finding a particle at position $\mathbf{q}^*$ at time t. Thereby $P(\mathbf{q}^*, t)$ describes the statistical properties of the particle motion which are captured by key transport quantities like the mean particle velocity in the long-time limit

$$\left\langle\, \mathbf{v}^0 \,\right\rangle = \lim_{t\to\infty} \langle\, \dot{\mathbf{q}}^*(t) \,\rangle = \lim_{t\to\infty} \frac{\langle\, \mathbf{q}^*(t) \,\rangle}{t}. \tag{2.6}$$

From Eq. (2.5), and with the properties of Gaussian white noise, Eqs. (2.3), it is straightforward to conclude that the *free mean particle velocity* equals $\left\langle\, \mathbf{v}^0 \,\right\rangle = \mathbf{F}/\gamma$. In the sense of linear response, the terminal drift velocity and the applied force are connected via the mobility tensor $\mathbb{M}$, $\mathbf{v} = \mathbb{M}\,\mathbf{F}$. For non-interacting particles moving through a spatially isotropic media $\mathbb{M}$ is diagonal, i.e., $\mathbb{M}_{m\,n} = \mu^0\,\delta_{m,n}$ for m, n are x, y, or z. The main diagonal elements equal the *free particle mobility*

$$\mu^0 = \frac{1}{\gamma}. \tag{2.7}$$

We emphasize that for a non-dilute particle concentration hydrodynamic interactions between the Brownian particles have to be taken into account. According to Faxen's law [Faxen, 1922], additional forces are exerted on a given particle caused by the flow fields induced by all the other particles. These hydrodynamic interactions can be included into the EOM via the hydrodynamic mobility tensor $\mathbb{M}^{\mathrm{hyd}}$ whose non-diagonal elements are different from zero; for details see Sect. 5.2.

The second quantity of interest, the dispersion tensor $\mathbb{D}$, concerns the temporal evolution of the mean square displacement (MSD) with respect to the mean position $\langle \mathbf{q}^* \rangle$

$$\left\langle \left(\mathbf{q}^* - \langle \mathbf{q}^* \rangle\right) \left(\mathbf{q}^* - \langle \mathbf{q}^* \rangle\right)^T \right\rangle = 2\,\mathrm{tr}[\mathbb{D}]\,t. \tag{2.8}$$

In the case of normal diffusion, the MSD grows linearly in time in the long time limit. For a spatially isotropic medium, $\mathbb{D}$ is diagonal with main diagonal elements being equal to the *free diffusion constant* [von Smoluchowski, 1906]

$$D^0 = \frac{k_B T}{\gamma}. \tag{2.9}$$

In 1905 and 1906, Einstein showed that for Brownian particles the diffusion constant is connected to the friction coefficient γ via the fluctuation-dissipation theorem (Sutherland-Einstein relation) [Callen and Welton, 1951; Sutherland, 1905]. It is a remarkable feature that the diffusion coefficient does not depend on the mass of the Brownian particle [Reimann, 2002]. We emphasize that in contrast to the MSD measured with respect to the initial position, $\langle(\mathbf{q}^* - \mathbf{q}^*(0))\,(\mathbf{q}^* - \mathbf{q}^*(0))^T\rangle \propto (\mathbf{F}\,t/\gamma)^2$, the diffusion coefficient Eq. (2.9) does not change even if there is a constant external force $\mathbf{F}$ acting on the particle. This follows from the fact that the diffusion constant is invariant under Galilean transformation $\mathbf{q} \to \mathbf{q} - \mathbf{F}\,t/\gamma$. Comparing Eq. (2.9) and Eq. (2.7), one notices that the free diffusion constant and the free particle mobility are connected via the Sutherland-Einstein relation [Sutherland, 1905]

$$D^0 = \mu^0\,k_B T. \tag{2.10}$$

2.1. Macrotransport theory

The dynamics of Brownian particles and their transport properties, respectively, change if their motion becomes restricted by geometrical constraints. In typical transport processes through confined structures such as pores and channels, like the one depicted in Fig. 2.1 with period L and an area of local cross-section $Q(x)$, the impenetrability of the channel's walls has to be taken into account. Consequently, the mean particle velocity and the diffusion constant may differ from the free values. Macrotransport theory provides a rigorous method for extracting the mean particle velocity $\langle \dot{\mathbf{q}}^* \rangle$ and the effective dispersion tensor $\mathbb{D}^{\mathrm{eff}}$ without the need for solving Eq. (2.5) directly or performing the equivalent Langevin-type simulations [Brenner and Edwards, 1993]. The theory based on the decomposition of the position $\mathbf{q}^*$ within the periodic system into a "cell pointer" $\mathbf{R}_n$, where $-\infty < n < \infty$, and $\mathbf{R}_n - \mathbf{R}_{n-1} = L\,\mathbf{e}_x$. Then the local position within a cell reads $\mathbf{q} = \mathbf{q}^* - \mathbf{R}_n$. This results in the transformations $P(\mathbf{q}^*, t) \to P(n, \mathbf{q}, t)$ and $\langle \dot{\mathbf{q}}^*(\mathbf{q}^*) \rangle \to \langle \dot{\mathbf{q}}(\mathbf{q}) \rangle$. Using a moment-matching asymptotic procedure, $\langle \dot{\mathbf{q}} \rangle$ and $\mathbb{D}^{\mathrm{eff}}$ can be evaluated from the solution of two time-independent intracellular fields, which depend only on the local position $\mathbf{q} = (x, y, z)^T$ within the unit cell which, with no loss of generality, extends over the range $0 \le x \le L$. The theory is valid in the long-time limit, namely, when the residence time τ_R in the system satisfies the inequality $\tau_R \gg L^2/D^0$.

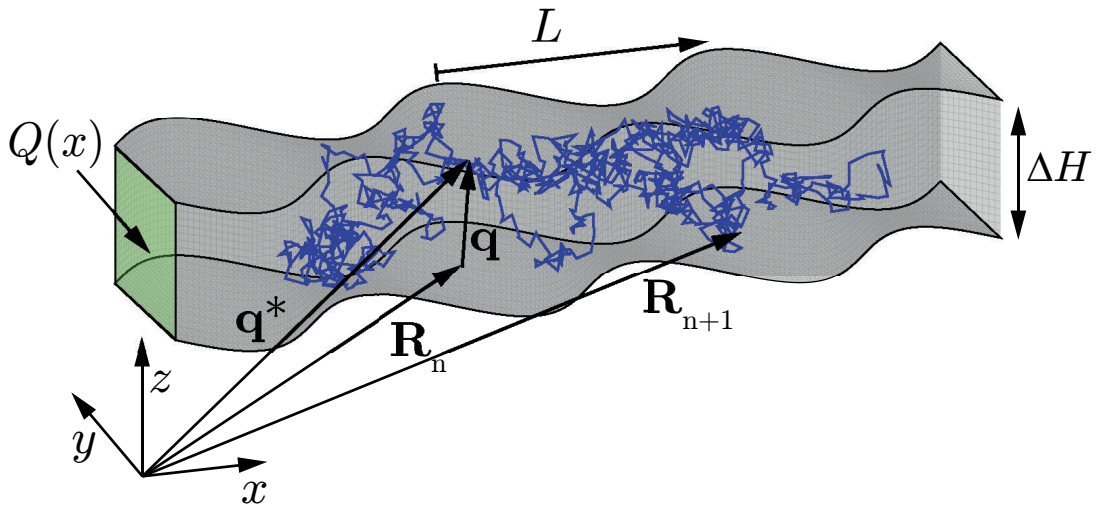

Figure 2.1.: Segment of 3D planar channel geometry with period L, height ΔH, and periodically varying cross-section $Q(x)$. An exemplary particle trajectory is indicated by the erratic line. Superimposed are the global position vector $\mathbf{q}^*$, lattice-point position vector $\mathbf{R}_n$, and the local position vector within a unit cell $\mathbf{q} = \mathbf{q}^* - \mathbf{R}_n$.

The first step in the macrotransport scheme entails computing the joint probability density function (PDF) $P(\mathbf{q}, t)$ of finding a particle at local position $\mathbf{q}$ at time t

$$P(\mathbf{q}, t) = \sum_{n=-\infty}^{\infty} P(n, \mathbf{q}, t), \tag{2.11}$$

regardless of the specific cell in which it resides. Its evolution is given by the Smoluchowski equation [Risken, 1989; von Smoluchowski, 1915]

$$\partial_t P(\mathbf{q}, t) + \boldsymbol{\nabla}_{\mathbf{q}} \cdot \mathbf{J}(\mathbf{q}) = 0, \tag{2.12}$$

where

$$\mathbf{J} = \mathbf{F}(\mathbf{q}, t)\ P(\mathbf{q}, t) - \frac{k_B T}{\gamma} \boldsymbol{\nabla}_{\mathbf{q}} P(\mathbf{q}, t), \tag{2.13}$$

is the probability current of $P(\mathbf{q}, t)$. Caused by impenetrability of the channel walls the probability current $\mathbf{J}(\mathbf{q}, t) = (J^x, J^y, J^z)^T$ is subject to no-flux boundary condition (bc), reading

$$\mathbf{J}(\mathbf{q}, t) \cdot \mathbf{n} = 0, \quad \forall\, \mathbf{q} \in \text{channel wall}, \tag{2.14}$$

where $\mathbf{n}$ denotes the outward-pointing normal vector at the channel walls. Note that the channel walls confine the particles motion inside the channel, but do not exchange energy with them otherwise. Especially, particle absorption and emission at boundaries are disregarded. Various kinds of boundary conditions exist that regulate the inward and outward probability fluxes at the ends of the channel [Burada et al., 2009]. If

the channel connects large, well-mixed particle reservoirs, constant PDFs $P_{L,R}$ may be assigned at the channel's end at x_L and x_R leading to Dirichlet boundary conditions, viz., $P(x_L, y, z) = P_L$ and $P(x_R, y, z) = P_R$. For an infinitely long channel consisting of many unit cells periodic boundary conditions are more appropriate [Risken, 1989]

$$P(\mathbf{q} + m\, L\, \mathbf{e}_x, t) = P(\mathbf{q}, t),\ m \in \mathbb{Z}. \tag{2.15}$$

Additionally, $P(\mathbf{q}, t)$ has to satisfy the normalization condition

$$\int\limits_{\text{unit cell}} P(\mathbf{q}, t)\, \mathrm{d}^3\mathbf{q} = 1, \tag{2.16}$$

in the case of periodic bc. In the long-time limit both the stationary joint PDF $P_{\text{st}}(\mathbf{q}) \equiv P(\mathbf{q}, t \to \infty)$ and its gradient must be continuous at the transition from $x = x_0$ to $x = x_0 + L$. Once, $P_{\text{st}}(\mathbf{q})$ is known, the mean particle current $\langle\, \dot{\mathbf{q}}\, \rangle$ can be computed by

$$\langle\, \dot{\mathbf{q}}\, \rangle = \int\limits_{\text{unit cell}} \mathbf{J}_{\text{st}}(\mathbf{q})\, \mathrm{d}^3\mathbf{q}. \tag{2.17}$$

Thereby, in the sense of linear response, the mean particle current vector and the applied force are connected via an effective mobility tensor $\langle\, \dot{\mathbf{q}}\, \rangle = \mathbb{M}^{\text{eff}}\, \mathbf{F}$. In what follows, we focus only on transport in the longitudinal (transport) channel direction, $\mu \equiv \mathbb{M}^{\text{eff}}_{x,x}$, and we call it particle mobility

$$\mu = \frac{\langle\, \dot{x}\, \rangle}{\mathbf{F}_x}. \tag{2.18}$$

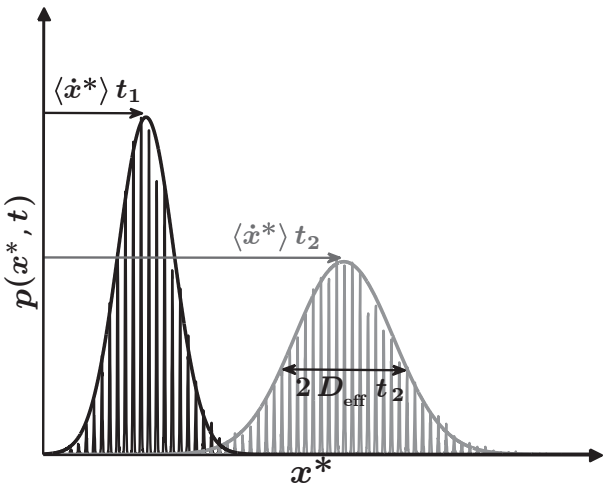

Figure 2.2: Time evolution of the marginal PDF $p(x^*, t)$ as a function of the global coordinate x^* in a confined geometry with periodically varying width. Mean position and mean square displacement grow linearly in time, viz., $\langle\, x^*(t)\, \rangle = \langle\, \dot{x}^*\, \rangle\, t$ and $\langle (x^* - \langle\, x^*\, \rangle)^2 \rangle = 2\, D_{\text{eff}}\, t$. The Gaussian distribution $p(x, t_i) \propto \exp\left[-(x - \langle\, \dot{x}^*\, \rangle\, t_i)^2 / (4\, D_{\text{eff}} t_i) \right]$ (solid lines) represents the envelope of the numerical simulation of Eq. (2.5) (peaked structure).

The second step involves the calculation of the so-called **B**-field [Brenner, 1980; Brenner and Edwards, 1993],

$$\mathbf{B}(\mathbf{q}) = \lim_{t\to\infty}\left[\sum_{n=-\infty}^{\infty}\frac{\mathbf{R}_n\, P(n,\mathbf{q},t)}{P_{\mathrm{st}}(\mathbf{q})} - \langle\,\dot{\mathbf{q}}\,\rangle\, t\right]. \tag{2.19}$$

This intracellular vector field arises from deviations of the tracer position $\mathbf{q}^*$ from the mean position $\langle\,\dot{\mathbf{q}}\,\rangle\, t$ and it is governed by a convection-diffusion equation in the i-th spatial direction

$$\mathbb{D}_{i,i}\boldsymbol{\nabla}_{\mathbf{q}}\cdot\left(P_{\mathrm{st}}\,\boldsymbol{\nabla}_{\mathbf{q}}\mathbf{B}_i\right) - \left(\mathbf{J}\cdot\boldsymbol{\nabla}_{\mathbf{q}}\right)\mathbf{B}_i = P_{\mathrm{st}}(\mathbf{q})\,\langle\,\dot{\mathbf{q}}_i\,\rangle, \quad \text{for} \quad i = x, y, \text{ or } z. \tag{2.20}$$

Any component $\mathbf{B}_i$ obeys the no-flux boundary condition

$$\boldsymbol{\nabla}_{\mathbf{q}}\mathbf{B}_i(\mathbf{q})\cdot\mathbf{n} = 0, \quad \forall\,\mathbf{q}\in\text{channel wall}, \tag{2.21}$$

and satisfies the requirement that $\mathbf{b} = \mathbf{B} + \mathbf{q}$ is a periodic function in the longitudinal channel direction (here in x), yielding

$$\mathbf{B}(x = x_0 + L) - \mathbf{B}(x = x_0) = -L\,\mathbf{e}_x. \tag{2.22}$$

Mathematically, the **B**-field can be interpreted as a dispersion "potential": once **B** is calculated, the elements of the effective dispersion tensor $\mathbb{D}^{\mathrm{eff}}$ can be computed by the following unit cell quadrature

$$\mathbb{D}^{\mathrm{eff}}_{i,j} = \mathbb{D}_{i,j}\int\limits_{\text{unit cell}} P_{\mathrm{st}}(\mathbf{q})\,\left(\boldsymbol{\nabla}_{\mathbf{q}}\mathbf{B}_i\right)\cdot\left(\boldsymbol{\nabla}_{\mathbf{q}}\mathbf{B}_j\right)\,\mathrm{d}^3\mathbf{q}, \quad \text{for} \quad i,j = x, y, \text{ or } z. \tag{2.23}$$

Here, we also concentrate only on the diffusion constant in longitudinal channel direction, $D_{\mathrm{eff}} \equiv \mathbb{D}^{\mathrm{eff}}_{x,x}$, and we call it effective diffusion coefficient (EDC).

2.2. Dimensionless units

We pass to dimensionless quantities, i.e., all lengths are measured in units of the channel period L, $\mathbf{q} \to \overline{\mathbf{q}}\,L$, the time is expressed in units of $\tau = L^2\gamma/(k_B\,T)$ which is twice the time the particle requires to overcome diffusively the distance L at zero bias $\|\mathbf{F}\| = \mathbf{0}$, i.e., $t \to \tau\,\bar{t}$, and all energies are scaled in units of the thermal energy k_BT. Furthermore, we define the dimensionless forcing parameter $\mathbf{f}$

$$\mathbf{f} = \frac{\mathbf{F}L}{k_BT}, \tag{2.24}$$

which characterizes the ratio of the work $\mathbf{F}L$ done on a particle when dragged by the constant force $\|\mathbf{F}\|$ along a distance of length L divided by the thermal energy k_BT. While the force $\mathbf{F}$ and the temperature T are independent variables in the case of purely energetic systems, these two quantities become coupled and tune the system's transport properties in geometries with spatial constraints [Burada, 2008; Burada et al., 2008b].

In an experimental setup, the value of $\mathbf{f}$ can be adjusted either by modifying the force strength or the thermal energy k_BT. After re-scaling the EOM of Brownian particles, Eq. (2.5) changes to

$$\dot{\overline{\mathbf{q}}}(\bar{t}) = \mathbf{f} + \overline{\boldsymbol{\xi}}(\bar{t}), \tag{2.25}$$

with $\boldsymbol{\xi}(t) \to \overline{\boldsymbol{\xi}}(\bar{t})/\sqrt{\tau}$. Additionally, the joint PDF reads $P(\mathbf{q},t) \to \overline{P}(\overline{\mathbf{q}},\bar{t})/L^3$ and the probability current is given by $\mathbf{J}(\mathbf{q},t) \to \overline{\mathbf{J}}(\overline{\mathbf{q}},\bar{t})/(\tau L^2)$. In the following, for convenience, we shall omit the overbar in our notation.

Assuming that the Sutherland-Einstein relation Eq. (2.10) is valid also for transport processes in confined geometries for any force strength $f = \|\mathbf{f}\|$, yields $D_{\text{eff}} = \mu\, k_BT$. After passing to dimensionless variables the relation reduces to

$$D_{\text{eff}}/D^0 = \mu/\mu^0. \tag{2.26}$$

Supposing that the particle dispersion in longitudinal channel direction is proportional to its mobility, as a consequence of the fluctuation-dissipation theorem, it turns out that the effective diffusion coefficient in units of its free value has to be equal to the particle mobility in units of the bulk mobility. By means of Eq. (2.26), we are able to identify values for the external force strength f where the Sutherland-Einstein relation is violated in confined geometries. A detailed discussion is given in Sect. 3.2.4.

2.3. Fick-Jacobs approach

As mentioned in the previous section, the first step to calculate the main transport quantities entails evaluating the stationary joint probability density function $P_{\text{st}}(\mathbf{q})$. The latter is determined by Eq. (2.12) and has to obey the no-flux bc Eq. (2.14) for any channel geometries. Below, we consider two realizations for three-dimensional (3D) channels which are relevant to experiments [Squires and Quake, 2005], viz., (i) a planar periodic channel geometry with unit period, constant height ΔH, and periodically varying transverse width $W(x)$, for details see Sect. 3.1, and (ii) a cylindrical tube with unit period and periodically varying radius $R(x)$ (see Sect. 3.3). First, we focus on the 3D planar problem[1]: the motion of a particle is confined by two planar walls at $z = 0$ and $z = \Delta H$ as well as by two perpendicular side-walls at $y = \omega_+(x)$ and $y = \omega_-(x)$. Thereby, the outward-pointing normal vectors read $\mathbf{n}_z = (0,0,\pm 1)^T$ at $z = 0(-), \Delta H(+)$ and $\mathbf{n}_y = (\mp\omega'_\pm(x), \pm 1, 0)^T$ at $(x, y = \omega_\pm(x))$. The prime denotes the differentiation with respect to x.

Integrating the Smoluchowski equation Eq. (2.12) over the local cross-section $Q(x)$ and respecting the no-flux bcs, yields

$$\partial_t\, p(x,t) = -\int_{\omega_-(x)}^{\omega_+(x)} \mathrm{d}y\, \partial_x \int_0^{\Delta H} \mathrm{d}z\, J^x(\mathbf{q},t) - \int_0^{\Delta H} \mathrm{d}z\, J^y(\mathbf{q},t)\Big|_{y=\omega_-(x)}^{y=\omega_+(x)}. \tag{2.27}$$

[1]The basic assumptions and considerations are identical for the cylindrical geometry.

Thereby, the marginal probability density function is defined by

$$p\,(x,t) = \int\limits_{\omega_-(x)}^{\omega_+(x)} \mathrm{d}y \int\limits_0^{\Delta H} \mathrm{d}z\; P(\mathbf{q},t). \tag{2.28}$$

Using the relation

$$\int\limits_{\alpha(x)}^{\beta(x)} \mathrm{d}y\, \partial_x f(x,y) = \partial_x \int\limits_{\alpha(x)}^{\beta(x)} \mathrm{d}y\, f(x,y) + \alpha'(x) f(x,\alpha(x)) - \beta'(x) f(x,\beta(x)), \tag{2.29}$$

we obtain for arbitrary boundary functions $\omega_\pm(x)$

$$\partial_t\, p\,(x,t) = -\,\partial_x \int\limits_{\omega_-(x)}^{\omega_+(x)} \mathrm{d}y \int\limits_0^{\Delta H} \mathrm{d}z\; \left[\mathbf{f}_x(\mathbf{q},t)\, P(\mathbf{q},t) - \partial_x P(\mathbf{q},t)\right] = -\partial_x J^x(x,t). \tag{2.30}$$

The principle problem that must be solved is to express the joint PDF $P(\mathbf{q},t)$ in terms of the marginal PDF $p\,(x,t)$. According to the Bayes theorem, the joint PDF is given by the product

$$P(\mathbf{q},t) = P(y,z|x,t)\, p(x,t) \tag{2.31}$$

of the conditional PDF $P(y,z|x,t)$ and the marginal PDF, cf. Eq. (2.28). In general, $P(y,z|x,t)$ cannot be calculated analytically for arbitrary channels and external forces. Several authors made either assumption for the conditional PDF or present expansion methods for the joint PDF. In their pioneering works M. H. Jacobs [Jacobs, 1967] and R. Zwanzig [Zwanzig, 1992] assumed a separation of the time scale between the "fast" transverse dynamics and the "slow" longitudinal one. A detailed derivation of their results is given below. Later other authors presented series expansion techniques based on the ratio of the time scales, respectively, length scales [Kalinay and Percus, 2006; Laachi et al., 2007; Yariv and Dorfman, 2007]. In Chapt. 3, we present an expansion method for the joint PDF $P(\mathbf{q},t)$ in a parameter measuring the corrugation of the local width $W(x)$.

In 1935, Merkel H. Jacobs studied diffusion processes in a symmetric tube whose cross-section $Q(x)$ varies along the x-axis, defined by the center line of the tube. He considered an elementary volume of thickness $\mathrm{d}x$ perpendicular to the axis of the tube, see Fig. 2.3. The rate of entrance $r_{\mathrm{in}} = -Q(x)\,\partial_x\,(p(x,t)/Q(x))$ and the rate of exit $r_{\mathrm{out}} = -\left[Q(x)\,\partial_x\,(p(x,t)/Q(x)) + \partial_x\,(Q(x)\partial_x\,(p(x,t)/Q(x))\;\mathrm{d}x) + O(\mathrm{d}x^2)\right]$ of the diffusing particles into the volume are given by Fick's 1st law (dimensionless). Thereby $p(x,t)/Q(x)$ is the local probability in units of the local cross-section area. For the problem at hand, both rates are different not only because the concentration gradient $\partial_x p(x,t)$ changes with $\mathrm{d}x$, but also due to the variation of the cross-section $Q(x)$. The difference between both rates provides the rate of change of the particles in the elementary volume, $\partial_t p(x,t)\,\mathrm{d}x$. Neglecting quadratic terms in $\mathrm{d}x$, Jacobs derived by means

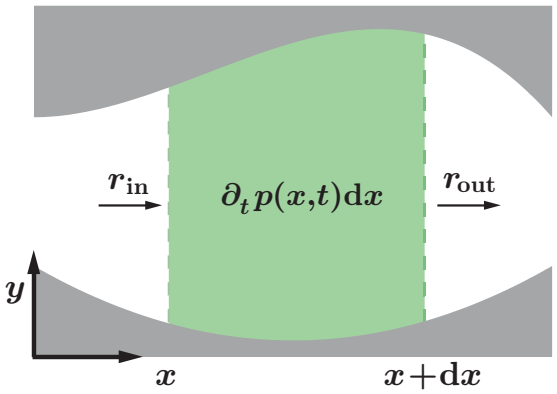

Figure 2.3: Sketch of Jacobs' approach to determine the Fick-Jacobs equation. An elementary volume of thickness $\mathrm{d}x$ is presented. The rates of entrance r_{in} and of exit r_{out} of the diffusing particles into the volume are given by Fick's 1st law. The difference between both rates provides the rate of change of the substance in the elementary volume, $\partial_t p(x,t)\,\mathrm{d}x$.

of these arguments an effective one-dimensional equation governing the diffusion within a channel geometry

$$\partial_t p(x,t) = \partial_x \left[Q(x) \partial_x \left(\frac{p(x,t)}{Q(x)} \right) \right], \tag{2.32}$$

which is referred to as the *Fick-Jacobs* (FJ) equation. Equation (2.32) represents a extension of the Fick's 2nd law which is recovered for non-modulated cross-sections $Q(x) = const$, $\partial_t p(x,t) = \partial_x^2 p(x,t)$. Note that the argumentation presented by Jacobs is not exact because it does not take account of the no-flux boundary conditions. Comparing Eq. (2.32) with the more general expression, Eq. (2.30), it turns out that $p(x,t) = P(\mathbf{q},t)\,Q(x)$. Hence the derivation of Jacobs implies that the Brownian particles distribute uniformly along the transverse direction(s) of the confined structure at any position x and at any given time t, i.e., $P(y,z|x,t) = 1/Q(x)$.

In 1992, Robert Zwanzig presented a more general derivation of the Fick-Jacobs equation by considering the diffusion in a potential $\Phi(\mathbf{q})$. This potential $\Phi(\mathbf{q})$ can be either an external potential confining the motion of the Brownian particles (Zwanzig's original idea), a scalar potential generating the external force,[2] $\mathbf{f} = -\boldsymbol{\nabla}\Phi(\mathbf{q})$ (shown later by other authors [Burada, 2008; Reguera and Rubí, 2001; Reguera et al., 2006]), or a combination of both [Martens et al., 2012a; Wang and Drazer, 2010]. Zwanzig derived the FJ equation by performing a reduction in the number of coordinates from the full 3D Smoluchowski equation to a one-dimensional description. Assuming that the distribution of the transverse coordinates y and z relaxes much faster to the equilibrium one than the longitudinal coordinate does (separation of time scales), the conditional PDF, Eq. (2.31), can be approximated by

$$P(y,z|x,t) \to P(y,z|x) = \frac{e^{-\Phi(\mathbf{q})}}{\int\limits_{\omega_-(x)}^{\omega_+(x)} \mathrm{d}y \int\limits_0^{\Delta H} \mathrm{d}z\; e^{-\Phi(\mathbf{q})}}. \tag{2.33}$$

[2] According to the Helmholtz's theorem, in general, every force $\mathbf{f}(\mathbf{q})$ can be decomposed into a curl-free component and a divergence-free component, $\mathbf{f}(\mathbf{q}) = -\boldsymbol{\nabla}\Phi(\mathbf{q}) + \boldsymbol{\nabla} \times \boldsymbol{\Psi}(\mathbf{q})$. An extension of the Fick-Jacobs approach to the most general force $\mathbf{f}(\mathbf{q})$ is presented and discussed in Chapt. 4.

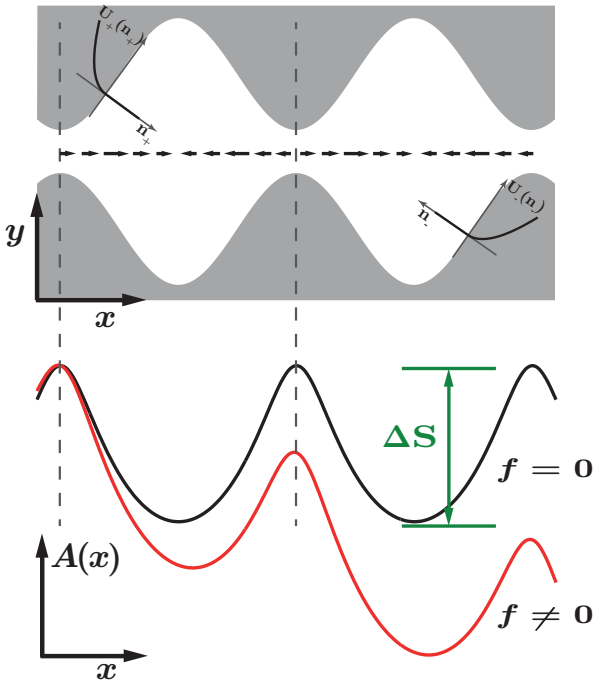

Figure 2.4: The effective entropic potential $A(x)$ as a function of the longitudinal coordinate x, Eq. (2.37b), for a channel with periodically varying local width $W(x)$ (plan view on a 3D planar channel). The arrows indicate the direction and strength of the mean force $\langle \mathbf{f}_x \rangle = -\mathrm{d}A(x)/\mathrm{d}x$ in the absence of external forces $\mathbf{f} = \mathbf{0}$. Superimposed are the maximum change of entropy ΔS and the particle-wall interaction potential $U_{\pm}(n_{\pm})$, Eq. (2.38).

Substituting Eq. (2.33) into Eq. (2.30), yields

$$\partial_t p\,(x,t) = \partial_x \left[e^{A(x)} \partial_x \left(e^{-A(x)} p\,(x,t) \right) \right], \tag{2.34}$$

where the *effective entropic potential* $A(x)$ (in units of $k_B T$) is explicitly given by

$$A(x) = -\ln \left[\int_{\omega_-(x)}^{\omega_+(x)} \mathrm{d}y \int_0^{\Delta H} \mathrm{d}z\; e^{-\Phi(\mathbf{q})} \right]. \tag{2.35}$$

The Smoluchowski equation for the marginal PDF, Eq. (2.34), is associated to a 1D particle dynamics evolving in the potential $A(x)$

$$\dot{x}(t) = -\frac{\mathrm{d}\,A(x)}{\mathrm{d}\,x} + \xi_x(t). \tag{2.36}$$

To conclude, the Fick-Jacobs approach enables a reduction of the problem's complexity from a 3D dynamics in a confined geometry with no-flux bcs to a 1D energetic description.

2.3.1. Potential of mean force – effective entropic potential

For the commonly discussed limits of either pure diffusion ($\Phi(\mathbf{q}) = 0$) [Dagdug et al., 2010; Kalinay and Percus, 2006; Makhnovskii et al., 2010], or an external force with magnitude f acting along the longitudinal (x) direction of the channel, i.e, $\Phi(\mathbf{q}) = -f\,x$ [Burada et al., 2007; Dagdug et al., 2011; Kalinay, 2009], the dimensionless effective

entropic potential simplifies to

$$A(x) = -\ln\left[Q(x)\right], \quad \text{if} \quad f = 0, \tag{2.37a}$$
$$A(x) = -f\,x - \ln\left[Q(x)\right], \quad \text{if} \quad f \neq 0. \tag{2.37b}$$

One immediately notices that substituting Eq. (2.37a) into Eq. (2.34) results in the Fick-Jacobs equation derived by Jacobs, cf. Eq. (2.32).

For illustration, the effective entropic potential is depicted in Fig. 2.4 for different values of f. $A(x)$ reflects the periodicity of the local cross-section $Q(x)$ and attains its maximum values at the minima of $Q(x)$ and vice versa. Even in the absence of external forces, $f = 0$, detailed balance is locally broken due to the uneven shape of the channel. Since the stationary joint PDF $P_{\mathrm{st}}(\mathbf{q})$ scales with $\exp(-A(x))$, the particle motion is rectified by the confinement, $P(x + \mathrm{d}x, y, z)/P(x - \mathrm{d}x, y, z) = Q(x + \mathrm{d}x)/Q(x - \mathrm{d}x) \neq 1$ for $\mathrm{d}x \neq 0$. It turns out that the probability for a particle to diffusive towards the constricting part of the channel is smaller compared to the one to move in opposite direction. The modulation of the channel's shape, or, equivalently, the entropy variations induces a symmetry breaking that biases the particles' diffusion. This fact is indicated by the arrows in Fig. 2.4. For $f \neq 0$, the effective entropic potential becomes tilted with slope f and therefore detailed balance is violated at any position x even in a straight channel, $Q(x) = const.$ Additionally, we depict the maximum change of entropy ΔS within a channel unit cell. For Brownian motion in a confined geometry the number of possible states Ω in transverse direction(s) is proportional to the local cross-section $\Omega \propto Q(x)$ for a given longitudinal position x. Within the Fick-Jacobs approach each transverse microstate is assumed to be occupied by equal probability. According to *the fundamental assumption of statistical thermodynamics* [Boltzmann, 1896], the entropy is given by $S = k_B \ln\left[\Omega\right]$ for any system if the occupation of any microstate is equally probable. Hence, the effective entropic potential $A(x)$, Eq. (2.37a), scales with the local entropy in the absence of external forces.

By introducing $A(x)$ one replaces the 3D full dynamics in a confined geometry with no-flux bc to an effective 1D description, cf. Eq. (2.36), where the particles evolve in an energetic potential. But what is the physical nature of the effective entropic potential? Referring to Sokolov, 2010, the interaction of the particles with the channel's wall can be mimicked by a quadratic potential growing in the direction normal to the wall,[3]

$$U_{\pm}(\mathbf{n}_{\pm}) = \frac{\kappa_w}{2}\,\mathbf{n}_{\pm}^2, \tag{2.38}$$

with interaction strength κ_w and $\mathbf{n}_{\pm}$ being the coordinate along the normal to the upper $\mathbf{n}_{+}$ and lower boundary $\mathbf{n}_{-}$ taken at the point $(x, \omega_{\pm}(x))$, see Fig. 2.4. When x is fixed, the energy depends solely on the y-coordinate and is given by

$$U_{\pm}(x, y) = \begin{cases} 0, & \text{if} \quad \omega_{-}(x) < y < \omega_{+}(x), \\ \frac{1}{2}\,\kappa_w\,\left(y - \omega_{\pm}(x)\right)^2\,\cos^2\alpha_{\pm}(x), & \text{otherwise}, \end{cases} \tag{2.39}$$

[3]Here, we restrict ourselves to a two-dimensional setup. A generalization to three dimensions is trivial.

with angle $\alpha_{\pm}(x) = \arctan\left(\omega'_{\pm}(x)\right)$. Then, the mean force acting on the particle during its motion through the confined geometry is given by

$$\langle\, \mathbf{f}_x \,\rangle = -\frac{\mathrm{d}\, A(x)}{\mathrm{d}\, x} = -\int_{-\infty}^{\infty} \mathrm{d}y\, \left(\partial_x \Phi(x,y) + \partial_x U_{\pm}(x,y)\right) P(y|x). \tag{2.40}$$

Interchanging derivation and integration, yields $A'(x) = -\partial_x \ln\Big[\int_{-\infty}^{\infty} \mathrm{d}y\, \exp\left(-\Phi - U_{\pm}\right)\Big]$. The integral over y can be divided into three parts, namely, $-\infty < y \leq \omega_-(x)$, $\omega_-(x) < y < \omega_+(x)$, and $\omega_+(x) < y < \infty$. Integrating $\int_{-\infty}^{\omega_-(x)} \mathrm{d}y \ldots$ by parts and using the substitution $\varsigma = y - \omega_-$ result in

$$\begin{aligned} \int_{-\infty}^{0} \mathrm{d}\varsigma\, e^{-[\Phi(x,\varsigma+\omega_-)+U_-(x,\varsigma)]} &= \sqrt{\frac{\pi}{2\kappa_w \cos^2\alpha_-}}\, \Big[e^{-\Phi(x,-\infty)} \\ - \int_{-\infty}^{0} \mathrm{d}\varsigma\, \partial_\varsigma e^{-\Phi(x,\varsigma+\omega_-(x))}\, \mathrm{erf}&\left(\sqrt{\frac{\kappa_w \cos^2\alpha_-}{2}}\,\varsigma\right)\Big]. \end{aligned} \tag{2.41}$$

In the same manner, we evaluate the integral $\int_{\omega_+(x)}^{\infty} \mathrm{d}y \ldots$. In the limit of hard walls, i.e., $\kappa_w \to \infty$, both integrals vanish and thus the mean force in the longitudinal direction reads

$$\langle\, \mathbf{f}_x \,\rangle = -\frac{\mathrm{d}\, A(x)}{\mathrm{d}\, x} = \partial_x \ln\left[\int_{\omega_-(x)}^{\omega_+(x)} \mathrm{d}y\, e^{-\Phi(x,y)}\right]. \tag{2.42}$$

It turns out that "the mean force is the conditional average of the mechanical force acting on the particle (here conditioned on its x-coordinate). This is essentially a mean constraint force caused by nonholonomic constraint stemming from the boundaries" [Sokolov, 2010]. The result that the potential of mean force equals the free energy associated with the partition function $Z(x) = \int_{\omega_-(x)}^{\omega_+(x)} \mathrm{d}y\, \exp\left(-\Phi(\mathbf{q})\right)$ is absolutely general[4] and it is intimately connected with equipartition.

2.4. Validity of the Fick-Jacobs approach – Spatially dependent diffusion coefficient

The reduction of dimensionality done implicitly in the formulation of the Fick-Jacobs equation, Eq. (2.34), relies on the assumption of equilibration in transverse directions. This approximation neglects the influence of relaxation dynamics in y and z, supposing that it is infinitely fast. In a more detailed view, we have to notice that the particles can flow from or to the wall in transverse direction(s) only at finite time. Therefore, particles may accumulate at the curved walls where the channel is getting narrower or depletion zones can occur where the channel becomes wider. By analyzing the

[4] In Martens et al., 2012a we have shown that the derivation of the potential of mean force is not only valid in the overdamped limit but also for arbitrary viscous friction coefficient γ, see Eq. (2.2). This fact is also discussed in depth in Sect. 6.2.

different time scales involved in the problem, Burada et al., 2007, see also [Burada, 2008], derived an estimate for the conditions under which equilibration occurs. In the case of forced Brownian motion, three characteristic processes with corresponding time scales can be identified in a 2D channel.[5] These are the times $\tau_y = \Delta y^2/2$ and $\tau_x = \Delta x^2/2$ to diffuse over distances Δy and Δx, respectively, and the characteristic drift time $\tau_{\text{drift}} = \Delta x/f$. In order to achieve equilibration in the transverse direction, the characteristic time scales associated with diffusion in this direction has to be much smaller than the other two characteristic time scales, yielding

$$1 \gg \frac{\tau_y}{\tau_x} = \left(\frac{\Delta y}{\Delta x}\right)^2 \sim W'(x)^2, \tag{2.43a}$$

$$1 \gg \frac{\tau_y}{\tau_{\text{drift}}} = f\,\frac{\Delta y^2}{2\,\Delta x} \sim \frac{f}{2}\,W(x)^2. \tag{2.43b}$$

Then, the criterion

$$\max\left(\tau_y/\tau_x, \tau_y/\tau_{\text{drift}}\right) \ll 1, \tag{2.44}$$

has to be satisfied at any position x and for any value of f.

Consequently, the accuracy of the FJ equation can be improved by either speeding up the transverse dynamics while keeping the longitudinal one fixed or slowing down the longitudinal dynamics. These imposed artificial separation of time scales can be realized e.g. by an anisotropy in the dispersion tensor, $\mathbb{D}_{y,y} \gg \mathbb{D}_{x,x}$ [Berezhkovskii and Szabo, 2011; Kalinay and Percus, 2006]. Hence, Zwanzig proposed the following correction to the Fick-Jacobs equation

$$\partial_t p\,(x,t) = \partial_x\left[D(x,f)e^{A(x)}\partial_x\left(e^{-A(x)}p\,(x,t)\right)\right], \tag{2.45}$$

which corresponds to a slow down of the longitudinal dynamics. Note that the function $D(x,f)$ corrects both the convection and the diffusion term in the same way, keeping (a kind of) the Sutherland-Einstein relation between them valid. We stress that the dynamics of $p(x,t)$, Eq. (2.45), differs from the one in systems with position-dependent diffusion [Büttiker, 1987; Lindner and Schimansky-Geier, 2002]. Since the criterion Eq. (2.44) depends on the magnitude of the external force f, the spatially dependent diffusion coefficient $D(x,f)$ (in units of D^0) has to be a function of f. Comparing Eqs. (2.30) and (2.45), the marginal probability current in longitudinal direction is given by

$$\begin{aligned} -J^x(x,t) &= D(x,f)e^{A(x)}\partial_x\left(e^{-A(x)}p\,(x,t)\right) \\ &= -\int_{\omega_-(x)}^{\omega_+(x)}\mathrm{d}y\;\int_0^{\Delta H}\mathrm{d}z\;\left[\mathbf{f}_x(\mathbf{q},t)\,P(\mathbf{q},t) - \partial_x P(\mathbf{q},t)\right]. \end{aligned} \tag{2.46}$$

[5] For the sake of simplicity, the authors focused on the situation of a two-dimensional (2D) channel, although the same discussion can readily be extended to 3D.

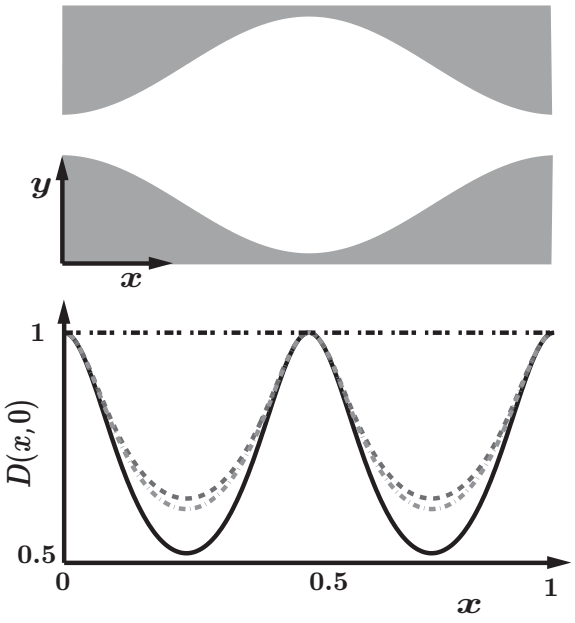

Figure 2.5: Sketch of one unit cell of a two-dimensional, confining geometry with unit period (top panel). The behavior of the spatially dependent diffusion coefficient $D(x,0)$ is depicted in the bottom panel. Solid line corresponds to Zwanzig's estimate Eq. (2.47), dashed line represents Reguera-Rubí's proposal Eq. (2.48), the result of Kalinay and Percus is indicated by the dashed-dotted line Eq. (2.49a), and the horizontal line corresponds to the free diffusion constant which is unity in our scaling. As an example for a periodically varying width we choose $W(x) = 0.7 - 0.5\,\cos(2\pi\,x)$.

The second equality determines the sought-after $D(x,f)$. Once the joint PDF $P(\mathbf{q},t)$ and marginal PDF are known the spatially dependent diffusion coefficient can be calculated according to Eq. (2.46).

Zwanzig calculated the first order correction to $P(\mathbf{q},t)$ and suggested

$$D_Z(x,0) = 1 - \frac{\alpha}{4}\,W'(x)^2 \simeq \frac{1}{1+\alpha\,W'(x)^2/4}, \tag{2.47}$$

for an axis-symmetric channel. Thereby, 3D planar structures are presented by $\alpha = 1/3$ and tubes by $\alpha = 1/2$. Reguera and Rubí, 2001, presented arguments for the corrected stationary FJ equation, cf. Eq. (2.45), within the framework of mesoscopic non-equilibrium thermodynamics. They improved Zwanzig's estimates of $D_Z(x,0)$, proposing

$$D_{RR}(x,0) = \frac{1}{\left[1+W'(x)^2/4\right]^{\alpha}}, \tag{2.48}$$

with $\alpha = 1/3$ (3D planar structures) and $\alpha = 1/2$ (tubes), respectively, with rather heuristic reasoning. A first systematic treatment taking the finite diffusion time into account was presented by Kalinay and Percus (KP). Their proposed mapping procedure enables the derivation of higher order corrections in terms of an expansion parameter ε_{KP}^2, which is the ratio of imposed anisotropic diffusion constants in the longitudinal and transverse direction [Kalinay and Percus, 2006]. Within this scaling, the "fast" transverse modes (transients) separate from the "slow" longitudinal ones and can be projected out by integration over the transverse directions. KP suggested an operator procedure mapping the solutions of the corrected FJ equation back onto the space of solutions of the original 3D problem. The resulting recurrence scheme provides

systematic corrections to the FJ equation resulting in

$$D_{KP}(x,0) = \frac{\arctan\left(W'(x)/2\right)}{W'(x)/2}, \quad \text{for 3D planar structures,} \tag{2.49a}$$

$$D_{KP}(x,0) = \frac{1}{\sqrt{1+W'(x)^2/4}}, \quad \text{for tubes.} \tag{2.49b}$$

In 2009, Kalinay extended the mapping procedure to the problem of biased ($\Phi(\mathbf{q}) \neq 0$) Brownian particles in a two-dimensional confinement. He presented a first order expansion for a generalized spatially dependent diffusion coefficient $D(x, \Phi(\mathbf{q}))$.

2.5. Mean first passage time

The mean first passage time (MFPT) approach [Arrhenius, 1889; Hänggi et al., 1990; Kramers, 1940; van't Hoff, 1884] enables the calculation of the transport characteristics like the mean particle current, Eq. (2.17), and effective diffusion coefficient, Eq. (2.23), of Brownian particles moving through a periodic channel by means of the moments of the first passage time distribution. The first passage time $t\left(x_0 \to x_0+1\right)$ is *the time an object needs to reach the final point* x_0+1 *for the first time when it starts at an arbitrary point* x_0. The n-th moment of the first passage time distribution is given by the average over the fluctuating force, $\left\langle\, t^n\left(x_0 \to x_0+1\right)\right\rangle$. For the one-dimensional Fick-Jacobs dynamics, Eq. (2.36), these moments are given by the well-closed analytical recursion [Burada, 2008, see appendix]

$$\left\langle\, t^n\left(a \to b\right)\right\rangle = n \int_a^b \mathrm{d}x\, \frac{e^{A(x)}}{D\left(x,f\right)} \int_{-\infty}^{x} \mathrm{d}y\, e^{-A(y)} \left\langle\, t^{n-1}\left(y \to b\right)\right\rangle. \tag{2.50}$$

The iteration starts with $\left\langle\, t^0(a \to b)\right\rangle = 1$ for $n = 0$.

For any non-negative force the mean particle current in periodic structures can be obtained via the Stratonovich formula [Stratonovich, 1958; Tikhonov, 1959]

$$\left\langle\, \dot{x}\,\right\rangle = \frac{1}{\left\langle\, t(x_0 \to x_0+1)\,\right\rangle} = \frac{1-e^{-f}}{\int_{x_0}^{x_0+1} \mathrm{d}x\, \frac{e^{A(x)}}{D(x,f)} \int_{x-1}^{x} \mathrm{d}x'\, e^{-A(x')}}. \tag{2.51}$$

Note that for a vanishing force $\mathbf{f} = \mathbf{0}$ the mean first passage time $\left\langle\, t(x_0 \to x_0+1)\,\right\rangle$ diverges and consequently $\left\langle\, \dot{x}\,\right\rangle$ vanishes. A non-zero force prevents the particle to make far excursions to the left or right, hence leading to a finite mean first passage time as well as a finite current.

Referring to Eq. (2.8), D_{eff} is defined as the asymptotic behavior of the variance of the position and can be computed analytically by regarding the hopping events [Lindner et al., 2001; Reimann et al., 2001] as manifestations of a renewal process [Ebeling and

Sokolov, 2005] in the overdamped regime

$$D_{\text{eff}}/D^0 = \frac{\langle\, t^2(x_0 \to x_0+1)\,\rangle - \langle\, t(x_0 \to x_0+1)\,\rangle^2}{2\,\langle\, t(x_0 \to x_0+1)\,\rangle^3}. \tag{2.52}$$

After algebraic manipulations the expression for D_{eff} can be transformed to read [Reimann et al., 2001, 2002]

$$D_{\text{eff}}/D^0 = \frac{\int_0^1 \mathrm{d}x\, I_{\mp}(x) I_{\pm}(x)^2}{\left[\int_0^1 \mathrm{d}x\, I_{\pm}(x)\right]^3}, \tag{2.53}$$

where the substitutes $I_+(x)$ and $I_-(x)$ are given by

$$I_+(x) = e^{-A(x)} \int_x^{x+1} \mathrm{d}x'\, \frac{e^{A(x')}}{D(x',f)}, \tag{2.54a}$$

$$I_-(x) = \frac{e^{A(x)}}{D(x,f)} \int_{x-1}^{x} \mathrm{d}x'\, e^{-A(x')}. \tag{2.54b}$$

In the diffusion dominated regime, $\|\mathbf{f}\| \ll 1$, the Sutherland-Einstein relation emerges and thus the particle mobility equals the effective diffusion coefficient, cf. Eq. (2.26). For any particle diffusing in a periodic potential $A(x+m) = A(x)$ with periodic function $D(x+m,f) = D(x,f), \forall m \in \mathbb{Z}$, $D_{\text{eff}}(f)/D^0$ can be calculated via the Lifson-Jackson formula [Lifson and Jackson, 1962]

$$\lim_{f\to 0} \mu(f)/\mu^0 = \lim_{f\to 0} D_{\text{eff}}(f)/D^0 = \frac{1}{\langle\, e^{-A(x)}\,\rangle_x \,\langle\, e^{A(x)}/D(x,f)\,\rangle_x}. \tag{2.55}$$

According to Eq. (2.37a), the potential of mean force simplifies to $A(x) = -\ln[Q(x)]$ for $f \to 0$ and thus one gets

$$\lim_{f\to 0} \mu(f)/\mu^0 = \lim_{f\to 0} D_{\text{eff}}(f)/D^0 = \frac{1}{\langle\, Q(x)\,\rangle_x \,\langle\, 1/\left(D(x,0)\,Q(x)\right)\,\rangle_x}. \tag{2.56}$$

Here, the average is taken over one period which is one in the considered scaling, i.e., $\langle\,\cdot\,\rangle_x = \int_0^1 \cdot\, \mathrm{d}x$. It turns out that the effective diffusion constant in longitudinal direction is solely determined by the channel geometry. In channels where the local equilibration assumption is always fulfilled, the expression for the spatially dependent diffusion coefficient $D(x,f)$ can be replaced by the bulk coefficient. The latter is one in our scaling.

2.6. Summary

In this chapter, we gave first a short overview over Brownian motion in systems without geometrical constraints. In the presence of spatially constrictions, one can compute the transport quantities like the mean particle current and the effective diffusion coefficient by means of macrotransport theory. The main task entails computing the joint probability density function $P(\mathbf{q}, t)$ for geometries with impenetrable boundaries. For arbitrary channel geometries and forces the problem usually cannot be solved analytically. Assuming that (i) the time scales in transverse directions separate from the longitudinal one, (ii) the distributions of the transverse coordinates equal the equilibrium distributions at any position x and time t, and (iii) equipartition holds, enable a reduction of the problem's dimensionality and leads to an effective one-dimensional kinetic description – the *Fick-Jacobs approach*. Within the latter, the particle dynamics is determined by the potential of mean force $A(x)$. The mean force $\langle \mathbf{f}_x \rangle = -A'(x)$ is essentially a mean constraint force caused by nonholonomic constraint originated from the boundaries. The reduction of dimensionality done implicitly in the formulation of the Fick-Jacobs equation neglects the influence of relaxation dynamics in transverse directions, supposing that it is infinitely fast. Therefore, the accuracy of the Fick-Jacobs equation can be improved by the introduction of a spatially dependent diffusion coefficient $D(x, f)$, which corresponds to an imposed artificial separation of time scales. Finally, concerning the reduced one-dimensional kinetic description, analytical expressions for the mean particle current and effective diffusion coefficient can be evaluated via the mean first passage time approach.

In the following chapter 3, we present a systematic treatment for entropic particle transport by performing asymptotic perturbation analysis of the stationary joint probability density function. We demonstrate that the leading order of the series expansion, in terms of an expansion parameter specifying the channel corrugation, is equivalent to the well-established Fick-Jacobs approach. The calculated higher-order corrections to the joint probability density function become significant for extremely corrugated confinements.

3. Biased particle transport in extremely corrugated channels – Higher-order corrections to Fick-Jacobs equation

In the previous chapter, we gave a short introduction into macrotransport theory for spatially periodic confinements which provides a generic scheme for computing the main transport quantities like the mean particle current and the effective diffusion coefficient (EDC). The first step to calculate these quantities entails calculating the joint PDF $P(\mathbf{q}, t)$ whose evolution is governed by the Smoluchowski equation, Eq. (2.12). In general, the problem's dimensionality (degrees of freedom) can be reduced by integrating the transverse coordinate(s) out, leading to an integro-partial differential equation, see Eq. (2.30). Then, the principle problem that must be solved is to express the 3D joint PDF $P(\mathbf{q}, t)$ in terms of the marginal PDF $p\,(x, t)$. This can only be done exactly in a few idealized cases.

Hence, many authors discussed different approaches in order to solve this problem. In their pioneering works M. Jacobs [Jacobs, 1967] and R. Zwanzig [Zwanzig, 1992] assumed a separation of the time scale between the "fast" transverse dynamics and the "slow" longitudinal one. This approach neglects the relaxation dynamics in transverse direction(s) and leads to an effective one-dimensional, energetic description for the problem of biased Brownian motion in system with spatial constraints.

In the sense of lubrication theory [Reynolds, 1886], several authors presented series expansion techniques for the 3D joint PDF based on the ratio of time scales or, equivalently, length scales involved in the problem. In principle, the Smoluchowski equation, Eq. (2.12), can be rewritten as a series expansion in a small parameter ε. Thereby, the *leading order* $O(\varepsilon^0)$ also denoted as *unperturbed* problem is assumed to be solvable. The expansion parameter ε measures how far the actual problem deviates from the unperturbed problem whereby the latter's solution equals the one of the Fick-Jacobs equation. The idea is to calculate both the 3D joint PDF and marginal PDF by successively finding the higher-order terms in a perturbation expansion series. The essential question here is the choice of the small parameter ε, in which one could do an expansion.

For instance, the disparity between the channel height and the period, $\varepsilon = \Delta H$, or between the averaged half width and channel's period, $\varepsilon = \langle\, W(x) \,\rangle_x$, serves as expansion parameter in [Laachi et al., 2007; Yariv and Dorfman, 2007]. Contrary, Kalinay and Percus [Kalinay and Percus, 2006, 2008] used as smallness parameter the ratio of an imposed anisotropy in the dispersion tensor, $\varepsilon_{KP}^2 = \mathbb{D}_{x,x}/\mathbb{D}_{y,y} \approx \tau_y/\tau_x \ll 1$. In both cases, a small value of ε corresponds to rapid transverse sojourns associated with quick relaxation of the transverse profile to the steady-state form. Based on an expansion in ε, Kalinay and Percus derived a rigorous mapping method where the n-th series expansion term of the 3D joint PDF have the form of an operator acting on

$p(x,t)$. Both choices of ε are appropriate if one focuses on the short time evolution of $P(\mathbf{q},t)$ when starting from a given initial PDF $P(\mathbf{q},0)$.

Our objective with this chapter is to provide a systematic treatment by applying the method of asymptotic perturbation analysis [Bruus, 2008] to the problem of biased Brownian motion in confined geometries. We purpose to calculate higher-order correction terms to the stationary joint PDF in terms of an expansion parameter, which specifies the channel corrugation. In particular, we limit our consideration to the stationary problem of Eq. (2.12), which is in fact, the only state necessary for deriving the main transport quantities, see Sect. 2.1. Once equilibration in transverse direction(s) is accomplished, the problem is well described by the FJ equation, Eq. (2.34), as long as the modulation of the channel walls is small compared to the period length. Hence, contrarily to the choices for ε stated above, we choose a quantity characterizing the deviation of the corrugated cross-section from the straight channel, corresponding to $\varepsilon = 0$. In detail, our dimensionless parameter ε measures the difference between the widest cross-section of the channel, $\Delta\Omega$, and the most narrow constriction at the bottleneck, $\Delta\omega$,[1] yielding

$$\varepsilon = \Delta\Omega - \Delta\omega. \tag{3.1}$$

Our choice of ε is supported by analysis of the time scales involved in the problem, see Sect. 2.4, leading to a criteria for the validity of the FJ equation. Burada et al. found the requirement $W'(x)^2 \simeq \varepsilon^2 \ll 1$ for diffusive motion, $\mathbf{f} = \mathbf{0}$.

Before we start to deduce the higher-order correction terms to the Fick-Jacobs solution, we briefly summarize the basic concept underlying asymptotic perturbation analysis. In general, the governing stationary Smoluchowski equation, cf. Eq. (2.12), can be reformulated in terms of the steady state Fokker-Planck operator $\mathfrak{L}$, yielding $\mathfrak{L}\,P_{\mathrm{st}}(\mathbf{q}) = 0$. First, one supposes that $\mathfrak{L}$ can be written as a series expansion in ε

$$\mathfrak{L} = \mathfrak{L}_0 + \varepsilon^2\,\mathfrak{L}_1, \tag{3.2}$$

where $\mathfrak{L}_0$ is a differential operator, which represents a simpler problem that is assumed to be solvable.[2] This simpler problem is also denoted as *unperturbed* problem or *leading order*. The idea is to calculate the stationary joint PDF $P_{st}(\mathbf{q})$ by successively finding the higher-order terms in the expansion $P_{st}(\mathbf{q}) = \sum_{n=0}^{\infty} \varepsilon^{2n} P_n(\mathbf{q})$. Since we suppose that the steady state Fokker-Planck operator depends of ε^2, Eq. (3.2), $P_{st}(\mathbf{q})$ is expanded solely in the form of a formal perturbation series in even orders of ε. Combining both expansions, the stationary Smoluchowski equation reads

$$\mathfrak{L}_0 P_0 + \varepsilon^2 (\mathfrak{L}_0 P_1 + \mathfrak{L}_1 P_0) + \varepsilon^4 (\mathfrak{L}_0 P_2 + \mathfrak{L}_1 P_1) + \ldots = 0. \tag{3.3}$$

Likewise, one has to expand the no-flux boundary condition, Eq. (2.14), in ε. For Eq. (3.3) to be true for any value of ε, each order must be zero, leading to an infinite,

[1] Please note that throughout this thesis all lengths are scaled in units of the channel period L. Considering dimensionful quantities leads to $\varepsilon = (\Delta\Omega - \Delta\omega)/L$.

[2] We emphasize that the described concept is not limited to three-dimensional problems. Mainly, we apply this method to effective 2D systems in the following sections.

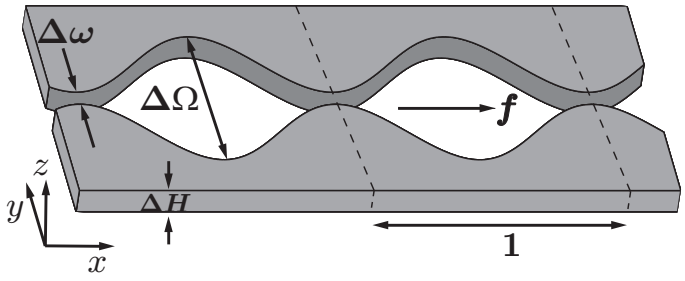

Figure 3.1.: Sketch of a segment of a 3D, reflection-symmetric periodically varying channel that is confining the motion of overdamped, point-like Brownian particles. The periodicity of the channel structures is unity, the height ΔH, the minimal and maximal channel widths are $\Delta\omega$ and $\Delta\Omega$, respectively. The size of a unit cell is indicated with the dashed lines.

hierarchic set of boundary value problems to solve. By assumption, the homogeneous zero-order equation is the unperturbed, solvable problem and $P_0(\mathbf{q})$ can therefore be found. This implies that the first-order equation $O(\varepsilon^2)$ becomes an inhomogeneous differential equation for the first-order correction $P_1(\mathbf{q})$ which in principle can be derived since $\mathfrak{L}_1 P_0$ is known. Then, the solution of the full problem can be calculated if any solutions of $\mathfrak{L}_0 P_n + \mathfrak{L}_1 P_{n-1} = 0$ with associated bc can be iteratively found.

In the following chapter, we calculate the higher-order corrections terms to Fick-Jacobs solution for two possible realizations of three-dimensional channels. That are (i) a periodic channel geometry with rectangular cross-section in Sect. 3.1 and (ii) a cylindrical tube with periodically varying radius $R(x)$ in Sect. 3.3. If not explicitly stated otherwise, we always restrict our studies to (i) axis-symmetric boundary functions $\omega_\pm(x) = \pm\omega(x)$ confining the particle's motion in transverse direction(s). Additionally, we assume throughout (ii) dilute particle concentration within each unit cell and (iii) negligible particle diameter (point-like) compared to the bottleneck width, $d_p \ll \Delta\omega$. Thus, hydrodynamic particle-wall, hydrodynamic and hard-core particle-particle interactions can safely be disregarded [Happel and Brenner, 1965]. Finally, (iv) the particles are subject to an external static force with static magnitude f acting only along the longitudinal direction of the channel $\mathbf{e}_x$ (the corresponding potential is $\Phi(\mathbf{q}) = -f\,x$).

3.1. Three-dimensional, planar channel geometry

In this section, we study the dynamics of point-size Brownian particles evolving under the action of an external static force $\mathbf{f} = f\,\mathbf{e}_x$ in a 3D planar channel geometry.[3] The confinements possess unit period, constant height ΔH, and a periodically varying rectangular cross-section $Q(x)$. The particle motion is confined by two planar

[3] I remark that several results and similar figures presented in this section have been previously published in Martens et al., 2011a.

walls at $z = 0$ and $z = \Delta H$ and by the perpendicular axis-symmetric side-walls at $y = \omega_+(x) = \omega(x)$ and $y = \omega_-(x) = -\omega(x)$ [Oliveira et al., 2007; Squires and Quake, 2005]. The corresponding local cross-section is given by $Q(x) = \Delta H\, W(x)$ with $W(x) = 2\,\omega(x)$. The minimal and maximal value of the local channel width are denoted as $\Delta\omega$ and $\Delta\Omega$. A sketch of a segment of the channel is depicted in Fig. 3.1.

We next measure, for the case of finite corrugation $\varepsilon \neq 0$, the transverse length y in units of ε, $y \to \varepsilon\, y$ and, likewise, the boundary functions $\pm\omega(x) \to \pm\varepsilon\, h(x)$. After re-scaling, the joint PDF reads $P\,(\mathbf{q}, t) \to \varepsilon\, P\,(\mathbf{q}, t)$, respectively, the probability current is given by $\mathbf{J}\,(\mathbf{q}, t) = (\varepsilon J^x, J^y, \varepsilon J^z)^T$. We emphasize that the scaling of time, energies, and the set of units are not influenced by this additional transverse scaling, see Sect. 2.2.

In dimensionless units, the Langevin equations, Eq. (2.25), describing the particle's dynamics are given by

$$\dot{x} = -\,\partial_x \Phi(\mathbf{q}) + \xi_x(t), \tag{3.4a}$$

$$\dot{y} = -\,\frac{1}{\varepsilon^2}\partial_y \Phi(\mathbf{q}) + \frac{1}{\varepsilon}\,\xi_y(t), \tag{3.4b}$$

$$\dot{z} = -\,\partial_z \Phi(\mathbf{q}) + \xi_z(t). \tag{3.4c}$$

The corresponding stationary[4] Smoluchowski equation, Eq. (2.12),

$$0 = \boldsymbol{\nabla}_{\mathbf{q}} \cdot \mathbf{J}_{\mathrm{st}}\,(\mathbf{q}) = -\boldsymbol{\nabla}_{\mathbf{q}} \left[e^{-\Phi(\mathbf{q})} \boldsymbol{\nabla}_{\mathbf{q}} \left(e^{\Phi(\mathbf{q})}\, P_{\mathrm{st}}\,(\mathbf{q}) \right) \right], \tag{3.5a}$$

simplifies to

$$0 = \varepsilon^2 \partial_x J^x_{\mathrm{st}} + \partial_y J^y_{\mathrm{st}} + \varepsilon^2 \partial_z J^z_{\mathrm{st}}, \tag{3.5b}$$

with $\boldsymbol{\nabla}_{\mathbf{q}} = (\partial_x, \varepsilon^{-1}\partial_y, \partial_z)^T$. The subscript *st* will be omitted in the following since we solely discuss the stationary problem. We postulate that the dynamics in z-direction is decoupled from the one in x and y-direction. Consequently, the separation ansatz $P(\mathbf{q}) = p(x, y)\, Z(z)$ in consideration of the boundary condition

$$J^z(\mathbf{q}) = 0, \quad \text{at } z = 0, \text{ and } z = \Delta H, \tag{3.6}$$

results in a non-trivial solution for $J^z\,(\mathbf{q}) = 0$ everywhere within the channel. For the studied situation, i.e., there is only a constant force acting in x-direction, the particles are uniformly distributed in z-direction and the form function $Z(z)$ equals the inverse of the dimensionless channel height at steady state, i.e., $Z = 1/\Delta H$. The separation ansatz can also be applied to more complicated forcing scenarios if the external potential can be written as a sum of two independent potentials, $\Phi(\mathbf{q}) = V(x, y) + W(z)$. In this

[4] For non-stationary problems, the left-hand side of Eq. (3.5b) reads $-\varepsilon^2 \partial_t P\,(\mathbf{q}, t)$. Hence, the time derivative is negligible for smoothly varying channel widths, respectively, small values for ε.

case, the stationary solution reads

$$P(\mathbf{q}) = p(x,y)\,\frac{e^{-W(z)}}{\int\limits_0^{\Delta H} \mathrm{d}z\, e^{-W(z)}}, \tag{3.7}$$

where the form function $Z(z)$ equals the Boltzmann-distribution. This allows a reduction of the problem's dimensionality from 3D to 2D:

$$\varepsilon^2 \partial_x J^x(x,y) + \partial_y J^y(x,y) = 0. \tag{3.8}$$

Comparing the last expression with Eq. (3.2), we identify $\mathfrak{L}_0 p(x,y) = \partial_y J^y(x,y)$ and $\mathfrak{L}_1 p(x,y) = \partial_x J^x(x,y)$. The 2D transport problem, stated in Eq. (3.8), was investigated for symmetric [Burada et al., 2008b; Laachi et al., 2007; Marchesoni and Savel'ev, 2009] as well as in asymmetric [Bradley, 2009; Kalinay and Percus, 2010; Yariv et al., 2004] channels.

For the considered re-scaled channel geometry, the outward-pointing normal vector reads $\mathbf{n}_y = (-h'(x), \pm 1, 0)^T / \sqrt{1 + h'(x)^2}$ at the perpendicular side-walls at $y = \pm h\,(x)$. The prime denotes the differentiation with respect to x. Therefore, the no-flux boundary conditions, Eq. (2.14), can be written as

$$\pm \varepsilon^2 h'(x)\, J^x = J^y, \quad \forall\,(x,y) \in \text{channel wall}. \tag{3.9}$$

Asymptotic perturbation analysis

In what follows, we perform asymptotic perturbation analysis of the problem stated by Eqs. (3.8) and (3.9). Therefore, the stationary joint PDF $p(x,y)$

$$p(x,y) = p_0(x,y) + \varepsilon^2\, p_1(x,y) + \ldots = \sum_{n=0}^{\infty} \varepsilon^{2n} p_n(x,y), \tag{3.10}$$

and, likewise, the stationary probability current $\mathbf{J}$

$$\mathbf{J}(x,y) = \sum_{n=0}^{\infty} \varepsilon^{2n} \mathbf{J}_n(x,y), \tag{3.11}$$

are expanded a perturbation series in even orders of the parameter ε. Substituting these expressions into Eqs. (3.8) and (3.9), we get a hierarchic set of inhomogeneous, partial differential equations

$$0 = \partial_y J_0^y(x,y) + \sum_{n=1}^{\infty} \varepsilon^{2n} \left\{ \partial_x J_{n-1}^x(x,y) + \partial_y J_n^y(x,y) \right\}, \tag{3.12a}$$

with associated boundary conditions at the channel walls $y = \pm h(x)$

$$0 = -J_0^y(x,y) + \sum_{n=1}^{\infty} \varepsilon^{2n} \left\{ \pm\, h'(x) J_{n-1}^x(x,y) - J_n^y(x,y) \right\}, \quad \forall\,(x,y) \in \text{wall}. \tag{3.12b}$$

For this to be true for any value of ε each term within the brackets must be zero, yielding to an infinite system of boundary value problems to solve. Basically, the solution of the full problem can be calculated if any solutions of Eq. (3.12) can be iteratively found.

Moreover, the stationary joint PDF has to be normalized for any value of ε. For simplification, we claim that the normalization requirement for $p(x, y)$ corresponds to the zeroth solution $p_0(x, y)$

$$\langle\, p_0(x,y)\,\rangle_{x,y} = \int_0^1 \mathrm{d}x \int_{-h(x)}^{h(x)} \mathrm{d}y\, p_0(x,y) = 1, \tag{3.13}$$

that is normalized to unity. Consequently, the unit-cell average of the higher-order correction terms must vanish

$$\langle\, p_n(x,y)\,\rangle_{x,y} = 0. \tag{3.14}$$

In order to prevent that the marginal PDF, Eq. (2.28), equals the FJ results for any value for ε, i.e., $p(x) = p_0(x)$, we claim that $\exists\, x \in [0,1] : \sum_{n=1}^{\infty} \varepsilon^{2n} \int_{-h(x)}^{h(x)} \mathrm{d}y\, p_n(x,y) \neq 0$. The normalization condition, Eq. (3.14), can be realized by introducing the centered functions

$$p_n(x,y) \longmapsto p_n\,(x,y) - \langle\, p_n\,(x,y)\,\rangle_{x,y}\,, \quad \text{for } n \in \mathbb{N}^+. \tag{3.15}$$

We emphasize that the latter are no probability densities functions anymore because they can assume negative values for a given x and y. Additionally, each order $p_n(x, y)$ has to obey the periodicity requirement $p_n(x + m, y) = p_n(x, y)$, $\forall\, m \in \mathbb{Z}$.

By means of the series expansion Eq. (3.12a) in combination with Eq. (3.14), the calculation of the mean particle current in longitudinal direction, Eq. (2.17), simplifies to

$$\langle\, \dot{x}\,\rangle = \langle\, \dot{x}\,\rangle_0 - \sum_{n=1}^{\infty} \varepsilon^{2n} \langle\, \partial_x p_n(x,y)\,\rangle_{x,y}\,. \tag{3.16}$$

We find that the mean particle current is composed of (i) the Fick-Jacobs result $\langle\, \dot{x}\,\rangle_0$ and (ii) becomes corrected by the sum of averaged derivatives of the higher-order correction terms $p_n(x, y)$. One immediately notices that the introduction of the centered functions, Eq. (3.15), does not influence the result for the mean particle current.

3.1.1. Zeroth Order: the Fick-Jacobs equation

First, we derive the solution for the leading order $p_0(x, y)$ and demonstrate that the latter is identical to the solution of the Fick-Jacobs equation, cf. Eq. (2.34). Comparing Eqs. (3.8) and (3.2), the unperturbed differential operator $\mathfrak{L}_0$ explicitly reads

$$\mathfrak{L}_0 = -\partial_y \left[e^{-V(x,y)} \partial_y e^{V(x,y)} \right] = -\partial_y^2, \tag{3.17}$$

for $\Phi(\mathbf{q}) = V(x,y) = -f\,x$. To derive the leading order term, one has to solve $\mathfrak{L}_0 p_0(x,y) = \partial_y J_0^y(x,y) = 0$ supplemented with the corresponding no-flux boundary condition $J_0^y(x,y) = 0, \forall\,(x,y) \in$ channel wall, Eqs. (3.12). It immediately follows that $p_0(x,y) = g(x)\,e^{-V(x,y)}$ where $g(x)$ is an unknown function which has to be determined from the second order $O\left(\varepsilon^2\right)$ balance of Eq. (3.3), $\mathfrak{L}_0 p_1(x,y) + \mathfrak{L}_1 p_0(x,y) = 0$, with

$$\mathfrak{L}_1 = -\partial_x \left[e^{-V(x,y)} \partial_x e^{V(x,y)}\right] = \left(f\,\partial_x - \partial_x^2\right). \tag{3.18}$$

Integrating the second order $O\left(\varepsilon^2\right)$ balance with respect to y, yields

$$\begin{aligned} 0 = \partial_x \left(\int_{-h(x)}^{h(x)} \mathrm{d}y\, e^{-V(x,y)} g'(x) \right) + h'(x) J_0^x(x,-h(x)) \\ + h'(x) J_0^x(x,h(x)) - J_1^y(x,h(x)) + J_1^y(x,-h(x)). \end{aligned}$$

Taking the no-flux boundary conditions, Eq. (3.12b), into account, we obtain

$$0 = \partial_x \left(e^{-A(x)} g'(x)\right), \tag{3.19}$$

where $A(x)$ is the potential of mean force previously introduced in Eq. (2.35). For the exactly-posed problem, $\Phi(\mathbf{q}) = -f\,x$, $A(x)$ looks like $A(x) = -f\,x - \ln(2\,h(x))$. For $f \neq 0$ and only if x is not multiplicative coupled to the other spatial coordinate(s), a closed-form for $p_0(x,y)$ can be found [Risken, 1989]:

$$p_0(x,y) = e^{-V(x,y)} g(x) = \mathcal{I}^{-1}\, e^{-V(x,y)} \int_x^{x+1} \mathrm{d}x'\, e^{A(x')}, \tag{3.20}$$

with substitutes

$$I(x) = e^{-A(x)} \int_x^{x+1} \mathrm{d}x'\, e^{A(x')}, \quad \text{and} \quad \mathcal{I} = \int_0^1 \mathrm{d}x\, I(x). \tag{3.21}$$

Further, the marginal probability density function, cf. Eq. (2.28), becomes

$$p_0(x) = e^{-A(x)} g(x) = \mathcal{I}^{-1}\, I(x). \tag{3.22}$$

In the pure diffusion limit, $f = 0$, the particles are uniformly distributed within each channel unit cell, $p_0(x,y) = const$, and the marginal PDF reduces to

$$p_0(x) = \frac{W(x)}{\int_0^1 \mathrm{d}x\, W(x)}. \tag{3.23}$$

Expressing next $g(x)$ by $p_0(x)$, Eq. (3.19) reduces to the stationary Fick-Jacobs equation

$$0 = \partial_x \left[e^{-A(x)} \partial_x \left(e^{A(x)}\, p_0(x) \right) \right], \tag{3.24}$$

previously presented in Sect. 2.3.

We demonstrated that the leading order term of the asymptotic perturbation analysis is equivalent to the solution of the FJ equation. Therein, the particles' distributions in transverse directions equal the equilibrium (canonical) one. In addition, we showed that whether one considers an energetic confining potential $V_{\mathrm{en}}(x, y)$ with natural boundary conditions $J_n^y(x, y = \pm\infty) = 0$ or the problem of Brownian motion in a confined region with corresponding no-flux boundary conditions Eq. (3.12b), the differential equation determining the unknown function $g(x)$, Eq. (3.19), is the same. Therefore, in zeroth order and for the given scaling, Brownian motion in an appropriately chosen confining potential $V_{\mathrm{en}}(x, y)$, obeying $\int_{-\infty}^{\infty} \mathrm{d}y \, \exp(-V_{\mathrm{en}}(x, y)) = \int_{-h(x)}^{h(x)} \mathrm{d}y \, \exp(-V(x, y))$, exhibits the same transport characteristics as those induced by a confining channel with hard walls [Sokolov, 2010; Wang and Drazer, 2010]. We emphasize that the above presented derivation of the FJ equation is neither limited to reflection symmetric channel geometries, $h_{\pm}(x) = \pm h(x)$, nor to the particularly chosen external potential: $V(x, y) = -f\, x$, see [Burada and Schmid, 2010; Burada et al., 2008a].

We evaluate the mean particle current in longitudinal direction by use of well-known analytic expressions [Burada et al., 2009; Stratonovich, 1958], to yield

$$\langle\, \dot{x}(f)\, \rangle_0 = \int_0^1 \mathrm{d}x \int_{-h(x)}^{h(x)} \mathrm{d}y \, J_0^x(x, y) = \mathcal{I}^{-1} \left(1 - e^{-f} \right). \tag{3.25}$$

Consequently, the particle mobility in units of the free mobility μ^0 is given by

$$\mu_0\,(f)\,/\mu^0 = \frac{\langle\, \dot{x}(f)\, \rangle_0}{f} = \frac{\left(1 - e^{-f} \right)}{f\, \mathcal{I}}. \tag{3.26}$$

in leading order. Basically, the stationary joint PDF of finding an overdamped Brownian particle budging in a two-dimensional periodic geometry is sufficiently described by Eq. (3.20) as long as the extension of the channel structure's bulges is small compared to the period, i.e., $\varepsilon \ll 1$. We next address the higher-order corrections $p_n(x, y)$ to the joint PDF which become necessary for more winding structures.

3.1.2. Higher order contributions to the Fick-Jacob equation

According to Eq. (3.3), one needs to iteratively solve $\mathfrak{L}_0 p_n + \mathfrak{L}_1 p_{n-1} = 0$ having regard to the boundary condition Eq. (3.12b). For the considered situation, the equation simplifies to

$$\partial_y^2 p_n(x, y) = \left(f\, \partial_x - \partial_x^2 \right) p_{n-1}(x, y), \quad n \in \mathbb{N}^+. \tag{3.27}$$

Each solution of this second order partial differential equation possesses two integration constants $d_{n,1}$ and $d_{n,2}$. The first one, $d_{n,1}$, is determined by the no-flux boundary condition Eq. (3.12b) whereas the second provides the normalization condition $\langle\, p_n(x,y)\,\rangle_{x,y} = 0$.

For the first order correction, the determining equation is

$$\partial_y^2 p_1(x,y) = \langle\, \dot{x}\,\rangle_0\; \partial_x \left(\frac{1}{2\,h(x)}\right), \tag{3.28}$$

and after integrating twice over y, we obtain

$$p_1(x,y) = -\,\langle\, \dot{x}\,\rangle_0 \left(\frac{h'(x)}{2\,h^2(x)}\right) \frac{y^2}{2!}. \tag{3.29}$$

Hereby, as previously requested above, the first integration constant $d_{1,1}(x)$ is set to 0 in order to fulfill the no-flux boundary condition, and the second must provide the normalization condition Eq. (3.13), i.e., $d_{1,2} = 0$. Obviously, the first correction to the joint PDF becomes positive if the confinement is constricting, i.e., for $h'(x) < 0$ and $\langle\, \dot{x}\,\rangle_0 \neq 0$. In contrast, the probability for finding a particle diminishes in unbolting regions of the confinement, i.e., for $h'(x) > 0$. Please note, that the first order correction scales linearly with the mean particle current $\langle\, \dot{x}\,\rangle_0$. Overall, the break of spatial symmetry observed within numerical simulations in previous works [Burada, 2008; Burada et al., 2007] is reproduced by this very first order correction. Particularly, with increasing forcing, the probability for finding particles close to the channel bottlenecks increases.

Upon recursively solving, the higher-order correction terms read

$$p_n\,(x,y) \simeq \mathfrak{L}_1^n p_0(x,y)\,\frac{y^{2n}}{(2n)!} + d_{n,2}, \quad n \in \mathbb{N}^+, \tag{3.30}$$

where the differential operator $\mathfrak{L}_1$ utilized n-times is given by

$$\mathfrak{L}_1^n = \sum_{k=0}^{n} \binom{n}{k} (-1)^k\, f^{n-k}\, \frac{\partial^{\,n+k}}{\partial\, x^{n+k}}\,. \tag{3.31}$$

We stress that each single correction term $p_n(x,y)$, Eq. (3.30), satisfies the normalization condition, $d_{n,2} = -\langle \mathfrak{L}_1^n p_0(x,y)\,(y^{2n})/(2n)!\rangle_{x,y}$, but does not obey the no-flux boundary condition at the channel wall, Eq. (3.12b). Referring to Eq. (3.10), the stationary PDF $p(x,y)$ is obtained by summing all correction terms $p_n(x,y)$, leading to

$$p(x,y) = \; p_0(x,y) + \sum_{n=1}^{\infty} \varepsilon^{2n} \left(\mathfrak{L}_1^n p_0(x,y) \frac{y^{2n}}{(2n)!} + d_{n,2}\right). \tag{3.32}$$

One can proof that the full solution, Eq. (3.32), obeys the no-flux bc by putting the

latter into Eq. (3.9), yielding

$$\varepsilon^2\,\partial_x \int\limits_{-h(x)}^{h(x)} \mathrm{d}y\, e^{-V(x,y)}\partial_x\left(e^{V(x,y)}p(x,y)\right) = 0. \tag{3.33}$$

Referring to Eq. (2.30), this expression vanishes identically at steady state.

The exact solution for the stationary joint probability density function of finding a biased Brownian particle in 3D, planar channel geometry is given by Eq. (3.32). The latter solves the stationary Smoluchowski equation, Eq. (3.8), under satisfaction of the normalization as well as the periodicity requirements. More importantly the solution, Eq. (3.32), obeys the no-flux boundary conditions at the center line $y = 0$ (caused by problem's axis-symmetry) as well as at the channel walls, $y = \pm h(x)$. Further, one notices that $p(x, y)$ is fully determined by the Fick-Jacobs results $p_0(x, y)$. Caused by $\mathfrak{L}_1\, p_0(x, y) \propto \langle\, \dot{x}(f)\,\rangle_0$, the higher order corrections to the PDF scales linearly with the mean particle current in the FJ limit $\langle\, \dot{x}\,\rangle_0$, and thus the stationary PDF equals the leading order (FJ) result, $p(x, y) = p_0(x, y) = const$, regardless the value of ε for $f = 0$ or, equivalently, for $\langle\, \dot{x}\,\rangle_0 = 0$.

In practice, it is only possible or worthwhile to calculate a few of the higher-order corrections terms. Then, the series is truncated and one has to take account of the integration constants $d_{n,1}$ in order to satisfy the no-flux bc. This results in an additional sum over odd powers of $|y|$ in Eq. (3.30), viz., $\sum_{k=1}^{n} \mathfrak{L}_1^{n-k} d_{k,1}(x)\, \frac{|y|^{2(n-k)+1}}{(2(n-k)+1)!}$. The integration constants $d_{n,1}(x)$ are proportional to the probability current of the previous order, $d_{n,1}(x) \propto -\partial_x(\int_{-h(x)}^{h(x)} \mathrm{d}y\, J_{n-1}^{x}\,(x, y))$. Caused by the $|y|$-terms, each probability current $J_n^y(x, y)$ is discontinuously at the center line at $y = 0$. The $|y|$-terms generate nonzero fluxes to or from the center line, despite that there are neither sources nor sinks. Solely, in the limit $n \to \infty$ all discontinuities vanishes.

We emphasize that the presented derivation of $p(x, y)$ is valid only if (i) the dynamics in z is decoupled from the dynamics in x and y-direction, $\Phi(\mathbf{q}) = V(x, y) + W(z)$, (ii) no forces act in y-direction, $\partial_y V(x, y) = 0$ or, equivalently, $\mathfrak{L}_0 = -\partial_y^2$, and (iii) the channel is axis-symmetric with respect to the y-axis. In this special case, the center line $C(x) = (\omega_+(x) + \omega_-(x))\,/2$ acts as a hard wall with an additional bc at $y = C(x) = 0$, viz., $\partial_y p(x, y) = 0$. One can easily check that our solution, Eq. (3.32), satisfies this bc at $y = 0$, too. From this follows that the above present solution is also exact for channel geometries with one flat boundary at $y = h_-(x) = 0$. In general, any solution for the stationary joint PDF depends both on the local width $W(x)$, respectively, local cross-section $Q(x)$ and on the center line's behavior. In 2009, Bradley presented a first derivation for higher order corrections to the diffusion problem in a narrow two-dimensional channel with arbitrary boundary functions $h_\pm(x)$, respectively, curved center line $C'(x)$. Very recently, Dagdug and Pineda, presented a generalization to the case of asymmetric channel geometries using the projection method introduced earlier by Kalinay and Percus, to project the 2D diffusion equation into an effective one-dimensional generalized Fick-Jacobs equation [Dagdug and Pineda, 2012].

According to Eq. (3.16), it follows that the mean particle current scales with the mean particle current obtained from the Fick-Jacobs formalism $\langle\, \dot{x}\,\rangle_0$ for any values of ε. In

what follows, we derive an expression for the spatially dependent diffusion coefficient $D(x, f)$ and for the mean particle current based on the above presented perturbation series expansion for the stationary PDF $P(\mathbf{q})$.

3.1.3. Spatially dependent diffusion coefficient

In Sect. 2.3, we showed that the reduction of dimensionality done implicitly in the formulation of the FJ equation relies on the assumption of equilibration in transverse direction(s). Referring to the previously presented series expansion, this approximation is sufficiently correct as long as the maximum change of the local cross-section is negligible compared to the channel period, $\varepsilon \ll 1$. Because the particles can move out from or to the channel's bulges only at finite rate, higher-order corrections to the joint PDF, Eq. (3.30), become important for $\varepsilon \gtrsim 1$. Basically, the accuracy of the FJ description can be improved by the introduction of a spatially dependent diffusion coefficient $D(x, f)$, see Eq. (2.45). In reference to Eq. (2.46), $D(x, f)$ is given by ratio of two equivalent expressions for the marginal probability current $J^x(x)$, viz.,

$$D(x,f) = -\frac{\int_{-h(x)}^{h(x)} \mathrm{d}y\ [f\, p(x,y) - \partial_x p(x,y)]}{e^{A(x)}\partial_x \left(e^{-A(x)} p(x)\right)}, \tag{3.34}$$

for the considered situation $\Phi(\mathbf{q}) = -f\, x$. The spatially dependent diffusion coefficient is solely determined by the stationary joint PDF $p(x, y)$ and the stationary marginal PDF $p(x)$. In what follows, we intend to calculate $D(x, f)$ based on our previous results for the asymptotic perturbation analysis, Eq. (3.32).

Let us start with the force dominated limit, $f \to \infty$, in which all terms proportional to f prevail, leading to

$$\lim_{f\to\infty} D(x,f) = \frac{f \int_{-h(x)}^{h(x)} \mathrm{d}y\, p(x,y)}{f\, p\,(x)} = 1. \tag{3.35}$$

We find that $D(x, f)$ equals the bulk diffusion coefficient, which is unity in our scaling, if the external bias dominates the diffusion. Then the particles' sojourn time within one unit cell goes to $1/f$, i.e., the particles move almost straight through a unit cell without having time to diffuse into the channel's bulges. Consequently, their motion is quasi one-dimensional and thus the change of the cross-section will not influence the diffusion in longitudinal direction.

Inserting Eq. (3.32) into Eq. (3.34), yields

$$\begin{aligned} D(x,f) &= \frac{\langle\, \dot{x}\,\rangle_0 - \sum_{n=1}^{\infty} \varepsilon^{2n} \int_{-h(x)}^{h(x)} \mathrm{d}y\ (\partial_x V(x,y) - \partial_x)\, p_n(x,y)}{\langle\, \dot{x}\,\rangle_0 - \sum_{n=1}^{\infty} \varepsilon^{2n}\, (A'(x) - \partial_x)\, p_n\,(x)} \\ &= \frac{\langle\, \dot{x}\,\rangle_0 + \sum_{n=1}^{\infty} \varepsilon^{2n}\, [f p_n(x) - \partial_x p_n(x)] + 2\sum_{n=1}^{\infty} \varepsilon^{2n}\, h'(x)\, p_n(x, h(x))}{\langle\, \dot{x}\,\rangle_0 + \sum_{n=1}^{\infty} \varepsilon^{2n}\, [f p_n(x) - \partial_x p_n(x)] + \sum_{n=1}^{\infty} \varepsilon^{2n} h'(x)\, p_n(x)/h(x)}. \end{aligned} \tag{3.36}$$

In the case that the stationary joint PDF is independent of y, i.e., flat profile in transverse direction which corresponds to $p_n(x) = 2\, h(x)\, p_n(x, h(x))$, $D(x, f)$ equals unity.

For smoothly varying channel geometries, $\varepsilon \lesssim 1$, it is worthwhile to calculate only the leading orders in ε. In detail, we expand the general expression for $D(x,f)$ up to the forth order resulting in

$$\begin{aligned} D(x,f) = 1 - \frac{h'(x)^2}{3}\,\varepsilon^2 + \frac{1}{90}\Big\{&18\,h'^4 - 13\,h\,h'^2\,h'' + 3\,h^2\,h'\,h''' \\ &+ f\,h\,h'^3 - 3\,f\,h^2\,h'\,h''\Big\}\,\varepsilon^4 + O(\varepsilon^6, f^2). \end{aligned} \tag{3.37}$$

We find that the second order solely depends on the first derivative of the boundary function while the forth order is composed of combinations of $h(x)$ and its derivatives as well as it depends linearly on the force magnitude f. The next higher orders ε^{2n} contains terms proportional to $(2n-1)$-th derivative of $h(x)$ and f^{n-1}.

Albeit the method gives $D(x,f)$ exactly, it is rather tedious and one cannot go to high orders in ε. Thus, it is necessary to make the ansatz that (i) all but the first derivative of the boundary function $h(x)$ are negligible and (ii) the external force magnitude is sufficiently small, $f \lesssim 1$. If so, $\mathfrak{L}_1$ simplifies to

$$\mathfrak{L}_1^n \simeq (-1)^n \frac{\partial^{\,2n}}{\partial\, x^{2n}} + (-1)^{n-1}\, n\, f\, \frac{\partial^{\,2n-1}}{\partial\, x^{2n-1}} + O(f^2). \tag{3.38}$$

Additionally, the m-th derivative of $h(x)^{-1}$ with respect to x can be approximated by

$$\partial_x^m \left(\frac{1}{h(x)}\right) \simeq (-1)^m\, m!\, \frac{h'(x)^m}{h(x)^{(m+1)}} + O\left(h''(x)\right). \tag{3.39}$$

With these simplifications, the n-th order of the joint PDF Eq. (3.10) reads

$$p_n(x,y) \simeq (-1)^n\, \frac{\langle\, \dot{x}\,\rangle_0}{4n\,h'(x)^2} \left[h'(x) + \frac{(n-1)}{2n-1}\, f\, h(x)\right] \left(\frac{y\,h'(x)}{h(x)}\right)^{2n} + d_{n,2}(f), \tag{3.40a}$$

respectively, the marginal PDF reduces to

$$p_n(x) \simeq (-1)^n\, \frac{\langle\, \dot{x}\,\rangle_0\, h(x)\, h'(x)^{2n}}{2n\,(2n+1)\,h'(x)^2} \left[h'(x) + \frac{(n-1)}{2n-1}\, f\, h(x)\right] + 2h(x)\, d_{n,2}(f), \tag{3.40b}$$

for $n \in \mathbb{N}^+$. Expanding next Eq. (3.36) in Taylor series in f, one gets

$$\begin{aligned} D(x,f) &= D_0(x) + D_1(x)\, f + O(f^2) \\ &= \frac{\langle\, \dot{x}\,\rangle_0 + A_1(f) + A_2(f)}{\langle\, \dot{x}\,\rangle_0 + A_1(f) + A_3(f)}\Big|_{f=0} + f\, \Bigg[\frac{A_1'(f) + A_2'(f)}{\langle\, \dot{x}\,\rangle_0 + A_1(f) + A_3(f)} \\ &\quad - \frac{\langle\, \dot{x}\,\rangle_0 + A_1(f) + A_2(f)}{\langle\, \dot{x}\,\rangle_0 + A_1(f) + A_3(f)}\, \frac{A_1'(f) + A_3'(f)}{\langle\, \dot{x}\,\rangle_0 + A_1(f) + A_3(f)}\Bigg]_{f=0} + O(f^2). \end{aligned} \tag{3.41}$$

Here, the prime denotes the derivative with respect to f. The auxiliary functions A_i read $A_1(f) = \sum_{n=1}^{\infty} \varepsilon^{2n}\, [f p_n(x) - \partial_x p_n(x)]$, $A_2(f) = \sum_{n=1}^{\infty} \varepsilon^{2n} 2\, h'(x)\, p_n(x, h(x))$, and

$A_3(f) = \sum_{n=1}^{\infty} \varepsilon^{2n} h'(x)\, p_n(x)/h(x)$. Inserting Eqs. (3.40) into $A_i(f)$, we derive

$$D_0(x) = 1 + \sum_{n=1}^{\infty} (-1)^n \, \frac{(\varepsilon\, h'(x))^{2n}}{2n+1} = \frac{\arctan\left(\varepsilon\, h'(x)\right)}{\varepsilon\, h'(x)} = \frac{\arctan\left(W'(x)/2\right)}{W'(x)/2}, \tag{3.42}$$

for the leading order and

$$\begin{aligned} D_1(x) &= \frac{h(x)}{2\, h'(x)} \sum_{n=1}^{\infty} (-1)^n \, \frac{(\varepsilon\, h'(x))^{2n}}{2n+1} - D_0(x)\, \frac{h(x)}{2h'(x)} \sum_{n=1}^{\infty} (-1)^n \, \frac{(\varepsilon\, h'(x))^{2n}}{(2n+1)(2n-1)} \\ &= \frac{W(x)}{4\, W'(x)} \left[-2 + D_0(x) + D_0(x)^2 + \arctan\left(W'(x)/2\right)^2 \right] \end{aligned} \tag{3.43}$$

for the first order correction term in f. One can proof that the integration constants $d_{n,2}(f)$ and its derivative with respect to f, $\partial_f d_{n,2}(f)$, are proportional to $h''(x)$ which is assumed to be negligible. Therefore, $d_{n,2}(f)$ and $\partial_f d_{n,2}(f)$ vanish approximately for $f = 0$ and $n \in \mathbb{N}^+$.

To briefly conclude, we verified the expression $\lim_{f\to 0} D(x,f) = D_0(x)$ proposed by Kalinay and Percus, cf. Eq. (2.49a), by means of an asymptotic perturbation analysis in orders of the expansion parameter ε. In compliance with the authors, we supposed that the second and all higher derivatives of the boundary function $h(x)$ are negligible. Furthermore, we calculated the first order correction term to $D(x,f)$ in f, Eq. (3.43). The latter is proportional to $W(x)/W'(x)$ and is determined by a combination of $W'(x)$ and $\arctan(W'(x)/2)$. In contrast to $D_0(x)$, the first order correction $D_1(x)$ in f is less practicable. Hence, below we limit the spatially dependent diffusion coefficient to its leading order for $f \leq 1$, $D(x,f) \simeq D_0(x)$.

Very recently, Dagdug and Pineda derived a more general expression for the spatially dependent diffusion coefficient for arbitrary channel geometries in 2D

$$\lim_{f\to 0} D_{DP}(x,f) = \frac{\arctan\left(C'(x) + W'(x)/2\right)}{W'(x)} - \frac{\arctan\left(C'(x) - W'(x)/2\right)}{W'(x)}. \tag{3.44}$$

The authors took only the first derivatives of the center line $C'(x)$ and of the local width $W'(x)$ into account [Dagdug and Pineda, 2012]. For channels that have a straight center line, $C(x) = 0$, or are composed of one flat wall, the expression in Eq. (3.44) simplifies to Eq. (3.42).

3.1.4. Corrections to the mean particle current

Next, we derive an estimate for the mean particle current $\langle\, \dot{x}(f)\,\rangle$ based on the higher expansion orders to the joint PDF, $p_n(x,y)$. Referring to Eq. (3.16), the mean particle current is composed of (i) the Fick-Jacobs result $\langle\, \dot{x}(f)\,\rangle_0$, cf. Eq. (3.25), and (ii) becomes corrected by the sum of the averaged derivative of the higher orders $\langle\, \partial_x p_n(x,y)\,\rangle_{x,y}$.

In accordance with the previous paragraph, we also suppose that (i) all but the first derivative of the boundary function $h(x)$ are negligible. Further, (ii) we focus on the diffusion dominated limit, i.e., $f \lesssim 1$. Then the partial derivative of $p_n(x,y)$ with

respect to x, Eq. (3.40a), reduces to

$$\partial_x p_n(x,y) = \langle\, \dot{x}(f)\,\rangle_0\, (-1)^{n+1} \frac{(h')^{2n}}{2\,h^{2n+1}} y^{2n} + O(h''(x)). \tag{3.45}$$

Integrating the latter over the local channel width and plugging the result into Eq. (3.16), lead to one of our main findings

$$\begin{aligned} \lim_{f\to 0} \langle\, \dot{x}(f)\,\rangle &\simeq \lim_{f\to 0} \langle\, \dot{x}(f)\,\rangle_0 \left\langle \frac{\arctan\left(\varepsilon h'(x)\right)}{\varepsilon h'(x)} \right\rangle_x + O\left(h''(x), f\right) \\ &\simeq \lim_{f\to 0} \langle\, \dot{x}(f)\,\rangle_0\, \langle\, D_{KP}(x,f)\,\rangle_x + O\left(h''(x), f\right), \end{aligned} \tag{3.46}$$

where we identify $\arctan\left(\varepsilon h'(x)\right)/\varepsilon h'(x)$ with the spatially dependent diffusion coefficient $D_{KP}(x,0)$ derived by Kalinay and Percus for 2D channel geometries, see Eqs. (2.49a) and (3.42). We obtain that the mean particle current is determined as the product of the Fick-Jacobs result, $\langle\, \dot{x}(f)\,\rangle_0$, and the expectation value of the spatially dependent diffusion coefficient $\langle\, D_{KP}(x,0)\,\rangle_x$ in the diffusion dominated regime, $f \lesssim 1$.

In the sense of linear response, the particle mobility is given by $\mu(f)/\mu^0 = \langle\, \dot{x}(f)\,\rangle/f$. Referring to the Sutherland-Einstein relation, the dimensionless EDC $D_{\text{eff}}(f)/D^0$ coincide with the dimensionless particle mobility for $f \ll 1$, see Eq. (2.26), leading to

$$\lim_{f\to 0} \mu(f)/\mu^0 = \lim_{f\to 0} D_{\text{eff}}(f)/D^0 \simeq \lim_{f\to 0} \mu_0(f)/\mu^0\, \langle\, D_{KP}(x,f)\,\rangle_x + O\left(h''(x)\right). \tag{3.47}$$

We stress that the correction derived above differs from the commonly used ansatz, cf. Eq. (2.56). In compliance with the MFPT approach, see Sect. 2.5, the leading order of the particle mobility can be evaluated via the well-known Lifson-Jackson formula [Lifson and Jackson, 1962]

$$\lim_{f\to 0} \mu_0(f)/\mu^0 = \lim_{f\to 0} D_{\text{eff}}(f)/D^0 = \frac{1}{\langle\, Q(x)\,\rangle_x\, \langle\, 1/Q(x)\,\rangle_x}. \tag{3.48}$$

Combining Eqs. (3.47) and (3.48), one gets

$$\begin{aligned} \lim_{f\to 0} \mu(f)/\mu^0 = \lim_{f\to 0} D_{\text{eff}}(f)/D^0 &\simeq \frac{\langle\, D_{KP}(x,0)\,\rangle_x}{\langle\, Q(x)\,\rangle_x\, \langle\, 1/Q(x)\,\rangle_x} \\ &\neq \frac{1}{\langle\, Q(x)\,\rangle_x\, \langle\, 1/(D_{KP}(x,0)\, Q(x))\,\rangle_x}. \end{aligned} \tag{3.49}$$

Although both derivations assume that higher derivatives of $h(x)$ are insignificantly small, the results differ as long as $\langle\, (D_{KP}(x,0)\, Q(x))^{-1}\,\rangle_x \neq \langle\, Q(x)^{-1}\,\rangle_x\, \langle\, D_{KP}(x,0)\,\rangle_x$.

3.2. Example: Channel geometry with sinusoidally varying rectangular cross-section

Throughout this work, we study the transport characteristics of Brownian particles with negligible diameter, $d_p \ll \Delta\omega$, moving under the action of an external force $\mathbf{f}$ through confining structures. It is supposed that the local, rectangular cross-section

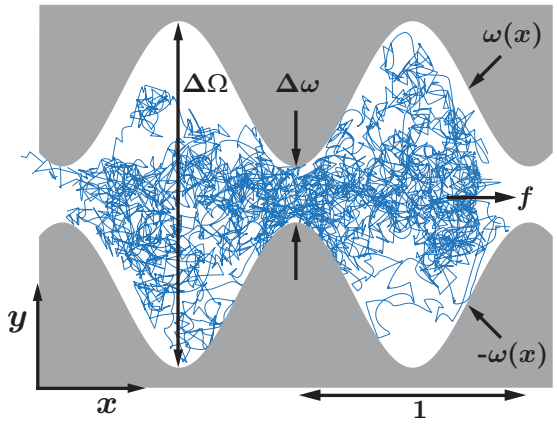

Figure 3.2.: Segment of 2D channel geometry with unit period and sinusoidally varying local width $W(x) = 2\omega(x)$. The particle transport occurs due to the combination of molecular diffusion and convective transport caused by the external force $\mathbf{f} = f\,\mathbf{e}_x$. An exemplary particle trajectory for $f = 1$ is indicated by the erratic line.

$Q(x) = \Delta H\, W(x)$ varies periodically in longitudinal direction whereby the system's period is unity in our scaling. Basically, any periodic function can be decomposed into a Fourier series [Fourier, 1807]

$$W(x) = \frac{a_0}{2} + \sum_{k=1}^{\infty} \left\{ a_k \cos\left(2\pi\, k\, x\right) + b_k \sin\left(2\pi\, k\, x\right) \right\}, \tag{3.50}$$

where a_k and b_k are the expansion coefficients associated to the k-th mode. Focusing on first sine harmonic, i.e., $k = 1$, the boundary functions at $y = \omega_{\pm}(x)$ read

$$\omega_{\pm}(x) = \pm\,\omega(x) = \pm \left[\frac{a_0}{4} + \frac{b_1}{2} \sin\left(2\pi\, x\right) \right], \tag{3.51}$$

for axis-symmetric boundaries. Thereby, the parameters a_0 and b_1 control the slope and the channel width at the bottleneck $\Delta\omega$. Here, the condition $a_0 > 2\,b_1$ should be satisfied in order to avoid a closed channel. The sum and difference of the two parameters, $0.5\,a_0 + b_1$ and $0.5\,a_0 - b_1$, yield the maximum width $\Delta\Omega$ and the minimum width of the channel $\Delta\omega$, respectively. Hence, the boundary function is given by

$$\omega(x) = \frac{1}{4} \left[(\Delta\Omega + \Delta\omega) + (\Delta\Omega - \Delta\omega) \sin\left(2\pi\, x\right) \right], \tag{3.52}$$

and is illustrated in Fig. 3.2. Moreover, the first coefficient coincides with the average channel's half width $\langle\, W(x)\,\rangle_x$. The maximum change of the local cross-section within a unit cell is represented by $\Delta\Omega - \Delta\omega$ which was previously denoted as ε, cf. Eq. (3.1). We emphasize that our performed asymptotic perturbation analysis in ε, presented in Sect. 3.1, agrees with an expansion of the transverse quantities in units of the amplitude of the first harmonics ("dominating" wavelength). Hence, the used method is often also called long-wave asymptotic analysis in literature [Laachi et al., 2007; Yariv and

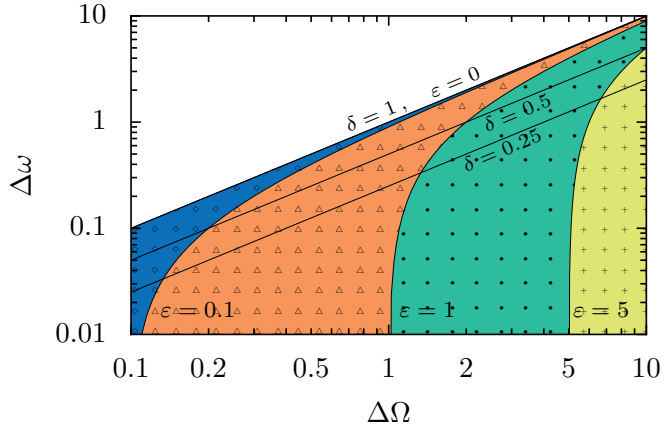

Figure 3.3.: Schematic sketch of the dependence of expansion parameter $\varepsilon = \Delta\Omega - \Delta\omega$ and aspect ratio $\delta = \Delta\omega/\Delta\Omega$ on the maximum width $\Delta\Omega$, respectively, the width at the bottleneck $\Delta\omega$. The dashed lines correspond to $\delta = 1, 0.5, 0.25$ (from above) whereas the colored areas illustrate pairs of $(\Delta\Omega, \Delta\omega)$ where $\varepsilon \leq 0.1$ (blue,diamonds), $\varepsilon \leq 1$ (red,triangles), $\varepsilon \leq 5$ (green,dots), and $\varepsilon > 5$ (yellow,plus signs).

Dorfman, 2007]. The dimensionless boundary $h(x)$ looks like

$$h(x) = \frac{1}{4}\left[\mathtt{b} + \sin\left(2\pi\, x\right)\right], \tag{3.53}$$

and contains only one free parameter $\mathtt{b} = (1+\delta)/(1-\delta)$ which is solely governed by the channel aspect ratio $\delta = \Delta\omega/\Delta\Omega$.

Obviously different realizations of channel geometries can possess the same value for δ. The number of orders have to taken into account in the perturbation series, Eq. (3.32), or, equivalently, the applicability of the Fick-Jacob approach to the problem, depends solely on the value of the expansion parameter $\varepsilon = \Delta\Omega\,(1-\delta)$ for a given aspect ratio δ. For clarity, the impact of maximum $\Delta\Omega$ and minimum width $\Delta\omega$ on ε and on δ is illustrated in Fig. 3.3.

In what follows, we study the key transport characteristics like particle mobility $\mu(f)/\mu^0$ and effective diffusion coefficient $D^0_{\text{eff}}(f)/D^0$ of point-like Brownian particles ($d_p \to 0$) evolving in a sinusoidally-shaped 2D geometry like the one in Fig. 3.2. Particularly, we compare the Fick-Jacobs approach with precise numerical simulations in order to validate our obtained analytic prediction, Eq. (3.47). As mentioned previously in Sect. 3.1, the stationary joint PDF in z-direction equals the Boltzmann distribution which permits us to integrate $P(\mathbf{q})$ with regard to z. Consequently, it is sufficient to consider only the particle dynamics in the $x-y$ plane.

Before we discuss the particle's transport characteristics, we focus first on the stationary joint PDF $p(x,y)$ with regard to the impact of the external bias $\mathbf{f}$ on the latter. In Fig. 3.4, we depict $p(x,y)$ (left column), the normalized transverse profiles at given x-values, and the marginal PDF $p(x)$ (right column). Thereby, the numerical result for $p(x,y)$, see Fig. 3.4 (iii), was obtained by solving the stationary 2D Smoluchowski equation Eq. (3.8) with the associated boundary conditions Eq. (3.12b) using finite

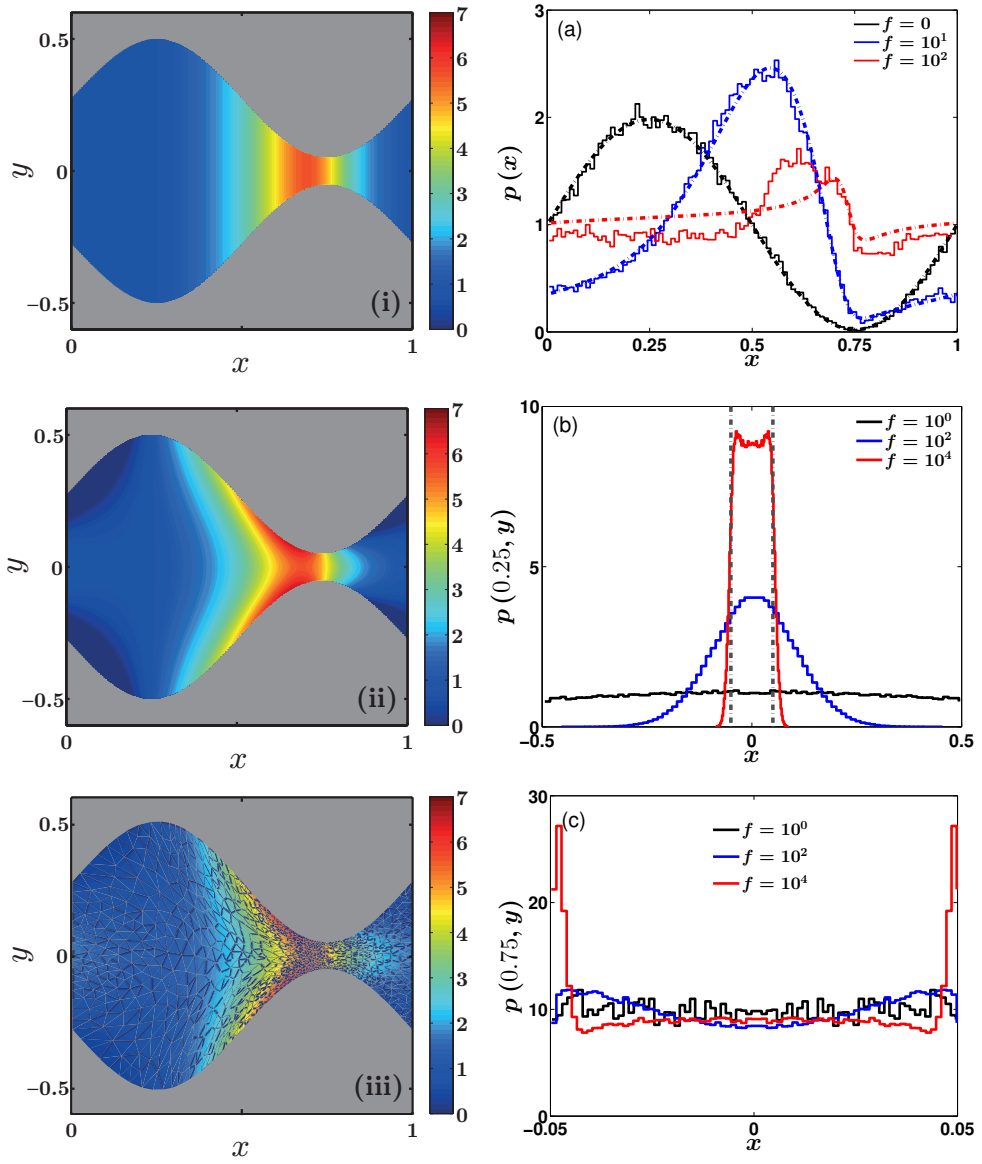

Figure 3.4.: Left column: Stationary 2D joint PDF $p(x, y)$ for $f = 10$; (i) leading order $p_0(x, y)$, Eq. (3.20), (ii) leading order plus first correction term $p_0 + \varepsilon^2 p_1$, Eq. (3.29), and (iii) the numerically obtained result using FEM. Right column: Stationary marginal PDF $p(x)$ for different force magnitudes f (a). Numerics are represented by staircase like solid lines whereas dashed-dotted lines correspond to the FJ solution $p_0(x)$, Eq. (3.22). Numerical obtained transverse profile of the stationary PDF (normalized with respect to the local width) at maximum width $x = 0.25$ (b) and at the bottleneck $x = 0.75$ (c) for various f values are depicted. The vertical dash-dotted lines indicate the width of the bottleneck. The channel parameters are $\Delta\Omega = 1$ and $\Delta\omega = 0.1$.

element method (FEM).[5] It is shown that the 2D joint PDF reflects the axis-symmetry with respect to x-axes of the channel since the latter is not broken by the external force, $\mathbf{f} = f\,\mathbf{e}_x$. In addition, accumulation of Brownian particles at the exit of the unit cell is found. This accumulation is due to, if a Brownian particle enters a cell through the preceding bottleneck, the applied force drags the particles in its direction. Simultaneously, the thermal fluctuations try to deviate this straight particle motion. As a result, Brownian particles may pile up at the bottleneck. Both accumulation and axis-symmetry can be found in the leading order solution $p_0(x, y)$ (FJ result), Eq. (3.20), as shown in Fig. 3.4 (i). If additionally the first order correction term is considered, Eq. (3.29), the superposition $p_0(x, y) + \varepsilon^2\, p_1(x, y)$ reproduces the particles' stickiness at the bottleneck quite well as shown in Fig. 3.4 (ii).

In the right column of Fig. 3.4, we present the dependence of the marginal PDF $p(x)$ and of the transverse profiles on the external force. If diffusion dominates external forcing, $f \lesssim 1$, equilibration in transverse direction is accomplished even for wider channel geometries. Then, the particles are uniformly distributed in y-direction (black lines) and the marginal PDF scales linearly with the local channel width $p(x) \propto W(x)$. In compliance with the time scales involved in the problem, see Sect. 2.4, an increase of the force magnitude results in the violation of the equilibration assumption. For large forces, the particles gather at the center of the channel. The initial step-like distribution at the bottleneck spreads to a bell-shaped distribution, see the blue line in Fig. 3.4 (b). Since the width of the joint PDF in transverse direction becomes broader than the subsequent bottleneck (indicated by the vertical dash-dotted lines) some particles are pushed against the boundary. These have to slide along the channel wall in order to leave the unit cell. This process takes some time and is revealed by the appearance of two distinct maxima at the left and right side of the bottleneck in $p(0.75, x)$. Of course, this behavior is also reflected by the marginal PDF. Namely, $p(x)$ exhibits an uneven shape and the position of the maximum starts to shift towards the bottleneck for larger forces. Nevertheless, the numerical result is well reproduced by the Fick-Jacobs solution even for a wide channel $\Delta\Omega = 1$ and moderate force magnitude $f = 10$. Especially, particle accumulation plays an important role in the diffusion process and results in enhancement of the effective diffusion coefficient as we will present below. For $f \to \infty$, the external drag is dominant compared to diffusion and thus the transverse PDF at the maximum width is almost equal to the one at the bottleneck, see Fig. 3.4 (b). In this situation, the Brownian particles do not feel any boundaries and the impact of entropic barriers disappears. Then, the particle motion is almost straight. Nevertheless, accumulation still can be observed at the channel walls, cf. Fig. 3.4 (c), in any kind of channel, no matter if it is rough [Dagdug et al., 2011; Marchesoni and Savel'ev, 2009] or smooth.

As already mentioned in Sect. 2.3, the problem's complexity is reduced from a three-dimensional dynamics in a confined geometry with no-flux boundary condition to an 1D energetic description within the Fick-Jacobs approach. The latter involves the potential of mean force $A(x)$, Eq. (2.36). For the problem at hand, the potential explicitly reads

[5] For details concerning the used numerical methods please see App. A.

$A(x) \simeq -f\,x - \ln\left[h(x)\right]$,[6] cf. Eq. (2.37b). Its extrema are located at

$$x_i = \frac{1}{2} + \frac{1}{2\pi}\,\arcsin\left(y_i\right) + k, \quad k \in \mathbb{Z} \quad \text{and} \quad i \in \{\,\min\,,\,\max\,\}, \tag{3.54}$$

for the boundary function given in Eq. (3.53). Thereby, the substitutes read

$$y_{\substack{\min\\\max}} = \frac{f^2\,\mathtt{b}}{f^2 + (2\pi)^2}\left[1 \mp \frac{2\pi}{\mathtt{b}\,f^2}\sqrt{(\mathtt{b}^2-1)\,(f_c^2 - f^2)}\right]. \tag{3.55}$$

For force magnitudes less than the critical value

$$f_c = \pi\,\frac{(1-\delta)}{\sqrt{\delta}}, \tag{3.56}$$

the potential of mean force possesses distinct extrema separating the adjacent basins of attraction. The entropic barrier (in units of k_BT) within each period is given by

$$\Delta A(f) = \frac{f}{2\pi}\left(\arcsin\left(y_{\min}\right) - \arcsin\left(y_{\max}\right)\right) + \ln\left(\frac{\mathtt{b} - y_{\min}}{\mathtt{b} - y_{\max}}\right), \tag{3.57}$$

and simplifies to

$$\Delta A(f) \simeq -\ln\left(\frac{\Delta\omega}{\Delta\Omega}\right) - \frac{f}{2} + O\left(f^2\right), \tag{3.58}$$

for small force magnitude $f \ll 1$. If $f < f_c$, the barrier height goes to infinity for closed channels, $\delta = \Delta\omega/\Delta\Omega \to 0$, and vanishes for straight channels, $\delta \to 1$. For $f = f_c$, the separating entropic barrier disappears.

3.2.1. Particle mobility

Let us first consider the particle mobility μ/μ^0 of one single Brownian particle in force direction. The particle mobility in periodic structures can be evaluated by means of the mean first passage time (MFPT), see Sect. 2.5, yielding

$$\mu/\mu^0 = \frac{1}{f\,\langle\, t(0\to 1)\,\rangle}, \tag{3.59}$$

for any non-zero force f. Within the Fick-Jacobs description (leading order), the MFPT of Brownian particles starting at $x = 0$ and arriving at $x = 1$ is given by $\langle\, t(0\to 1)\,\rangle = \mathcal{I}/\left(1 - \exp(-f)\right)$ with substitutes $\mathcal{I}$, see Eq. (3.21). For the explicitly

[6] The additive term $-\ln[2\,\Delta H]$ is irrelevant for the discussion.

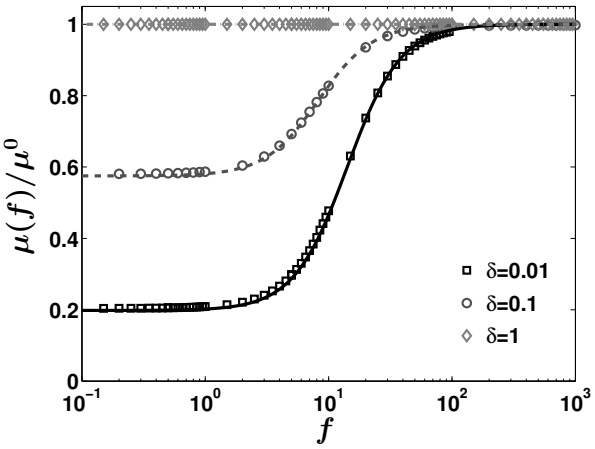

Figure 3.5: Particle mobility versus external force magnitude f for different aspect ratios δ is presented. Numerically obtained results are represented by markers. Exact analytic results for the leading order, Eq. (3.61), are indicated by lines. The maximum channel width is kept fixed $\Delta\Omega = 0.1$.

considered boundary, Eq. (3.52), the leading order result for $\langle\, t(0 \to 1)\,\rangle$ reads

$$\begin{aligned}\langle\, t(0 \to 1)\,\rangle &= \frac{1}{1-e^{-f}} \int_0^1 \mathrm{d}x\, \frac{e^{-f\,x}}{\mathtt{b} + \sin(2\pi\, x)} \int_{x-1}^{x} \mathrm{d}x'\, e^{f\,x'} \left(\mathtt{b} + \sin(2\pi\, x')\right) \\ &= \frac{1}{f}\, \frac{f^2 + \frac{1}{2}(2\pi)^2 \left\{\sqrt{\delta} + 1/\sqrt{\delta}\right\}}{f^2 + (2\pi)^2}. \end{aligned} \tag{3.60}$$

Immediately, one derives

$$\mu_0(f)/\mu^0 = \frac{f^2 + (2\pi)^2}{f^2 + \frac{1}{2}(2\pi)^2 \left\{\sqrt{\frac{\Delta\Omega}{\Delta\omega}} + \sqrt{\frac{\Delta\omega}{\Delta\Omega}}\right\}}. \tag{3.61}$$

for the particle mobility in units of its bulk value μ^0. We derive that $\mu_0(f)$ is solely determined by the aspect ratio $\delta = \Delta\omega/\Delta\Omega$ for any given value of f. Due to the reflection symmetry of the boundary function $\omega(x)$ with respect to $x = 0.25$ and $x = 0.75$, respectively, the particle mobility is a symmetric function $\mu_0(-f) = \mu_0(f)$. Thus it is sufficient to discuss only the behavior for $f \geq 0$.

In Fig. 3.5, we compare numerics (markers) with analytic results (lines), Eq. (3.61), for the particle mobility as a function of f for different aspect ratios δ. Thereby, the different aspect ratios are adjusted by fixing the maximum width $\Delta\Omega$ and varying bottleneck width $\Delta\omega$. The numerical results were obtained by calculating the stationary joint PDF and subsequently evaluating the mean particle current Eq. (3.25) using FEM. The FEM results were also double-checked by Brownian dynamics (BD) simulations. The numerical simulation methods are presented in depth in App. A. We emphasize that numerical errors are of the size of the markers so we do not indicate them.

In the limiting case of infinite large force strengths, i.e., drift is the dominating process, the particles move mostly close to the center line of the channel because diffusive spreading in y-direction is comparatively slow, see Fig. 3.4 (b). Hence, the transport is not inhibited by the confinement and particles' sojourn times to stay within one unit

cell equal the free value $\langle\, t(0 \to 1)\,\rangle = 1/f$, see Eq. (3.60). Consequently, the particle mobility tends to

$$\lim_{f\to\infty} \mu_0(f)/\mu^0 = 1, \tag{3.62}$$

as shown in Fig. 3.5. With decreasing dimensionless force magnitude f, i.e., the impact of thermal fluctuations becomes stronger, the spreading of the probability density in y-direction increases and the mean sojourn time within one unit cell grows. Thus, the particle mobility lessens. At

$$f_{ip} = 2\pi\sqrt{\left\{\sqrt{\delta} + 1/\sqrt{\delta}\right\}/6}\,, \tag{3.63}$$

$\mu_0(f)/\mu^0$ possesses its inflection point. After further reduction of f, diffusion dominates and $\mu(f)$ converges to its asymptotic value

$$\lim_{f\to 0} \mu_0(f)/\mu^0 = \frac{1}{\langle\, h(x)\,\rangle_x \,\langle\, 1/h(x)\,\rangle_x} = \frac{2\sqrt{\Delta\omega/\Delta\Omega}}{1+\Delta\omega/\Delta\Omega}. \tag{3.64}$$

In the diffusion dominated regime, $f \ll 1$, the mobility of Brownian particles is solely determined by the geometry – more precisely by the aspect ratio of the channel. In the limit of straight channels $\delta = 1$, i.e., there is no restriction of the phase space, the entropic barriers vanish and hence $\mu(f)/\mu^0$ attains always unity. With decreasing bottleneck width, the motion of the particles becomes inhibited and thus they accumulate at the cell's exit. In addition, the mean sojourn time grows, respectively, μ goes down even for small force magnitudes $f \to 0$. For very narrow bottlenecks $\Delta\omega \to 0$, the entropic barrier separating the adjacent basins of attraction goes to infinity, cf. Eq. (3.58), and the mobility converges to zero.

Noteworthy, it is shown that the exact analytic result for $\mu_0(f)/\mu^0$, Eq. (3.61), matches very well with numerics for all values of f and δ, see Fig. 3.5.

We stress that transport in periodically varying channel structures with associated entropic barriers is totally different from the one in 1D energetic, periodic potentials [Burada et al., 2009; Hänggi et al., 1990]. The fundamental difference is the temperature dependence of these models. In an energetic periodic potential, the MFPT from one period to the subsequent one grows with decreasing temperature according to the Arrhenius law $\langle\, t(0 \to 1)\,\rangle \propto \exp[\Delta\Phi]$ [Arrhenius, 1889]. Thereby, $\Delta\Phi$ denotes the activation energy (in units of thermal energy k_BT) necessary to proceed by a period [Hänggi et al., 1990]. Therefore, decreasing the temperature leads to a diminishing mobility $\propto \langle\, t(0 \to 1)\,\rangle^{-1}$. In contrast, in systems with geometrical constraints a decrease of the thermal energy leads to growing values of the dimensionless force parameter f and, consequently, to a shortening of the MFPT $\langle\, t(0 \to 1)\,\rangle$, see Fig. 3.5.

Wang and Drazer considered biased transport of Brownian particles confined by a soft channel. The latter was described by a parabolic potential $V_{\rm en}(x,y) = 0.5\,(y/W(x))^2$ with periodically varying curvature $W(x) = \sqrt{2}\,(\mathtt{b} + \cos(2\pi\,x))$. The potential of mean force, associated to $\Phi(\mathbf{q}) = -f\,x + V_{\rm en}(x,y)$, is given by $A(x) \simeq -f\,x - \ln[\mathtt{b} + \cos(2\pi\,x)]$.

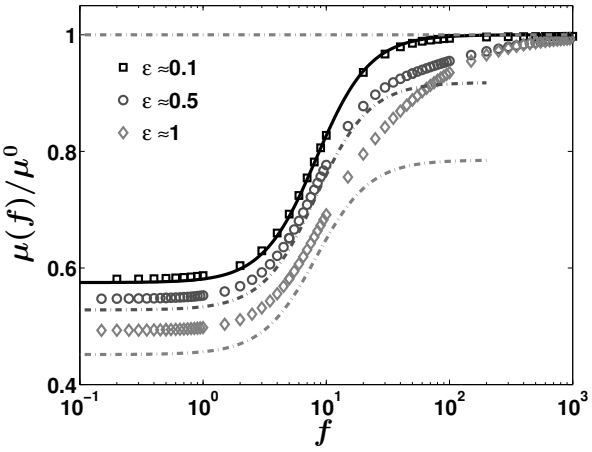

Figure 3.6: Comparison of numerically obtained results for the particle mobility (markers) with the analytic result $\mu_0(f)/\mu^0$ (solid line), Eq. (3.61), for various values of the expansion parameter ε. Additionally the estimate Eq. (3.66) including higher order corrections is presented (dash-dotted lines). The aspect ratio is set to $\delta = 0.1$.

The latter coincides with Eq. (2.37b) for the explicitly studied channel structure, Eq. (3.52). Therefore, the authors derived the identical result for the particle mobility, cf. Eq. (3.61) and Eq. (51) in [Wang and Drazer, 2009]. This agreement exemplifies that an appropriately chosen confining energetic potential may lead to the same transport characteristics as those induced by the smoothly varying channel with hard walls; for details see Sect. 3.1.1.

In Sect. 3.1.1, we demonstrated that the solution of the FJ equation is identical to the leading order of an asymptotic perturbation analysis of the 2D joint PDF in the expansion parameter ε. In Fig. 3.6, we present the influence of ε on the particle mobility. The value for ε is adjusted by changing the maximum width $\Delta\Omega$ for a fixed aspect ratio $\delta = 0.1$, see Fig. 3.3. We observe that the exact analytic solution, Eq. (3.61), is in very good agreement with the numerics for $\varepsilon \lesssim 0.1$. This validates that the dynamics of single particles can be well described by the FJ approach as long as the maximum channel width is of the order of 10% of its period. With growing ε value, as expected, the deviation between the analytic and the numerical result becomes distinct. Particularly, one recognizes that μ/μ^0 decreases with increasing maximum width $\Delta\Omega$ or, equivalently, with growing area of the channel's bulges. More available space in transverse direction enhances the probability for excursions into the channel's bulges, or, equivalently, the probability for long sojourn times. Therefore, the MFPT grows and the particle current lessens with $\Delta\Omega$. In agreement with the analysis of the time scales involved in the system, see Sect. 2.4, the leading order $\mu_0(f)/\mu^0$ is valid for $1 \ll f \ll \varepsilon^{-2}$. In the case of wide channels, the Fick-Jacobs approach becomes untenable already for relatively small forces f, whereas for $\varepsilon \ll 1$, its validity extends to significantly larger drives [Burada et al., 2007, 2008b].

3.2.2. Verification of the correction to the particle mobility

In Sect. 3.1.4, we derived that the higher-order correction to the particle mobility is proportional to the expectation value of the spatial dependent diffusion coefficient

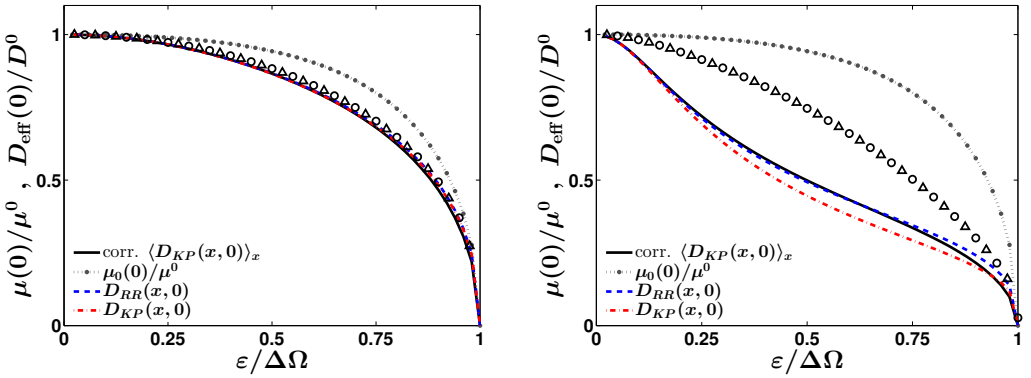

(a) $\Delta\Omega = 1$ **(b)** $\Delta\Omega = 5$

Figure 3.7.: Comparison of analytic theory versus precise numerics: Mobility (squares) and effective diffusion coefficient (triangles) for confined Brownian particles versus $\varepsilon/\Delta\Omega$ for different maximum channel widths $\Delta\Omega$ and bias $f = 10^{-3}$ (corresponding to the diffusion dominated regime). The left curves correspond to $\Delta\Omega = 1$ and the right ones to $\Delta\Omega = 5$. Superimposed are the limit behavior of the zeroth order mobility $\mu_0(0)/\mu^0$ (dotted line), Eq. (3.64), the higher-order corrections (solid lines), Eq. (3.65), the Lifson-Jackson approach using $D_{RR}(x,0)$ (dashed lines), and $D_{KP}(x,0)$ (dash-dotted lines).

$\langle\, D_{KP}(x,f)\,\rangle_x$, Eq. (3.47). Calculating the period average of $D_{KP}(x,f)$ results in

$$\lim_{f\to 0}\mu(f)/\mu^0 = \lim_{f\to 0} D_{\rm eff}(f)/D^0 \simeq \frac{4\sqrt{1-\varepsilon/\Delta\Omega}}{2-\varepsilon/\Delta\Omega}\,\frac{\operatorname{asinh}(\pi\varepsilon/2)}{\pi\,\varepsilon} + O(h''(x)) \qquad (3.65)$$

for 3D, planar confinements with sinusoidally varying rectangular width Eq. (3.52).

In Fig. 3.7, we depict the dependence of the particle mobility (squares) and the effective diffusion coefficient (triangles) on the expansion parameter ε for $f \ll 1$ in depth. The results for $D_{\rm eff}/D^0$ were obtained by calculating the stationary joint PDF, solving the convection-diffusion equation for the **B**-field, Eq. (2.20), and subsequent evaluation of the unit cell quadrature, Eq. (2.23), using FEM; for details see App. A. In order to modify the value of ε, the minimum width $\Delta\omega$ is changed while the maximum width $\Delta\Omega$ is kept fixed. It is demonstrated that the numerical results for $D_{\rm eff}(f)/D^0$ and $\mu(f)/\mu^0$ coincide for all values of ε, thus corroborating the Sutherland-Einstein relation for $f \ll 1$. Particularly, we compare the numerical results with our analytic estimates, viz., the zeroth order μ_0/μ^0 (dotted lines), Eq. (3.64), and the higher-order correction (solid lines), Eq. (3.65). Additionally, we evaluated the Lifson-Jackson formula, Eq. (2.56), by using the expression derived by Reguera and Rubí $D_{RR}(x,0)$, Eq. (2.48), as well as the one obtained by Kalinay and Percus $D_{KP}(x,0)$, Eq. (2.49a). Note that we do not present any results for the Lifson-Jackson formula using the expression proposed by Zwanzig $D_Z(x,0)$, Eq. (2.47). The discrepancies are much bigger compared with $D_{RR}(x,0)$ and $D_{KP}(x,0)$ for any value of ε.

$\Delta\Omega$	$\varepsilon/\Delta\Omega$	FJ, Eq. (3.64)	Eq. (3.65)	$D_{RR}(x,0)$	$D_{KP}(x,0)$
0.5	0.5	0.022	-0.002	-0.002	-0.002
	0.8	0.049	-0.011	-0.003	-0.003
1	0.5	0.068	-0.019	-0.018	-0.020
	0.8	0.153	-0.033	-0.017	-0.024
2	0.5	0.151	-0.096	-0.097	-0.112
	0.8	0.355	-0.108	-0.082	-0.117
5	0.5	0.264	-0.326	-0.342	-0.398
	0.8	0.679	-0.317	-0.288	-0.401

Table 3.1.: Relative error $\mu^{\text{theo}}(0)/\mu^{\text{num}}(0) - 1$ between theoretical estimates and numerics are presented for two given ratios $\varepsilon/\Delta\Omega$. The maximum channel width is varied from $\Delta\Omega = 0.5$ to $\Delta\Omega = 5$. The third column represents the results for the Fick-Jacobs approach $\lim_{f\to 0}\mu_0(f)/\mu^0$, Eq. (3.64), and the values in the 4th column corresponds to our correction estimate Eq. (3.65). Additionally the results based on the Lifson-Jackson formula with $D_{RR}(x,0)$ (5th column) and $D_{KP}(x,0)$ (6th column) are presented.

Although not explicitly shown here, all analytic expressions are in excellent agreement with the numerics in the case of smoothly varying channel geometry, $\Delta\Omega \ll 1$. Basically, the zeroth order result $\mu_0(0)/\mu^0$ matches sufficiently well with the simulation results, indicating the applicability of the Fick-Jacobs approach. In virtue of Eq. (3.1), the dimensionless expansion parameter is defined by $\varepsilon = \Delta\Omega - \Delta\omega$ and hence the maximal value for ε equals $\Delta\Omega$, see Fig. 3.3. Consequently, the influence of the higher expansion orders $\varepsilon^{2n}\langle\,\partial_x p_n(x,y)\,\rangle$ on the mean particle current as well as on the particle mobility becomes negligible if the maximum channel width $\Delta\Omega$ is small.

With increasing maximum width the deviation between the FJ result and the numerics grows. Specifically, $\mu_0(0)/\mu^0$ overestimates the particle mobility and the effective diffusion coefficient. In Tab. 3.1, we display the relative error $\mu^{\text{theo}}(0)/\mu^{\text{num}}(0) - 1$ between theoretical estimates and numerics for two selected ratios $\varepsilon/\Delta\Omega = 0.5, 0.8$. At these values, the size of the bottleneck is 50% ($\varepsilon/\Delta\Omega = 0.5$), respectively, 20% ($\varepsilon/\Delta\Omega = 0.8$) of the maximum channel width. Note that a negative value of the relative error, $\mu^{\text{theo}}(0)/\mu^{\text{num}}(0) - 1$, indicates that the theoretical result underestimates the true result while a positive value corresponds to overestimation of μ. We find that the relative error between the FJ result and the simulation results grows from 2% to 15% for $\Delta\Omega = 1$. Higher-order corrections need to be included and therefore all other theoretical estimates provide a very good agreement for a wide range of ε-values for which the maximum width $\Delta\Omega$ is on the scale to the channel period, i.e., $\Delta\Omega \sim 1$. The relative errors are below 4%. We emphasize that any estimate including geometrical corrections underestimates the simulation results.

Upon further increasing the maximum width $\Delta\Omega$, the range of applicability of the derived higher-order corrections diminishes. This is due to the neglect of correction terms which scale with higher derivatives of the boundary function $h(x)$. Put differently, the higher derivatives of $h(x)$ become significant for $\Delta\Omega > 1$. The relative error grows from nearly 3% ($\Delta\Omega = 1$) to at least 30% ($\Delta\Omega = 5$) for all estimates. Thereby, our estimate Eq. (3.65) provides almost identical results for mobility and effective

diffusion coefficient as the Lifson-Jackson formula with $D_{RR}(x, f)$. Notably, Eq. (3.65) agrees better with numerics compared to the Lifson-Jackson formula with $D_{KP}(x, f)$, although, both use the same expression for the spatially dependent diffusion coefficient.

To summarize, we found that our estimate for the particle mobility, respectively, the EDC matches very well with numerical results for the entire range of ε-values, for which maximum widths $\Delta\Omega$ are on the scale to the channel period, i.e., $\varepsilon \in [0, 1)$. For all values of ε and $\Delta\Omega$, the mobility is bounded from above by the FJ result $\mu_0(0)/\mu^0$ and from below by the estimates including the channel corrugation. Remarkable, Eq. (3.65) can be calculated exactly in contrast to the integrals appearing in the Lifson-Jackson formula our estimate. More importantly, our estimate provides equally good or even better agreement with the simulation results.

Motivated by the small discrepancy between the higher-order results, Eq. (3.47), and the numerically evaluated results in the diffusion dominated limit, we propose that $\mu(f)/\mu^0$ is given by the product of the FJ result, Eq. (3.61), and the expectation value of $D_{KP}(x, 0)$ for any force magnitude f

$$\mu(f)/\mu^0 \equiv \mu_0(f)/\mu^0 \, \langle D_{KP}(x,0) \rangle_x \simeq \frac{2 \operatorname{asinh}(\pi\varepsilon/2)}{\pi\,\varepsilon} \, \mu_0(f)/\mu^0 + O(h''(x)). \quad (3.66)$$

In Fig. 3.6, we indicate this estimate by dash-dotted lines. As expected, the ansatz underestimates the true mobility for all force magnitudes. For small up to moderate force strengths, Eq. (3.66) matches the true result quite well. However, for large values of f the asymptotic limits are not reached for $\varepsilon \neq 0$. The differing saturation values are due to the application of the force-independent expression for $D(x, f)$. Referring to Sect. 3.1.3, $D(x, f)$ equals the bulk diffusion coefficient for $f \to \infty$ and thus $\lim_{f\to\infty} \mu(f)/\mu^0 = \lim_{f\to\infty} \mu_0(f)/\mu^0 = 1$. Furthermore, it turns out that the range of applicability of Eq. (3.66) diminishes with growing maximum channel width $\Delta\Omega$.

3.2.3. Effective diffusion coefficient

In this paragraph, we focus on the second transport quantity of interest, the effective diffusion coefficient $D_{\text{eff}}(f)/D^0$. The latter is defined as the asymptotic behavior of the variance of the position, Eq. (2.8), and, in principle, it can be computed analytically by regarding the hopping events in the overdamped regime as manifestations of a renewal process [Lindner et al., 2001; Reimann et al., 2001]. In leading order in ε (FJ limit), the EDC is determined by

$$D^0_{\text{eff}}/D^0 = \mathcal{I}^{-3} \int_0^1 \mathrm{d}x \int_{x-1}^{x} \mathrm{d}x' \, e^{A(x)-A(x')} \, I^2(x). \quad (3.67)$$

Unfortunately, a closed-form expression for $I(x)$ cannot be found for the considered boundary function, Eq. (3.52).

Nevertheless, we derive an estimate for D^0_{eff}/D^0 based on its limiting behavior in what follows. For infinite strong forces the particle moves close to the channel's center line, see Fig. 3.4 (b), and thus the diffusion coefficient equals the free value, i.e., $D_{\text{eff}}(f)/D^0 \to 1$. Referring to Eq. (3.61), the dominating power of $I(x)$ has

to be $(1-e^{-f})\,f^2/(f^3+(2\pi)^2\,f)$. In the opposite limit, $f\to 0$, the integral $I(x)$ simplifies to $I(x)=h(x)\,\langle 1/h(x)\rangle_x$. Therefore, we assume the following structure $I(x)=(1-e^{-f})\left(f^2+k(x)\,f+(2\pi)^2\,h(x)/\sqrt{\mathtt{b}^2-1}\right)/\,(f^3+(2\pi)^2\,f)$ where $k(x)$ is an unknown function. The latter has to be periodic in order to fulfill the condition $\int_0^1 \mathrm{d}x\, I(x)=(1-e^{-f})/(\mu_0(f)/\mu^0\,f)$. From numerical evaluation of $I(x)$, we propose

$$I(x)\approx\frac{1-e^{-f}}{f^3+(2\pi)^2\,f}\left[f^2+\frac{(\mathtt{b}+\sin(2\pi\,x))}{\sqrt{\mathtt{b}^2-1}}\left\{\pi^2-\frac{2\pi\,f}{\mathtt{b}}\,\cos(2\pi\,x)\right\}\right]. \tag{3.68}$$

By plugging the latter into Eq. (2.53), we get the following result for the EDC in units of the bare diffusion coefficient

$$D^0_{\mathrm{eff}}(f)/D^0\approx 1+\frac{c_1(\mathtt{b})f^4+c_2(\mathtt{b})\,f^2+c_3(\mathtt{b})}{\left(\sqrt{\mathtt{b}^2-1}\,f^2+(2\pi)^2\,\mathtt{b}\right)^3}, \tag{3.69}$$

where the coefficients c_1,c_2, and c_3 read

$$c_1(\mathtt{b})=(2\pi)^2\left(\mathtt{b}^3-\sqrt{\mathtt{b}^2-1}^{\,3}-1/\mathtt{b}\right), \tag{3.70a}$$

$$c_2(\mathtt{b})=(2\pi)^4\left(6\,\mathtt{b}^2\left(\mathtt{b}-\sqrt{\mathtt{b}^2-1}\right)-5\,\mathtt{b}+3\,\sqrt{\mathtt{b}^2-1}\right), \tag{3.70b}$$

$$c_3(\mathtt{b})=(2\pi)^6\,\mathtt{b}^3\left(\sqrt{1-1/\mathtt{b}^2}-1\right). \tag{3.70c}$$

In Fig. 3.8, we depict the impact of the aspect ratio $\delta=\Delta\omega/\Delta\Omega$ on $D_{\mathrm{eff}}(f)/D^0$. The aspect ratio is adapted by fixing the maximum width $\Delta\Omega$ and varying the minimum width at the bottleneck $\Delta\omega$. The EDC was numerically computed by FEM, see App. A. The analytic estimate Eq. (3.69) is represented by lines in Fig. 3.8. In the drift dominated regime $f\gg 1$, the effective diffusion coefficient equals unity independent of the chosen aspect ratio. In the opposite limit, $f\ll 1$, $D_{\mathrm{eff}}(f)$ attains the asymptotic value $\lim_{f\to 0} D_{\mathrm{eff}}(f)/D^0=\lim_{f\to 0}\mu(f)/\mu^0$. The latter can be adjusted by the channel aspect ratio δ. For narrow bottlenecks, $\Delta\omega\to 0$, the entropic barrier separating the adjacent basins of attraction goes to infinity, cf. Eq. (3.58), and thus the diffusion coefficient converges to 0. With growing bottleneck width, $\Delta\omega\to\Delta\Omega$, the asymptotic value for the effective diffusion coefficient tends to the bulk value. This behavior is in compliance with experiments [Jovanovic-Talisman et al., 2009; Martin et al., 2005] in which was found that the diffusion of nano- or micro-sized colloid objects [Siwy et al., 2005] and DNA [Meller et al., 2001] can be controlled by changing the pore size (bottleneck width) of the channel. Moreover, in between the asymptotic limits, $f\ll 1$ and $f\gg 1$, an enhancement of $D_{\mathrm{eff}}(f)/D^0$, with maximum exceeding the free diffusion constant, is observed [Burada et al., 2008b; Reguera et al., 2006; Yariv and Dorfman, 2007]. In particular, one notices that the maximum value of the EDC grows with lessening aspect ratio δ, respectively, bottleneck width, see Fig. 3.8. Noteworthy, our analytic estimate (lines), Eq. (3.69), reproduces well the asymptotic limits as well as the peak of $D_{\mathrm{eff}}(f)$ for a wide range of aspect ratios.

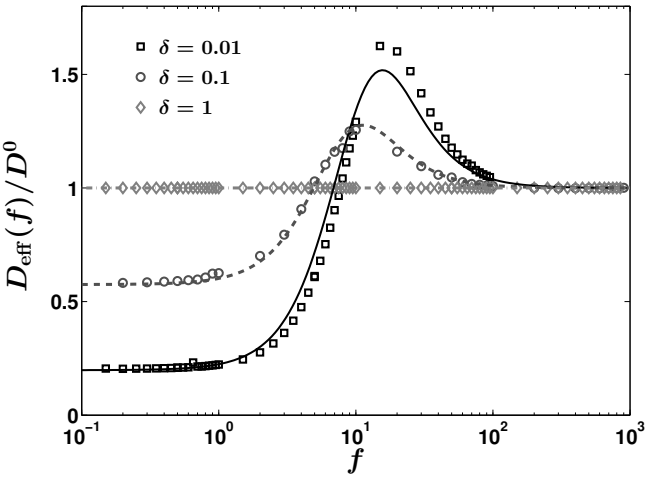

Figure 3.8: Effective diffusion coefficient as a function of the external force magnitude f for different aspect ratios δ. Simulation results (markers) are compared to the estimate for $D^0_{\mathrm{eff}}(f)/D^0$ (lines), Eq. (3.69). The maximum channel width is kept fixed $\Delta\Omega = 0.1$.

In Burada et al., 2008b, the authors showed that entropic effects increase the randomness of transport through a channel in such a way that the particle mobility decrease and the effective diffusivity increase. They found that a growth in the maximum channel width $\Delta\Omega$, while the aspect ratio is kept fixed, results not only in a dramatical enhancement of the maximal diffusion value but also in a broadening of the diffusion peak. Consequently, the value of f where D_{eff}/D^0 attains unity becomes larger with $\Delta\Omega$. Additionally, as anticipated, the deviation between the zeroth order estimate and the numerical result grows with ε. The described behavior is not explicitly shown here.

Referring to Costantini and Marchesoni, 1999, the f-dependence of the diffusion constant can be interpreted analytically in the framework of linear response theory resulting in

$$D_{\mathrm{eff}}(f)/D^0 = \frac{\mathrm{d}}{\mathrm{d}\,f}\,\langle\,\dot{x}(f)\,\rangle = \mu(f)/\mu^0 + f\frac{\mathrm{d}}{\mathrm{d}\,f}\,\left[\mu(f)/\mu^0\right], \tag{3.71}$$

for overdamped Brownian motion in period energetic potentials. Then "the bump in the $D_{\mathrm{eff}}(f)/D^0$ is related to the jump of $\mu(f)$ at the locked-to-running transition threshold $f = f_c$"[Costantini and Marchesoni, 1999]. The authors found that for energetic potentials "the resonance-like behavior of the diffusion coefficient is around the value for the tilt f for which the potential in Eq. (2.36) ceases to exhibit local extrema" and the peak "gets more and more pronounced as the thermal noise strength decreases" [Reimann et al., 2002]. Replacing the particle mobility by our exact zeroth order result, Eq. (3.61), and calculating the derivative with respect to f in Eq. (3.71), the effective diffusion coefficient may attains its maximum at

$$f_{\mathrm{Cost.}} = \pm\pi\sqrt{6\left(\sqrt{\delta} + 1/\sqrt{\delta}\right)}\,. \tag{3.72}$$

So far, we have restricted ourselves tacitly to $f > 0$. It is not difficult to see that the results remain valid for $f < 0$.

In order to simplify the estimate Eq. (3.69), we expand the latter for large aspect ratios or, equivalently, small value for $1/\mathtt{b}$, leading to

$$D^0_{\text{eff}}/D^0 \approx 1 - 2\pi^2 \, \frac{4 + 3\, f^2}{\left(f^2 + (2\pi)^2\right)^2} \frac{1}{\mathtt{b}^2} + O\left(\frac{1}{\mathtt{b}^4}\right). \tag{3.73}$$

Then the EDC reaches its maximum value

$$\max\left(D^0_{\text{eff}}/D^0\right) = 1 + \frac{9}{32}\left(\frac{1-\delta}{1+\delta}\right)^2, \quad \text{at} \quad f_{\max} = \pm\sqrt{\frac{20}{3}}\,\pi. \tag{3.74}$$

In Fig. 3.9, we depict the impact of the aspect ratio δ on the position of the diffusion peak $f_{\max}$ (a) as well as on the peak height $\max(D^0_{\text{eff}}/D^0)$ (b). To do this, we numerically evaluated the maximum of $D_{\text{eff}}(f)/D^0$ from the exact expression (squares), Eq. (2.53), and from our estimate (circles), Eq. (3.69).

Concerning the peak position, see Fig. 3.9 (a), one observes that the value of $f_{\max}$ decreases with growing aspect ratio δ. Whereas our estimate , Eq. (3.69), underestimates $f_{\max}$ for very narrow bottlenecks, the agreement becomes better with growing bottleneck width $\Delta\omega$. For $\delta > 0.1$, both results coincide within the errors. Additionally, we notice that the peak position saturates for wider bottlenecks and finally converges to $f_{\max} = \sqrt{20/3}\,\pi$ (dash-dotted line). More interestingly, it turns out that the enhancement of diffusion is not initiated by the locked-to-running transition. The value for $f_{\max}$ where D_{eff}/D^0 attains its maximum neither coincides with the critical force magnitude f_c (solid line), Eq. (3.56), nor with the estimate derived by Constantini et al. (dashed line), Eq. (3.72). Consequently, the mechanism entailing the enhancement of diffusion for biased transport in confined geometries is different to the one in energetic periodic potential despite that D_{eff}/D^0 is well reproduced by the 1D kinetic FJ description. Moreover, the enhancement is comparatively weak – maximal factor of $2\,D^0$ – in contrast to energetic potential where the diffusion may be enhanced up to multiple orders of magnitude [Reimann et al., 2002]. An explanation for the enhancement of diffusion can be given by the ratio of the diffusion time in transversal direction to the drift time in transport direction. For $f \to \infty$, the drift time is much short than the diffusive time scale and thus the particles gather at the channel's center line. Hence, the effective diffusivity approaches the bulk value. With decreasing dimensionless force strength, the initial step-like distribution at the bottleneck becomes bell-shaped in transversal direction, see the blue line in Fig. 3.4 (b). Therefore, some particles pile up at the bottleneck and hence move slower than the mean. Consequently, the joint PDF spreads in x-direction and the EDC exceeds its bulk value. With upon decreasing value of f, diffusion starts to dominate and the particle transport becomes irregular. If so, the drift time is much larger than the diffusive time and thus equilibration in transversal direction is accomplished; see the black line in Fig. 3.4 (b). In this limit, the majority of the particles stay together for long times in a unit-cell and, consequently, diffusion in longitudinal direction is diminished such that the effective diffusion coefficient is less than free diffusion.

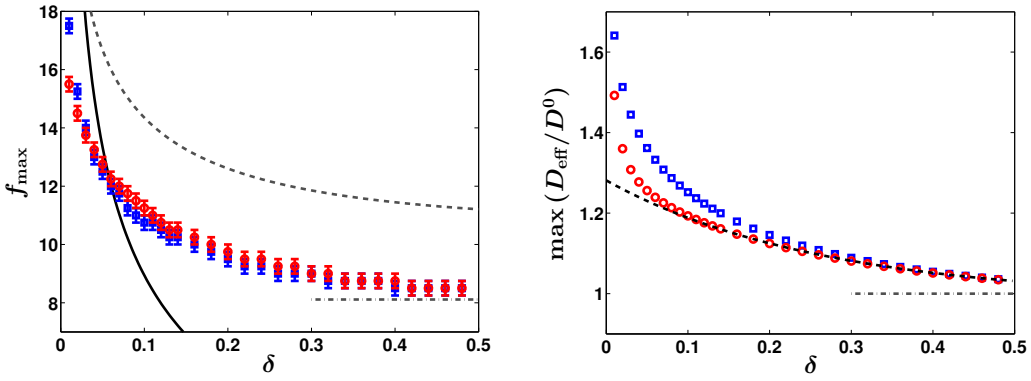

Figure 3.9.: The impact of aspect ratio $\delta = \Delta\omega/\Delta\Omega$ on the position of the diffusion peak $f_{\max}$ (left panel) and the peak height $\max(D_{\text{eff}}/D^0)$ (right panel) is depicted. The peak height as well as the position are numerically evaluated for the exact result (squares), Eq. (2.53), and for the estimate (circles), Eq. (3.69). Superimposed are in (a): the critical force magnitude f_c (solid line), Eq. (3.56), the estimate of Constantini et al. (dashed line), Eq. (3.72), and the asymptotic limit for $f_{\max}$ (horizontal dash-dotted line), Eq. (3.74); in (b): the estimate for $\max(D_{\text{eff}}/D^0)$ (dotted line), Eq. (3.74), and the asymptotic value unity (dash-dotted line). For all graphs the maximum width is set to $\Delta\Omega = 0.1$.

In Fig. 3.9 (b), we present the influence of the aspect ratio δ on the diffusion peak height $\max(D^0_{\text{eff}}/D^0)$. We find that our analytic result, Eq. (3.69), underestimates the true peak height for the entire range of aspect ratios. Further, it is shown that the discrepancy becomes smaller with growing value of δ. More importantly, the result Eq. (3.74) matches the maximum value obtained from Eq. (3.69) for $\delta > 0.1$. Additionally, as expected, the peak height $\max(D^0_{\text{eff}}/D^0)$ goes to unity in the limit of a straight channel, $\delta \to 1$.

3.2.4. Transport quality – Péclet number

In order to qualify the particle transport in confined geometries, we consider the Péclet number Pe [Landau and Lifschitz, 1991; Péclet, 1841]. Originally, the Péclet number was used in the context of heat transfer in fluids and was defined as the ratio of heat transfer in horizontal direction of the fluid surface to the diffusion. Large values of Pe correspond to ordered and directed motion whereas small Péclet numbers are associated with irregular motion. In the context of particulate motion, the Péclet number reflects the ratio of convective to diffusive motion on a characteristic length. For some problems, it is desirable that particles starting at sharp distribution reach a certain region without much spreading [Freund and Schimansky-Geier, 1999; Romanczuk et al., 2010]. If so, convective motion dominates and this results in a large Péclet number. In honor of Howard Brenner the number has also been called *Brenner number* Br [Rose, 1973]. In

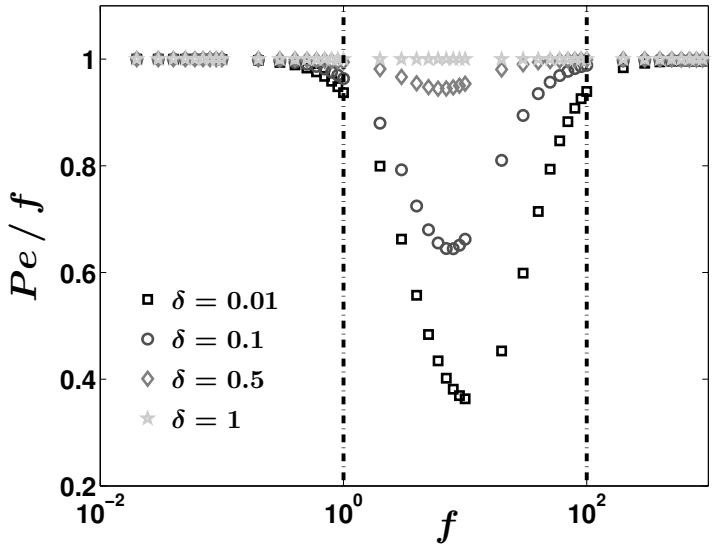

Figure 3.10: Simulation results for Peclet number Pe versus external force magnitude f for different aspect ratios δ. The maximum channel width is kept fixed $\Delta\Omega = 0.1$.

detail, the Péclet number is given by

$$Pe = \frac{\langle \dot{x} \rangle L}{D^0}, \tag{3.75}$$

for dimensionful quantities. Immediately, one recognizes that our dimensionless force magnitude $f = F L/k_B T$ equals the Péclet number for the problem of biased Brownian motion in systems without geometrical constraints, i.e., $Pe^0 = f$. Passing to dimensionless quantities, the Péclet number in units of its free value reads

$$Pe/f = \frac{\mu(f)/\mu^0}{D_{\text{eff}}(f)/D^0}. \tag{3.76}$$

According to Eq. (2.26), Pe/f equals unity if the Sutherland-Einstein relation holds. Consequently, the Péclet number can be used to identify parameter ranges where this relation is violated.

The impact of the external force magnitude on the Péclet number is depicted in Fig. 3.10. Obviously, Pe/f equals unity regardless the value of f if the channel is straight, i.e., $\delta = 1$. With decreasing aspect ratio we observe that the Sutherland-Einstein relation gets violated for an intermediate range of force strengths [Burada, 2008]. In compliance with the previously presented results for the mobility and the effective diffusion coefficient, cf. Sect. 3.2.1 and 3.2.3, the Péclet number attains unity either for very small, $f \lesssim 1$, of for very large force magnitudes, $f \gtrsim 100$. In between $D_{\text{eff}}(f)/D^0$ shows a resonance-like behavior and attains values larger than one. In the same interval the particle mobility changes from $\lim_{f\to 0} \mu(f)/\mu^0 \leq 1$ to its asymptotic value 1 without exceeding unity. As a consequence, one observes that the Péclet number attains a minimum for $f \in [1, 100]$. In this parameter range, the transport in confined geometries exhibiting entropic barriers is more irregular and diffusive compared to the free situation. Unlike the maximal value of $D_{\text{eff}}(f)/D^0$ increases with shrinking bottleneck size, the minimal value for Pe/f decreases with $1/\Delta\omega$. In addition, it turns

out that the interval where the Sutherland-Einstein relation is violated becomes wider with lessening bottleneck width for a given $\Delta\Omega$. It can be seen that not only the Péclet number attains smaller values but also that the dent becomes broader for channels with larger bulges (not explicitly shown).

3.3. Three-dimensional, cylindrical tube with periodically changing cross-section

In Sect. 3.1, we provided a systematic treatment for biased Brownian motion in a three-dimensional, planar channel with periodically varying, rectangular cross-section. There, the expansion of the stationary probability density function in a series in terms of the geometric parameter ε which specifies the channel corrugation was presented. In particular, we have demonstrated that the consideration of the higher order corrections to the stationary joint PDF leads to a substantial improvement of the commonly employed Fick-Jacobs approach towards extremely corrugate channels. The object of this section is to provide a similar analytic treatment to the problem of biased Brownian motion in *three-dimensional, cylindrical tubes* with periodically varying radius $R(x)$.[7]

In detail, we consider the overdamped dynamics of point-like Brownian particles in a cylindrical tube with periodically modulated radius $R(x)$, respectively, cross-section $Q(x) = \pi\, R(x)^2$. For simplification, we suppose a radial symmetric channel resulting in a straight and position independent channel center line $C(x) = 0$. A sketch of a tube segment with unit period is depicted in Fig. 3.11. As before in Sect. 3.1, the particles are subject to an external force with static magnitude f acting along the longitudinal direction of the tube $\mathbf{e}_x$, i.e., the corresponding potential reads $\Phi(\mathbf{q}) = -f\, x$. Additionally, the particle size is considered to be negligibly small (point-like). Thus, hydrodynamic as well as hard-core particle-particle interactions can safely be disregarded.

For the studied cylindrical geometry it is appropriate to change from Cartesian representation to Polar coordinates $(x, y, z) \to (x, r, \varphi)$ with distance $r = \sqrt{y^2 + z^2}$ and angle $\varphi = \arctan(z/y)$. The evolution of the joint probability density function $P(\mathbf{q}, t)$ of finding the particle at the local position $\mathbf{q} = (x, r, \varphi)^T$ at time t is governed by the 3D Smoluchowski equation Eq. (3.5a) with associated probability current $\mathbf{J}(\mathbf{q}, t) = (J^x, J^r, J^\varphi)^T$. Additionally, $\mathbf{J}(\mathbf{q}, t)$ has to obey the no-flux boundary condition at the tube's wall, $\mathbf{J}(\mathbf{q}, t) \cdot \mathbf{n} = 0$, where $\mathbf{n}$ is the outward-pointing normal vector at the boundary, reading explicitly

$$R'(x) J^x(\mathbf{q}, t) = J^r(\mathbf{q}, t), \quad \text{at} \quad r = R(x). \tag{3.77a}$$

The prime denotes the derivative with respect to x. As a result of symmetry arguments the probability current must be parallel with the tube's center line at $r = 0$

$$J^r(\mathbf{q}, t)\,|_{r=0} = 0. \tag{3.77b}$$

[7] I remark that several results and similar figures presented in this section have been previously published in Martens et al., 2011b.

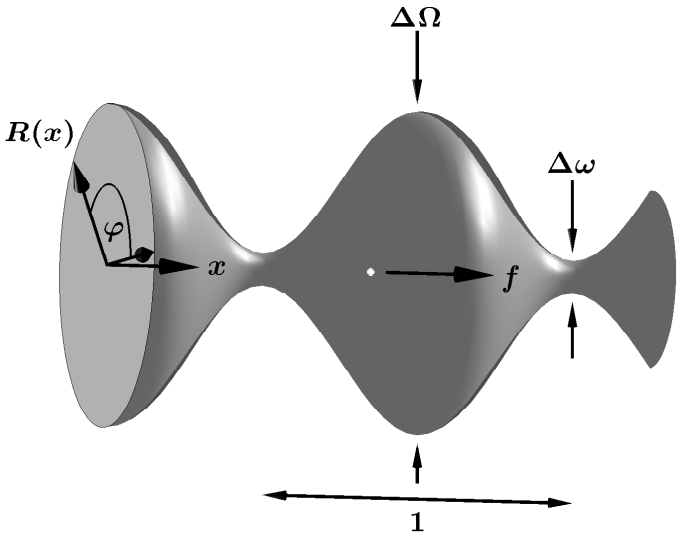

Figure 3.11.: Sketch of a segment of a cylindrical tube with sinusoidally varying radius $R(x)$ that is confining the motion of an overdamped, point-like Brownian particle. The periodicity of the tube structures is unity, the minimal and maximal tube widths are $\Delta\omega$ and $\Delta\Omega$, respectively. The constant force f pointing in the direction of the tube is applied on the particle.

Further, $P(\mathbf{q},t)$ satisfies the normalization condition Eq. (2.16) as well as the periodicity requirement $P(x+m\,L,r,\varphi+n\,2\pi,t)=P(x,r,\varphi,t),\forall\, m,n\in\mathbb{Z}$.

Since the external force $\mathbf{f}=f\mathbf{e}_x$ acts only in longitudinal channel direction, the probability density $P\left(\mathbf{q},t\right)$ is radial symmetric. This allows a reduction of the problem's dimensionality from 3D to 2D by integrating Eq. (3.5a) with respect to the angle φ, yielding

$$\partial_t p\left(x,r,t\right)=\partial_x\left[e^{-\Phi(x)}\partial_x\left(e^{\Phi(x)}\,p(x,r,t)\right)\right]+\frac{1}{r}\partial_r\left[r\,\partial_r p(x,r,t)\right]. \tag{3.78}$$

Thereby, the joint PDF is defined as

$$p(x,r,t)=\frac{1}{2\pi}\int_0^{2\pi}\mathrm{d}\varphi\,P\left(x,r,\varphi,t\right), \tag{3.79}$$

and the marginal probability density reads

$$p(x,t)=\frac{1}{2\pi}\int_0^{R(x)}\mathrm{d}r\,r\int_0^{2\pi}\mathrm{d}\varphi\,P\left(x,r,\varphi,t\right). \tag{3.80}$$

Both are connected via

$$\partial_t p(x,t) = \partial_x \int_0^{R(x)} \mathrm{d}r\; r \left[e^{-\Phi(x)} \partial_x \left(e^{\Phi(x)}\, p(x,r,t) \right) \right], \tag{3.81}$$

which can be obtained by integrating Eq. (3.78) over the local cross-section and taking the boundary conditions, Eqs. (3.77), into account.

Below we measure, for the case of finite corrugation $\varepsilon \neq 0$, the radius r in units of ε, i.e., $r \to \varepsilon\, r$ and, likewise, the local channel radius $R(x) \to \varepsilon\, h(x)$. Consequently, the joint PDF reads $P(\mathbf{q},t) \to \varepsilon^2\, P(\mathbf{q},t)$, respectively, the probability current is given by $\mathbf{J}(\mathbf{q},t) = \left(\varepsilon^2 J^x, J^r, \varepsilon^2 J^\varphi\right)^T$ after re-scaling. We emphasize that the scaling of time, energies, and the set of units are not influenced by this additional transformation, see Sect. 2.2.

In the same manner as done before in Sect. 3.1, we concentrate only on the steady state, $\lim_{t\to\infty} p(x,r,t) := p(x,r)$. The Smoluchowski equation, Eq. (3.78), becomes

$$\varepsilon^2 \partial_x \left[e^{-\Phi} \partial_x \left(e^{\Phi} p(x,r) \right) \right] + \frac{1}{r} \partial_r \left[r\, \partial_r p(x,r) \right] = 0, \tag{3.82}$$

and the no-flux bcs, Eqs. (3.77), read

$$0 = \left[\partial_r p(x,r) - \varepsilon^2 h'(x) e^{-\Phi} \partial_x \left(e^{\Phi} p(x,r) \right) \right]_{(x,r=h(x))}, \tag{3.83a}$$

$$0 = \partial_r p(x,r)|_{(x,r=0)}. \tag{3.83b}$$

in dimensionless units. Comparing Eqs. (3.82) and Eq. (3.2), we identify the unperturbed, steady state Fokker-Planck operator, $\mathfrak{L}_0 = \frac{1}{r}\partial_r \left[r\, \partial_r \right]$, and the perturbed one, $\mathfrak{L}_1 = \partial_x [e^{-\Phi(x)} \partial_x e^{\Phi(x)}] = (f \partial_x - \partial_x^2)$.

Asymptotic perturbation analysis

Next, we perform asymptotic perturbation analysis of the problem stated by Eqs. (3.82) and (3.83). Therefore, we expand the stationary joint PDF $p(x,r)$

$$p(x,r) = p_0(x,r) + \varepsilon^2\, p_1(x,r) + \ldots = \sum_{n=0}^{\infty} \varepsilon^{2n} p_n(x,r), \tag{3.84}$$

and, likewise, the probability current $\mathbf{J}(x,r) = \sum_{n=0}^{\infty} \varepsilon^{2n} \mathbf{J}_n(x,r)$ at steady state in the form of a formal perturbation series in orders of ε^2. Substituting these expressions into Eq. (3.82), we find

$$\begin{aligned} 0 &= \mathfrak{L}_0\, p_0(x,r) + \sum_{n=1}^{\infty} \varepsilon^{2n} \left\{ \mathfrak{L}_0\, p_n(x,r) + \mathfrak{L}_1\, p_{n-1}(x,r) \right\}, \\ 0 &= \frac{1}{r} \partial_r \left[r \partial_r p_0 \right] + \sum_{n=1}^{\infty} \varepsilon^{2n} \left\{ \frac{1}{r} \partial_r \left[r \partial_r p_n \right] + \partial_x \left[e^{-\Phi} \partial_x \left(e^{\Phi} p_{n-1} \right) \right] \right\}. \end{aligned} \tag{3.85}$$

The no-flux bc at the tube wall at $r = h(x)$, Eq. (3.83a), turns into

$$0 = \partial_r p_0(x,r) + \sum_{n=1}^{\infty} \varepsilon^{2n} \left\{ \partial_r p_n(x,r) - h'(x) e^{-\Phi} \partial_x \left(e^{\Phi} p_{n-1}(x,r) \right) \right\}, \tag{3.86a}$$

and the bc at the tube's center line at $r = 0$, Eq. (3.83b), reads

$$0 = \sum_{n=0}^{\infty} \varepsilon^{2n} \partial_r p_n(x,r). \tag{3.86b}$$

Further, we claim that the normalization condition for $p(x,r)$ corresponds to the zeroth solution $p_0(x,r)$ that is normalized to unity,

$$\langle\, p_0(x,r) \,\rangle_{x,r} = \int_0^1 \mathrm{d}x \int_0^{h(x)} \mathrm{d}r\, r\, p_0(x,r) = 1. \tag{3.87}$$

Therefore, all higher orders term p_n have zero average, $\langle\, p_n(x,r) \,\rangle_{x,r} = 0, n \in \mathbb{N}^+$, and have to obey the periodic boundary condition $p_n(x+m,r) = p_n(x,r), \forall\, m \in \mathbb{Z}$.

3.3.1. Zeroth Order: the Fick-Jacobs equation

Let us start with the leading order of the perturbation series $p_0(x,r)$. To derive the latter, one has to solve $\mathfrak{L}_0\, p_0(x,r) = 0$ supplemented with the associated no-flux bc $\partial_r p_0(x,r) = 0$ at $r = 0$ and at $r = h(x)$. We propose the ansatz $p_0(x,r) = g(x)\, e^{-\Phi(x)}$ where $g(x)$ is an unknown function which has to be determined from the second order $O(\varepsilon^2)$ balance of Eq. (3.85), viz., $\mathfrak{L}_0\, p_1(x,r) + \mathfrak{L}_1\, p_0(x,r) = 0$. Integrating the latter with respect to the radius r and taking the no-flux boundary conditions Eqs. (3.86) into account, we get $0 = \partial_x(e^{-A(x)} g'(x))$. Here, $A(x)$ also denotes the potential of mean force, defined as $A(x) = -\ln[\int_0^{h(x)} \mathrm{d}r\, r\, e^{-\Phi(x)}]$. The latter explicitly reads $A(x) = -f\,x - \ln[h^2(x)]$ for the considered situation $\Phi(\mathbf{q}) = -f\,x$. Note that upon the irrelevant additive constant $\ln(\pi)$ the potential of mean force corresponds to that given in [Jacobs, 1967].

Referring to Sect. 3.1.1, the normalized leading order of stationary joint PDF is given by

$$p_0(x,r) = e^{-\Phi} g(x) = \mathcal{I}^{-1}\, e^{-\Phi(x)} \int_x^{x+1} \mathrm{d}x'\, e^{A(x')}, \tag{3.88}$$

and, moreover, the marginal probability density, Eq. (3.80), becomes

$$p_0(x) = e^{-A(x)}\, g(x) = \mathcal{I}^{-1}\, e^{-A(x)} \int_x^{x+1} \mathrm{d}x'\, e^{A(x')}, \tag{3.89}$$

with substitute $\mathcal{I}$ previously defined in Eq. (3.21). In the case $f \to 0$, the stationary

joint PDF passes into a uniform distribution $p_0(x,r) = const$ and the marginal PDF scales with the cross-section $p_0(x) \propto Q(x)$. Expressing next $g(x)$ by $p_0(x)$ yields the stationary Fick-Jacobs equation $0 = \partial_x\big[e^{-A(x)}\partial_x(e^{A(x)}\, p_0(x))\big]$, previously discussed in Sect. 2.3. In the same manner as done before for 3D, planar confinements, we demonstrate that the leading order term of the asymptotic perturbation analysis is equivalent to the FJ-equation. Naturally, the joint pdf is sufficiently reproduced by Eq. (3.88) as long as the modulation of the tube radius is small compared to its periodicity, i.e. $\varepsilon \ll 1$.

By using $p_0(x,r)$, the leading order of the mean particle current is evaluated the Stratonovich formula [Stratonovich, 1958]

$$\langle\, \dot{x}(f)\,\rangle_0 = \int_0^1 \mathrm{d}x \int_0^{h(x)} \mathrm{d}r\, r\, J_0^x(x,r) = \mathcal{I}^{-1}\left(1 - e^{-f}\right). \tag{3.90}$$

Additionally, the mean particle current Eq. (2.6) simplifies to

$$\langle\, \dot{x}\,\rangle = \langle\, \dot{x}\,\rangle_0 - \sum_{n=1}^{\infty} \varepsilon^{2n}\, \langle\, \partial_x p_n(x,r)\,\rangle_{x,r}\,, \tag{3.91}$$

due to the normalization condition Eq. (3.87). Similar to the problem stated in Sect. 3.1, the mean particle current in longitudinal tube direction (here x-direction) is composed of (i) the Fick-Jacobs result $\langle\, \dot{x}\,\rangle_0$, Eq. (3.90), and (ii) becomes corrected by the sum of averaged derivatives of the higher orders $p_n(x,r)$. We next address the higher order corrections $p_n(x,r)$ of the probability density which become necessary for extremely corrugated structures.

3.3.2. Higher order contributions to the Fick-Jacobs equation

In reference to Eq. (3.85), one has to recursively solve $\mathfrak{L}_0\, p_n(x,r) + \mathfrak{L}_1\, p_{n-1}(x,r) = 0$ bearing in mind the no-flux bcs, Eqs. (3.86). In detail, the determining equations read

$$\frac{1}{r}\partial_r\left[r\partial_r p_n(x,r)\right] = \left(f\partial_x - \partial_x^2\right)\, p_{n-1}(x,r), \quad n \in \mathbb{N}^+. \tag{3.92}$$

Any solution of this second order partial differential equation has two integration constants $d_{n,1}$, determined by the no-flux bc at the center line at $r = 0$, Eq. (3.86b), and $d_{n,2}$, providing the zero average condition $\langle\, p_n(x,r)\,\rangle_{x,r} = 0$, $n \in \mathbb{N}^+$.

The determining equation for the first order correction reads

$$\frac{1}{r}\partial_r\left[r\partial_r p_1(x,r)\right] = 2\, \langle\, \dot{x}\,\rangle_0\, \partial_x\left(\frac{1}{h^2(x)}\right), \tag{3.93}$$

and after integrating twice with respect to r, we obtain

$$p_1(x,r) = -\,\langle\, \dot{x}\,\rangle_0\, \left(\frac{h'(x)}{h^3(x)}\right) r^2. \tag{3.94}$$

Upon recursively solving, the higher order corrections are given by

$$\begin{aligned} p_n(x,r) &\simeq \mathfrak{L}_1^n p_0(x,r)\,\frac{r^{2n}}{\left(2^n n!\right)^2} + d_{n,2}, \\ &\simeq 2\,\langle\,\dot{x}\,\rangle_0\,\frac{r^{2n}}{\left(2^n n!\right)^2}\,\mathfrak{L}_1^{n-1}\partial_x\left(\frac{1}{h^2(x)}\right) + d_{n,2}, \quad n\in\mathbb{N}^+, \end{aligned} \tag{3.95}$$

where $\mathfrak{L}_1^n$ is given by Eq. (3.31). According to Eq. (3.84), $p(x,r)$ is obtained by summing all correction terms $p_n(x,r)$, yielding

$$p(x,r) = p_0(x,r) + \sum_{n=1}^{\infty}\varepsilon^{2n}\left(\mathfrak{L}_1^n\,p_0(x,r)\,\frac{r^{2n}}{\left(2^n n!\right)^2} + d_{n,2}\right). \tag{3.96}$$

To conclude, the exact solution for the joint PDF $p(x,r)$ for finding a biased Brownian particle ($\Phi(\mathbf{q}) = -f\,x$) in cylindrical tube with periodically varying radius at steady state is given by Eq. (3.96). The latter solves the stationary Smoluchowski equation, Eq. (3.82), under satisfaction of the normalization as well as the periodicity requirements. More importantly the solution, Eq. (3.96), obeys both no-flux boundary conditions at $r = 0$ and at $r = h(x)$. We stress that in contrast to the full solution, Eq. (3.96), each correction term p_n, Eq. (3.95), does not satisfy the no-flux bc at the channel wall since all terms scaling with integration constants $d_{n,1}$ are missing. Furthermore, one notices that $p(x,r)$ is solely determined by the leading order solution (FJ result) $p_0(x,r)$. As a consequence of $\mathfrak{L}_1\,p_0(x,r) \propto \langle\,\dot{x}(f)\,\rangle_0$, higher order contributions to $p(x,r)$ scale linearly with $\langle\,\dot{x}\,\rangle_0$, cf. Eq. (3.95). Since $\langle\,\dot{x}\,\rangle_0$ is determined by the external force, in force free limit the stationary PDF equals its zeroth order $p(x,r) = p_0(x,r) = const$ regardless of the value of ε. With increasing force magnitude f, the probability for finding particles close to the constricting part of the confinement grows, see Fig. 3.4(a).

According to Eq. (3.91), the average particle current scales with the mean particle current obtained from the Fick-Jacobs formalism $\langle\,\dot{x}\,\rangle_0$ for all values of ε. Therefore, in order to validate the exact result for $p(x,r)$ as well as to derive corrections to the mean particle current it is required to calculate $\langle\,\dot{x}\,\rangle_0$ first.

3.4. Example: Sinusoidally modulated cylindrical tube

Below, we study the key transport quantities like the particle mobility $\mu(f)/\mu^0$ and the EDC $D_{\text{eff}}(f)/D^0$ of point-like Brownian particles moving through a tube with sinusoidally varying cross-section $Q(x)$, Eq. (3.52). The associated dimensionless boundary function reads $h\,(x) = 0.25\;(\mathtt{b} + \sin\,(2\pi\,x))$, Eq. (3.53), and it is illustrated in Fig. 3.11. The function $h(x)$ is solely governed by the aspect ratio $\delta = \Delta\omega/\Delta\Omega$, respectively, the auxiliary parameter $\mathtt{b} = (1+\delta)/(1-\delta)$.

First, we calculate the leading order (Fick-Jacobs approximation) for the particle mobility μ_0/μ^0 in units of its bulk value. Referring to Eqs. (3.90) and (2.18), the particle

mobility is given by

$$\left[\mu_0(f)/\mu^0\right]^{-1} = \frac{1}{2\sqrt{\mathtt{b}^2-1}^3}\left\{\mathtt{b}\left(2\mathtt{b}^2+1\right) - \frac{4\mathtt{b}f^2}{f^2+(2\pi)^2} + \frac{\left(2\sqrt{\mathtt{b}^2-1}^3 - 2\mathtt{b}^3 + 3\mathtt{b}\right)f^2}{f^2+(4\pi)^2}\right\}. \tag{3.97}$$

Due to the reflection symmetry of the boundary function $R(x)$ with respect to $x = 0.25$ and $x = 0.75$, the particle mobility $\mu(f)/\mu^0$ is also a symmetric function, $\mu(-f) = \mu(f)$. Therefore, it is sufficient to discuss only the behavior for $f \geq 0$.

In the limiting case of infinite large force strength, the particle mobility equals the bulk value

$$\lim_{f\to\infty} \mu_0(f)/\mu^0 = 1, \tag{3.98}$$

regardless of the channel parameters $\Delta\Omega$ and $\Delta\omega$. With decreasing force magnitude f, $\mu_0(f)/\mu^0$ lessens till it attains the asymptotic value

$$\lim_{f\to 0} \mu_0(f)/\mu^0 = \lim_{f\to 0} D_{\text{eff}}(f)/D^0 = \frac{8\,\delta}{3\delta^2+2\delta+3}\,\frac{2\sqrt{\delta}}{1+\delta}, \tag{3.99}$$

which coincides with the value for $\lim_{f\to 0} D_{\text{eff}}(f)/D^0$ in accordance with the Sutherland-Einstein relation, Eq. (2.26). In the limit of vanishing bottleneck width, $\delta \to 0$, the mobility and the effective diffusion constant tend to zero. On the contrary, both transport quantities attains their free values for straight tubes corresponding to $\delta = 1$, respectively, $\varepsilon = 0$.

Comparing the asymptotic value Eq. (3.99) with the one for three-dimensional, planar channels, Eq. (3.64), one notices that the mobility and the effective diffusion coefficient in a tube are much smaller. What is the reason for this reduction? For weak forces, the particles are uniformly distributed over an area of maximum size $\max(Q(x)) = \pi\Delta\Omega^2$ in a tube. In order to induce directed motion, the particles has to be dragged through the much smaller bottleneck of size $\min(Q(x)) = \pi\Delta\omega^2$. Hence, the total change of available space scales with $(\Delta\omega/\Delta\Omega)^2$ for cylindrical tubes compared to $\Delta\omega/\Delta\Omega$ for planar channels. Having in mind that the change of the cross-section's area is reflected by the entropic barrier ΔA separating the adjacent basins of attraction (unit cells), it turns out that ΔA for cylindrical channels, $\lim_{f\to 0}\Delta A = -2\ln(\delta)$, doubles the one for planar geometries, cf. Eq. (3.58).

In Fig. 3.12, we depict the dependence of $\mu(f)/\mu^0$ and $D_{\text{eff}}(f)/D^0$ on the force magnitude f.[8] Referring to Fig. 3.12 (a), we recognize that the analytic result for the mobility, Eq. (3.97), is corroborated by the numerics. Further, it is shown that in the case of weakly modulated tubes, $\Delta\Omega \ll 1$, our analytic result is in excellent agreement with the numerics for all values of f, indicating the applicability of the FJ approach.

[8] The numerical results were obtained by FEM. For details please see App. A. The numerical errors are of the size of the markers so we do not indicate them.

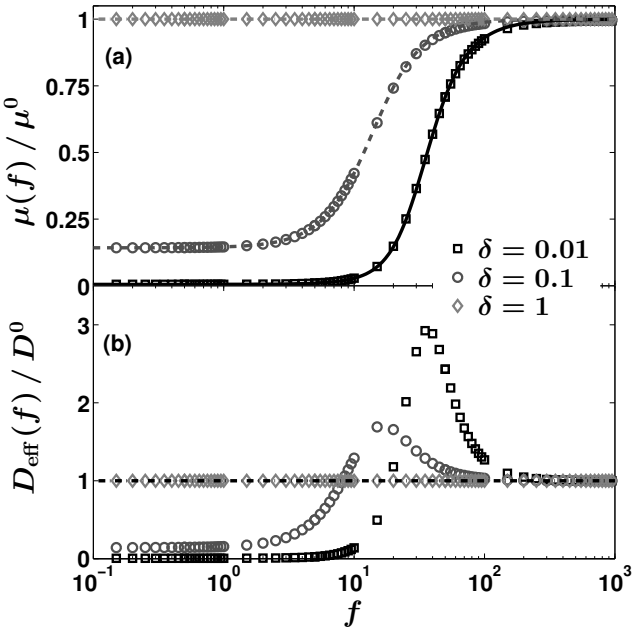

Figure 3.12: Particle mobility (a) and effective diffusion constant (b) for Brownian particles moving inside a sinusoidal tube as function of the force magnitude f. The maximum tube width is kept fixed, $\Delta\Omega = 0.1$, while the aspect ratio is varied $\delta = 0.01, 0.1, 1$, respectively, the corresponding values of ε are $\varepsilon = 0.099, 0.09, 0$. The markers correspond to the simulation results for the mobility and the effective diffusion coefficient. In panel (a) the lines represent the analytic result Eq. (3.97).

The EDC $D_{\rm eff}(f)$ exhibits a non-monotonic dependence on f, see Fig. 3.12 (b). It starts with the value Eq. (3.99) which is less than the free diffusion constant in the diffusion dominated regime, i.e., $|f| \ll 1$. Then it reaches a maximum with increasing f and finally approaches the value for the free diffusion from above. In addition, we observe that the location of the diffusion peak as well as the peak height depends on the aspect ratio δ. With diminishing bottleneck width, while keeping the maximum channel width $\Delta\Omega$ fix, the diffusion peak is shifted towards larger force magnitude f. Simultaneously the peak height grows. In the limit of straight tubes, $\delta \to 1$, as expected, the EDC coincides with its free value D^0 which is one in the considered scaling.

In Fig. 3.13, we depict the impact of the expansion parameter ε on the particle mobility. It turns out that for values of $\varepsilon \lesssim 0.1$ the Fick-Jacobs approach is in very good agreement with the simulation. The difference between the FJ-result (solid line) and the numerics grows with the value of ε. In detail, we find that the larger the available space inside the tube the less is the particle mobility. Consequently, the higher order corrections to $p(x, r)$, Eq. (3.84), and to the $\mu(f)/\mu^0$, Eq. (3.91), need to be included in order to provide a better agreement. This is done in the next paragraph.

3.4.1. Spatially dependent diffusion coefficient and corrections to particle mobility

The commonly studied idea to enhance the applicability of the Fick-Jacobs approach based on the introduction of the spatially dependent diffusion coefficient $D(x, f)$, for details please see Sect. 2.4, which can be derived by means of the marginal probability

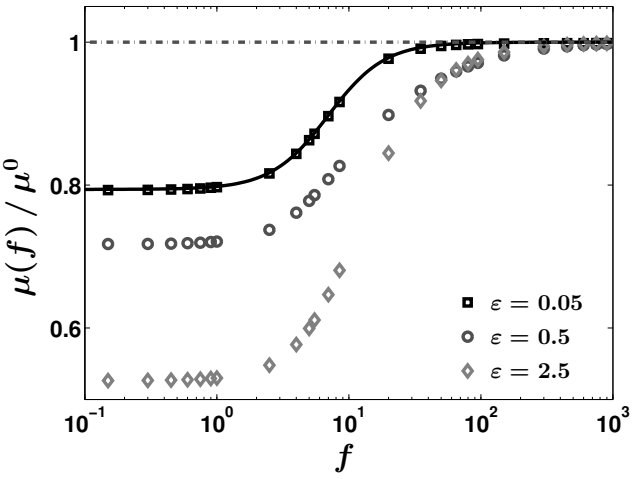

Figure 3.13: Influence of geometric parameter ε on particle mobility is presented. The value of ε is varied, $\varepsilon = 0.05, 0.5, 2.5$, while the aspect ratio is kept fixed, $\delta = 0.5$. The solid line corresponds to the analytic result Eq. (3.97) whereas the dash-dotted line indicates the asymptotic value unity.

current in longitudinal direction

$$-J^x(x) = D\,(x,f)\,e^{-A(x)}\partial_x\left(e^{A(x)}p\,(x)\right) = \int_0^{h(x)} \mathrm{d}r\, r\, e^{-\Phi(\mathbf{q})}\partial_x\left(e^{\Phi(\mathbf{q})}p\,(x,r)\right). \quad (3.100)$$

The second equality determines $D(x,f)$ which is governed by the stationary joint PDF $p(x,r)$ and the stationary marginal PDF $p(x)$. Below, we calculate $D(x,f)$ by means of the result from asymptotic perturbation analysis, Eq. (3.96).

One immediately notices that in the force dominated regime $|f| \gg 1$, Eq. (3.100) simplifies to $D(x,f)\,f\,p(x) = \int_0^{h(x)} \mathrm{d}r\, r\, f\, p(x,r)$. Thus, the spatially dependent diffusion coefficient equals the bulk value D^0, which is one in our scaling,

$$\lim_{f\to\infty} D(x,f) = 1. \quad (3.101)$$

In the opposite limit of small force strengths, $|f| \ll 1$, diffusion is the dominating process and Eq. (3.100) reduces to

$$D\,(x,f)\,h^2(x)\partial_x\left(\frac{p\,(x)}{h^2(x)}\right) = \int_0^{h(x)} \mathrm{d}r\, r\, \partial_x p\,(x,r)\,. \quad (3.102)$$

By inserting Eq. (3.96) into Eq. (3.102), we are able to calculate an expression for $D(x,f)$. In compliance with other authors [Kalinay and Percus, 2006; Reguera and Rubí, 2001], we assume that all but the first derivative of the boundary function $h(x)$ are negligible. If so, the n-times applied operator $\mathfrak{L}_1$, Eq. (3.31), reduces to $\mathfrak{L}_1^n = (-1)^n \frac{\partial^{2n}}{\partial x^{2n}}$; yielding

$$p_n(x,r) = 2\,(-1)^n\,\langle\,\dot{x}\,\rangle_0\,\frac{(2n)!}{(2^n n!)^2}\frac{(h')^{2n-1}}{h^{2n+1}}r^{2n} + O(h''(x)). \quad (3.103)$$

Putting the latter into Eq. (3.100) and calculating the complete sum, we get

$$\lim_{f\to 0} D(x,f) = \frac{1}{\sqrt{1+W'(x)^2/4}} + O\left(h''(x)\right), \tag{3.104}$$

for the spatially dependent diffusion coefficient in the diffusion dominated regime $|f| \ll 1$. To conclude, we confirm the expression for $D_{RR}(x,0)$ previously suggested by Reguera and Rubí, cf. Eq. (2.48), and derived by Kalinay and Percus, see Eq. (2.49b), using our exact analytic result for $p(x,r)$.

Next, we derive an estimate for the particle mobility $\mu(f)/\mu^0$ based on the higher expansion orders $p_n(x,r)$, $n \in \mathbb{N}^+$. From Eqs. (3.91) and (2.18) follow that the mean particle current is composed of (i) the Fick-Jacobs result $\mu_0(f)/\mu^0$, Eq. (3.90), and (ii) becomes corrected by the sum of the averaged derivatives of the higher orders $p_n(x,r)$. Immediately, one notices that the additive integration constants $d_{n,2}$, resulting from the normalization condition Eq. (3.87), do not influence the result for $\mu(f)/\mu^0$.

In particular, we concentrate on the diffusion dominated limit, $|f| \ll 1$. Furthermore, we suppose once more that all but the first derivative of the boundary function $h(x)$ are negligible. If so, the partial derivative of $p_n(x,r)$ with respect to x reduces to

$$\partial_x p_n(x,r) = 2\left\langle \dot{x} \right\rangle_0 (-1)^{n+1} \frac{(h')^{2n}}{h^{2n+2}} \frac{(2n+1)!\, r^{2n}}{\left(2^n n!\right)^2} + O(h''(x)), \tag{3.105}$$

and, finally, we obtain

$$\begin{aligned}
\lim_{f\to 0} \mu(f)/\mu^0 &\simeq \lim_{f\to 0} \mu_0(f)/\mu^0 \sum_{n=0}^{\infty} \frac{(-1)^n (2n+1)!}{2^{2n+1}(n!)(n+1)!} \left\langle \left(\varepsilon h'(x)\right)^{2n} \right\rangle_x \\
&\simeq \lim_{f\to 0} \mu_0(f)/\mu^0 \left\langle \frac{2}{\left(\varepsilon h'(x)\right)^2} \left(1 - \frac{1}{\sqrt{1+\left(\varepsilon h'(x)\right)^2}}\right) \right\rangle_x \\
&\neq \lim_{f\to 0} \mu_0(f)/\mu^0 \left\langle D_{RR}(x,f) \right\rangle_x .
\end{aligned} \tag{3.106}$$

We derive that the most important transport quantities like mean particle current, particle mobility, and effective diffusion coefficient are determined by the product of their zeroth order result and the expectation value of a complicated function, including the slope of the boundary. In contrast to the previously studied case of biased Brownian motion in a 3D, planar channel geometry, Sect. 3.1.4, the multiplicative correction term to the transport quantities does not coincide with the expectation value of $D_{RR}(x,0)$.

Evaluating the sum in Eq. (3.106), for a cylindrical tube with sinusoidally modulated radius, Eq. (3.53), leads to the estimate

$$\lim_{f\to 0} \mu(f)/\mu^0 \simeq \lim_{f\to 0} \mu_0(f)/\mu^0 \; {}_2F_1\left(\frac{1}{2}, \frac{1}{2}, 2, -\left(\frac{\varepsilon\pi}{2}\right)^2\right), \tag{3.107}$$

where ${}_2F_1(\cdot)$ is the first hypergeometric function.

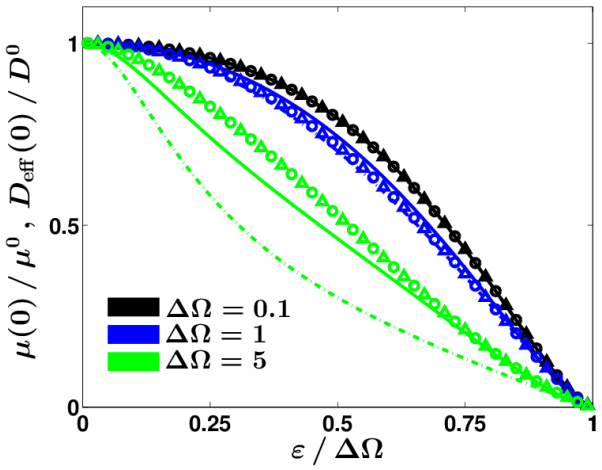

Figure 3.14.: Comparison of the analytic theory versus precise numerics: Mobility and effective diffusion constant of Brownian particles moving inside a tube with sinusoidal varying radius are depicted as a function of geometric parameter ε in units of $\Delta\Omega$. The latter is varied $\Delta\Omega = 0.1, 1, 5$ (from top to bottom) while the external bias is kept fixed $f = 10^{-3}$ (corresponding to the diffusion dominated regime). The symbols correspond to the numerically obtained mobility (triangles) and effective diffusion coefficient (circles). Solid lines represent the analytic higher order result, Eq. (3.107). The zeroth order (Fick-Jacobs) results, Eq. (3.99), collapse to a single curve hidden by the solid line for $\Delta\Omega = 0.1$. In addition, numerical evaluations of the Lifson-Jackson formula with $D_{RR}(x,0)$, Eq. (2.56), are represented by the dash-dotted lines.

We stress that considering the first derivative of the boundary function $h'(x)$ only results in an additional term proportional to $\varepsilon^2\, {}_2F_1\left(3/2, 3/2, 3, -(\varepsilon\pi/2)^2\right)$. Taking the second derivative $h''(x)$ into account indicates that this additional term is negligible compared to ${}_2F_1\,(1/2, \ldots)$ regardless of the value of ε.

In Fig. 3.14, we present the dependence of $\mu(f)/\mu^0$ (triangles) and $D_{\rm eff}(f)/D^0$ (circles) on the slope parameter ε for $f = 10^{-3}$. We find that the numerical results for the EDC and the particle mobility coincide for any values of ε corroborating the Sutherland-Einstein relation. In addition, the Fick-Jacobs result, given by Eq. (3.99), the higher order result (solid lines), Eq. (3.107), and the numerical evaluation of the Lifson-Jackson formula using $D_{RR}(x,0)$ (dash-dotted lines), Eq. (2.56), are depicted in Fig. 3.14.

For the case of smoothly varying tube geometry, $\Delta\Omega \ll 1$, all analytic expressions are in excellent agreement with the numerics, indicating the applicability of the Fick-Jacobs approach. With upon growing maximum width, discrepancies between the FJ-result, Eq. (3.99), and the numerics become larger. Specifically, the FJ-approximation overestimates μ/μ^0 and $D_{\rm eff}/D^0$. Consequently, the corrugation of the tube geometry needs to be included. The Lifson-Jackson formula using $D_{RR}(x,0)$, Eq. (2.56), provides a good agreement for a wide range of ε-values as long as the maximum width $\Delta\Omega$ is on the scale to the period length of the tube, i.e., $\Delta\Omega \sim 1$. The rela-

$\Delta\Omega$	$\varepsilon/\Delta\Omega$	FJ, Eq. (3.99)	Eq. (3.107)	$D_{RR}(x,0)$
1	0.25	0.027	0.008	-0.007
	0.5	0.009	0.021	-0.035
	0.8	0.179	0.027	-0.024
5	0.25	0.159	-0.106	-0.289
	0.5	0.460	-0.150	-0.449
	0.8	1.342	-0.002	-0.281

Table 3.2.: Relative error $\mu^{\text{theo}}(0)/\mu^{\text{num}}(0) - 1$ between theoretical estimates and numerics are presented for three given ratios $\varepsilon/\Delta\Omega$. The maximum channel width is varied from $\Delta\Omega = 1$ to $\Delta\Omega = 5$. The third column represents the results for the Fick-Jacobs approach $\lim_{f\to 0}\mu_0(f)/\mu^0$, Eq. (3.99), and values in the 4th column correspond to our correction estimate Eq. (3.107). Additionally, the results derived from the Lifson-Jackson formula with $D_{RR}(x,0)$ (5th column) are presented.

tive error $\mu^{\text{theo}}(0)/\mu^{\text{num}}(0) - 1$ is below 4% for all values of $\varepsilon/\Delta\Omega$, see 5th column in Tab. 3.2. Upon further increasing the maximum width $\Delta\Omega$ diminishes the range of applicability of the presented concept. In detail, the Lifson-Jackson formula using $D_{RR}(x,0)$, Eq. (2.56), drastically underestimates the simulation results (rel. error of 45% for $\varepsilon/\Delta\Omega = 0.5$) due to the neglect of the higher derivatives of $h(x)$. Put differently, the higher derivatives of $h(x)$ become significant for $\Delta\Omega \gtrsim 1$.

In contrast, we observe that our estimate, Eq. (3.107), for the particle mobility and the diffusion coefficient, based on the higher order corrections to the stationary joint PDF, is in very good agreement with the numerics. For tube geometries where the maximum width $\Delta\Omega$ is on the scale to the period length, $\Delta\Omega \sim 1$, the correction estimate matches perfectly with the numerical results (rel. errors are below 3%). A further growth of the tube width results in small deviations from the simulation results. Noteworthy, the relative errors between the analytic estimate and the numerics are less than 15%. Additional, it is remarkable that the agreement becomes much better with shrinking bottleneck width $\Delta\omega$, respectively, larger value of $\varepsilon/\Delta\Omega$.

3.5. Summary

In this chapter, we considered the transport of Brownian particles under the action of a static and spatially homogeneous force field through a 3D, planar channel geometry and 3D cylindrical tube with both periodically varying cross-section.

For both geometries, we presented a systematic treatment for particle transport by performing asymptotic perturbation analysis of the stationary joint probability density function (PDF) in terms of an expansion parameter specifying the channel corrugation. Exact solutions for the associated stationary Smoluchowski equation were derived for point-like Brownian particles moving in axis-symmetric channels. In particular, it turned out that the zeroth order of the series expansion is equivalent to the well-established *Fick-Jacobs approach*. The higher-order corrections to the joint PDF become significant for extreme bending of the channel walls. Interestingly, these correction terms scale with the zeroth order of the mean particle current.

Moreover, by means of the exact solutions for the stationary joint PDF, we presented an alternative derivation for the spatially dependent diffusion coefficient $D(x, f)$ substituting the constant diffusion coefficient present in the common Fick-Jacobs equation. Based on similar assumptions as those previously suggested by other authors, we validated both the result for 3D, planar geometries (Kalinay and Percus) and the one for cylindrical tubes (Rubí and Reguera).

In particular, we applied the analytic results to a specific example, namely, the particle transport through confinements with sinusoidally varying cross-section. Our theoretical predictions for the particle mobility and the effective diffusion coefficient were corroborated by precise numerical results. It turned out that the dynamics of single particles can be well described by the Fick-Jacobs approach as long as the maximum channel width is of the order of 10% of its period. Furthermore, we derived that in the diffusion dominate regime $|f| \ll 1$ the key transport quantities like mean particle current, particle mobility, and effective diffusion coefficient are determined by the product of their zeroth order result and the expectation value of a function, including the channel wall's corrugation. Remarkably, our analytic result can be calculated exactly for sinusoidal boundaries in contrast to the integrals appearing the commonly used Lifson-Jackson formula and it provides equally good or even better agreement with the numerics.

So far, the Fick-Jacobs approach has been limited to scalar potentials which solely generates conservative forces exerted on the particles. In the following chapter 4, we overcome this restriction by extending the Fick-Jacobs description to the most general external force which is composed of a curl-free (conservative) and a divergence-free component.

4. Hydrodynamically enforced entropic trapping of Brownian particles – Fick-Jacobs approach to vector potentials

In the previous chapter, we presented a systematic treatment for particle transport by performing an asymptotic perturbation analysis of the stationary joint PDF in terms of an expansion parameter specifying the corrugation of the channel walls. Exact solutions for the stationary Smoluchowski equation were derived for point-like Brownian particles moving under the action of a static, spatially homogeneous force ($\Phi(\mathbf{q}) = -f\,x$) in axis-symmetric channels. Possible realizations of this simplest form of an external force are e.g. gravity and electric fields. In particular, electric fields are generated by two oppositely charged cathodes placed at entrance and exit of the channel.

As an obvious extension, one may consider the superposition of a longitudinal $f_\parallel$ and a perpendicular force $f_\perp$ [Burada and Schmid, 2010]. The associated energetic potential reads $\Phi(\mathbf{q}) = -f_\parallel\,x - f_\perp\,y$ and the force field is given by $\mathbf{f} = (f\,\cos(\beta), f\,\sin(\beta), 0)^T$. Thereby, $f = \sqrt{f_\parallel^2 + f_\perp^2}$ is the force magnitude and $\beta = \arctan(f_\perp/f_\parallel)$ represents the force orientation angle measured from the x-axis. Burada and Schmid, showed that "by changing the angle of the external bias, the nature of the potential barriers, separating two adjacent unit cells, changes from purely entropic to energetic, which in turn affects the diffusion process in the system. Especially, at an optimum angle of the bias, the particle mobility exhibits a striking bell-shaped behavior. Moreover, the enhancement of the effective diffusion coefficient can be efficiently controlled by β". These facts are presented in Fig. 4.1. Albeit, the consideration of a superposition of a longitudinal and perpendicular force component or, equivalently, the introduction of a force orientation angle β is quite simple its influence on the particle transport quantities is very strong.

However, the situation is often not so simple in nature. Many forces acting on a suspended particle can be exerted, for instance, by surrounding walls [Israelachvili, 2011], by neighboring particles and molecules via hydrodynamic interactions [Happel and Brenner, 1965, for a discussion see Sect. 5.2], by external fields and solvent flows. For example, a solid surface submerged in aqueous (polar) solutions acquires electrical charges which attract counterions and repel co-ions. To maintain the electoneutrality of the system, electric double layer (EDL)[1] which excess the counterions must be formed to counterbalance the surface charge. Evidently due to thermal motion there is no perfect charge neutrality within the EDL whose thickness is approximately determined

[1] Although it is traditionally termed "double" layer, its structure can be very complicated and may contains three or more layers in most instances [Zhao and Yang, 2012].

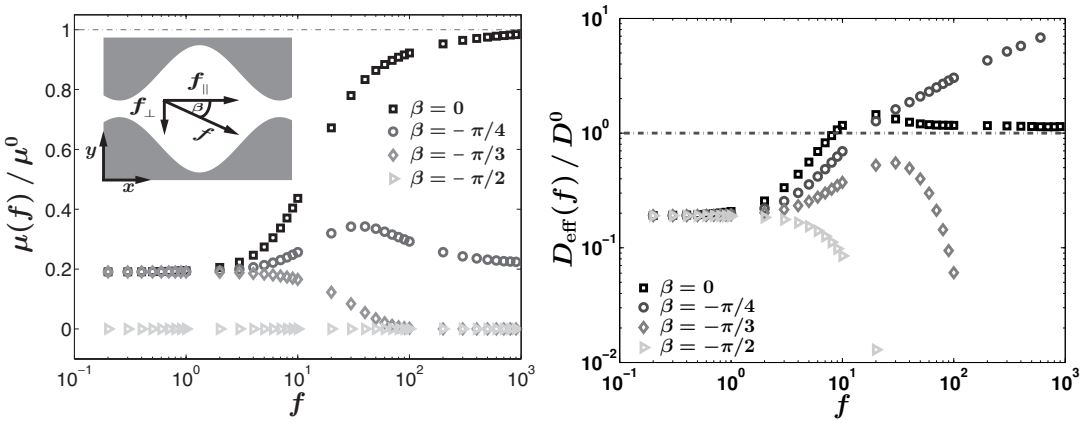

Figure 4.1.: Particle mobility $\mu/\mu^0 = \langle \dot{x} \rangle / f_\parallel$ (left) and effective diffusion coefficient (right) versus force magnitude f for various forcing angles β. Inset: Sketch of a channel unit cell and the force orientation are depicted. In compliance with Burada and Schmid the channel parameters are $\Delta\Omega = 0.6$ and $\Delta\omega = 0.06$.

by Debye length λ_D. Furthermore, the ionic charges in the EDL gradually screen the electric field generated by the charged surface with zeta potential ζ. The latter is a measure of the surface charge density. In the case of two parallel walls, the opposite surface attains as surface potential $-\zeta$ in order to maintain system's electoneutrality.

Although the application of external driving electric fields does not influence the surface charge on insulating (non-conducting) surfaces, electrokinetic phenomena occur. The two most prominent are electroosmosis – the movement of the liquid relative to a stationary charged surface – and electrophoresis – the movement of a charged suspended object relative to a stationary liquid. Electroosmotic flows emerge along charged solid walls subjected to a tangential electric field. The externally applied electric field exerts body force on the net charge density in the diffusive part of the EDL, driving ions and the liquid into motion [Dukhin and Shilov, 1969]. It is a unique feature that the electroosmotic flow does not depend an the channel geometrie that stands in contrast to pressure-driven flows. Due to this property the combination of electroosmotic and pressure-driven flows are used as micropumps [Brask et al., 2005; Mishchuk et al., 2009].

On the other hand, the electroosmotic slip velocity over the surface of a freely suspended, charged particle in an electrolyte solution [Teubner, 1982] gives rise to particle motion, known as electrophoresis. The particle motion is oppositely directed to the electroosmotic slip velocity. However, in the case of electrokinetic motion of charged particles inside a channel of μm-size, electrophoresis and electroosmosis are not independent of each other.

When polarizable (conducting) surfaces are subject to external electric fields, the external driving electric field induces surface polarization charges [Bazant and Squires, 2010; Daghighi and Li, 2010] in addition to the physiochemical bond charges on the surface, which generate additional effects like non-linear induced-charge electrokinetic flows [Dukhin, 1991; Squires and Bazant, 2006]. Such flows arise when the applied electric field interacts with the EDL that is induced by the applied field itself. Without surface conduction or Faradaic currents, ionic charges suspended in the aqueous solvent

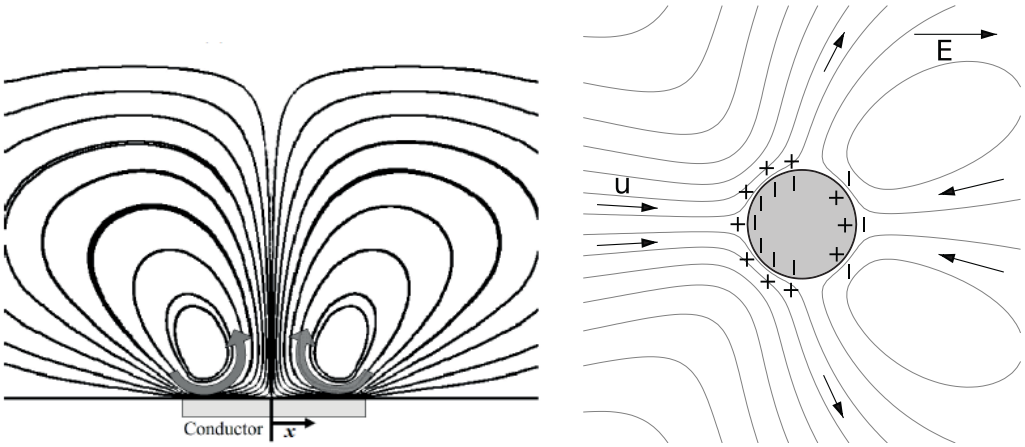

Figure 4.2.: Left: Induced-charge electroosmotic (ICEO) flow streamlines over conducting patch. Reprinted with permission from Soni et al., 2007. Right: ICEO flow **u** around a charged polarizable cylindrical wire which is placed in an electrolyte under the action of a weak electric field **E**. Reprinted with permission from Bazant and Squires, 2004. *Copyright (2012) by The American Physical Society.*

accumulate in the EDL. The induced charge is non-uniform – negative ($\zeta > 0$) where the initial current leaves the surface and positive ($\zeta < 0$) where it enters [Anderson, 1985]. Then the flow pattern is "simply a superposition of a non-linear quadrupol flow and the linear streaming flow of electrophoresis" [Bazant and Squires, 2004] in a dc field. It is evident that the basic pattern of such non-linear electrokinetic flows is a pair of symmetric counter-rotating vortices above the conducting path [Squires and Bazant, 2004; Zhao and Yang, 2012].

Moreover, acousto- [Petersson et al., 2007], magneto- [Pamme and Wilhelm, 2006], and dielectrophoretic forces [Gascoyne and Vykoukal, 2002] can also be exerted on particles. Dielectrophoretic forces arise from the interaction between a dielectric particle in a dielectric suspending medium and either rapidly changing electric fields gradients or non-uniform electric fields [Voldman, 2006].

To sum up, in experimental devices like micro- or nanofluidic devices mass transport occurs due to the combination of molecular diffusion, passive transport arising from complicated force fields, and hydrodynamic solvent flow fields. Consequently, various forces act on the particles which together add up to the most general external force $\mathbf{f}(\mathbf{q})$. According to the Helmholtz decomposition any twice continuously differentiable vector field $\mathbf{f}(\mathbf{q})$ can be decomposed into a curl-free and a divergence-free component:

$$\mathbf{f}(\mathbf{q}) = -\boldsymbol{\nabla}\Phi(\mathbf{q}) + \boldsymbol{\nabla} \times \boldsymbol{\Psi}(\mathbf{q}). \tag{4.1}$$

Thereby, $\Phi(\mathbf{q})$ denotes the scalar potential

$$\Phi(\mathbf{q}) = \frac{1}{4\pi} \int_V \frac{\boldsymbol{\nabla}_{\mathbf{q}'} \cdot \mathbf{f}(\mathbf{q}')}{\|\mathbf{q} - \mathbf{q}'\|} \, \mathrm{d}V' - \frac{1}{4\pi} \int_S \frac{\mathbf{f}(\mathbf{q}') \cdot \mathrm{d}\mathbf{S}'}{\|\mathbf{q} - \mathbf{q}'\|}, \tag{4.2}$$

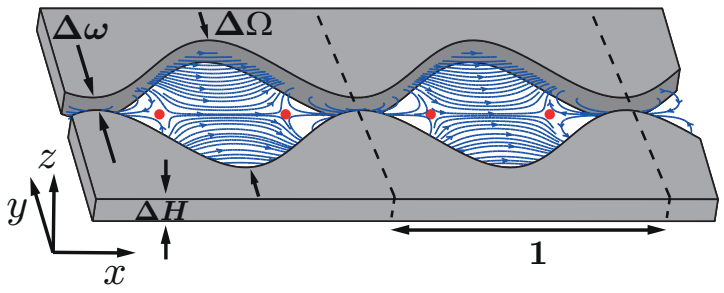

Figure 4.3.: Sketch of a segment of a reflection-symmetric sinusoidally varying channel that is confining the motion of overdamped, point-like Brownian particles. The periodicity of the channel structures is unity, ΔH represents the channel height, and the minimal and maximal channel widths are $\Delta\omega$ and $\Delta\Omega$, respectively. The size of a unit cell is indicated with the dashed lines. Superimposed is an exemplary force field $\mathbf{f}(\mathbf{q})$ which contains vortices and stagnation points (solid circles).

and $\mathbf{\Psi}(\mathbf{q})$ is the vector potential

$$\mathbf{\Psi}(\mathbf{q}) = \frac{1}{4\pi}\int_V \frac{\boldsymbol{\nabla}_{\mathbf{q}'}\times\mathbf{f}(\mathbf{q}')}{\|\mathbf{q}-\mathbf{q}'\|}\,\mathrm{d}V' + \frac{1}{4\pi}\int_S \frac{\mathbf{f}(\mathbf{q}')\times\mathrm{d}\mathbf{S}'}{\|\mathbf{q}-\mathbf{q}'\|}. \tag{4.3}$$

Thus far, the Fick-Jacobs approach has mainly been limited to energetic potentials generating conservative forces on the particles, as given by the first term in Eq. (4.1). In what follows, we overcome this restriction by extending the FJ formalism to the most general external force $\mathbf{f}(\mathbf{q})$, Eq. (4.1), exerted on particles.[2]

4.1. Fick-Jacobs approach to vector potentials

We start by considering the dynamics of point-like, spherical Brownian particles at position $\mathbf{q} = (x, y, z)^T$ moving under the action of a most general, static force field $\mathbf{f}(\mathbf{q})$ Eq. (4.1) through a planar, three-dimensional channel with unit period and constant height ΔH. The periodically varying side-walls at $y = \omega_+(x)$ and $y = \omega_-(x)$ confine the particle motion, see Fig. 4.3. Assuming throughout (i) dilute particle density, (ii) negligible particle diameter ($d_p \ll \Delta\omega$), and (iii) a strong viscous dynamics, implies that inertial effects, hydrodynamic particle-particle and particle-wall interactions, and the effects that can be initiated by rotation of particles can be neglected [Happel and Brenner, 1965; Maxey and Riley, 1983]. If so, the particles' dynamics is well described by the overdamped Langevin equation[3]

$$\dot{\mathbf{q}}(t) = -\boldsymbol{\nabla}\,\Phi(\mathbf{q}) + \boldsymbol{\nabla}\times\mathbf{\Psi}(\mathbf{q}) + \sqrt{2}\,\boldsymbol{\xi}(t), \tag{4.4}$$

[2] I remark that several results and similar figures presented in this chapter will be published in Martens et al., 2012b.

[3] By passing to dimensionless quantities the energetic potential $\Phi \to \Phi\, k_B T$ and the vector potential $\mathbf{\Psi} \to \mathbf{\Psi}\, k_B T$ are scaled in units of the thermal energy $k_B T$.

with Gaussian random force $\boldsymbol{\xi} = (\xi_x, \xi_y, \xi_z)^T$ obeying $\langle\, \xi_i(t)\xi_j(s)\,\rangle = \delta_{ij}\delta(t-s)$ and $\langle\, \xi_i(t)\,\rangle = 0$; $i, j = x, y$ or z. Although formally Eq. (4.4) is stated for a quiescent liquid, the case of moving solvent can be treated via the term $\boldsymbol{\nabla} \times \boldsymbol{\Psi}(\mathbf{q})$, as discussed later in Sect. 4.2.

At first, we aim an approximated one-dimensional description of the above stated 3D problem, Eq. (4.4). In the spirit of the Fick-Jacobs approach, we consider the corresponding Smoluchowksi equation for the stationary joint PDF $P\,(\mathbf{q})$, Eq. (3.5a), and perform asymptotic perturbation analysis, cf. Sect. 3.1, in the expansion parameter ε, Eq. (3.1), to the problem. Therefore, we measure the transverse quantities in ε, i.e., $y \to \varepsilon\, y$ and $\omega_\pm(x) \to \varepsilon\, h_\pm(x)$, and expand the stationary joint PDF $P(\mathbf{q}) = P_0(\mathbf{q}) + \varepsilon^2\, P_1(\mathbf{q}) + O(\varepsilon^4)$ and similar $\Phi(\mathbf{q}) = \Phi_0(\mathbf{q}) + O(\varepsilon^2)$ in a series in even orders of ε. Due to the invariance of $\boldsymbol{\nabla} \times \boldsymbol{\Psi}$ under the scaling in y, the series expansion of the vector potential reads $\boldsymbol{\Psi}(\mathbf{q}) = (\varepsilon\Psi_0^x + O(\varepsilon^3), \Psi_0^y + O(\varepsilon^2), \varepsilon\Psi_0^z + O(\varepsilon^3))^T$. Substituting this ansatz into the stationary Smoluchowksi equation

$$0 = -\boldsymbol{\nabla} \cdot \mathbf{J}(\mathbf{q}), \quad \text{where} \quad \mathbf{J} = \left[-\boldsymbol{\nabla}\, \Phi(\mathbf{q}) + \boldsymbol{\nabla} \times \boldsymbol{\Psi}(\mathbf{q})\right] P - \boldsymbol{\nabla} P, \tag{4.5}$$

together with the no-flux boundary condition $\mathbf{J} \cdot \mathbf{n} = 0$, we obtain a hierarchic set of partial differential equations. With the conditions that (i) the x-component of $(\boldsymbol{\nabla} \times \boldsymbol{\Psi}_0(\mathbf{q}))$ is periodic in x with unit period and (ii) its z-component $(\boldsymbol{\nabla} \times \boldsymbol{\Psi}_0(\mathbf{q}))_z$ vanishes at the upper and lower confining boundary, i.e., for $z = 0, \Delta H$, the stationary marginal PDF yields

$$p_0(x) = \frac{e^{-\mathcal{F}(x)} \int_x^{x+1} \mathrm{d}x'\, e^{\mathcal{F}(x')}}{\int_0^1 \mathrm{d}x\, e^{-\mathcal{F}(x)} \int_x^{x+1} \mathrm{d}x'\, e^{\mathcal{F}(x')}}. \tag{4.6}$$

Here, $\mathcal{F}(x)$ is the *generalized* potential of mean force, reading

$$\begin{aligned} \mathcal{F}(x) = &-\ln\left[\int_{h_-(x)}^{h_+(x)} \mathrm{d}y \int_0^{\Delta H} \mathrm{d}z\, e^{-\Phi_0(\mathbf{q})}\right] \\ &- \int_0^x \mathrm{d}x' \int_{h_-(x')}^{h_+(x')} \mathrm{d}y \int_0^{\Delta H} \mathrm{d}z\, \left(\boldsymbol{\nabla} \times \boldsymbol{\Psi_0}\right)_x P_{\mathrm{eq}}(y, z|x'), \end{aligned} \tag{4.7}$$

where $P_{\mathrm{eq}}(y, z|x) = e^{-\Phi_0(\mathbf{q})} \Big/ \int_{h_-(x)}^{h_+(x)} \mathrm{d}y \int_0^{\Delta H} \mathrm{d}z\, e^{-\Phi_0(\mathbf{q})}$ is the equilibrium PDF of y and z, conditioned on x. The derivation of Eq. (4.6) is presented in depth in App. B.

Note that a closed-form expression for $p_0(x)$ exists only if the scalar potential is either independent of the x-coordinate or scales linearly with x, and if and only if the longitudinal coordinate x is not multiplicatively connected to the transverse coordinates. Further, Eq. (4.6) is only valid if the generalized potential of mean force fulfills the condition $\Delta\mathcal{F} = \mathcal{F}(x+1) - \mathcal{F}(x) \neq 0$. For $\Delta\mathcal{F} = 0$, the stationary joint PDF is con-

stant, $P_0(\mathbf{q}) = const$, and the marginal PDF scales with the local channel cross-section $p_0(x) \propto Q(x)$.

We reveal that the generalized potential of mean force $\mathcal{F}(x)$ comprises the known effective entropic potential $A(x)$ (the logarithmic term), Eq. (2.35), caused by the non-holonomic constraints stemming from the boundaries, see Sect. 2.3.1, and the newly energetic contribution, the part stemming from $\mathbf{\Psi}_0$. The latter is associated with the conditional average of the x-component of the divergence-free forces exerted on the particle weighted by its equilibrium conditional PDF $P_{\mathrm{eq}}(y, z|x)$. In the absence of divergence-free forces, Eqs. (4.6) and (4.7) reduce to the commonly known results of the Fick-Jacobs approximation, cf. Eqs. (3.22) and (2.35).

The kinetic equation for the time-dependent marginal PDF $p_0(x, t)$ can be deduced from its steady state solution, Eq. (4.6), resulting in the *generalized* Fick-Jacobs equation

$$\partial_t p_0(x,t) = \partial_x \left[\frac{\mathrm{d}\,\mathcal{F}(x)}{\mathrm{d}\,x}\; p_0(x,t) \right] + \partial_x^2 p_0(x,t). \tag{4.8}$$

We evaluate the stationary average particle current by making use of the well-known Stratonovich formula [Stratonovich, 1958], to yield

$$\langle\, \dot{x} \,\rangle_0 = \frac{1 - e^{\Delta\mathcal{F}}}{\int\limits_0^1 \mathrm{d}x\; e^{-\mathcal{F}(x)} \int\limits_x^{x+1} \mathrm{d}x'\, e^{\mathcal{F}(x')}}. \tag{4.9}$$

The effective diffusion coefficient (in units of the bulk diffusivity D^0) is calculated via the first two moments of the first passage time distribution, cf. Sect. 2.5:

$$D_{\mathrm{eff}}/D^0 = \frac{\int\limits_0^1 \mathrm{d}x\, e^{\mathcal{F}(x)} \int\limits_x^{x+1} \mathrm{d}x'\; e^{\mathcal{F}(x')} \left[\int\limits_{x-1}^{x} \mathrm{d}x'\, e^{-\mathcal{F}(x')} \right]^2}{\left[\int\limits_0^1 \mathrm{d}x\; e^{\mathcal{F}(x)} \int\limits_{x-1}^{x} \mathrm{d}x'\, e^{-\mathcal{F}(x')} \right]^3}. \tag{4.10}$$

4.2. Poiseuille flow in shape-perturbated channels

Generally, the external force consists of two terms, Eq. (4.1), and the interpretation of results based on Eq. (4.7) may be not straightforward. To elucidate the newly obtained contribution and make comparison with previous results more transparent, we apply the developed approach to Brownian motion under the influence of both, an external constant bias with magnitude f in x-direction and the Stokes drag force caused by the difference between the particle velocity $\dot{\mathbf{q}}$ and the instantaneous solvent flow field in the absence of the particle $\mathbf{u}(\mathbf{q}, t)$. Accordingly, the particle dynamics is determined by

$$\dot{\mathbf{q}}(t) = f\,\mathbf{e}_x + \mathbf{u}(\mathbf{q},t) + \sqrt{2}\,\boldsymbol{\xi}(t), \tag{4.11}$$

with scalar potential $\Phi(\mathbf{q}) = -f\,x$ and vector potential $\mathbf{u}(\mathbf{q}, t) = \boldsymbol{\nabla} \times \mathbf{\Psi}(\mathbf{q})$.

In the equation of motion for a spherical particle, Eq. (4.11), we disregard the effects of solvent inertia $\propto \dot{\mathbf{u}}$, including those described by the Basset history term; added mass force; and Saffman lift force [Saffman, 1965], effects that can be initiated by rotation of particles (e.g., Magnus force, modified drag, and rotational Brownian diffusion [Favro, 1960]), particle acceleration, the Oseen correction [Faxen, 1922; Oseen, 1910] to the Stokes drag, side forces due to shear of the undisturbed flow, etc. [Hess and Klein, 1983; Maxey and Riley, 1983, see references within]. All these effects are small compared to the Stokes drag force with the assumption of low Reynolds number Re (laminar solvent flow) and for particle with density ρ_p comparable to the solvent's density ρ_f. Additionally, our model implies one-way coupling between the solvent and the particles, i.e., the particle dynamics is influenced by the solvent flow but not *vice versa*. To be precise, we suppose that $\mathbf{u}$ is superimposed and is not affected by the particle motion [Straube, 2011]. This is ensured by the adopted assumption of the dilute suspension and negligible particle size, $d_p \ll \Delta\omega$ [Faxen, 1922]. Furthermore, we emphasize that the Stokes drag formula is only valid in infinite containers in which the solvent moves very slowly. Hence, for microfluidic systems the formula is solely applicable for low Reynolds numbers, $Re \ll 1$, and given that the spherical particle is moving at distances several times their diameter away from the channel walls [Bruus, 2008].

The time and spatial evolution of the fluid with density ρ_f is determined by the dimensionless Navier-Stokes equation (NSE) [Landau and Lifschitz, 1991]

$$Re\,\{\partial_t \mathbf{u}(\mathbf{q},t) + (\mathbf{u}\cdot\boldsymbol{\nabla})\,\mathbf{u}(\mathbf{q},t)\} = -\boldsymbol{\nabla}\mathcal{P}(\mathbf{q},t) + \triangle\mathbf{u}(\mathbf{q},t)\,, \tag{4.12}$$

where $\triangle$ is the Laplace operator, $\mathbf{u} = (u^x, u^y, u^z)^T$ denotes the solvent flow field in units of L/τ, $\mathcal{P}(\mathbf{q},t)$ is the sum of the hydrodynamic and hydrostatic pressures in units of η/τ, and the Reynolds number $Re = \rho_f L^2/(\eta\tau)$. Here, we presume that the solvent viscosity η is independent of the channel's dimensions like it is true for most microfluidic devices [Gravesen et al., 1993]. The NSE is composed of the convective acceleration term $(\mathbf{u}\cdot\boldsymbol{\nabla})\,\mathbf{u}$, which is caused by the change in velocity over position, the pressure gradient $\boldsymbol{\nabla}\mathcal{P}(\mathbf{q},t)$, and the internal friction is described by the term $\triangle\mathbf{u}(\mathbf{q},t)$. Sometimes additional body forces that act on a unit volume of fluid ΔV must be taken into account in Eq. (4.12). These body forces are often so-called conservative forces and may be represented as the gradient of some scalar quantity. This implies that solving the NSE without body force $\mathbf{f}_{\text{ext}}$ can be mended by introducing an *effective* local pressure field $-\boldsymbol{\nabla}\mathcal{P}_{\text{eff}}(\mathbf{q},t) = -\boldsymbol{\nabla}\mathcal{P}(\mathbf{q},t) + \mathbf{f}_{\text{ext}}/\Delta V$.

Assuming conservation of mass and the constraint that the solvent density ρ_f remains constant within a moving unit volume of fluid, the continuity equation for an incompressible flow reads

$$\boldsymbol{\nabla}\cdot\mathbf{u}(\mathbf{q},t) = 0. \tag{4.13}$$

The fluid flow field may obeys the slip or so-called Navier boundary conditions at every point of the boundary

$$\mathbf{u}(\mathbf{q},t) - \mathbf{u}_{\text{wall}}(\mathbf{q},t) = \lambda_s \frac{\partial\,\mathbf{u}(\mathbf{q},t)}{\partial\,n}\,, \quad \forall\,\mathbf{q} \in \text{channel wall}, \tag{4.14}$$

where λ_s is the slip length or Navier length and $\partial\mathbf{u}/\partial n = (\mathbf{n}\cdot\boldsymbol{\nabla})\mathbf{u}$ represents the gradient perpendicular to the boundary. For typical slip lengths $\lambda_s = 50\,\mathrm{nm} \pm 50\,\mathrm{nm}$ [Joseph and Tabeling, 2005, for water on glas] the right hand side of Eq. (4.14) is negligible if $\Delta\omega \gg \lambda_s$. If so, Eq. (4.14) simplifies to the no-slip bc

$$\mathbf{u}\,(\mathbf{q},t) = 0, \quad \forall\,\mathbf{q} \in \text{channel wall}, \tag{4.15}$$

for a resting wall $\mathbf{u}_{\text{wall}}\,(\mathbf{q},t) = 0$. In what follows, we employ the no-slip bc to the discussed problem since we solely consider micro-sized fluidic systems. For nanofluidic devices slip bcs, Eq. (4.14), have to be considered.

Bearing in mind microfluidic applications, for most devices with rectangular cross-section the aspect ratio of the transverse length scales can often be so large that the channel is well approximated by an infinite parallel-plate configuration $\Delta H \gg \Delta\Omega$. Then, the velocity profiles for u^x and u^y are flat in the wide direction except near the walls, cf. Fig. C.2. By rotation, this situation can always be realized in experiments for any shape of the cross-section. On contrary, if both length scales are of the same size the best we can do analytically is to find a Fourier sum representation of the solution for weakly shape-perturbed channels. Then, the flow components depend on all channel directions. For the interested reader, we present the derivation of an estimate for flow velocities of an incompressible fluid through an arbitrary 3D channel with periodically varying rectangular cross-section in App. C in depth.

If we neglect the top and bottom side walls completely, we arrive at the case of an infinitely high channel. For $\Delta H \gg 1$, the pressure is uniform in wide direction which permits us to integrate $\mathbf{u}(\mathbf{q},t)$ with regard to z and thus to consider the flow field only in x and y-direction. Additionally, from the uniformity of the pressure in z directly follows that $u_z(\mathbf{q}) = 0$. Applying the curl to both sides of Eq. (4.12) results in the elimination of the local pressure $p(\mathbf{r})$. Then, the NSE for incompressible flows degrades into one equation

$$Re\,\{\partial_t \triangle\,\Psi + \partial_y\Psi\,\partial_x\,(\triangle\Psi) - \partial_x\Psi\,\partial_y\,(\triangle\Psi)\} = \triangle^2\,\Psi, \tag{4.16}$$

for the stream function $\Psi(x,y)$, $\boldsymbol{\Psi} = \Psi(x,y)\,\mathbf{e}_z$. Here $\triangle^2 = \boldsymbol{\nabla}^4$ is the biharmonic operator. Defining the stream function through $u^x = \partial_y\Psi$ and $u^y = -\partial_x\Psi$ results in continuity equation, Eq. (4.13), being unconditionally satisfied. In order to solve Eq. (4.16), one has to take account of the no-slip bcs, $\partial_y\Psi = 0$ at $y = \omega_\pm(x)$, and of the conditions specifying the flow discharge, $\Psi = 0$ at $y = \omega_-(x)$ and $\Psi = -\Delta p/(12\langle W^{-3}(x)\rangle_x)$ at $y = \omega_+(x)$ [Kettner et al., 2000; Kitanidis and Dykaar, 1997; Mortensen et al., 2005]. In analogy to the derivation of the generalized FJ equation, we measure all transverse quantities in units of the expansion parameter ε which results in $y \to \varepsilon y$, $\partial_y \to \varepsilon^{-1}\partial_y$, and $\Psi \to \varepsilon\Psi$. Substituting the expansion of Ψ into Eq. (4.16) yields $0 = \partial_y^4\Psi_0(x,y) + O(\varepsilon^2)$. After tedious calculations, we finally obtain

$$\Psi_0(x,y) = -\frac{\mathcal{P}_0'(x)}{12}\,(y-\omega_-(x))^2\,(3\,\omega_+(x) - \omega_-(x) - 2y)\,. \tag{4.17a}$$

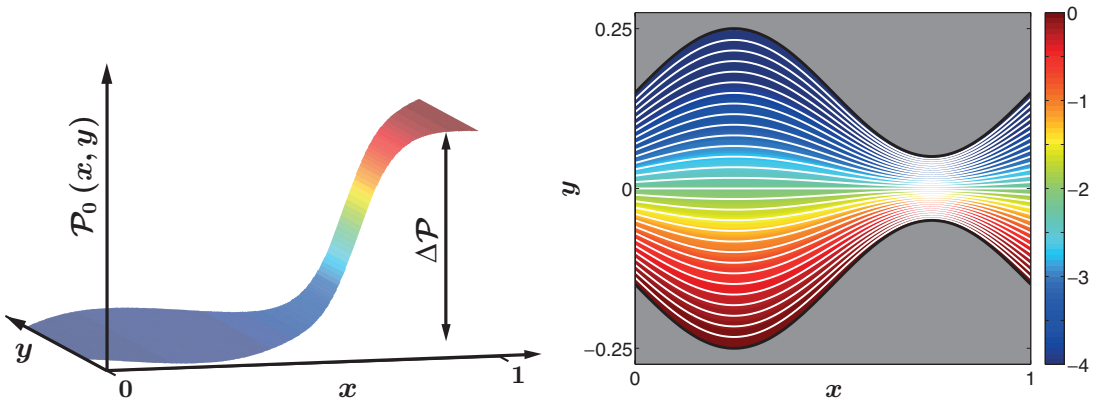

Figure 4.4.: The leading order solutions for the locale pressure $\mathcal{P}_0(x,y)$ (left panel) and the flow velocity field $\mathbf{u}_0(x,y) = (u_0^x, u_0^y)^T$ (right panel) are depicted. The associated stream function is indicated by the colored background where blue represents small values and red high values of Ψ_0. The chosen channel parameters are $\Delta\Omega = 0.5$ and $\Delta\omega = 0.1$.

The solution for the flow field components reads

$$\partial_y \Psi_0 = u_0^x(x,y) = -\frac{\mathcal{P}_0'(x)}{2}\left(\omega_+(x) - y\right)\left(y - \omega_-(x)\right), \tag{4.17b}$$

$$-\partial_x \Psi_0 = u_0^y(x,y) = \frac{1}{12}\partial_x\left[\mathcal{P}_0'(x)\left(y-\omega_-(x)\right)^2\left(3\omega_+(x) - \omega_-(x) - 2y\right)\right], \tag{4.17c}$$

and the local pressure is given by

$$\mathcal{P}_0(x,y) = \Delta\mathcal{P}\,\frac{\int_0^x \mathrm{d}x'\, W(x)^{-3}}{\int_0^1 \mathrm{d}x\, W(x)^{-3}}, \tag{4.17d}$$

plus an additive constant which can be set to zero. Thereby, the change of pressure along one unit cell is denoted by $\Delta\mathcal{P} = \mathcal{P}(x+1,y) - \mathcal{P}(x,y)$ and $W(x) = \omega_+(x) - \omega_-(x)$ is the local width. Note that we scaled the transverse quantities back in order to enhance the readability. We emphasize that both the time derivative and the convective advection term are proportional to $Re\,\varepsilon^2$. Therefore, as long as the product is small $Re\,\varepsilon^2 \ll 1$, the left hand side in Eqs. (4.12) and (4.16) can be disregarded, which leaves us with the Stokes equation, respectively, the so-called "creeping flow" equation [Landau and Lifschitz, 1991]. In most microfluidic applications $Re \ll 1$. Because of the smallness of the Reynolds number most well known flow instabilities leading to period doubling [von Stamm et al., 1996], chaos [Hall and Papageorgiou, 1999], turbulence [Karniadakis and Triantafyllou, 1992], and the formation of eddies [Oliveira et al., 2008] are absent. Beside the absence of flow instabilities, low Reynolds number $Re \ll 1$ is even more essential to safely disregard many forces exerted by the fluid on a spherical particle.

Note that in the limit of straight channels $W(x) = \Delta\Omega$, Eqs. (4.17b)-(4.17d) give the known Poiseuille flow results $u^x(x,y) = -\Delta\mathcal{P}\,(y^2 - (\Delta\Omega/2)^2)/2$, $u^y(x,y) = 0$, and $\mathcal{P}(x,y) \sim \Delta\mathcal{P}\,x$ between two flat walls at $y = \omega_\pm = \pm\Delta\Omega/2$. According to Eq. (4.17b), the longitudinal flow component u_0^x is inversely proportional to the third power of the local channel width $W(x)$ for arbitrary boundary functions $\omega_\pm(x)$. Consequently, u_0^x attains its maximum values at the bottlenecks where the gradient of the local pressure is maximal $\partial_x \mathcal{P}_0(x,y) \propto W(x)^{-3}$. Interestingly, the local pressure sharply increases, respectively, decreases at the channel bottlenecks instead of the linear growth which is known for straight channels, see Fig. 4.4. Further, the flow velocity in longitudinal direction is limited from above by the value $\max(|u_0^x|) \leq |\Delta\mathcal{P}|\,(\Delta\Omega)^3/(8\,\Delta\omega)$. Consequently, the flow velocity grows with lessening bottleneck width.

As mentioned previously, various forces exerted on a spherical particle can be safely disregarded under the assumption of low Reynolds number Re. Usually the Reynolds number is defined as $Re = \rho_f\, V_0\, L_0/\eta$, where L_0 is a characteristic length scale and V_0 is a characteristic velocity scale. Following the convention that the Reynolds number should contain the smallest length scale of the system, here $\Delta\omega$, we evaluating Re at the channel bottleneck where the longitudinal flow component is the strongest, resulting in $Re = \rho_f\,|\Delta\mathcal{P}|\,(\Delta\Omega)^3/(8\eta^2\,L)$ in dimensional units. If we claim that the Reynolds number is small [Gravesen et al., 1993], $Re < 1$, we obtain an upper limit for the applied pressure drop, viz.,

$$\Delta\mathcal{P} < 10\,\mathrm{kPa}, \tag{4.18}$$

for typical channel parameters $L = 100\,\mu$m, $\Delta\Omega = 50\,\mu$m, see Tab. 5.1, and water as solvent ($\rho_f = 998\,\mathrm{kg/m^3}$ and $\eta = 10^{-3}\,\mathrm{kg/(m\,s)}$) at room temperature $T = 293,15\,$K. We emphasize that even if we suppose that the characteristic length scale equals the unit cell period length, the upper limit for the maximal pressure drop decreases only by one order of magnitude. Furthermore, the characteristic quantities are of the order $\tau = 10^3\,$s, $\langle\, v^0\,\rangle = L/\tau = 0.1\,\mu$m/s, and $\mathcal{P}^{\mathrm{ref}} = \eta/\tau = 1\,\mu$Pa for tracer particles of size $d_p = 0.1\mu$m. Consequently, we can apply pressure drops of the order $|\Delta\mathcal{P}| = 10^{10}$ in our Brownian dynamics simulations without worrying about influences caused by flow instabilities. Lastly, we stress that hydrodynamic acceleration effects like added mass become important only on a time scale of the order $\tau_f \approx 1\,\mathrm{ns} \ll \tau$ for micro-sized particles ($d_p = 0.1\mu$m) in water [Hinch, 1975].

4.3. Example: Transport in sinusoidally varying channels

To elucidate the intriguing feature caused by the divergence-free force, Eqs. (4.17), and its interplay with the constant bias which represents the curl-free force, we limit our consideration to particles moving in our standard example for a 2D channel geometry, viz., the reflection symmetric sinusoidally-shaped channel Eq. (3.52) [Hoagland and Prud'Homme, 1985; Kitanidis and Dykaar, 1997]. All numerical results presented below were obtained by Brownian dynamics simulation of Eq. (4.11) in which the flow field $\mathbf{u}$ was calculated by solving the "creeping flow" equation (right-hand side of Eq. (4.12)) using FEM.

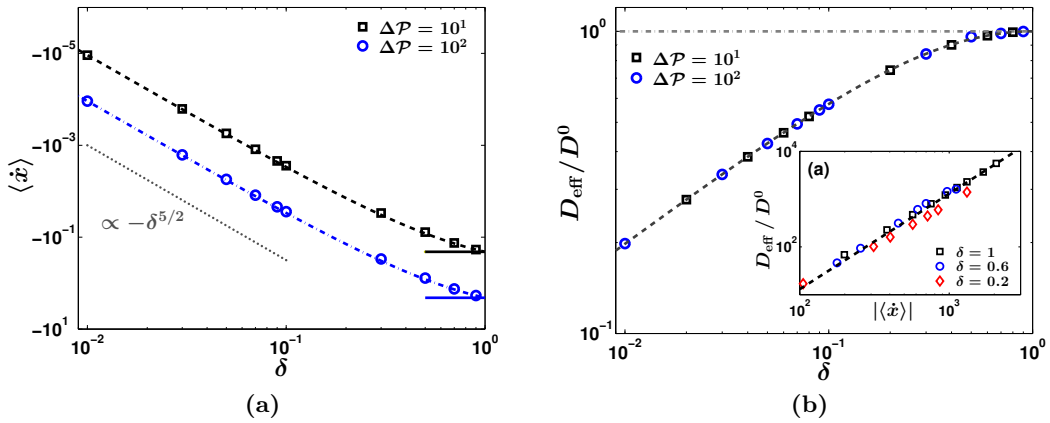

Figure 4.5.: Left panel: Comparison of numerical results from BD simulations for the mean particle current (markers) and the analytic estimate Eq. (4.20) (lines) versus the aspect ratio δ for two different pressure drops $\Delta\mathcal{P}$. The solid lines represent the Poiseuille flow result $\langle\, \dot{x}\, \rangle = -\Delta\mathcal{P}\,(\Delta\Omega)^2/12$. Right panel: Simulation results for the EDC $D_{\rm eff}/D^0$ (markers) as a function of δ. Superimposed is the estimate $D_{\rm eff}/D^0 = 2\sqrt{\delta}/(1+\delta)$ (dashed line). The horizontal dash-dotted line indicates unity. Impact of $|\langle\, \dot{x}\, \rangle|$ on $D_{\rm eff}/D^0$ is presented in inset (a): markers represent numerical results and the estimate $D_{\rm eff}/D^0 \propto (\Delta\Omega\, \langle\, \dot{x}\, \rangle)^2/192$ is indicated by the dashed line. The remaining parameters are $\Delta\Omega = 0.5$ and $f = 0$.

Next, we investigate the dependence of the key transport quantities, such as the average particle velocity $\langle\, \dot{x}\, \rangle$ and the effective diffusion coefficient $D_{\rm eff}/D^0$, on the force magnitude f and the applied pressure drop $\Delta\mathcal{P}$. Both parameters generally control the curl-free and the divergence-free contributions to the force field $\mathbf{f}(\mathbf{q})$, cf. Eq. (4.1).

4.3.1. Purely flow driven transport

First, we shortly discuss the purely flow driven case. In the absence of scalar potentials, $\Phi(\mathbf{q}) = 0$, and in the case of vanishing flow velocity $\mathbf{u} = \boldsymbol{\nabla} \times \boldsymbol{\Psi}$ normal to the channel wall, $\mathbf{u} \cdot \mathbf{n} = 0$, only uniform distributions are allowed, $p(x,y) = 1/\langle\, W(x)\, \rangle_x$. If so, no particle separation could ever be achieved. Any inhomogeneity in the spatial distribution of non-interacting suspended particles can only be caused by hydrodynamic interaction between particles and walls [Happel and Brenner, 1965; Schindler et al., 2007]. In the purely flow driven case the mean particle current is given by

$$\langle\, \dot{x}\, \rangle_0^{\rm flow} = \frac{1}{\langle\, W(x)\, \rangle_x} \int_0^1 \mathrm{d}x \int_{\omega_-(x)}^{\omega_+(x)} \mathrm{d}y\, u_0^x(x,y) = -\frac{\Delta\mathcal{P}}{12\, \langle\, W\, \rangle_x\, \langle\, W^{-3}\, \rangle_x}, \tag{4.19}$$

and, in particular, reads

$$\langle \dot{x} \rangle_0^{\text{flow}} = -\frac{4\,\Delta\mathcal{P}\,(\Delta\Omega)^2\,\sqrt{\delta}^5}{3\,(1+\delta)\,(3+2\delta+3\delta^2)}, \quad \text{for } f=0, \tag{4.20}$$

for the considered channel geometry Eq. (3.52). We obtain that the mean particle current is proportional to $\Delta\Omega^2$ and scales linearly with the applied pressure drop $\Delta\mathcal{P}$. For $\Delta\mathcal{P} < 0$ the solvent flows left to right and *vice versa* for $\Delta\mathcal{P} > 0$. Figure 4.5 (a) shows that $\langle \dot{x} \rangle_0^{\text{flow}} \propto \delta^{5/2}$ for $\delta \ll 1$ and that the latter converges to the Poiseuille result for $\delta = 1$, viz., $\langle \dot{x} \rangle^{\text{Pois}} = -\Delta\mathcal{P}\,(\Delta\Omega)^2/12$. The variations in the flow field at the microscale contribute significantly to the macroscale effective diffusion coefficient D_{eff}/D^0. For sufficiently small pressure drops $|\Delta\mathcal{P}|$ or, equivalently, slow mean particle velocity, $\langle \dot{x} \rangle \lesssim 1$, the particles' dynamics is dominated by diffusion. Hence, the EDC starts from the value of $D_{\text{eff}}/D^0 = 2\sqrt{\delta}/(1+\delta)$, Eq. (3.47), see Fig. 4.5 (b). With growing pressure drop which leads to higher flow velocity, the EDC exhibits Taylor-Aris dispersion [Aris, 1956; Taylor, 1953] regardless of the channel constriction, i.e., $D_{\text{eff}}/D^0 \propto (\Delta\Omega\,\langle \dot{x} \rangle)^2/192$ for $\langle \dot{x} \rangle \gg 1$. This fact is presented in the inset of Fig. 4.5 (b). Due to the invariance of the effective diffusivity under the transformation $\langle \dot{x} \rangle \to -\langle \dot{x} \rangle$, one observes the same dependence of D_{eff}/D^0 on the pressure drop for $\Delta\mathcal{P} < 0$ (not shown).

The opposite limit of solely curl-free forces was previously discussed in detail in Sect. 3.2. Analytic results for the mean particle current and the EDC are known.

4.3.2. Interplay of solvent flow and external forcing

Below, we study the interplay of both the external bias and the Stokes drag acting on the Brownian particles. Because all required conditions for the derivation of the generalized FJ equation are fulfilled, cf. App. B, the studied problem of forced Brownian dynamics in a confined 2D geometry can by replaced by Brownian motion in the tilted, periodic potential of mean force Eq. (4.7); yielding

$$\mathcal{F}(x) = -f\,x - \ln\left[2\,\omega(x)\right] - \int_0^x \mathrm{d}x' \int_{-\omega(x')}^{\omega(x')} \mathrm{d}y\, \frac{u_0^x(x',y)}{2\,\omega(x')}\,. \tag{4.21}$$

In Fig. 4.6, we present the impact of the external bias and the solvent flow ($\Delta\mathcal{P}$) on the steady state marginal PDF. If the Brownian particles experience solely the Stokes drag force, $f = 0$, the stationary joint PDF simplifies to $p(x,y) = 1/\langle W(x) \rangle_x$ and thus the stationary marginal PDF scales with the local channel width $p(x) \propto W(x)$. In the opposite limit of biased transport in a resting solvent, $\Delta\mathcal{P} = 0$, the particles accumulate at the channel bottleneck. Thus, $p(x)$ exhibits an uneven shape whose maximum is shifted towards the constricting part of the channel. If both forces are acting simultaneously but in opposite directions, i.e, $f > 0$ and $\Delta\mathcal{P} > 0$, the large longitudinal flow velocities lead to the appearance of vortices in total force field $f\mathbf{e}_x + \mathbf{u}$ near the bottleneck, see Fig. 4.8. Obviously, the force field points oppositely to the external bias near the vortices. As a consequence, the bias-induced accumulation of

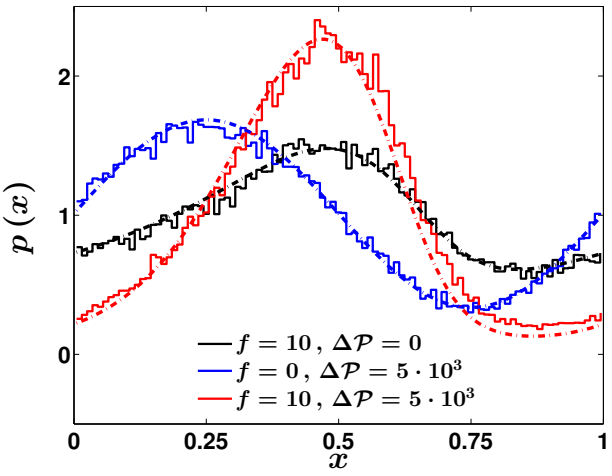

Figure 4.6: Stationary marginal PDF $p(x)$ as a function of force magnitude f and pressure drop $\Delta\mathcal{P}$. Numerical results are represented by staircase like solid lines whereas dashed-dotted lines correspond to general FJ solution $p_0(x)$, cf. Eq. (4.6). The channel parameter values are $\Delta\Omega = 0.5$ and $\Delta\omega = 0.1$.

particles at the bottleneck is inhibited, cf. Fig. 3.4(iii). Since the vortex size grows with the applied pressure drop, the maximum of the stationary marginal PDF shifts towards the left with $\Delta\mathcal{P}$. Additionally, one observes that the peak height grows with the pressure drop indicating accumulation of particles. Notably, the numerical results are well reproduced by the generalized FJ solution, Eq. (4.6), even for moderate corrugated channels $\varepsilon = 0.4$, cf. Fig. 4.6.

Figure 4.7 shows the impact of the pressure drop $\Delta\mathcal{P}$ on the mean particle current (left panel) for different values of external bias f. Only at $f = 0$, $\langle \dot{x} \rangle = \langle \dot{x} \rangle_0^{\text{flow}}$, cf. Eq. (4.20), is point symmetric with respect to $\Delta\mathcal{P}$. The behavior changes drastically for $f \neq 0$. For $\Delta\mathcal{P} < 0$ with $|\Delta\mathcal{P}| \gg 1$, u^x and f are both positive, the Stokes drag force dominates over the constant bias and thus $\langle \dot{x} \rangle \simeq \langle \dot{x} \rangle_0^{\text{flow}} \propto -\Delta\mathcal{P}$. The increase in $\Delta\mathcal{P}$ results in a systematic crossover from flow driven transport to biased entropic transport. We observe a broad range of $|\Delta\mathcal{P}|$ values in which the presence of the flow is insignificant and thus $\langle \dot{x} \rangle$ remains almost constant. In this interval the external bias dominates and hence $\mathcal{F}(x)$ is approximately given by $\mathcal{F}(x) \simeq -f\,x - \ln[2\omega(x)]$. According to Eq. (4.9), the mean particle current reads

$$\langle \dot{x} \rangle_0^{\text{ent}} = f\,\mu_0(f)/\mu^0 = \frac{f^3 + (2\pi)^2\, f}{f^2 + \frac{1}{2}\,(2\pi)^2 \left\{ \sqrt{\frac{\Delta\Omega}{\Delta\omega}} + \sqrt{\frac{\Delta\omega}{\Delta\Omega}} \right\}}, \quad \text{for } \Delta\mathcal{P} = 0, \tag{4.22}$$

whereas the result for the associated particle mobility was previously presented in Eq. (3.61). The width of the interval where $\langle \dot{x} \rangle \simeq \langle \dot{x} \rangle_0^{\text{ent}}$ holds, scales linearly with f. With further growing pressure drop $\Delta\mathcal{P} \gg 1$ – the solvent flow $u_0^x < 0$ drags the particles in opposite direction to the external force $f > 0$ – one notices that a sharp jump of $\langle \dot{x} \rangle$ from positive to negative velocities occurs. In other words, the particle current reverses its direction. Although strong non-vanishing local forces $f\mathbf{e}_x + \mathbf{u}(x, y)$ are acting on the particles, there exists a critical ratio of force magnitude to applied pressure drop $(f/\Delta\mathcal{P})_{\text{crit}}$ such that $\langle \dot{x} \rangle = 0$. As follows from Eq. (4.9), this occurs if

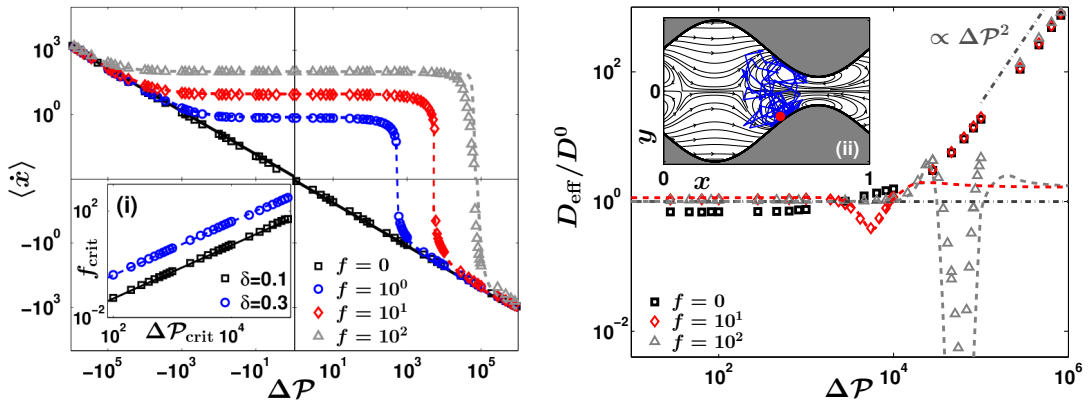

Figure 4.7.: Results for BD simulations in a channel geometry like Fig. 4.3 with $\Delta\Omega = 0.5$ and $\Delta\omega = 0.1$. Left: Mean particle current $\langle \dot{x} \rangle$ versus pressure drop $\Delta\mathcal{P}$ for different force magnitudes f. The solid line indicate the analytic estimate for $f = 0$, Eq. (4.20), and the dashed lines correspond to Eq. (4.9). Comparison of numerics (markers) and Eq. (4.23) (lines) for the critical force magnitude $f_{\rm crit}$ versus $\Delta\mathcal{P}_{\rm crit}$ is presented in the inset (i). Right: $D_{\rm eff}/D^0$ as a function of $\Delta\mathcal{P}$ for various values of f. The dashed lines represent the numerical evaluation of Eq. (4.10) and the horizontal dash-dotted line is for $D_{\rm eff} = D_0$. Exemplary trajectory corresponding to HEET ($f = 10^2$ and $\Delta\mathcal{P} = 6.5 \cdot 10^4$) of a point-like Brownian particle (red circle) is depicted in inset (ii).

$\Delta\mathcal{F} = 0$, yielding for the critical ratio

$$\left(\frac{f}{\Delta\mathcal{P}}\right)_{\rm crit} = \frac{1}{12}\frac{\langle W(x)^{-1}\rangle_x}{\langle W(x)^{-3}\rangle_x} = \frac{2\,\Delta\Omega^2\,\delta^2}{3\,(3+2\delta+3\delta^2)}. \tag{4.23}$$

The critical ratio is solely determined by the channel geometry, see Fig. 4.7(i). Especially, the smaller the maximum channel width the less is the ratio $f/\Delta\mathcal{P}$ in order to inhibit particle transport for a given aspect ratio δ. While $(f/\Delta\mathcal{P})_{\rm crit}$ goes to zero for almost closed channels $\delta \to 0$, Eq. (4.23) resembles the Poiseuille flow result $f/\Delta\mathcal{P} = \Delta\Omega^2/12$ for straight channels $\delta = 1$. Finally, upon further increasing pressure drop, the flow-induced drag force starts to dominate over the external bias again and thus we observe $\langle \dot{x} \rangle \approx \langle \dot{x} \rangle_0^{\rm flow} \propto -\Delta\mathcal{P}$. In Fig. 4.7, we compare the numerically evaluated results for Eq. (4.9) with the predictions of Eq. (4.21) (dashed lines). In compliance with the very good agreement between the leading order estimates for the marginal PDF and the numerics we observe that the mean particle current is also strikingly well reproduced by the generalized potential of mean force.

4.3.3. Hydrodynamically enforced entropic trapping

The role of $\Delta\mathcal{P}$ and f on the EDC $D_{\rm eff}/D^0$ is presented in the right panel of Fig. 4.7. As previously mentioned, in the purely flow driven case, $f = 0$ (squares), the EDC starts from the value of $D_{\rm eff}/D^0 = 2\sqrt{\delta}/(1+\delta)$ for $\langle \dot{x} \rangle \lesssim 1$, i.e., small $|\Delta\mathcal{P}|$. It exhibits so termed Taylor-Aris dispersion [Aris, 1956; Taylor, 1953] $D_{\rm eff}/D^0 \propto \Delta\mathcal{P}^2$ for $\langle \dot{x} \rangle \gg 1$

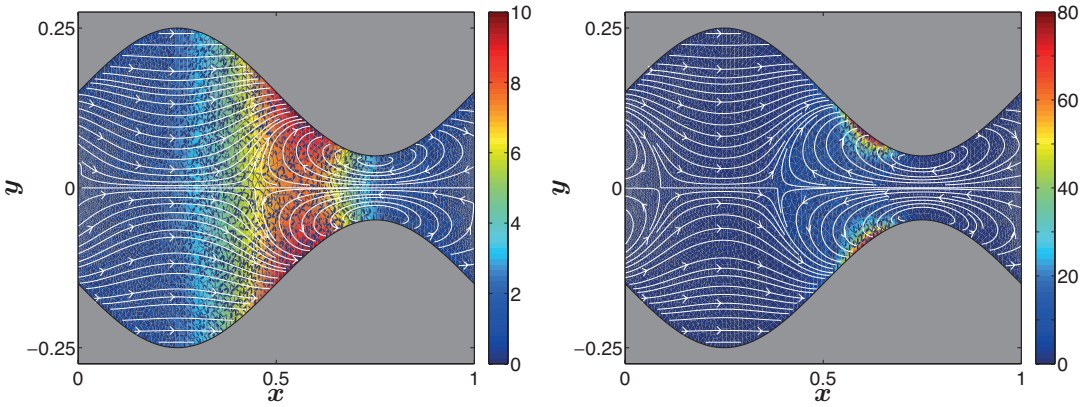

Figure 4.8.: Stationary joint PDF $p(x, y)$ and force field $\mathbf{f}$ (lines) for parameter sets where HEET was observed. Left panel: $f = 10$ and $\Delta\mathcal{P} = 5.5 \cdot 10^3$. Right panel: $f = 100$ and $\Delta\mathcal{P} = 6.5 \cdot 10^4$. The channel parameters are $\Delta\Omega = 0.5$ and $\Delta\omega = 0.1$.

or, equivalently, large $|\Delta\mathcal{P}|$. In the opposite limit of a resting fluid, $\Delta\mathcal{P} = 0$, such that solely static bias induced transport occurs, D_{eff}/D^0 exhibits the known bell shape structure as a function of f, see Sect. 3.2.3.

A new intriguing effect emerges if the Stokes drag ($\mathbf{u}(\mathbf{q})$) and the external force ($f\mathbf{e}_x$) exerted on the particles start to counteract. Especially, if $u^x \propto -\Delta\mathcal{P}$ and f are comparable, but of opposite sign. In this case, their superposition, $\mathbf{f} = f\mathbf{e}_x + \mathbf{u}$, contains stagnation points – points of zero force – and vortices leading to *hydrodynamically enforced entropic trapping* (HEET). We find that at the critical ratio $(f/\Delta\mathcal{P})_{\text{crit}}$, Eq. (4.23), at which the mean particle current vanishes, the EDC displays an abrupt decrease and becomes several magnitudes smaller than the bulk one D^0. Although the particles experience continuous thermal fluctuations, they exhibit long residence times in the regions where the force field pushes the particles against the channel wall, see inset (ii) in Fig. 4.7. In these regions of the channel, we observe strong particle accumulation resulting in a more localized distribution or, equivalently, larger depletion zones., cf. Fig. 4.8. Moreover, one notices that the vortices counteract the focusing structure of the channel. As previously mentioned in Sect. 3.2, one also finds particle accumulation for biased transport in a resting solvent $\Delta\mathcal{P} = 0$. There. the particles follow the force field $\mathbf{f} = f\mathbf{e}_x$ and may slide along the constricting boundary in order to leave the unit cell. This leads to particle accumulation at the bottlenecks and results in an enhancement of the EDC. In flowing solvent, $\Delta\mathcal{P} \neq 0$, the biased particles stick to the boundary and the probability to find a particle at the channel's center line, $y = 0$, is severely reduced which suppresses diffusion.

Particularly, HEET becomes more pronounced for larger f_{crit} and $\Delta\mathcal{P}_{\text{crit}}$, resulting in a stronger localized particle distribution or, equivalently, larger depletion zones, see Fig. 4.8. Therefore, the minimum of D_{eff}/D^0 decreases with the growth in f, cf. Fig. 4.7, leading to a stiffer trap. HEET can be understood in terms of the generalized potential of mean force $\mathcal{F}(x)$. Upon glancing at the energy barrier within one unit cell, $\delta\mathcal{F} = \max(\mathcal{F}(x)) - \min(\mathcal{F}(x))$, we notice that the latter is solely determined by the channel's aspect ratio δ and increases linearly with f_{crit} for $f \gg 1$, cf. Fig. 4.9.

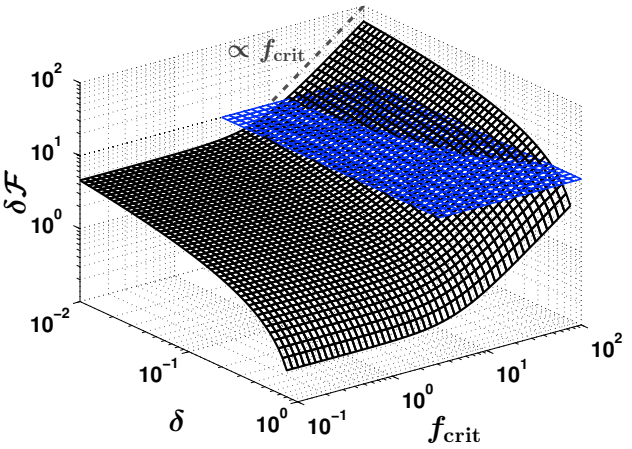

Figure 4.9: Impact of critical force magnitude f_{crit} and aspect ratio δ on the energy barrier within one unit cell $\delta\mathcal{F} = \max(\mathcal{F}(x)) - \min(\mathcal{F}(x))$. The corresponding pressure is determined by Eq. (4.23). The horizontal surface represents $\delta\mathcal{F} = 10$ (in units of k_BT). The chosen channel parameters are $\Delta\Omega = 0.5$ and $\Delta\omega = 0.1$.

Additionally, we compare the numerical results for Eq. (4.10) with Eq. (4.21) (dashed lines) in the right panel of Fig. 4.7. It is demonstrated that the dependence of the EDC on the applied pressure drop is well described by Eq. (4.10) for many values for $\Delta\mathcal{P}$. Especially, one observes a satisfactory agreement for $\langle \dot{x} \rangle \simeq \langle \dot{x} \rangle_0^{\mathrm{entr}}$ and, more importantly, at the minimum of D_{eff}/D^0. Merely for $\Delta\mathcal{P} \gg 1$ where Stokes' drag force dominates and thus the EDC shows Taylor-Aris dispersion, $D_{\mathrm{eff}}/D^0 \propto \Delta\mathcal{P}^2$, not surprisingly, strong deviations occur. On the one hand, the tilt of $\mathcal{F}(x)$ decreases with $\Delta\mathcal{P}$ ($u^x < 0$), and thus the separating energy barrier $\delta\mathcal{F}$ eventually disappears which leads to a directed motion $D_{\mathrm{eff}} \simeq D^0$. On the other hand, Taylor-Aris dispersion is caused by the transverse diffusion that transports the particle among layers with different longitudinal velocities $u_0^x(x,y) \propto (\omega(x)^2 - y^2)$. This microscopic effect is not incorporated in the effective one-dimensional energetic picture.

HEET offers a unique opportunity to efficiently separate particles of the same size based on their different response to applied stimuli, e.g., to sift healthy cells from deceased and dead cells [Becker et al., 1995; Hu et al., 2005; Voldman, 2006]. With regard to Fig. 4.7, even small distinctions in the response can be used to achieve opposite transport directions for those particles by tuning f at a fixed $\Delta\mathcal{P}$ (or, equivalently, $\Delta\mathcal{P}$ at a fixed f) such that their ratio is close to the value given by Eq. (4.23). Figure 4.10 shows the temporal evolution of three different non-interacting particle species starting with delta distribution $p(x,y) = \delta(x - 0.25)\delta(y)$ at $t = 0$. While particles with $f < f_{\mathrm{crit}}$ move to the left, they remain for quite long time within the starting unit cell at $f = f_{\mathrm{crit}}$, and move to the right for $f > f_{\mathrm{crit}}$. Thus, one can efficiently separate particles by adjusting the pressure drop in such a way that the associated critical force strength lays in between the specific species' force magnitudes. Assisted by the suppressed effective diffusion, the marginal PDFs are much narrower compared to the free case at a given time t. In the right panel of Fig. 4.10, we depict the temporal evolution for the probability $P(0 \leq x \leq 1, t)$ of a particle to be found within the starting unit cell at time t. Albeit, strong local forces and continuous fluctuations are acting on the particles, the probability slowly decays for the critical parameter values. In detail, the probability reduces to almost 30% at $t = 100$ which corresponds to one hundred times the characteristic diffusion time τ in dimensional units. For $f < f_{\mathrm{crit}}$ and $f > f_{\mathrm{crit}}$,

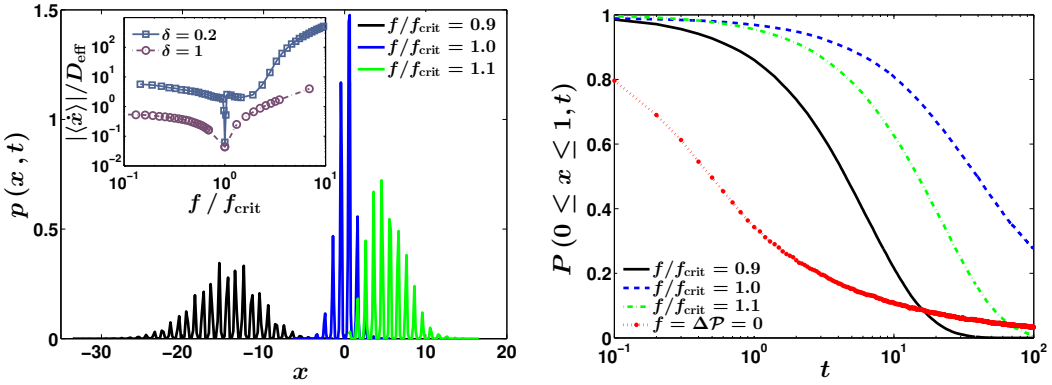

Figure 4.10.: Left panel: Snapshot of marginal PDF $p(x,t)$ at $t = 100$ for different force strengths f in units of $f_{\mathrm{cr}} = 100$ in a corrugated channel with $\Delta\omega = 0.1$. The width of $p(x,t)$ is several magnitudes smaller compared to the case of unbounded geometry $\propto D_0\, t$. Inset: Péclet number $|\langle \dot{x} \rangle|/D_{\mathrm{eff}}$ versus f/f_{cr} for $\delta = 0.2$ and $\delta = 1$ (straight channel). Right panel: Time evolution for probability $P(0 \le x \le 1, t)$ to find a particle within the starting unit cell at time t. Superimposed is the result for purely diffusive particle motion (red dots), i.e., $f = \Delta\mathcal{P} = 0$. The remaining parameter values are $\Delta\Omega = 0.5$, $\Delta\omega = 0.1$, and $\Delta\mathcal{P} = 6.5 \cdot 10^4$.

the probability decays faster, nevertheless, the decrement is much slower compared to diffusion (red dots). There, $P(0 \le x \le 1, t)$ reduces to almost 30% at the characteristic diffusion time $t = 1$.

Importantly, we stress that the converging-diverging nature of the channel geometry, $\delta \neq 1$, is a crucial prerequisite to observe HEET. Despite that for a straight channel ($\delta = 1$) a critical force magnitude also can be found where the transport direction reverses, viz., $f_{\mathrm{crit}} = -\langle \dot{x} \rangle^{\mathrm{Pois}}$, the force field $\mathbf{f}(\mathbf{q})$ lacks vortices which are responsible for particle accumulation. As a result, the effective diffusion coefficient behaves like $D_{\mathrm{eff}}/D^0 = 1 + (\Delta\Omega \langle \dot{x} \rangle^{\mathrm{Pois}})^2/192$ and it is bounded from below by the value of bulk diffusivity, $D_{\mathrm{eff}} \ge D^0$. Consequently, HEET is impossible and the Péclet number $|\langle \dot{x} \rangle|/D_{\mathrm{eff}}$, which quantifies the transport of the objects, is strongly reduced compared to channels with finite corrugation, $\delta \neq 1$, cf. inset in Fig. 4.10. Note that in contrast to corrugated channels, D_{eff}/D^0 is independent of the external force for $\delta = 1$ since Galilei transformation $x \to x - f\,t$ leaves the latter invariant.

4.4. Summary

Let us summarize our findings presented in this chapter. First, we generalized the Fick-Jacobs approach to the most general force acting on the particle, Eq. (4.1), which can involve both the curl-free and the divergence-free component. In the spirit of chapter 3, we applied asymptotic perturbation analysis in the geometric parameter ε to the problem of Brownian motion in a 3D, planar channel geometry. By doing this, the problem reduces to an effective one-dimensional kinetic system in which the particle dynamics is

determined by the *generalized* potential of mean force $\mathcal{F}(x)$, where x is the coordinate along the channel. The latter comprised the known *entropic* contribution caused by the non-holonomic constraint stemming from the boundaries, which is equivalent to that obtained in Sect. 2.3.1, and a second novel energetic contribution associated with the divergence-free force exerted on the particle. In the absence of divergence-free forces, the leading order solutions resemble the common Fick-Jacobs result.

The interpretation of the leading order results may be not straightforward. To elucidate the intriguing feature caused by the divergence-free force, we applied the developed approach to the problem where Brownian particles are subject to both, an external constant bias f and to a pressure-driven flow controlled by the applied pressure drop $\Delta\mathcal{P}$. The leading order expressions for the local pressure and the solvent's flow components were derived. In particular, we corroborated these results by a specific example, namely, biased particle transport through 2D confinements with sinusoidally modulated width. Analytic estimates for the mean particle current and the effective diffusion coefficient are available in the limiting case of particle diffusion in a moving solvent. Especially, we found that the effective diffusion coefficient (EDC) is solely determined by the aspect ratio δ if the mean solvent velocity is small, however, the EDC shows Taylor-Aris dispersion for high flow velocity.

Intriguing novel effects emerge when the Stokes drag and the external force acts simultaneously but in opposite directions. For example, the mean particle current changes from biased entropic to flow driven transport controlled by the applied pressure drop. Furthermore, during this transition the transport direction reverses. Remarkably, we identified a critical ratio of force magnitude to applied pressure drop, $(f/\Delta\mathcal{P})_{\text{crit}}$, at which the mean particle current turns to zero despite that strong non-vanishing local forces are acting. Being accompanied by a significant suppression of diffusion and therefore robust against thermal fluctuations, the effect is caused by the existence of vortices in the force fields $\mathbf{f}(\mathbf{q})$. These vortices lead to strong particle accumulation at the channel walls, referred to as *hydrodynamically enforced entropic trapping* (HEET). Counterintuitively, HEET becomes more pronounced for larger f_{crit} and $\Delta\mathcal{P}_{\text{crit}}$, respectively, and, more importantly, it is a purely *entropic* effect caused by the converging-diverging nature of the channel geometry, $\delta \neq 1$. Despite that for a straight channel, $\delta = 1$, one also finds a critical force magnitude resulting in a vanishing mean current, the force field lacks vortices which are responsible for particle accumulation. As a result, the EDC is bounded from below by the value of bulk diffusivity and it is solely determined by the applied pressure drop. Furthermore, we showed that HEET offers the opportunity to efficiently separate particles of the same size based on their different response to external stimuli.

Beside the opportunity to separate Brownian particles of the same size, a main challenge in basic research is to obtain pure single-size suspensions by filtering wanted from unwanted material. The impact of the particle size which affects numerous physical properties like the mass, the viscous friction coefficient, the strength of the external force, and the accessible space within the channel, on the particle dynamics is studied in the subsequent chapter 5. In particular, we investigate the simplifications made in our preceding theoretical considerations for their applicability in experiments.

5. Entropic transport of spherical finite size particles

In the last two chapters, we solely focused on the transport quantities of Brownian particles with negligible diameter $d_p \to 0$ (point-like) in 3D confinements with periodically modulated cross-section. Obviously, assuming that the particle size is much smaller compared to the bottleneck width is a strong limitation which might not feasible in experiments. A main challenge in basic research, industrial processing, and in nanotechnology is to separate particles by their size. Separation techniques use the fact that the response of the particles to an external stimulus depends on their size. Filtering objects of different size is traditionally performed by means of centrifugal fractionation [Harrison et al., 2002], external fields [MacDonald et al., 2003] or phoretic forces [Bruus, 2008]. Unquestionably, electrophoretically separating DNA by size is one of the most important tools in molecular biology [Slater et al., 2002]. By means of these methods, the sorting of particles proceeds either by size exclusion, as happens in a sieve, or by migration through the host medium, a gel or porous media [Voldman, 2006]. Contrary to our method proposed in Sect. 4.3.3, in these cases all particles move in the same direction but at different speeds. In the last decade, various separation techniques have been proposed which take account of the impact of the particle size on the environment where they are located in [Duke and Austin, 1998; Martin et al., 2005; Reguera et al., 2012].

In this chapter, we study the dynamics of spherical objects with mass m and finite diameter d_p evolving under the action of an external static force $\mathbf{F} = F\,\mathbf{e}_x$ in a resting solvent, $\mathbf{u}(\mathbf{q}) = \mathbf{0}$, with dynamic viscosity η [Cheng et al., 2008; Reguera et al., 2012; Riefler et al., 2010]. Their motion is confined by a 2D channel geometry[1] which is depicted in Fig. 5.1. Here, we also restrict our studies to symmetric channel geometries, i.e., $\omega_{\pm}(x) = \pm\omega(x)$. The finite particle size influences numerous physical properties like (i) the effective mass $m^* = \pi(\rho_p + 0.5\,\rho_f)d_p^3/6$, (ii) the viscous friction coefficient $\gamma = 3\pi\eta\,d_p$, (iii) the external force $\mathbf{F} = F_0\,d_p^{\alpha}\,\mathbf{e}_x$, and (iv) the accessible space within one unit cell.

How the external force $\mathbf{F}$ depends on the particle diameter is determined by the exponent α. The latter can attain the values $\alpha = 0$ (idealized situation [Riefler et al., 2010]), $\alpha = 2$ for surface-charged colloids [Hänggi and Marchesoni, 2009] and for DNA electrophoresis[2][Volkmuth and Austin, 1992], and $\alpha = 3$ for gravitational, buoyant and

[1] In Sect. 3.1, we have shown that the particles' dynamics in a 3D, planar confinement can be reduced to a 2D problem. Thereby, the channel height reduces to $\Delta H - d_p$ for extended particles.

[2] Double-stranded DNA is a semiflexible heteropolymer whose structure is characterized by a cascade of nucleotides [Dorfman, 2010]. Rather than model DNA as thousands of bases, one can adopt a coarser approach by treating the DNA instead as a homopolymeric chain consisting of N_k Kuhn segments of Kuhn length l_k [Kuhn, 1934]. Each Kuhn segment consists of approximately $N_0 = 300$

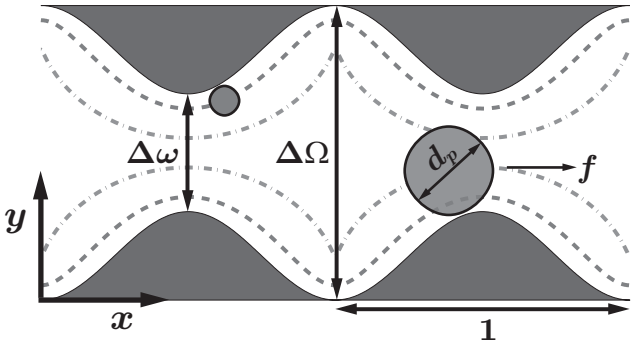

Figure 5.1.: Sketch of 2D sinusoidally modulated channel $\omega(x)$ with unit period, maximum width $\Delta\Omega$, and bottleneck width $\Delta\omega$. The spherical particle of diameter d_p is subject to the external force $\mathbf{f} = f\,\mathbf{e}_x$. Superimposed are the effective boundary function for the center of a particle $\omega_{\text{eff}}(x)$ with $d_p/\Delta\omega = 0.4$ (dashed line) and $d_p/\Delta\omega = 0.8$ (dash-dotted line).

electric force with charge density ρ_q. Furthermore, F_0 denotes the α-dimensional force density.

As mentioned above, the accessible space within each unit cell depends on the particle size too. Caused by the finite particle size its center position $\mathbf{q}$ can approach the hard walls only up to its radius $d_p/2$. Therefore, the particle's center never reaches the channel wall for finite radius and thus it is restricted to a portion of the unit cell area. Consequently, the dynamics of the particle's center is confined by an *effective boundary* $\omega_{\text{eff}}(x)$ and thus it takes place in channel geometries with *effective local width* $W_{\text{eff}}(x) = 2\,\omega_{\text{eff}}(x)$. The effective upper boundary is determined by the map $(x^\dagger, \omega_{\text{eff}}(x^\dagger))^T \to (x, \omega(x))^T - d_p/2\,\mathbf{n}$; yielding

$$x^\dagger = x + d_p\,\omega'(x)/2, \tag{5.1a}$$

$$\omega_{\text{eff}}(x^\dagger) = \omega(x) - d_p/2, \tag{5.1b}$$

with outward-pointing normal vector $\mathbf{n} = (-\omega'(x), 1)^T$. Unfortunately, the inverse function $x = \mathfrak{F}^{-1}(x^\dagger)$ associated with Eq. (5.1a) can only be found for some special cases [Berezhkovskii and Dagdug, 2010; Reguera et al., 2012] and thus the effective boundary function $\omega_{\text{eff}}(x)$ cannot be determined explicitly for arbitrary channel geometry.

If the maximal curvature of $\omega(x)$ is smaller than the one of the particle, $2/d_p$, the effective boundary and its derivatives are continuous. Then, the bottleneck width and the maximum channel width for $\omega_{\text{eff}}(x)$ read $\Delta\omega - d_p$ and $\Delta\Omega - d_p$, respectively. The

base pairs. In the local force model, the electric force acting on the DNA molecule is $F_{\text{elec}} = q_k\,N_k\,E$, where q_k is the charge per Kuhn segment and E is the magnitude of the electric field. In free solution, the configurational entropy of the chain is maximized by the random coil configuration. For an ideal chain (no excluded volume interactions) the radius of gyration of the coil scales as $R_g \sim l_k\,N_k^\nu$ with Flory exponent $\nu = 1/2$ [Flory, 1942]. Consequently, the number of Kuhn segments are proportional to R_g^2, yielding $F_{\text{elec}} \sim q_k\,(R_g/l_k)^2\,E$ for ideal chains. Taking excluded volume interactions into account which are important for long DNA the Flory exponent reads $\nu = 3/5$ for a swollen chain in a good solvent [Doi, 1996]. Then the electric force scales $F_{\text{elec}} \sim q_k\,(R_g/l_k)^{5/3}\,E$. This limit is not discussed in detail here.

associated aspect ratio changes to $\delta_{\text{eff}} = (\Delta\omega - d_p)/(\Delta\Omega - d_p)$ while the value for the expansion parameter maintains, $\varepsilon_{\text{eff}} = \varepsilon$. In the opposite limit where the particle's curvature is smaller than the maximal channel's curvature, i.e., $\max(|\omega''(x)|) > 2/d_p$, $\omega_{\text{eff}}(x)$ exhibits kinks and therefore its derivatives are discontinuous. Then, both the effective aspect ratio and the value for ε decrease, viz., $\delta_{\text{eff}} < (\Delta\omega - d_p)/(\Delta\Omega - d_p)$ and $\varepsilon_{\text{eff}} < \Delta\Omega - \Delta\omega$. An illustration of the effective boundary is depicted in Fig. 5.1.

The Langevin equation Eq. (2.2) for extended, spherical Brownian particles reads explicitly

$$m^* \ddot{\mathbf{q}} + 3\pi\eta\, d_p\, \dot{\mathbf{q}} = F_0\, d_p^\alpha\, \mathbf{e}_x + \sqrt{6\pi\eta\, d_p\, k_B T}\, \boldsymbol{\xi}(t), \tag{5.2}$$

with Gaussian white noise $\boldsymbol{\xi}(t)$, Eq. (2.3). Passing to re-scaled quantities $\mathbf{q} \to \mathbf{q}\, L$, $d_p \to d_p\, L$, $t \to \tau\, t$, and $\boldsymbol{\xi}(t) \to \sqrt{\tau}\boldsymbol{\xi}(t)$, the dimensionless EOM is given by[3]

$$\Lambda\, \ddot{\mathbf{q}} + d_p\, \dot{\mathbf{q}} = f_0\, d_p^\alpha\, \mathbf{e}_x + \sqrt{2\, d_p}\, \boldsymbol{\xi}(t), \tag{5.3}$$

with $f_0 = F_0 L^{\alpha+1}/k_B T$, $\Lambda = m^* L^2/(k_B T\, \tau^2)$ and characteristic time $\tau = 3\pi\eta L^3/(k_B T)$. The parameter Λ measures the ratio of the velocity correlation time $\tau_{\text{corr}} = m^*/\gamma(d_p)$ to the diffusion time $\tau_{\text{diff}} = \gamma(d_p) L^2/k_B T$, i.e., $\Lambda = \tau_{\text{corr}}/\tau_{\text{diff}}\, d_p^2$. Usually Λ is small for Brownian particles moving inside a medium and thus inertial effects can be neglected in Eq. (5.3); resulting in the overdamped limit. Furthermore, we disregard both hydrodynamic particle-wall and hydrodynamic particle-particle interactions (supposed dilute particle concentration), and, as well, all effects initiated by rotation of the particles. Moreover, the effect of hard-core particle-particle interaction (collision) is not considered. Otherwise, especially for large particles, $2\, d_p > \Delta\Omega$, the mutual passage of particles is excluded which leads to single file diffusion [Hahn et al., 1996; Keil et al., 2000; Wei et al., 2000]. In this case, the sequence of particles remains the same resulting in strong deviations from normal diffusion, i.e., the particle MSD grows $\propto \sqrt{t}$.

The evolution of the joint PDF $p(\mathbf{q}, t)$ following Eq. (5.3) is governed by the Smoluchowski equation $\partial_t p(\mathbf{q}, t) = -\boldsymbol{\nabla}_{\mathbf{q}} \cdot \mathbf{J}(\mathbf{q}, t)$. The probability flux $\mathbf{J}(\mathbf{q}, t)$ obeying no-flux bcs at $y = \pm\omega_{\text{eff}}(x)$, $\mathbf{J} \cdot \mathbf{n} = 0$, reads $\mathbf{J}(\mathbf{q}, t) = [f_0\, d_p^\alpha\, p(\mathbf{q}, t)\, \mathbf{e}_x - \boldsymbol{\nabla}_{\mathbf{q}} p(\mathbf{q}, t)]/d_p$. The outward-pointing normal vectors read $\mathbf{n} = (-\omega'_{\text{eff}}(x), \pm 1)^T$. Despite the inherent complexity of this problem, an approximated solution can be given within the concept of the potential of mean force $A_d(x) = -f_0\, d_p^\alpha - \ln[2\omega_{\text{eff}}(x)]$. The corresponding Fick-Jacobs equation reads $\partial_t p(x, t) = d_p^{-1}\, \partial_x\, [A'_d(x)\, p(x, t) + \partial_x p(x, t)]$, see Sect. 2.3. As previously shown in Sect. 3.2, this approach is expected to be accurate for weakly corrugated channel geometries $\varepsilon_{\text{eff}}^2 \ll 1$. Within this 1D kinetic description the most important particle transport quantities can be calculated by means of the moments of the first

[3] We emphasize that by re-scaling the variables in same way like done in Sect. 2.2, the characteristic time scale $\tau = \gamma(d_p)\, L^2/(k_B T)$ becomes a function of the particle size d_p. Then, each spherical Brownian particle obeys the dimensionless Langevin equation, $\Lambda^\dagger\, \ddot{\mathbf{q}} + \dot{\mathbf{q}} = f_0\, d_p^\alpha\, \mathbf{e}_x + \sqrt{2}\, \boldsymbol{\xi}(t)$, with $\Lambda^\dagger = m^* L^2/(k_B T\, \tau^2)$. Since, our main object is to study the influences of d_p on the particle dynamics, here, we intentionally choose a different scaling. Certainly, the results for the particle mobility and the EDC in units of their free values do not depend on the considered scaling.

passage time distribution, see Sect. 2.5,

$$\mu/\mu^0 = \frac{1-\exp(-f_0\, d_p^\alpha)}{f_0\, d_p^\alpha \int\limits_0^1 \mathrm{d}x\, e^{A_d(x)} \int\limits_{x-1}^{x} \mathrm{d}x'\, e^{-A_d(x')}}, \tag{5.4a}$$

$$D_{\text{eff}}/D^0 = \frac{\int\limits_0^1 \mathrm{d}x\, e^{A_d(x)} \int\limits_x^{x+1} \mathrm{d}x'\, e^{A_d(x')} \left[\int\limits_{x-1}^{x} \mathrm{d}x'\, e^{-A_d(x')}\right]^2}{\left[\int\limits_0^1 \mathrm{d}x\, e^{A_d(x)} \int\limits_{x-1}^{x} \mathrm{d}x'\; e^{-A_d(x')}\right]^3}. \tag{5.4b}$$

Thereby, the free values $\mu^0 = 1/d_p$ and $D^0 = 1/d_p$ also depend on the particle size; yielding that smaller objects diffuse faster and response stronger to external stimuli compared to larger ones.

5.1. Sinusoidally modulated two-dimensional channel geometry

In what follows, we evaluate the particle mobility μ/μ^0 and the effective diffusion coefficient D_{eff}/D^0 for finite size Brownian particles moving through a 2D channel geometry with sinusoidally modulated boundary $\omega(x)$, Eq. (3.52). In Fig. 5.2, we present μ/μ^0 and D_{eff}/D^0 as a function of the external force $f_0\, d_p^\alpha$ for different particle diameters d_p and for $\alpha = 0$. We emphasize that the shown results are independent of the explicitly chosen exponent α as long as the product $f_0\, d_p^\alpha$ attains the same value for a given particle diameter d_p, cf. Fig. 5.4. For weakly corrugated channels, e.g., $\Delta\Omega = 0.2$, one recognizes that the general behavior of both μ/μ^0 and D_{eff}/D^0 do not change with growing particle diameter. In detail, the particle mobility is a monotonously growing function which starts from a value smaller than 1 for small forces and goes to unity for large forces. For weak forces, the asymptotic value decreases with growing d_p due to the reduction of the effective boundary's aspect ratio $\delta_{\text{eff}} = (\Delta\omega - d_p)/(\Delta\Omega - d_p)$. This is in compliance with Eq. (3.64). Further, D_{eff}/D^0 exhibits a non-monotonic dependence on the force magnitude, see Fig. 5.2 (b). It starts with a value which is less than the free diffusion constant in the diffusion dominated regime, i.e., $|f_0\, d_p^\alpha| \ll 1$. With increasing force magnitude it reaches a maximum and finally approaches from above the value for free diffusion. Additionally, we observe that the location of the diffusion peak as well as the peak height grow with particle size d_p.

In Sect. 3.2.1, we demonstrated that the analytic result for $\mu(f)$, Eq. (3.61), matches perfectly for weakly modulated channels and tends to overestimate the true result with growing channel width. Based on this, we propose an estimate for the mobility of finite size Brownian particles. By simply replacing $f \to f_0\, d_p^\alpha$ and $\delta \to (\Delta\omega - d_p)/(\Delta\Omega - d_p)$ in Eq. (3.61), we get

$$\mu/\mu^0 \lesssim \frac{\left(f_0\, d_p^\alpha\right)^2 + 4\pi^2}{\left(f_0\, d_p^\alpha\right)^2 + 2\pi^2 \left\{\sqrt{\frac{\Delta\Omega - d_p}{\Delta\omega - d_p}} + \sqrt{\frac{\Delta\omega - d_p}{\Delta\Omega - d_p}}\right\}}. \tag{5.5}$$

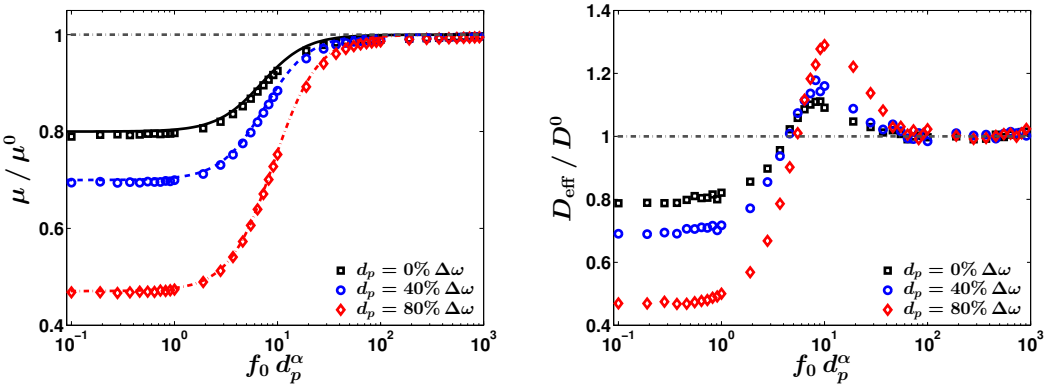

Figure 5.2.: Particle mobility μ/μ^0 (left panel) and effective diffusion coefficient D_{eff}/D^0 (right panel) versus external force magnitude $f_0\, d_p^\alpha$ for different particle diameters d_p. The force is adjusted by varying the force density f_0 for a chosen diameter d_p. The lines represent the analytic estimate Eq. (5.5). The remaining parameter values are $\Delta\Omega = 0.2$, $\Delta\omega = 0.05$, and $\alpha = 0$.

According Eq. (5.5), the associated MFPT reads $\langle\, t(0 \to 1)\,\rangle = (f_0\, d_p^\alpha\, \mu)^{-1}$ for finite size particles. In Fig. 5.2 (a), the estimate Eq. (5.5) is indicated by lines. One observes that the agreement with the numerics is satisfying. In contrast to point-like particles where the FJ approach is accurate only for $\varepsilon \ll 1$, we expect that our analytical result additionally works well for big particles. In this limit, the effective boundary function exhibits an kink-like structure, as shown in Fig. 5.1, and thus the corresponding slope parameter $\varepsilon_{\text{eff}} < \Delta\Omega - \Delta\omega$ is smaller than the one for point-like particles, see Fig. 5.3.

In exact the same manner, we can derive an estimate for the effective diffusion coefficient by substituting $f \to f_0\, d_p^\alpha$ and $\mathtt{b} \to (\Delta\Omega + \Delta\omega - 2d_p)/(\Delta\Omega - \Delta\omega)$ in Eq. (3.69). This fact is not presented in depth.

The impact of force magnitude $f_0\, d_p^\alpha$ and of particle size d_p on the particle mobility and the effective diffusion coefficient is presented in Fig. 5.4. The markers represent different combinations of values for f_0, d_p, and α, viz., $\alpha = 0$ (squares), $\alpha = 2$ (circles), and $\alpha = 3$ (diamonds). In order illustrate the dependence of μ/μ^0 and D_{eff}/D^0 on $f_0\, d_p^\alpha$ and d_p better, we superimpose associated surface plots which were obtained by cubic interpolation of the scattered data points.

For moderately corrugated channels Fig. 5.4 (a)-(b), i.e., $\Delta\Omega = 1$ and $\Delta\omega = 0.5$, the effective boundary function $\omega_{\text{eff}}(x)$ is continuous and thus the corresponding bottleneck width and maximum channel width are given by $\Delta\omega - d_p$ and $\Delta\Omega - d_p$, respectively. As a consequence, the bottleneck width becomes smaller and the entropic effects stronger with growing particle size while the value for ε remains constant. Hence, we basically observe that the particle mobility μ/μ^0 decreases monotonously with growing particle size. Thereby, one notices that the values of μ/μ^0 are almost equal for a broad range of particle diameters, $d_p \in [0, \Delta\omega/2]$, regardless of the force magnitude $f_0\, d_p^\alpha$. This indicates that particles with diameter up to the half bottleneck width can be satis-

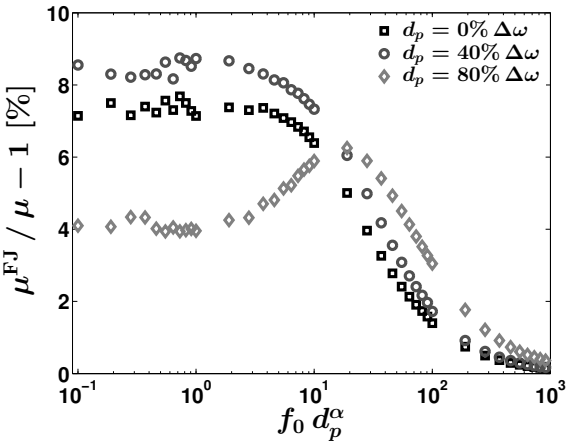

Figure 5.3: Relative error $\mu^{\mathrm{FJ}}/\mu - 1$ between FJ estimate Eq. (5.5) and the numerically obtained particle mobility μ/μ^0 as a function of external force magnitude $f_0\, d_p^\alpha$ and for various particle diameters d_p. The remaining parameters are $\Delta\Omega = 1$, $\Delta\omega = 0.5$, and $\alpha = 0$.

factorily described as point-like. In the opposite limit $d_p \to \Delta\omega$, the effective channel for the particle's center is closed and thus both μ/μ^0 and D_{eff}/D^0 go to zero. This behavior is in compliance with the previously presented results for point-like particles, cf. Fig. 3.5. It can be approximately described by $\mu/\mu^0 \propto \sqrt{\delta_{\mathrm{eff}}}/(1+\delta_{\mathrm{eff}})$ for sufficiently weak forces. In addition, it turns out that μ/μ^0 grows monotonously with the force magnitude regardless of the particle size d_p and the channel size. In particular, it is remarkable that the mobility exhibits a step-like dependence on the particle size for $f_0\, d_p^\alpha \gg 1$; μ/μ^0 is almost constant for a broad range of d_p values before it sharply decreases to zero for $d_p \to \Delta\omega$.

Likewise, the effective diffusion coefficient shows a similar dependence on $f_0\, d_p^\alpha$ and d_p for moderate corrugated confinements, see Fig. 5.4 (b). For weak forces, D_{eff}/D^0 monotonously decreases with the particle size and coincides with μ/μ^0, thus corroborating the Sutherland-Einstein relation. Keeping the particle's diameter fixed while increasing the force magnitude, one observes the typical bell-shaped structure of D_{eff}/D^0 on $f_0\, d_p^\alpha$, cf. Fig. 5.2b. Thereby, the asymptotic value for weak forces becomes less for bigger particles whereas the peak height slightly grows with d_p. For infinite strong forces the effective diffusion coefficient attains its D^0 for $d_p \neq \Delta\omega$.

The behavior of μ/μ^0 and D_{eff}/D^0 drastically changes for extremely modulated confinements, $\Delta\Omega = 10$ and $\Delta\omega = 1$, as shown in Fig. 5.4 (c)-(d). For instance, the particle mobility shows a resonance-like behavior as a function of the particle size for weak forces. While the bottleneck width decreases linearly with d_p, the maximum channel width shows a much stronger decline if $\max(|\omega''(x)|) > 2/d_p$. With growing particle diameter, the size of the effective channel's bulges lessens and the sojourn time, which the particle spends on average within one unit cell, shortens. Despite the intimately connected reduction of the bottleneck size, the particle mobility grows with the particle size till it attains its maximum value for a given diameter. With further increasing particle size, the particle motion gets more and more hindered by the shrinking bottleneck size and thus μ/μ^0 decreases. The impact of d_p on the mobility lessens for larger force strengths, i.e., the mobility is almost independent of the particle size for $f \gg 1$. In the force dominated regime, we observe that μ/μ^0 exhibits an almost step-like dependence on d_p.

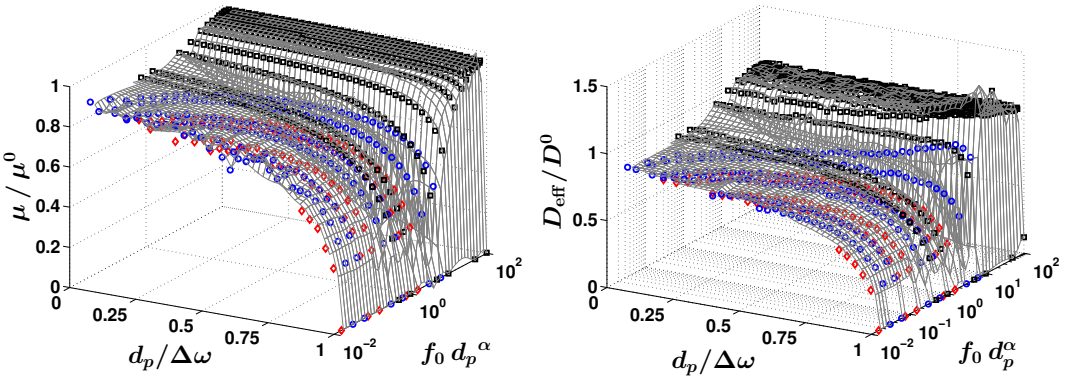

(a) $\Delta\Omega = 1$, $\Delta\omega = 0.5$ (b) $\Delta\Omega = 1$, $\Delta\omega = 0.5$

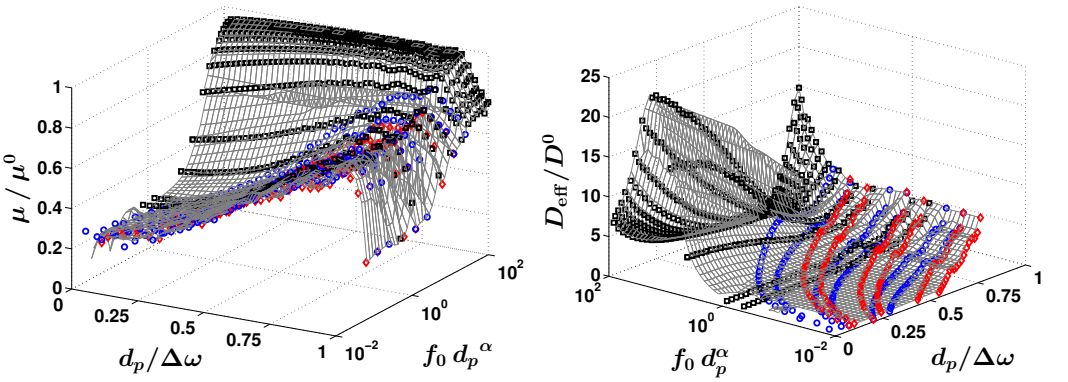

(c) $\Delta\Omega = 10$, $\Delta\omega = 1$ (d) $\Delta\Omega = 10$, $\Delta\omega = 1$

Figure 5.4.: Particle mobility μ/μ^0 (left column) and effective diffusion coefficient D_{eff}/D^0 (right column) as a function of force $f_0\, d_p^\alpha$ and particle diameter d_p. The markers represent the simulation results for various values of α, viz., $\alpha = 0$ (squares), $\alpha = 2$ (circles), and $\alpha = 3$ (diamonds). Additionally, we depict the associated surface plots obtained by cubic interpolation of the scattered data points. The channel parameters are $\Delta\Omega = 1$, $\Delta\omega = 0.5$ (top row) and $\Delta\Omega = 10$, $\Delta\omega = 1$ (bottom row).

	L [μm]	$\Delta\Omega$ [μm]	$\Delta\omega$ [μm]	d_p [μm]
Sven and Müller, 2003	8.4	4.8	2.5	1
Marquet et al., 2002	50		6-12	1-6
Mathwig et al., 2011	110	3.8	2	0.1-0.5
Groisman and Quake, 2004	230	330	37	
Yang et al., 2012	250	120	40	5-10

Table 5.1.: Experimentally used channel parameters and values for colloid diameters d_p are gathered from various sources.

Furthermore, the effective diffusion coefficient exhibits a complex dependence on the particle diameter and the force magnitude. In the limiting case of point-like particles $d_p/\Delta\omega \ll 1$, we notices the typical bell-shaped structure of D_{eff}/D^0 as a function of $f_0\, d_p^\alpha$. Noteworthy, the maximal diffusivity exceeds the free value D^0 for more than one magnitude, viz., $\max(D_{\text{eff}}) \simeq 20\, D^0$. Interestingly, an increase of the particle size leads to a growth of D_{eff}/D^0 for weak forces and a decline of the peak's height at moderate forces. In the asymptotic limit $d_p \to \Delta\omega$, the effective diffusion coefficient grows with d_p regardless of the force strength. In particular, one observes that D_{eff}/D^0 increases with growing force magnitude for $d_p \to \Delta\omega$. In contrast to point-like particles, the peak position is shifted towards stronger forces, however, the peak height also exceeds the free value D^0 for more than one magnitude. We expect that in the limit $f_0\, d_p^\alpha \to \infty$ the EDC converges to the free value regardless of the particle diameter.

5.2. Discussion on the applicability in experiments

In the previous section, we presented Brownian dynamics simulation results for the particle mobility and the effective diffusion coefficient of spherical objects with diameter d_p. We disregard (i) inertial effects $\Lambda \ll 1$, (ii) hydrodynamic particle-particle interactions as well as (iii) hydrodynamic particle-wall interaction in our study. Furthermore, we assume that the objects are subject to an idealized spatial homogeneous and static external force whose magnitude vary from $10^{-2} - 10^2$.

In what follows, we quantify the simplifications made for their applicability in experiments. Tab. 5.1 presents a small collections of channel parameter values and particle diameters used in experiments. For colloidal particles of size $d_p = 0.1 - 1\,\mu$m moving freely in water $\rho_f = 998\,\text{kg/m}^3$, $\eta = 10^{-3}\,\text{kg/(m s)}$, the free particle mobility is of the order $\mu^0 \approx 10^8 - 10^9\,\text{s/kg}$ and the free diffusion constant is nearly $D^0 \approx 0.1 - 1\,\mu\text{m}^2/\text{s}$ at room temperature $T = 293,15\,\text{K}$. Thereby smaller objects diffuse faster and response stronger (larger free mobility) to external stimuli. In numerical simulations we can easily vary the dimensionless force magnitude $f_0\, d_p^\alpha$ from $10^{-2}-10^2$ like done in chapters 3-5. One may ask if such values are accessible in experiments?

Assuming that the colloids are subject to gravity and buoyancy acting along longitudinal channel direction, but with opposite orientation, one gets $F_{\text{grav}} \approx 10^{-4} - 10^{-1}\,\text{fN}$ for polystyrene beads[4] of size $d_p = 0.1 - 1\,\mu$m, Tab. 5.1, and density $\rho_p = 1050\,\text{kg/m}^3$. For

[4] `http://www.polyscience.com`

silica beads, $\rho_p = 2000\,\mathrm{kg/m^3}$, of the same size one calculates $F_{\mathrm{grav}} \approx 10^{-2} - 10^{1}\,\mathrm{fN}$. The corresponding free particle velocity is in a range from $\langle\, v^0 \,\rangle = 0.01\mu\mathrm{m/s}$ ($d_p = 0.1\mu\mathrm{m}$) to $\langle\, v^0 \,\rangle = 1\mu\mathrm{m/s}$ ($d_p = 1\mu\mathrm{m}$). For a typical unit cell period length $L = 100\,\mu\mathrm{m}$, Tab. 5.1, the dimensionless force magnitude is of the order $f_{\mathrm{Poly}} \approx 10^{-3} - 10^{0}$ for polystyrene and $f_{\mathrm{Sil}} \approx 10^{-1} - 10^{2}$ for silica beads at room temperature. Albeit, gravity is a comparably weak force the values of f are of right order. Concerning the impact of inertial effects on the particles dynamics, we obtain $\Lambda \approx 10^{-18} - 10^{-15}$ for both polystyrene and silica beads ($d_p = 0.1 - 1\,\mu\mathrm{m}$) suspended in water at room temperature. Consequently, this assumption to neglect the inertial term $\Lambda\ddot{\mathbf{q}}$ is justified for spherical objects evolving in a aqueous solvent.

Apart from separating colloidal dispersion by size, electrophoretically separating of DNA or RNA by size is unquestionably one of the most important tools in molecular biology. While the understanding of DNA at the nucleotide level is critical for many biophysical studies, one can capture many physical properties using coarse-grained models. For example, DNA can be treated as a homopolymeric chain consisting of N_k Kuhn segments of Kuhn length l_k [Kuhn, 1934]. Each Kuhn segment consists of approximately $N_0 = 300$ base pairs. In free solution, the DNA coils with an associated radius of gyration $R_g \sim l_k \sqrt{N_k}$ for ideal chains (no excluded volume interactions) [Doi, 1996]. Supposing that the coil diameter is of the size of the bottleneck, $\Delta\omega = 1 - 10\,\mu\mathrm{m}$, cf. Tab. 5.1, results in an upper limit for the number of base pairs, $N_{bp} \approx 10^4 - 10^5$ for ideal chains. The canonical example for long DNA is λ-DNA which consists of $N_{bp} = 48502$ and has a radius of gyration of $R_g = 0.73\,\mu\mathrm{m}$. If the DNA is confined to a length scale smaller than the Kuhn length $l_k \approx 0.1\mu\mathrm{m}$ [Smith et al., 1996, for λ-DNA], a finer-scale model is needed [Odijk, 1983].

Calculating the prefactor Λ in Eq. (5.3), one gets $\Lambda \approx 10^{-29} - 10^{-28}$ for DNA with $N_{bp} \approx 10^4 - 10^5$ in water at room temperature.[5] In contrast to colloid particles, gravity applies only $F_{\mathrm{grav}} \approx 10^{-5} - 10^{-4}\,\mathrm{fN}$ on DNA; yielding $f \approx 10^{-3} - 10^{-2}$ for $N_{bp} = 10^4 - 10^5$ and $L = 100\,\mu\mathrm{m}$ at room temperature. We emphasize that even for long DNA ($N_{bp} = 4.85 \cdot 10^4$ and $q_k \sim 0.3\,\mathrm{electron/\AA}$ [Volkmuth and Austin, 1992]) one has to apply strong electric field strengths $E = 10^0 - 10^4\,\mathrm{V/cm}$ to achieve $f_{\mathrm{elec}} = 10^{-2} - 10^2$.

Hydrodynamic particle-particle interaction

Next, we briefly discuss the strength of hydrodynamic interaction between rigid spherical objects with diameter d_p moving slowly through a viscous fluid (low Reynolds number dynamics). It is assumed that the particles are sufficiently distant from the boundary walls to be regarded as unbounded. Attention will be predominantly directed to the situation where the fluid at infinity is at rest. According to Faxen's law [Faxen, 1922; Happel and Brenner, 1965], an additional force $\mathbf{f}_{ji}$ acts on the j-th particle at

[5] The mass of the adenine-thymine base pair is given by phosphate(95) + sugar(115) + adenine(134) + phosphate(95) + sugar(115) + thymine(125)=679 Da. For the cytosine-guanine complex one finds phosphate(95) + sugar(115) + cytosine(110) + phosphate(95) + sugar(115) + guanine(150)=680 Da. Thereby, one Dalton is $1\,\mathrm{Da} = 10^{-27}\,\mathrm{kg}$.

position $\mathbf{r}_0$

$$\mathbf{f}_{ji} = d_p \left[\mathbf{u}_i(\mathbf{r}_0) + \frac{d_p^2}{24} \triangle \mathbf{u}_i(\mathbf{r}_0) \right], \tag{5.6}$$

caused by the flow field $\mathbf{u}_i(\mathbf{r})$ induced by the i-th particle located at $(0,0)^T$. These hydrodynamic interactions can be included into the EOM

$$d_p \begin{pmatrix} \dot{\mathbf{q}}_1(t) \\ \dot{\mathbf{q}}_2(t) \\ \vdots \\ \dot{\mathbf{q}}_N(t) \end{pmatrix} = \mathbb{M}^{\text{hyd}} \begin{pmatrix} \mathbf{f}_1 \\ \mathbf{f}_2 \\ \vdots \\ \mathbf{f}_N \end{pmatrix} + \sqrt{2\, d_p} \begin{pmatrix} \boldsymbol{\xi}_1(t) \\ \boldsymbol{\xi}_2(t) \\ \vdots \\ \boldsymbol{\xi}_N(t) \end{pmatrix}, \tag{5.7}$$

by means of the Rodne-Prager tensor $\mathbb{M}^{\text{hyd}}$

$$\mathbb{M}_{ii}^{\text{hyd}} = \mathbb{I}, \tag{5.8a}$$

$$\mathbb{M}_{ij}^{\text{hyd}} = \left[\frac{3\, d_p}{8\, r_{ij}} \left(\mathbb{I} + \frac{\mathbf{r}_{ij}\, \mathbf{r}_{ij}}{r_{ij}^2} \right) + \frac{d_p^3}{16\, r_{ij}^3} \left(\mathbb{I} - 3 \frac{\mathbf{r}_{ij}\, \mathbf{r}_{ij}}{r_{ij}^2} \right) \right]. \tag{5.8b}$$

Here $r_{ij} = \|\mathbf{r}_{ij}\|$ denotes the distance between the i-th and j-th particle and $\mathbb{I}$ represents the unit matrix. One notices that hydrodynamic interactions are of repulsive character. Furthermore it turns out that the average distance between two particles of size d_p has to be $\langle\, r_{ij} \,\rangle \geq d_p/\Delta f$ if an additional force of magnitude Δf is maximally tolerated. For $d_p = 0.1 - 1\,\mu$m and 10% tolerance for the force magnitude, we derive that the mean distance must be at least $\langle\, r_{ij} \,\rangle = 1 - 10\,\mu$m which is of the size of the bottleneck width, cf. Tab. 5.1. Thus, the particle concentration has to be diluted in order to guarantee that only one particle is in the bottleneck's vicinity at any time.

Hydrodynamic particle-wall interaction

Concerning the particle-wall interaction it is necessary to establish the effect of walls on the particle dynamics separately. These effects may then be combined with those due to particle-particle interaction. In general, the interaction of a particle with the wall depends on the particle shape, orientation, and position, as well as on the geometry of the channel walls [Happel and Brenner, 1965]. For simplification, we suppose that the particle at distance l moves parallel to a infinite long horizontal wall located at $y = 0$ in a strong viscous media (low Reynolds number). Referring to Happel and Brenner, 1965, an additional force with magnitude

$$\Delta f = \frac{d_p}{2\, l - d_p}\, f + O\left(\left(\frac{d_p}{2l} \right)^2 \right) \tag{5.9}$$

acts on the particle due to the wall. From Eq. (5.9) follows that the additional force vanishes if the particle is far away from the wall, $l \gg d_p$. With decreasing distance l, the force strength Δf grows and finally goes to infinity for $l \to d_p/2$. Since Δf acts parallel to the particle's direction of motion and is oppositely directed, one can interpret

Δf as an additional drag force. Consequently, the asymptotic particle velocity lessens if the particle approaches the wall. In the limit $l \to d_p/2$, no-slip velocity $\mathbf{v} = 0$ is accomplished at the wall.

According to Eq. (5.9), the distance between particle and wall has to be at least $l \geq 0.5\,(1 + f/\Delta f)\,d_p$ if an additional force of magnitude Δf is tolerated. For diameter $d_p = 0.1 - 1\,\mu$m and 10% force tolerance, we calculate that the distance must be at least $l = 0.55 - 5.5\,\mu$m which is of the size of half the bottleneck width, cf. Tab. 5.1. In agreement with the condition for the mean particle distance, it has to be guaranteed that only one particle is in the bottleneck's vicinity at any time in order to safely disregard any hydrodynamic interactions. If this requirement is violated, as expected, particle-wall interaction becomes significant at the bottleneck. In particular, accumulation of particles at the constricting bottleneck may become enhanced due to the interaction with the wall [Schindler et al., 2007].

5.3. Summary

To conclude, we studied the impact of finite particle size on the key transport quantities. Since numerous physical properties like the particle mass, the friction coefficient, the external force magnitude, the accessible space or, equivalently, the entropic barrier within the channel depend on the particle diameter, the particle dynamics may change drastically. We validated that the transport quantities are well described by the Fick-Jacobs approach for weakly modulated channels as well as for strongly corrugated channels and large particles. In the latter limit, the effective boundary function exhibits a kink-like structure and consequently the corresponding channel slope is much smaller than the one for point-like particles. Interestingly, due to the nonlinear dependence of both the channel aspect ratio and the slope parameter on particle size, we found a resonance-like behavior of the particle mobility on the diameter for extreme corrugated channels and weak forces. Such a sensitive dependence offers the possibility to separate Brownian objects of different size.

Finally, we tested the simplifications made in our theoretical consideration for their applicability in experiments. In particular, limits for the ratio of particle size to pore size and the mean distance between the particles were identified. Both demonstrate that dilute particle concentration is essential for finite particle size. Namely, it has to be guaranteed that only one single particle stays in the bottleneck's vicinity at any time. If so, hydrodynamic particle-particle and particle-wall interactions can safely be disregarded. Additionally, the particles have to be much smaller compared to the pore size. For such diameter values, we found that the transport quantities in units of their free values are similar to the ones for idealized, point-like particles.

Regarding the impact of inertia on the particle dynamics, we demonstrate that the prefactor Λ, appearing in the equation of motion Eq. (5.3), is negligible small. Thus, the inertial term in Eq. (5.3) can be safely disregarded for colloid particles and DNA in an aqueous solvent. Nevertheless, if particles are confined in narrow channels and the dynamic viscosity of the surrounding medium is low, as it is e.g. in acetone $\eta = 3 \cdot 10^{-4}\,\mathrm{kg/(m\,s)}$ or in gases $\eta \simeq 10^{-5}\,\mathrm{kg/(m\,s)}$ [Li et al., 2010; Roy et al., 2003], the thermal correlation length, $l_{\mathrm{corr}} = \sqrt{m\,k_B T}/\gamma$, can be of the order of the bottleneck

size $\Delta\omega$. Moreover, the length scale on which the particle motion is spatially correlated grows in the presence of an external force (acceleration). Hence, it is of interest to investigate the impact of the viscous friction coefficient $\gamma(\eta)$ on the particle dynamics. This is done in detail in the subsequent chapter 6.

6. Impact of inertia on biased Brownian transport in confined geometries

In the previous chapters, we showed that the Fick-Jacobs approach, in which the elimination of the "fast" transversal degree(s) of freedom results in an effective description for the longitudinal coordinate, provides a powerful tool to describe particle transport through weakly corrugated channel geometries. The applicability of this approach depends on the existence of a hierarchy of relaxation times [Wilemski, 1976] governed by the geometry of the channel and by the viscous friction coefficient γ [Skinner and Wolynes, 1979; Titulaer, 1978]. This hierarchy guarantees separation of time scales and equipartition of energy; both are necessary conditions for applying the method. The core physical assumption behind the Fick-Jacobs approach is that the dynamics of particles in a fluid is the overdamped Langevin one (for a discussion see Chapt. 2). In the overdamped regime, the particle's velocity becomes uncorrelated during the time the particle needs to move a characteristic length l_{corr} forward, $m^*/\gamma < l_{\mathrm{corr}}/v$. If so, the inertia term $m^*\,\ddot{\mathbf{q}}(t)$ is negligibly small compared to the other acting forces and thus one can formally set the (added) mass of the particle to zero, $m^* = 0$, or, equivalently, make the viscous friction coefficient tend to infinity (Smoluchowski approximation [von Smoluchowski, 1906]).

But how large is an "infinite" γ or how small can be a "zero" mass? In cases that particles are confined in channels with narrow openings ($l_{\mathrm{corr}} \simeq \Delta\omega \lesssim 1\,\mu$m), the dynamic viscosity η of the surrounding medium is very low [Li et al., 2010], or particles move with relatively high velocities like in gases [Roy et al., 2003], the inequality $m^*/\gamma < l_{\mathrm{corr}}/v$ is not always satisfied. Hence, one expects that inertial effects become important as long as the particle's motion is spatially correlated on a length of the order of, or larger than, the smallest length scale of the system; the bottleneck width $\Delta\omega$ [Ghosh et al., 2012b,c]. The correlation length crucially depends on γ, the external force strength, and the environmental temperature T.

In the limit of vanishing viscous dissipation, $\gamma \to 0$, the considered problem resembles deterministic billiards where correlations are long-ranged [Machta, 1983]. Billiard-type dynamical systems are at the heart of the foundations of statistical mechanics and the theory of dynamical systems [Kozlov and Treshchëv, 1991]. These are suitable models for attempting to understand non-equilibrium statistical mechanics showing very rich dynamics, e.g., chaos [Gaspard et al., 1998], ergodicity [Sinai, 1970], defocusing [Bunimovich, 1974], stickiness to KAM tori [Arnold, 1963], Fermi acceleration [Fermi, 1949], etc. One of the most famous billiard-type system in statistical mechanics is a Lorentz gas [Bunimovich and Sinai, 1981; Gaspard and Baras, 1995] generated by a motion of a point particle in a periodic array of immovable scatterers. These confined geometries are ideal systems for studying deterministic diffusion which refers to the

asymptotically linear growth of the mean square displacement in purely deterministic and typically chaotic dynamical systems [Klages, 1996, 2002; Machta and Zwanzig, 1983].

Finite damping, $\gamma \neq 0$, and non-zero environmental temperature, $T \neq 0$, guarantee the existence of a hierarchy of relaxation times which may leads to an effective description for the longitudinal coordinates (FJ approach). Within the latter, the damped particle motion takes place in the one-dimensional, spatially periodic potential of mean force. Its purely energetic correspondent, a tilted periodic potential, is one of the most studied nonequilibrium system [Risken, 1989] and gained great interest due to its wide application and practical importance in many fields including Josephson tunnelling junctions [Barone and Paternò, 1982], rotation of dipoles, diffusion of atoms and molecules on crystal surfaces [Patriarca et al., 2005], to name a few. The associated particle dynamics is characterized by random switches occurring either between a locked state and a running state (small friction) or between two locked states (strong damping) [Hänggi and Marchesoni, 2009]. The transition rates between the locked and running state crucially depends on the force magnitude, the thermal fluctuation strength, and the viscous friction coefficient. As a consequence, analytic results are only known in some limits [Hänggi et al., 1990]. Caused by the interplay of chaotic and stochastic dynamics, in particular, time-periodically forced Brownian particles exhibit a variety of interesting phenomena like hysteresis loops [Borromeo et al., 1999], dynamical stochastic resonance [Borromeo and Marchesoni, 2000; Costantini and Marchesoni, 1999], absolute negative mobility [Machura et al., 2007; Nagel et al., 2008], and feedback control [Hennig et al., 2009; Pyragas, 1992].

Our objective with the chapter at hand is to investigate the impact of the viscous friction coefficient γ on point-size Brownian particles evolving in two-dimensional confining geometries. We demonstrate that if the time scales involved in the problem separate, the previously derived result for the potential of mean force $A(x)$, see Sect. 2.3.1, is absolutely general for arbitrary friction coefficients and it is intimately connected with equipartition.[1]

6.1. Model for inertial Brownian motion in periodic channels

In the following, we consider point-sized[2] Brownian particles with mass m whose motion in the $x-y-$ plane is confined by the top and bottom boundaries given by the functions $\omega_+(x)$ and $\omega_-(x)$, respectively, both periodic with unit period, see Fig. 6.1. For the sake of simplicity, we focus on the situation of a two-dimensional channel, although the same discussion can readily be extended to 3D. The directed motion of the particles is induced only by an external curl-free force $\mathbf{f} = f\,\mathbf{e}_x$ which acts along the channel's longitudinal (x-) direction (scalar potential $\Phi(\mathbf{q}) = -f\,x$). Hydrodynamic particle-particle as well as particle-wall interactions within the system can be neglected provided particles are

[1] I remark that several results and similar figures presented in this chapter have been previously published in Martens et al., 2012a.

[2] In Sect. 5.1, we showed that the results for the transport quantities (in units of their free values) are almost independent of the particle size if $d_p < \Delta\omega/2$. Thus, we simplify our model by considering idealized, point-like Brownian particles.

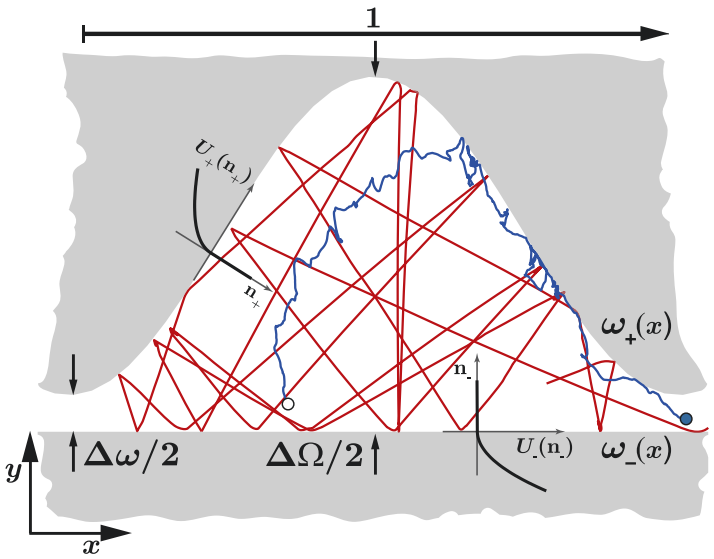

Figure 6.1.: Sketch of a segment of a sinusoidally-shaped 2D channel that confines the motion of a point-like Brownian particle (circle). The periodicity of the structures is unity, the minimal and maximum channel widths are $\Delta\omega$ and $\Delta\Omega$, respectively. The constant force f points in longitudinal (x-) direction. Shown are also the potentials describing the particle-wall interaction $U_\pm(n_\pm)$, cf. Eq. (2.38), as well as exemplary particle trajectories ($f = 100$) for $\gamma = 1$ (red line) and for $\gamma = 100$ (blue line).

small, $d_p \ll \Delta\omega$, and their concentration is low; see Sect. 5.2. In compliance with the preceding chapters, we also pass to re-scaled (dimensionless) variables $\mathbf{q} \to \mathbf{q}\,L$ and $\Phi \to \Phi\,k_BT$. But in contrast to the previous scaling, cf. Sect. 2.2, we chose the time the particle requires to overcome the distance L with rms thermal velocity $\sqrt{k_BT/m}$, viz., $\tau = L\sqrt{m/k_BT}$, as unit of time τ. Accordingly, the dimensionless vicous friction coefficient reads $\gamma \to \gamma\,m/\tau$. Further, we define the system of units with $m = L = k_BT = 1$. The velocity $\mathbf{v} = (v_x, v_y)^T$ of a particle (measured in units of $\sqrt{k_BT/m}$) is governed by the Langevin equation[3]

$$\dot{\mathbf{v}} = -\gamma\,\mathbf{v} - \nabla_{\mathbf{q}}\Phi(\mathbf{q}) + \sqrt{2\,\gamma}\,\boldsymbol{\xi}(t), \tag{6.1}$$

with delta-correlated Gaussian random force $\boldsymbol{\xi} = (\xi_x, \xi_y)$: $\langle\,\xi_i(t)\,\rangle = 0$, $\langle\,\xi_i(t)\xi_j(s)\,\rangle = \delta_{ij}\delta(t-s)$; i, j are x or y. In order to make the comparison with previously presented results for overdamped ($\gamma \gg 1$) Brownian motion in weakly corrugated channels more transparent, here, we also consider a quiescent solvent $\mathbf{u}(\mathbf{q}, t) = \mathbf{0}$.

[3]We emphasize that by re-scaling the variables in same way like done in Sect. 2.2, the characteristic time scale $\tau = \gamma L^2/(k_BT)$ becomes a function of the viscous friction coefficient γ. Thus, each Brownian particle obeys the dimensionless Langevin equation, $\Lambda^\dagger\,\ddot{\mathbf{q}} + \dot{\mathbf{q}} = f\,\mathbf{e}_x + \sqrt{2}\,\boldsymbol{\xi}(t)$, with $\Lambda^\dagger = m\,k_BT/(\gamma\,L)^2$. Since, our main object is to study the impact of γ on the particle dynamics, here, we intentionally choose a different scaling. Certainly, the results for the particle mobility and the EDC in units of their free values do not depend on the considered scaling.

The Langevin equation Eq. (6.1) is equivalent to the Klein-Kramers equation [Hänggi et al., 1990] for the joint PDF $P(\mathbf{q}, \mathbf{v}, t)$ of a particle to be found at position $\mathbf{q} = (x, y)^T$ with velocity $\mathbf{v}$ at time t:

$$\partial_t P = L_{x,v_x} P + L_{y,v_y} P, \tag{6.2a}$$

with

$$L_{q,v} = -v\partial_q + \partial_q \Phi(\mathbf{q})\partial_v + \gamma \partial_v \left[v + \partial_v\right]. \tag{6.2b}$$

Both the $\mathbf{q}$- and the $\mathbf{v}$-component of the probability current

$$\mathbf{J_q} = \mathbf{v}\, P, \quad \text{and} \quad \mathbf{J_v} = -\boldsymbol{\nabla}_\mathbf{q} U\, P - \gamma \left[\mathbf{v} + \boldsymbol{\nabla}_\mathbf{v}\right] P, \tag{6.3}$$

obey the no-flow condition which leads to vanishing probability currents normal to the channel's boundary

$$\mathbf{J_q}(\mathbf{q}, \mathbf{v}, t) \cdot \mathbf{n} = 0, \quad \text{and} \quad \mathbf{J_v}(\mathbf{q}, \mathbf{v}, t) \cdot \mathbf{n} = 0, \quad \forall\, \mathbf{q} \in \text{channel wall}, \tag{6.4}$$

where $\mathbf{n}$ denotes the outward-pointing normal vector at the channel walls. We stress that any solution of the Klein-Kramers equation, Eq. (6.2a), exhibits a kinetic boundary layer near a completely or partially absorbing wall [Harris, 1981]. Such kinetic boundary layers occur when one imposes boundary conditions that cannot be satisfied by a distribution function of local equilibrium type [Kainz and Titulaer, 1991; Selinger and Titulaer, 1984]. Hence, for simplification all particle-wall collisions are treated as perfectly elastic $\mathbf{v} \cdot \mathbf{n} = 0$, i.e., the angle of incidence just before the collision is equal to the angle of reflection just after the collision with the boundaries. Consequently, the bc for $\mathbf{J_q}$ is unconditionally satisfied. In the same manner, we claim that the normal component of $\mathbf{J_v}$ equals zero at the moment of collision. Periodic boundary conditions are appropriate [Risken, 1989]

$$P(x + m, y, v_x, v_y, t) = P(x, y, v_x, v_y, t),\ m \in \mathbb{Z}, \tag{6.5}$$

for an infinitely long channel consisting of many unit cells. Additionally, $P(\mathbf{q}, \mathbf{v}, t)$ satisfies the normalization condition in every unit

$$\int_0^1 \mathrm{d}x \int_{\omega_-(x)}^{\omega_+(x)} \mathrm{d}y \int_{-\infty}^{\infty} \mathrm{d}v_x \int_{-\infty}^{\infty} \mathrm{d}v_y\, P(x, y, v_x, v_y, t) = 1. \tag{6.6}$$

Approximations to Eq. (6.2a) give rise to effective theories concentrating on the relevant x-coordinate and suppressing the irrelevant y-one. In what follows, we first discuss necessary conditions for such a reduced description.

6.2. Fick-Jacobs approach for arbitrary friction

According to the Bayes theorem, the joint PDF of the position and the velocity is given by the product

$$P(\mathbf{q},\mathbf{v},t) = P(y,v_y|x,v_x,t)\,p(x,v_x,t), \tag{6.7}$$

of the marginal probability density

$$p(x,v_x,t) = \int\limits_{\omega_-(x)}^{\omega_+(x)} \mathrm{d}y \int\limits_{-\infty}^{\infty} \mathrm{d}v_y\, P(\mathbf{q},\mathbf{v},t), \tag{6.8}$$

and the joint PDF of y and v_y conditioned on x, v_x, and t, $P(y,v_y|x,v_x,t)$. The fast relaxation approximation [Berezhkovskii and Szabo, 2011] assumes that $P(y,v_y|x,v_x,t)$ equals the equilibrium PDF of y and v_y, conditioned on x:

$$\Phi(y,v_y|x,v_x,t) = \Phi(y,v_y|x) = \frac{e^{-[v_y^2/2+\Phi(\mathbf{q})]}}{\sqrt{2\pi}\int\limits_{\omega_-(x)}^{\omega_+(x)} \mathrm{d}y\, e^{-\Phi(\mathbf{q})}}. \tag{6.9}$$

In this case the full dynamics, Eq. (6.1), can be replaced by the motion of a particle in the potential of mean force $A(x)$

$$\frac{\mathrm{d}\,A(x)}{\mathrm{d}\,x} = \int\limits_{\omega_-(x)}^{\omega_+(x)} \mathrm{d}y \int\limits_{-\infty}^{\infty} \mathrm{d}v_y\, \partial_x\Phi(\mathbf{q})\, P(y,v_y|x), \tag{6.10}$$

yielding

$$\dot{v}_x = -\gamma\, v_x - \frac{\mathrm{d}\,A(x)}{\mathrm{d}\,x} + \sqrt{2\gamma}\,\xi_x(t). \tag{6.11}$$

The assumption Eq. (6.9) is valid if (i) the distribution of y relaxes fast enough to the equilibrium one (separation of time scales), (ii) equipartition of the kinetic energies corresponding to v_x and v_y holds (outside of energy-diffusion regime), and (iii) v_x and v_y are uncorrelated at any time τ, $\langle\, v_x(\tau)v_y(0)\,\rangle = 0$. Burada et al., 2007, analyzed the time scales involved in the problem. These are the times $\tau_y = \gamma\,\Delta y^2/2$ and $\tau_x = \gamma\,\Delta x^2/2$ to diffuse over distances Δy and Δx, the characteristic drift time $\tau^x_{\mathrm{drift}} = \min(\gamma\,\Delta x/f, \Delta x/v_x)$ and $\tau^y_{\mathrm{drift}} = \Delta y/v_y$, and the velocity correlation time $\tau_{\mathrm{corr}} = 1/\gamma$. A criterion to be satisfied is

$$\max\left(\tau_y/\tau_x, \tau^y_{\mathrm{drift}}/\tau^x_{\mathrm{drift}}, \tau_{\mathrm{corr}}/\tau_y, \tau_{\mathrm{cor}}/\tau^y_{\mathrm{drift}}\right) \ll 1, \tag{6.12}$$

whereas $\tau_y/\tau_x \ll 1$ and $\tau^y_{\mathrm{drift}}/\tau^x_{\mathrm{drift}} \ll 1$ represent the supposed separation of the transverse to the longitudinal time scales. This can be achieved either for anisotropic friction $\gamma_x \gg \gamma_y$ [Berezhkovskii and Szabo, 2011], or, equivalently, for anisotropic diffusion co-

efficients $D_y \gg D_x$ [Kalinay and Percus, 2006]. The last two conditions $\tau_{\rm corr}/\tau_y \ll 1$ and $\tau_{\rm corr}/\tau^y_{\rm drift} \ll 1$ should ensure that the velocity components are uncorrelated at any time. In the considered situation, Eq. (6.1), correlation between v_x and v_y can only occur due to reflection at the corrugated boundaries, where the acceleration in x-direction ($f\mathbf{e}_x$) is transfered to the transverse velocity component. This means that the ansatz, Eq. (6.9), is not valid as long as the Brownian motion is spatially correlated on a length (thermal length $l_{\rm therm} = 1/\gamma$ ($f \ll 1$) or the drift length $l_f = f/\gamma^2$ ($f > 1$) of the order of, or larger than, the smallest length scale of the system, viz., the bottleneck width $\Delta\omega$. Consequently, the criterion Eq. (6.12) can be formulated in an alternative way [Ghosh et al., 2012b,c]:

$$\gamma\,\Delta\omega \gg 1, \quad \text{and} \quad \frac{\gamma^2\,\Delta\omega}{f} \gg 1. \tag{6.13}$$

Violation of time scale separation

If the fast relaxation approximation (separation of time scales) fails, Eqs. (6.12) and (6.13), Berezhkovskii and Szabo proposed to add an additional term to Eq. (6.7) which describes the deviation from the local equilibrium $\Delta(\mathbf{q},\mathbf{v},t)$, yielding

$$P(\mathbf{q},\mathbf{v},t) = P(y,v_y|x)\,p(x,v_x,t) + \Delta(\mathbf{q},\mathbf{v},t). \tag{6.14}$$

Substituting Eq. (6.14) into Eq. (6.2a) and integrating the result over y and v_y, leads to

$$\partial_t p(x,v_x,t) = L^{MF}_{x,vx} - \partial_{v_x} \int\limits_{\omega_-(x)}^{\omega_+(x)} \mathrm{d}y \int\limits_{-\infty}^{\infty} \mathrm{d}v_y\, \delta F_x(y)\,\Delta(\mathbf{q},\mathbf{v},t), \tag{6.15}$$

where $L^{MF}_{x,vx}$ is obtained from L_{x,v_x}, Eq. (6.2b), by replacing $\partial_x\Phi(\mathbf{q})$ by $\mathrm{d}A(x)/\mathrm{d}x$, Eq. (6.10), and $\delta F_x(y) = -\partial_x\Phi(x,y) + \mathrm{d}A(x)/\mathrm{d}x$ measures the difference between the locally acting force and the mean force. The evolution of $\Delta(\mathbf{q},\mathbf{v},t)$ is determined by

$$\begin{aligned}\partial_t\Delta(\mathbf{q},\mathbf{v},t) = {} & L_{x,v_x}\Delta + L_{y,v_y}\Delta + P(y,v_y|t)\,\partial_{v_x} \int\limits_{\omega_-(x)}^{\omega_+(x)} \mathrm{d}y \int\limits_{-\infty}^{\infty} \mathrm{d}v_y\, \delta F_x(y)\,\Delta(\mathbf{q},\mathbf{v},t) \\ & - P(y,v_y|t)\,\delta F_x(y)\,[v_x + \partial_{v_x}]\,p(x,v_x,t).\end{aligned} \tag{6.16}$$

We emphasize that the last two equations are exact. By omitting the last term in Eq. (6.15), i.e., putting $\Delta(\mathbf{q},\mathbf{v},t) = 0$, one recovers the familiar result that the motion along x occurs in the presence of the potential of mean force with intrinsic mass and friction Eq. (6.11). Berezhkovskii and Szabo, 2011, showed further that the dynamics along y influences the dynamics along x (through $\delta F_x(y) \neq 0$) in two ways. It leads to an additional friction force as well as an additional thermal force (second heat bath), the two being related by the fluctuation-dissipation theorem. In the Markovian limit, the additional forces result in a position-dependent friction coefficient $\gamma(x)$, respectively, position-dependent diffusion coefficient $D(x)$, cf. Sect. 2.4. Then, the particle's velocity

along x is approximately governed by

$$\dot{v}_x = -\gamma(x)\, v_x - \frac{\mathrm{d}\, A(x)}{\mathrm{d}\, x} + \sqrt{2\gamma(x)}\, \xi_x(t). \tag{6.17}$$

High-friction limit

Referring to Kramers, 1940, see also Becker, 1985, the Fick-Jacobs equation, Eq. (2.34), can be derived directly from the Klein-Kramers equation, Eq. (6.15). Paraphrasing the latter leads to

$$\begin{aligned} \partial_t p(x, v_x, t) = (\gamma \partial_{v_x} - \partial_x) \left[v_x + \partial_{v_x} + \frac{1}{\gamma}\partial_x + \frac{1}{\gamma}\frac{\mathrm{d}\, A(x)}{\mathrm{d}\, x} \right] p(x, v_x, t) \\ + \frac{1}{\gamma}\partial_x \left[\frac{\mathrm{d}\, A(x)}{\mathrm{d}\, x}\, p(x, v_x, t) + \partial_x p(x, v_x, t) \right], \end{aligned} \tag{6.18}$$

where $\delta F_x(y)$ is set to zero. Integrating Eq. (6.18) along the line $G : v_x = \gamma\,(x_0 - x)$ results in

$$\int_G \mathrm{d}s\, \partial_t p(x, v_x, t) = \frac{1}{\gamma} \int_G \mathrm{d}s\, \partial_x \left[\frac{\mathrm{d}\, A(x)}{\mathrm{d}\, x}\, p(x, v_x, t) + \partial_x p(x, v_x, t) \right]. \tag{6.19}$$

If both the mean force $\mathrm{d}A(x)/\mathrm{d}x$ and the joint PDF $p(x, v_x, t)$ do not change much along x during the correlation length v_x/γ, the integration along $G : v_x$ can be replaced by $\int_{-\infty}^{\infty} \mathrm{d}v_x$ for any value for x, give rise to

$$\partial_t p(x, t) = \frac{1}{\gamma}\partial_x \left[\frac{\mathrm{d}\, A(x)}{\mathrm{d}\, x}\, p(x, t) \right] + \frac{1}{\gamma}\partial_x^2 p(x, t). \tag{6.20}$$

One expects that Eq. (6.20) is valid as long as

$$\frac{\mathrm{d}^{\,2} A(x)}{\mathrm{d}\, x^2}\, \frac{1}{\gamma} \ll \frac{\mathrm{d}\, A(x)}{\mathrm{d}\, x}, \quad \text{and} \quad \partial_x p(x, v_x, t) \frac{1}{\gamma} \ll p(x, v_x, t) \quad (f \ll 1). \tag{6.21a}$$

or

$$\frac{\mathrm{d}^{\,2} A(x)}{\mathrm{d}\, x^2}\, \frac{f}{\gamma^2} \ll \frac{\mathrm{d}\, A(x)}{\mathrm{d}\, x}, \quad \text{and} \quad \partial_x p(x, v_x, t) \frac{f}{\gamma^2} \ll p(x, v_x, t) \quad (f > 1), \tag{6.21b}$$

are satisfied. By re-scaling the time as suggested in Sect. 2.2, Eq. (6.20) goes over to the time-dependent Fick-Jacobs equation, cf. Eq. (2.34). Accordingly, the conditional PDF, Eq. (6.9), simplifies to Eq. (2.33) by integrating the transverse velocity v_y out. By expanding the Klein-Kramers equation, Eq. (6.18), in orders of the relaxation time $1/\gamma$ (Chapman-Enskog procedure), Tikhonov derived the first order correction to Eq. (6.20)

$$\partial_t p(x, t) = \frac{\partial}{\partial\, x} \left\{ 1 + \frac{1}{\gamma^2} \frac{\mathrm{d}^{\,2} A(x)}{\mathrm{d}\, x^2} \right\} \left[\frac{\mathrm{d}\, A(x)}{\mathrm{d}\, x}\, p(x, t) + \partial_x p(x, t) \right], \tag{6.22}$$

which scales with the second derivative of the potential of mean force with respect to the coordinate x [Titulaer, 1978; Wilemski, 1976].

The analytic expression for the potential of mean force $A(x)$ for arbitrary viscous friction coefficient can be derived along the lines of Sect. 2.3.1: Following Sokolov, 2010, the interaction of the particles with the wall can be mimicked by a quadratic potential acting in the direction normal to the wall, $U_{\pm}(\mathbf{n}_{\pm}) = 0.5\,\kappa_w\,\mathbf{n}_{\pm}^2$ with interaction strength κ_w and $\mathbf{n}_{\pm}$ being the coordinate along the normal to the upper and lower boundary taken at the point $(x, \omega_{\pm}(x))^T$. When x is fixed, $U_{\pm}(\mathbf{n}_{\pm})$ depends only on the y-coordinate and is given by Eq. (2.39). Equation (6.10) then reduces to $\mathrm{d}A(x)/\mathrm{d}x = \int_{\omega_-(x)}^{\omega_+(x)} \mathrm{d}y \int_{-\infty}^{\infty} \mathrm{d}v_y\, [\partial_x \Phi + \partial_x U_{\pm}]\, P(y, v_y|x)$. Integrating the latter with respect to the transverse velocity leads to Eq. (2.40) and, finally, we derive Eq. (2.42):

$$-\frac{\mathrm{d}\,A(x)}{\mathrm{d}\,x} = \partial_x \ln \left[\int_{\omega_-(x)}^{\omega_+(x)} \mathrm{d}y\, e^{-\Phi(x,y)} \right]. \tag{6.23}$$

The mean force is the conditional average of the mechanical forces exerted on the particle caused by non-holonomic constraint originated from the boundaries. Furthermore, the corresponding potential of mean force $A(x)$ is the free energy associated with the partition function $Z(x) = \int_{\omega_-(x)}^{\omega_+(x)} \mathrm{d}y\, \exp\left(-\Phi(\mathbf{q})\right)$ and, more importantly, it does not depend on the viscous friction coefficient γ. Referring to Pope and Ching, 1993, this result relies on the Maxwell distribution of v_y, i.e., on equipartition. Based on purely probabilistic considerations, Pope and Ching derived an equation connecting the stationary PDF $p(x)$ of any variable x with the mean conditional acceleration $\langle\, \ddot{x}|x \,\rangle$ at x and the mean conditional squared velocity at x, $\langle\, \dot{x}^2|x \,\rangle$:

$$\langle\, \ddot{x}|x \,\rangle\, p(x) = \frac{\mathrm{d}}{\mathrm{d}\,x} \left[\left\langle\, \dot{x}^2|x \,\right\rangle p(x) \right]. \tag{6.24}$$

If the equipartition theorem holds, the mean squared velocity of the particle does not depend on its position in a canonical ensemble and it equals unity in our scaling, $\langle\, \dot{x}^2|x \,\rangle = 1$. If so, the mean force or, equivalently, the mean conditional acceleration is given by

$$\langle\, \ddot{x}|x \,\rangle = \frac{\mathrm{d}}{\mathrm{d}\,x} \ln\left[p(x)\right], \tag{6.25}$$

which coincides with Eq. (6.23). As we proceed to show, equipartition breaks down if the particle motion is not overdamped.

6.3. Particle transport through sinusoidally-shaped channels

In this section, we focus on the particle mobility $\mu/\mu^0 = \lim_{t\to\infty} \gamma\, \langle\, x(t) \,\rangle / (f\, t)$ and the effective diffusion coefficient $D_{\mathrm{eff}}/D^0 = \lim_{t\to\infty} \gamma\, (\langle\, x(t)^2 \,\rangle - \langle\, x(t) \,\rangle^2)/(2\, t)$ of particles moving in a sinusoidally-shaped channel with top boundary given by

$$\omega_+(x) = \frac{1}{4} \left[\Delta\Omega + \Delta\omega - (\Delta\Omega - \Delta\omega) \cos\left(2\pi\, x\right) \right], \tag{6.26}$$

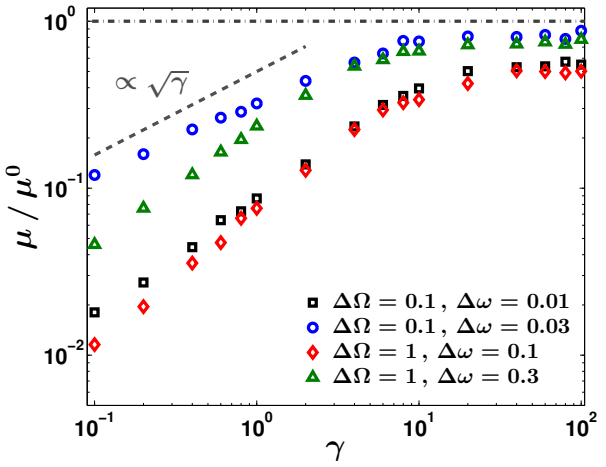

Figure 6.2: Particle mobility μ/μ^0 in a sinusoidally-shaped channel with profile Eq. (6.26) as a function of viscous friction coefficient γ for different channel widths $\Delta\Omega = 0.1, 1$ and aspect ratios $\delta = 0.1, 0.3$. The force magnitude is kept fixed $f = 0.1$.

and with flat bottom boundary, $\omega_-(x) = 0$. $\Delta\Omega$ and $\Delta\omega$ denote the maximal and the minimal width of the channel, respectively, with aspect ratio $\delta = \Delta\omega/\Delta\Omega$. An exemplary segment of the considered 2D channel geometry is depicted in Fig. 6.1. Since the external force acts only along the channel axis and all reflections at the boundary are treated as elastic, it is sufficient to consider only one half of the channel instead of the complete reflection symmetric geometry with $\omega_-(x) = -\omega_+(x)$. Both configurations lead to the same results for the transport quantities, cf. [Ghosh et al., 2012b,c]. Solely the correlation between the velocity components changes, however, the latter is assumed to be zero within the fast relaxation approximation Eq. (6.9).

Inertial effects in shape modulated channels become apparent if the Brownian motion is spatially correlated on a length of the order of the bottleneck width $\Delta\omega$. According to Eqs. (6.12) and (6.13), this is true both for small friction coefficient γ and for strong external forces f. Figures 6.2 and 6.3 show the impact of γ on the particle mobility in a sinusoidally-shaped channel with profile Eq. (6.26). The numerical results were obtained by Brownian dynamics simulation. For this reason, the Langevin equation Eq. (6.1) was numerically integrated by Euler's method [Kloeden and Platen, 1999] with a position dependent time step Δt. For each parameter set, Δt was set small enough for the output to be independent of it. Averages were performed over an ensemble of $3 \cdot 10^4$ initially equilibrated trajectories and collisions of the particle with the boundaries were treated as elastic [for details see App. A]. The numerical errors were of the size of the markers so we don't indicate them.

By inspecting Fig. 6.2 and 6.3, one immediately recognizes that inertial effects (small value of γ) suppresses the particle mobility in corrugated channels, i.e., particles respond much weaker to external stimuli. In the opposite limit of strong viscous friction, $\gamma \to \infty$, the mobility becomes independent of γ and tends to an asymptotic value, as expected in the Smoluchowski approximation $m \to 0$. For weakly modulated channels $\varepsilon = \Delta\Omega - \Delta\omega \lesssim 0.1$ and $\gamma \gg 1$, this asymptotic value is given by Eq. (3.61) for the considered geometry, Eq. (6.26). At low friction coefficient $\gamma \ll 1$, the particle mobility μ/μ^0 grows with γ as a power of γ, $\mu/\mu^0 \simeq \gamma^\chi$, where χ depends on f, see Fig. 6.3 (insets), and on the geometry parameters $\Delta\Omega$ and $\Delta\omega$, see Fig. 6.2. In particular, the exponent is close to $\chi \simeq 1/2$, i.e., $\mu/\mu^0 \simeq \sqrt{\gamma}$, for narrow channels $\Delta\Omega \ll 1$. Such a

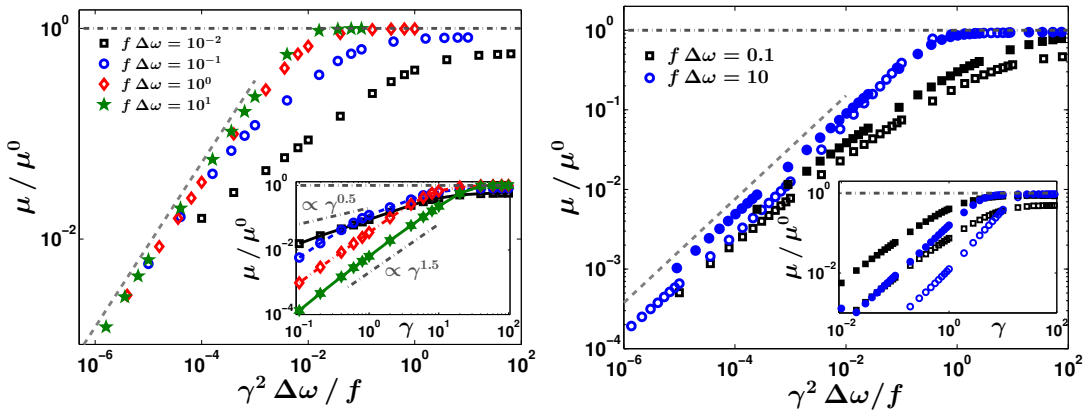

Figure 6.3.: Particle mobility μ/μ^0 as a function the rescaled friction coefficient $\gamma^2\,\Delta\omega/f$ and of γ (insets) for different values for f. Left: The raising branch of the collapsing curves is fitted by a power law $(\gamma^2\,\Delta\omega/f)^{\chi_S}$ with exponent $\chi_S = 0.75 \pm 0.02$ for $\Delta\Omega = 0.1$ and $\Delta\omega = 0.01$. Right: μ/μ^0 vs. γ for different bottleneck widths $\Delta\omega = 0.1$ (blank symbols) or $\Delta\omega = 0.5$ (filled symbols) and force strengths $f\,\Delta\omega$. The maximum channel width is kept fixed $\Delta\Omega = 1$. All data points collapse to one unique curve which scales like $(\gamma^2\,\Delta\omega/f)^{\chi_S}$ with exponent $\chi_S = 0.65 \pm 0.01$.

dependence is known for weakly damped Brownian motion in 1D, periodic energetic potentials, cf. [Risken, 1989, Eq. (11.135)], and might witness for the applicability of the reduced description. In the opposite limit of wide channels, $\varepsilon \gtrsim 1$, the exponent is unity, $\chi = 1$, regardless of the bottleneck width or the aspect ratio (see inset in Fig. 6.4 (ii)), i.e., $\lim_{f\to 0} \mu/\mu^0 \propto \gamma$. Comparing Fig. 6.4 (i) and (ii), we observe that the particle mobility and the effective diffusion coefficient coincide if diffusion dominates $f \ll 1$; thus corroborating the Sutherland-Einstein relation Eq. (2.26). In this limit, the motion within the unit cell of the channel is practically ballistic at a speed of the order of the rms thermal velocity $\langle\, v \,\rangle$ (scaled to unity). The typical time to traverse the cell is $T_e = 1/\langle\, v \,\rangle$, and the probability to leave the cell for another one, making a unit displacement, is of the order of the aspect ratio δ [Ghosh et al., 2012b]. Therefore, the EDC scales like $D_{\text{eff}}(0) \propto \delta/T_e \simeq \delta$ and one gets

$$\lim_{f\to 0} \mu(f)/\mu^0 = \lim_{f\to 0} D_{\text{eff}}(f)/D^0 \propto \delta\,\gamma, \quad \text{for} \quad \gamma \ll 1. \tag{6.27}$$

Although, the last equation agrees quite well with numerics for $\Delta\Omega = 1$ (see Fig. 6.4 (b)) it does not reproduce the results for narrow channels $\Delta\Omega = 0.1$ (see Fig. 6.4 (a)). To be more precise, for $\delta = 0.1$ and $f = 0.1$ we found $\chi \simeq 0.75, 0.94, 0.99$ for $\Delta\Omega = 0.1, 0.2,$ and 1.

Remarkable, expressing the viscous friction coefficient in units of $\sqrt{f/\Delta\omega}$, all curves tends to collapse on one unique curve which scales like $(\gamma^2\,\Delta\omega/f)^{\chi_S}$. The exponent was fitted as $\chi_S = 0.75 \pm 0.02$ for $\Delta\Omega = 0.1$ and $\Delta\omega = 0.01$ regardless of the value of f. For wider channels $\Delta\Omega = 1$, the particle mobility grows with exponent $\chi_S = 0.65 \pm 0.01$ independent of the value of the bottleneck width and the force strength. Surprisingly, while one observes that the value of γ, where μ/μ^0 attains its asymptotic value, grows

with the force magnitude it turns out that the value of the re-scaled friction coefficient $\gamma^2\,\Delta\omega/f$ decreases with f. Whereas it is of the order of unity for wide channels, $\Delta\Omega = 1$, the value decreases to approximately 0.01 for $f\,\Delta\omega = 10$ in narrow channels, $\Delta\Omega = 0.1$. This contradicts the argumentation based on the length scales, Eq. (6.13). Furthermore, it indicates that the analytic form of a function for $\gamma(f, \Delta\Omega, \Delta\omega)$ at which the particle's dynamics can be treated as overdamped is more complicated.

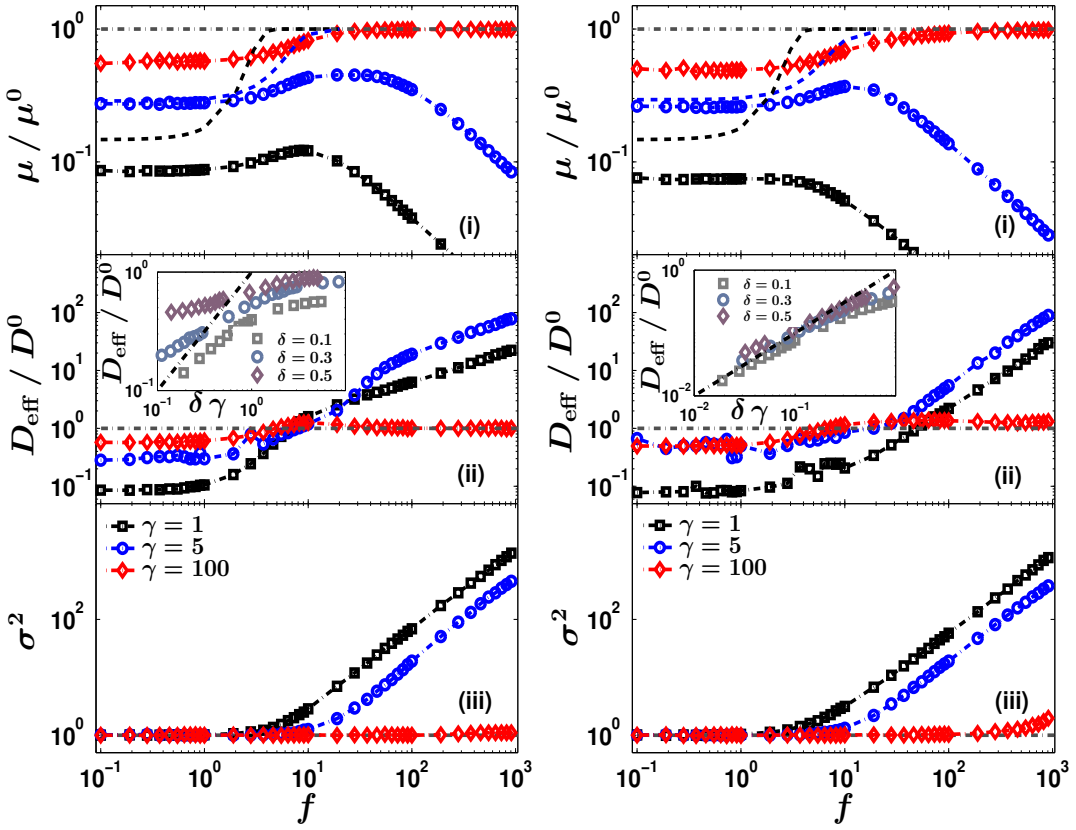

(a) $\Delta\Omega = 0.1$, $\Delta\omega = 0.01$ **(b)** $\Delta\Omega = 1$, $\Delta\omega = 0.1$

Figure 6.4.: Results of simulation of full dynamics, Eq. (6.1), in a sinusoidally modulated channel geometry of Fig. 6.1 with $\Delta\Omega = 0.1$ and $\Delta\omega = 0.01$ (a), and $\Delta\Omega = 1$ and $\Delta\omega = 0.1$ (b). In panel (i)-(iii), the force dependence of different dynamical characteristics of the system are depicted for $\gamma = 1, 5$ and 100. (i) Particle mobility μ/μ^0 (symbols). Superimposed are numerical results for reduced dynamics, Eq. (6.11) (dashed lines). (ii) The effective diffusion coefficient, D_{eff}/D^0 versus f. Inset: D_{eff}/D^0 versus $\delta\,\gamma$ for $f = 0.1$. Dash-dotted line indicates $\delta\,\gamma$. (iii) The 2nd central moment $\sigma^2 = \langle v_y^2 \rangle - \langle\, v_y \,\rangle^2$ of v_y. The horizontal dash-dotted lines indicate unity.

Figure 6.4 shows the influence of the force strength f on the particle mobility (see panel (i)) for various viscous friction coefficients γ. Since $\mu(f)$ and $D_{\text{eff}}(f)$ are reflection symmetric functions caused by the symmetry of the boundary function $\omega_+(x)$, viz., $\mu(-f) = \mu(f)$ and $D_{\text{eff}}(-f) = D_{\text{eff}}(f)$, for the sake of clarity, we discuss the behavior for $f > 0$ only. For $\gamma \gg 1$, we recognize the already known dependence of μ/μ^0 on f, cf. Sect. 3.2.1: Starting from the asymptotic value $\mu/\mu^0 = 2\sqrt{\delta}/(1+\delta)$ for $f \ll 1$, Eq. (3.64), the mobility increases with force magnitude till the asymptotic value $\mu/\mu^0 = 1$ is reached for $f \to \infty$. In the limiting case $\varepsilon = \Delta\Omega - \Delta\omega \lesssim 0.1$ and $\gamma \gg 1$, the dependence of the particle mobility on f is well reproduced by Eq. (3.61) for the considered geometry Eq. (6.26).[4] In the diffusion dominated regime, $f < 1$, the particle mobility and the effective diffusion coefficient (Fig. 6.4 (i) and (ii)) coincide. Furthermore, it is demonstrated that the scaled particle mobility μ/μ_0 and the EDC D_{eff}/D^0 grow with γ for $f < 1$, see Fig. 6.2. Noteworthy, the particle mobility and the mean particle current $\langle \dot{x} \rangle$ differ from zero even for sufficient weak, non-zero forces. In 2D confining channels, no locked state with zero mean particle current exists for $f \neq 0$, contrary to biased Brownian motion in 1D energetic potentials. Only in the limit of vanishing pore sizes, $\Delta\omega \to 0$, the MFPT diverges and particles are trapped.

For stronger external force, the particle mobility grows with f, reaches its maximum at $f_{\max}$, whose value depends on the friction coefficient and goes to infinity for $\gamma \to \infty$, and then decays as $\mu/\mu^0 \propto f^{-\epsilon_f}$ with $\epsilon_f < 1$. It turns out that the particles' response to an external force diminishes with its strength for a finite value of γ. In Tab. 6.1, we list some values of ϵ_f for different channel parameters and viscous friction coefficients. It turns out that the particle mobility is well fitted by an exponent $\epsilon_f \simeq 0.65$ for low friction and strong force. In the opposite limit of strong friction, $\gamma\Delta\omega > 1$ and $\gamma^2\Delta\omega/f > 1$, the Smoluchowski approximation $m \to 0$ is valid and thus the particle mobility tends to μ^0 for $f \to \infty$. Consequently, the exponent ϵ_f goes to zero.

Below, we discuss the impact of γ on the effective diffusion coefficient. In the high friction limit, we reproduce the results from Sect. 3.2.3: starting from $D_{\text{eff}}/D^0 = 2\sqrt{\delta}/(1+\delta)$ for $f \to 0$, Eq. (3.64), the EDC grows with increasing f until it reaches its maximum, then decays, and finally tends to the bulk value $D_{\text{eff}} = D^0$ for $f \to \infty$. For low γ and for small forces, all numerical results for the EDC collapse to one unique curve which scales linearly with γ, $D_{\text{eff}}/D^0 \propto \gamma\,\delta$ for $\Delta\Omega = 1$, and attain values smaller than D^0. For narrow geometries, D_{eff}/D^0 grows with γ too, but the slope diminishes with lessening channel width (see left inset in Fig. 6.4 (ii)). For moderate to strong forces, $f \gtrsim 10$, the behavior of D_{eff}/D^0 as a function of γ is non-monotonic. For weak to moderate damping the EDC grows monotonically with γ whereby the attained values are larger than the bulk value $D^0 = 1/\gamma$. In the opposite limit of high friction, the EDC is almost equal to D^0. Consequently, D_{eff}/D^0 attains a maximum at a given value of γ which depends on the force magnitude and on the channel geometry. For $f \to \infty$, the effective diffusion coefficient diverges like $D_{\text{eff}}/D^0 \propto f^{\varsigma_D}$ caused by the (chaotic) mechanism of ballistic collisions. From the numerical data we conclude that the exponent ς_D solely depends on the geometry parameters. In detail, we find $\varsigma_D \simeq 0.5$ for $\Delta\Omega = 0.1$ and $\varsigma_D \simeq 1$ for $\Delta\Omega = 1$. Especially, the last value coincides with the numerical results and a heuristic explanation presented in Ghosh et al., 2012b.

[4] Since we have demonstrated the good agreement already in Sect. 3.2.1, for sake of clarity, we abandon

$\Delta\Omega$	$\Delta\omega$	$\gamma\,\Delta\omega$	ϵ_f
0.1	0.01	0.01	0.69 ± 0.05
0.1	0.01	0.1	0.46 ± 0.03
0.1	0.01	1	0.01 ± 0.01
1	0.1	0.1	0.63 ± 0.04
1	0.1	1	0.68 ± 0.02
1	0.1	10	0.06 ± 0.02
1	0.5	0.1	0.60 ± 0.05
1	0.5	1	0.57 ± 0.03
1	0.5	10	0.05 ± 0.01

Table 6.1: The value of the exponent ϵ_f which determines the particle mobility's decay for $f \to \infty$ was fitted from the numerical data. Its dependence on the channel parameters $\Delta\omega$ and $\Delta\Omega$ and on the friction coefficient γ is presented.

6.4. Applicability of the Fick-Jacobs approach

In Sect. 6.2, we demonstrated that the full dynamics, Eq. (6.1), can be replaced by the motion of a particle evolving in the potential of mean force $A(x)$, Eq. (6.11). Above, we showed that both the particle mobility and the EDC grow with the viscous friction coefficient γ as a power of γ if diffusion dominates, $f < 1$. A similar dependence is known for weakly damped Brownian motion in 1D periodic potentials [Risken, 1989] and might be witness for the applicability of the reduced description, Eq. (6.11).

In Fig. 6.4 (i), the particles mobility for the reduced dynamics (dashed lines) obtained by simulating Eq. (6.11) is additionally presented. We observe that within the FJ approach μ/μ^0 is a monotonous function of f which starts from an asymptotic value, which is less than μ^0, for $f < 0$ and tends to the bulk value for $f \to \infty$. Comparing the results for reduced dynamics with numerical results for the full problem, one notices that the reduced description overestimates the mobility. However, the accuracy of the approximation is sufficiently good for $\gamma \geq 5$ and small forces $f < f_{\max}$. Additionally, we recognize that there exists a characteristic force strength f_c beyond which the reduced description fails. The force f_c gets smaller with decreasing friction and thus the discrepancy is large even for $\gamma = 1$ in the diffusion dominated regime, $f \ll 1$. Introducing the position-dependent friction $\gamma(x)$, as proposed in [Berezhkovskii and Szabo, 2011], gives corrections of the order of $(\Delta\Omega)^2$ and does not sufficiently improve the agreement (not explicitly shown).

Our derivation of the effective dynamics, Eq. (6.9), implies (i) homogeneous distribution of y (fast relaxation approximation), (ii) vanishing correlation between v_x and v_y, and (iii) most importantly equipartition of the kinetic energies (Maxwell distribution) corresponding to v_x and v_y holds. Figure 6.5 (a) presents the velocity PDFs $P(v_x)$ and $P(v_y)$ centered at their means $\langle\, v_x \,\rangle$ and $\langle\, v_y \,\rangle$ for different γ values and fixed force strength, $f = 100$. The distribution $P(v_x)$, Fig. 6.5 (a,i), undergoes a transition from a normal (Maxwell) one with unit variance for $\gamma = 100$ over an asymmetric form for $\gamma = 10$ to an even broader symmetric function for $\gamma = 1$. While the largest absolute value of v_x is much smaller than the asymptotic one for $\gamma = 1$, viz. $|v_x| \ll f/\gamma$, the maximum of $P(v_x)$ coincides with asymptotic value $v_x \simeq f/\gamma$ for $\gamma = 10$. The

to repeat it here.

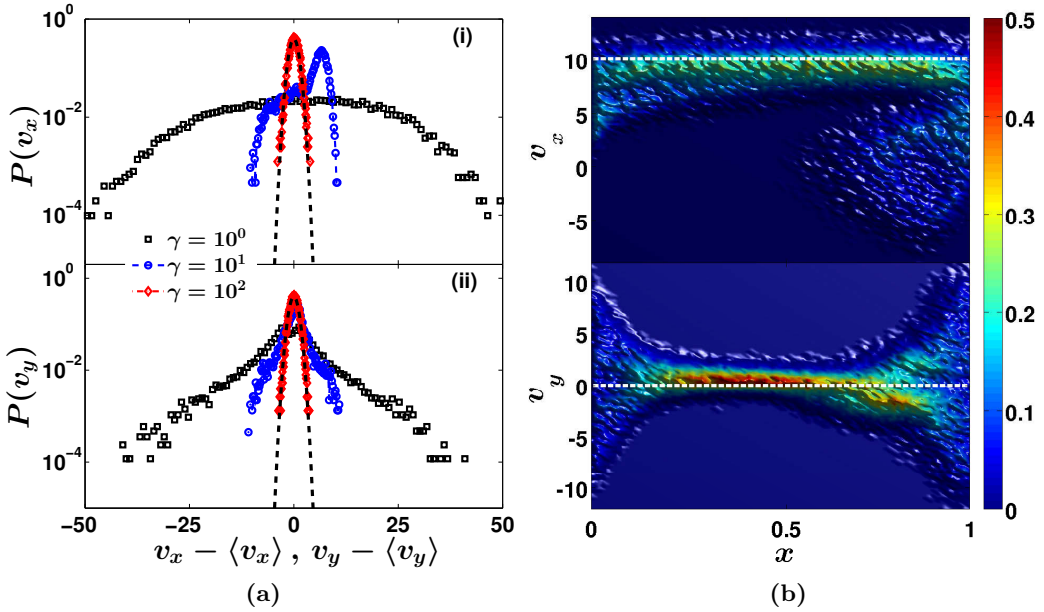

Figure 6.5.: Left panel: Normalized stationary probability distribution functions of v_x and v_y as functions of the friction coefficient γ. The mean values are $\langle v_x \rangle \approx 3.46, 6.78, 0.99$ (for $\gamma = 10^0, 10^1, 10^2$) and $\langle v_y \rangle \simeq 0$ (for all γ values). The black dashed lines indicate the normalized Maxwell velocity distribution $\exp(-v_i^2/2)/\sqrt{2\pi}$ with $i = x, y$. Right panel: Contour plots of the stationary joint PDFs $P(x, v_x)$ (top) and $P(x, v_y)$ (bottom) for $\gamma = 10$. The dashed lines represent the asymptotic values for the particle velocity, viz., f/γ for v_x and zero for v_y. For all panels the remaining parameters values are $\Delta\Omega = 0.1$, $\Delta\Omega = 0.01$, and $f = 100$.

PDF $P(v_y)$, Fig. 6.5 (a,ii), also broadens with decreasing viscous friction coefficient but stays symmetric. The corresponding mean values are always zero, $\langle v_y \rangle = 0$. The deviation of $P(v_y)$ from equilibrium distribution is indicated by its second central moment $\sigma^2 = \langle v_y^2 \rangle - \langle v_y \rangle^2$, see Fig. 6.4 (iii), which is unity for Maxwellian distribution in our scaling. For subcritical force magnitudes $f < f_c(\gamma)$, the velocity distribution $P(v_y)$ are always Maxwellian and thus $\sigma^2 \approx 1$. If f exceeds a critical magnitude f_c, we find $\sigma^2 \propto f^{\varsigma_v}$ with $\varsigma_v \gtrsim 1$. Consequently, the PDF $P(v_y)$ broadens with decreasing viscous friction coefficient for $f > f_c$. In other words, the decrease of the particle mobility goes hand in hand with violation of equipartition. The 2nd central moment of v_x shows the same dependence on the external force magnitude and the friction coefficient as the one of v_y (not explicitly shown). Furthermore, we find that the critical value f_c is bounded by $\gamma \leq f_c \leq 10\,\gamma$, see Fig. 6.6.

Let us discuss the nature of the equipartition violation. While changes in γ hardly influence the properties of the free motion (up to timescales), its value is crucial when the motion is confined, see Fig. 6.1. The latter changes from erratic $\gamma \gg 1$ to almost regular – like in the deterministic case [Cecconi et al., 2003; Harayama et al., 2002] – for $\gamma \to 0$. In Fig. 6.5 (b), we depict the stationary joint PDFs $P(x, v_x)$ and $P(x, v_y)$ ob-

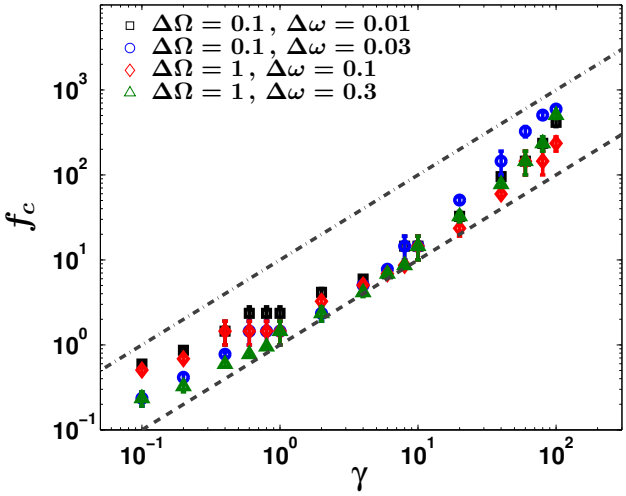

Figure 6.6: Dependence of the critical force magnitude f_c, where $\sigma^2(f_c) = 1.1$, on the viscous friction coefficient and on the channel parameters. Superimposed are $f_c = \gamma$ (dashed line) and $f_c = 10\,\gamma$ (dashed dotted line).

tained by BD simulation of 10^5 individual trajectories. We notice that the acceleration in x-direction is transferred to the transversal velocity component v_y due to reflections at the boundaries. The latter were treated as elastic. As a consequence, the probability that v_x attains negative values, i.e., the particles move in opposite direction to the force, increases at the bottleneck. At the same time, the variance $\langle v_x^2 \rangle - \langle\, v_x \,\rangle^2$ becomes a function of the position x and thus the equipartition condition $\langle\, \dot{x}^2 | x \,\rangle = \text{const}$ gets violated. Furthermore, one observes that the transversal component v_y is strongly enhanced due to the transfer of acceleration at the channel's constricting part. Hence, v_y increases with f leading to violation of equipartition, $\langle\, \dot{y}^2 | x \,\rangle \neq \text{const}$, and to the monotonous growth of σ^2 with f, cf. Fig. 6.3(iii). Integrating $P(x, v_x)$ and $P(x, v_y)$ with respect to x results in the blue curves presented in Fig. 6.5 (a).

The behavior in the x-direction is more complex. Particles reflected at an "optimal" angle can fly over several cells to the left or to the right. Since this "optimal" reflections happen randomly there are always particles moving in opposite direction to the external force at any time. These particles need a given time to turn their direction of motion, $t_{\text{turn}} = \ln\left(1 + \gamma |v_x| / f\right) / \gamma$ (without subsequent collision at the boundaries), which causes the decay of $\mu/\mu_0 \propto f^{-\epsilon_f}$ and the growth of the effective diffusivity $D_{\text{eff}}/D_0 \propto f^{\varsigma_D}$. In particular, we measured the distance d between two subsequent collisions and it turns out that the probability for long stretches $d > 1$ increases with external force and with decreasing γ (not explicitly shown). Likewise, the smaller the friction the higher is the probability to escape to the left $P(x \to x-1)$, see Fig. 6.7 (a). Nevertheless, long excursions in force direction are more probable than in opposite direction, $P(x \to x+1) > P(x \to x-1)$, due to the broken symmetry in x-direction. Additionally, we depict the first passage time PDF $P(t(x_0 \to x_0 + 1))$ for $f = 100$ in Fig. 6.7 (b). $P(t(x_0 \to x_0 + 1))$ undergoes a transition from a Gaussian distribution with mean $\langle\, t(x_0 \to x_0 + 1) \,\rangle = f/\gamma$ for $\gamma = 100$ to a broader bimodal one for $\gamma = 10$, whose maxima are located at $t(x_0 \to x_0 + 1) = f/\gamma$ and $t(x_0 \to x_0 + 1) \simeq 3\, f/\gamma$ (for the given channel parameters). With further reduction of γ, the first passage time PDF broadens and its most probable value shifts towards larger times. Likewise, the mean first passage time grows with ongoing reduction of γ and thus the average particle

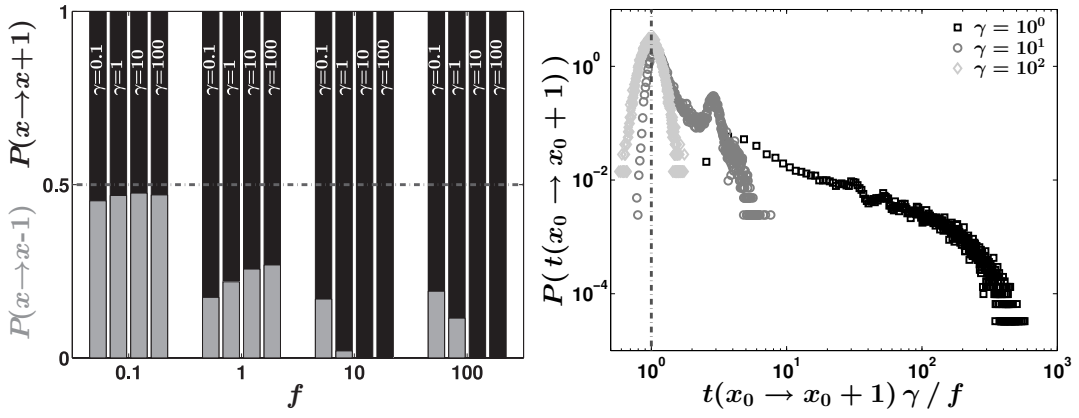

Figure 6.7.: Probability to leave a unit cell to the left or right and first passage time PDF for $\Delta\Omega = 0.1$ and $\Delta\omega = 0.01$. Left: Impact of γ and force magnitude f on probability to leave one unit cell to the left $P(x \to x-1)$ or to the right $P(x \to x+1)$. Right: Normalized PDF of first passage time $t(x_0 \to x_0 + 1)$ (in units of free value f/γ) to reach the final point $x_0 + 1$ for the first time when it starts at an arbitrary point x_0. The force magnitude is set to $f = 100$.

velocity $\langle\, v_x \,\rangle = 1/\langle\, t(x_0 \to x_0 + 1) \,\rangle$ or, equivalently, the particle mobility lessens with the value of γ. The latter is in compliance with the results depicted in Fig. 6.4 (a).

Nevertheless that equipartition of the kinetic energy corresponding to v_y holds for $f < f_c$, we found a large discrepancy between the particle mobility of the full problem and the one of the reduced dynamics for $\gamma \lesssim 1$, cf. Fig. 6.4. The derivation of the effective dynamics, Eq. (6.9), additionally implies that both velocity components are uncorrelated at any time τ, i.e., $\langle\, v_x(\tau) v_y(0) \,\rangle = 0$. According to the solution of Eq. (6.1) in the absence of spatial constraints (the *free* case),

$$\mathbf{v}(t) = \mathbf{v}(0)\, e^{-\gamma\, t} + \frac{\mathbf{f}}{\gamma}\left(1 - e^{-\gamma\, t}\right) + \int_0^t \mathrm{d}t'\, e^{-\gamma\,(t-t')}\boldsymbol{\xi}(t'), \tag{6.28}$$

where $\mathbf{v}(0)$ is the particle velocity at time $t = 0$, cf. Eq. (2.4), the velocity correlation function (VCF) $C_{v_x,v_y}(\tau) = \langle\, v_x(\tau) v_y(0) \,\rangle$ reads

$$\begin{aligned}\langle\, v_i(t) v_j(s) \,\rangle = &\left[\left(\langle\, v_i(0) \,\rangle - \frac{f_i}{\gamma}\right) e^{-\gamma\, t} + \frac{f_i}{\gamma}\right]\left[\left(\langle\, v_j(0) \,\rangle - \frac{f_j}{\gamma}\right) e^{-\gamma\, s} + \frac{f_j}{\gamma}\right] \\ &+ e^{-\gamma|t-s|} - e^{-\gamma(t+s)}, \quad \text{for} \quad i, j = x \,\text{or}\, y,\end{aligned} \tag{6.29}$$

for Gaussian white noise $\boldsymbol{\xi}(t')$, see Eq. (2.3). For large times t and s, i.e., $\gamma t \gg 1$ and $\gamma s \gg 1$, the VCF is independent of the initial velocity $\mathbf{v}(0)$ and becomes a function of the time difference $\tau = t - s$ only. Normalizing Eq. (6.29) by the VCF at $\tau = 0$, we

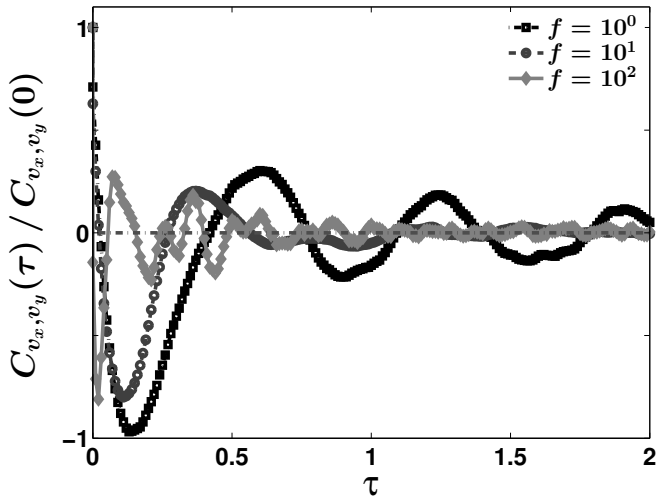

Figure 6.8: Impact of force strength f on the normalized velocity correlation function $C_{v_x,v_y}(\tau) = \langle\, v_x(\tau)v_y(0)\,\rangle$ associated with the confined Brownian motion in a 2D channel. The remaining parameter values are $\gamma = 1$, $\Delta\Omega = 0.1$, and $\Delta\omega = 0.01$.

obtain

$$\frac{C_{v_i,v_j}(\tau)}{C_{v_i,v_j}(0)} = \frac{\langle\, v_i(\tau)v_j(0)\,\rangle}{\langle\, v_i(0)v_j(0)\,\rangle} = \frac{f_i\, f_j + \gamma^2\delta_{i,j}e^{-\gamma|\tau|}}{f_i\, f_j + \gamma^2\,\delta_{i,j}}, \quad \text{for} \quad i = x, y. \tag{6.30}$$

It turns out that the normalized velocity correlation function between the velocity components decays exponentially with the characteristic correlation time $t_{\text{corr}} = 1/\gamma$. The velocity auto-correlation function (VACF) of any component remains finite and different from zero for all time differences τ if an external force is applied in the corresponding direction. For large times, each component converges to its asymptotic value, f_i/γ, and thus the normalized VCF equals $\lim_{\tau\to\infty} C_{v_i,v_j}(\tau)/C_{v_i,v_j}(0) = f_i\, f_j/(f_i\, f_j + \gamma^2\,\delta_{i,j})$ for $i, j = x, y$. For the considered situation where the force acts only along the longitudinal channel direction, $f_y = 0$, the VCF vanishes identically for all times, i.e., $C_{v_x,v_y}(\tau)/C_{v_x,v_y}(0) = 0$.

Figure 6.8 shows the normalized VCF as a function of the external force magnitude f for $\gamma = 1$. In contrast to free case, where $C_{v_x,v_y}(\tau) = 0$, we observe a non-vanishing correlation between the longitudinal and the transverse velocity component. The VCF is determined by subsequent positively correlated and anti-correlated intervals which are caused by the transfer of the acceleration from the longitudinal v_x to the transversal velocity component v_y during collisions with boundaries. Since the time between two successive collisions with the boundary shortens with f, the durations of positively correlated or anti-correlated intervals become less with growing force magnitude. Additionally, we notice that both the envelope's amplitude and its characteristic decay time decrease with increasing force strength. Consequently, the VCF is different from zero for short times and the velocity components become uncorrelated only for $\tau \gg 1$.

Additionally, we depict the dependence of the normalized VACF of the longitudinal v_x, Fig. 6.9 (left), and the transverse velocity component v_y, Fig. 6.9 (right), on the force magnitude f. While $C_{v_x,v_x}(\tau)$ shows anti-correlation in a certain time interval for $f \leq 1$, with growing force strength this interval shortens and finally vanishes identically for $f \gg 1$. Noteworthy, the longitudinal velocity component decorrelates for large time

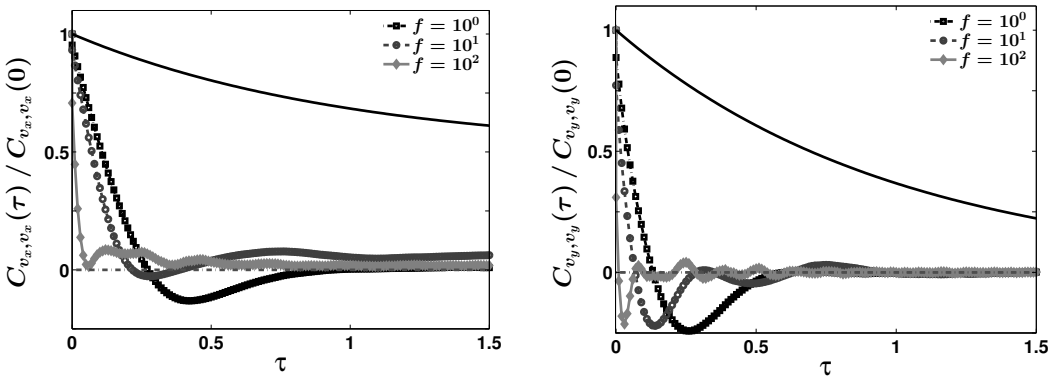

Figure 6.9.: Influence of force magnitude f on normalized velocity auto-correction functions $C_{v_x,v_x}(\tau)$ (left) and $C_{v_y,v_y}(\tau)$ (right) associated with the confined Brownian motion in a 2D channel. Superimposed is the free VACF, Eq. (6.30), for $f = 1$ by the solid line. The remaining parameter values are $\gamma = 1$, $\Delta\Omega = 0.1$, and $\Delta\omega = 0.01$.

differences τ in contrast to free motion. On the other hand, $C_{v_y,v_y}(\tau)$ is governed by subsequent positively correlated and anti-correlated intervals regardless of f. Interestingly, we observe that the envelopes of the VACF decay much faster compared to the free motion (solid lines), indicating that the persistent of the particle motion is disturbed by the collisions with the channel walls. Despite that the duration of anti-correlated particle motion depends on f, the characteristic decay time, $C_{v_y,v_y}(\tau^\dagger) \simeq 0$, seems to be independent of the force magnitude, viz., $\tau^\dagger \simeq 1$.

We conclude that the discrepancy between the reduced dynamics and the full one is caused by the non-vanishing correlation of the particle's velocity components $C_{v_x,v_y}(\tau)$. Since the correlation between v_x and v_y becomes amplified with decreasing external force magnitude, the decay time of the VCF scale inversely proportional to f. In other words, the time scale conditions t_{corr}/τ_y and $t_{\mathrm{corr}}/\tau^y_{\mathrm{drift}}$ are solely satisfied for strong forces or wide channels. This might explain our previous observation that the value of $\gamma^2\,\Delta\omega/f$, where the particle mobility attains its asymptotic value, decreases with the force strength, cf. Fig. 6.3.

6.5. When dissipation helps: Enhancement of particle transport through inelastic collision

In the sections above, we demonstrated that the full dynamics, Eq. (6.1), is sufficiently well reproduced by the reduced description involving the potential of mean force, Eq. (6.11), for moderate up to strong viscous friction coefficients $\gamma \geq 5$ and weak forces $f < f_c$. If f exceeds f_c, the reduced dynamics fails caused by violation of the equipartition conditions, $\langle \dot{x}^2|x\rangle = \text{const}$ and $\langle \dot{y}^2|x\rangle = 1$. Nevertheless that $\langle \dot{y}^2|x\rangle = 1$ holds for $f < f_c$, we found a large discrepancy between the particle mobility of the full problem and the one of the reduced dynamics for weak damping, $\gamma \lesssim 1$. We concluded that this discrepancy is caused by the non-vanishing correlation between the particle's velocity

components due to the transfer of the acceleration in x-direction to the transversal velocity component at the moment of collision with the boundaries. Before, reflections at the boundaries were treated as elastic. But, experiments clearly demonstrate that surface roughness of both the walls and the particles have a significant impact on the particle dynamics, because contact occur through microscopic surface imperfections [Bennett and Mattsson, 1989; Joseph et al., 2001]. Sommerfeld, 1992, showed that the rebound velocity depends on the impact Stokes number $\mathrm{St} \propto \|\mathbf{v}\|/\gamma$ and weakly on the elastic properties of the material. Below a Stokes number of approximately 10, no rebound of the particle occurred. For large impact Stokes number, the coefficient of restitution appears to asymptote to the values for elastic collision. In the following, we discuss the impact of inelastic collision and random elastic scattering on the key particle transport quantities. In particular, we ask if additional sources of dissipation or randomness help to enhance the accuracy of the reduced dynamics.

Caused by the impenetrability of the channel walls, the particle's velocity normal to the wall vanishes identically at the moment of collision. In principle, these collisions can be treated either as elastic or inelastic. The amount of energy dissipation due to the inelasticity of the contacts [Brilliantov and Pöschel, 2001] is often characterized by the coefficient of restitution C_R, defined by the ratio of the rebound to impact velocity. Basically, the particle velocity after collision $\mathbf{v}'$ is given by

$$\mathbf{v}' = \mathbf{v} - (1 + C_R)\ (\mathbf{v} \cdot \mathbf{n})\ \mathbf{n}, \tag{6.31}$$

where $\mathbf{n}$ is the outward-pointing normal vector at the collision point. According to Eq. (6.31), the tangential component of $\mathbf{v}$ does not change, $v_t' = v_t$, while the rebound normal component reads $v_n' = -C_R\, v_n$. $C_R = 1$ corresponds to the limit of ideal elastic collision (specular reflection): here the angle of incidence equals the angle of reflection with respect to the surface normal vector $\mathbf{n}$. The opposite limit of perfectly inelastic collision is represented by $C_R = 0$. There, the normal velocity component after collision vanishes, $v_n' = 0$, and only the tangential component remains, $\mathbf{v} = v_t\, \mathbf{e}_t$. The associated change of kinetic energy reads

$$\Delta E_{\mathrm{kin}} = E_{\mathrm{kin}}' - E_{\mathrm{kin}} = \frac{v_n^2}{2}\left(C_R^2 - 1\right). \tag{6.32}$$

For $C_R < 1$, ΔE_{kin} is negative and thus the systems losses energy caused by its interaction with the channel boundaries. In detail, we assume that the kinetic energy is lost due to e.g. surface friction, emission of heat, or transferred into elastic energy of the boundary, without changing the shape of both collision partners.

Ofter, the impact of microscopic surface imperfections (rough surfaces) is modeled by uniformly distributed reflection angles taken randomly from $\phi \in [0, \pi]$ [Bennett and Mattsson, 1989]. Then, the rebound velocity $\mathbf{v}'$ is determined by

$$\mathbf{v}' = \|\mathbf{v}\| \begin{pmatrix} \cos(\phi) & \sin(\phi) \\ -\sin(\phi) & \cos(\phi) \end{pmatrix} \mathbf{e}_t. \tag{6.33}$$

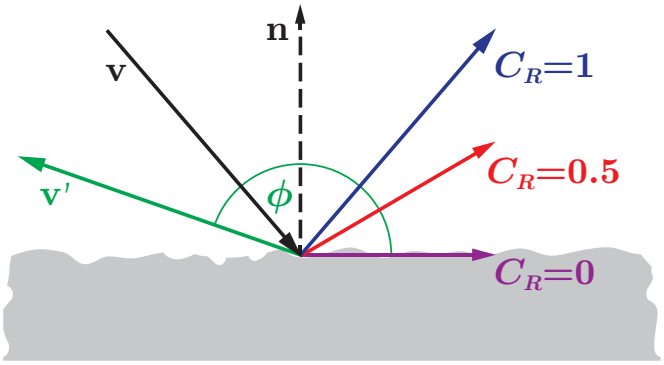

Figure 6.10: Illustration of impact of the coefficient of restitution C_R on the rebound particle velocity vector. The case of scattering with random uniformly distributed reflection angle ϕ is represented by the green arrow. $\mathbf{n}$ is the normal surface vector.

Obviously, kinetic energy and momentum are conserved during the collision. Nevertheless, the scattering procedure will influence the correlation between the velocity components. All discussed reflection methods are illustrated in Fig. 6.10.

The influence of the value of C_R on the transport quantities like the particle mobility μ/μ^0 and the EDC D_{eff}/D^0 is depicted in Fig. 6.11 (a). The numerical results (markers) were obtained by BD simulations in which collisions with the flat boundary, $y = \omega_-(x) = 0$, were always treated as ideal elastic regardless of the considered reflection procedure at the top boundary $\omega_+(x)$. Thus, our numerical results correspond to a reflection symmetric geometry with $\omega_-(x) = -\omega_+(x)$.

At first glance, we observe that the particle mobility grows with decreasing value of C_R or, equivalently, with increasing loss of kinetic energy due to collision. For $C_R = 0.5$, we find that the mobility is almost one magnitude larger compared to the limit of elastic reflection, $C_R = 1$, for any value of f. A further reduction of C_R results only in a weak enhancement of μ/μ^0. In particular, μ/μ^0 is close to unity for $C_R = 0$ and $f \leq f_{\text{max}}$. Basically, one notices that the dependence of the particle mobility on f is independent of the considered reflection method: μ/μ^0 starts from an asymptotic value which coincides with D_{eff}/D^0 for $f \ll 1$, grows with f till it reaches its maximum at f_{max}, and finally decays as a power of f. Interestingly, the value of f_{max} is independent of the considered method, too. In contrast to inelastic particle-wall collisions, elastic scattering leads to smaller mobility values compared to the results for $C_R = 1$. Since the reflection angles are randomly chosen, the particles may change their direction of motion independent of the force orientation. Consequently, the probability to move in opposite direction to f grows and thus μ/μ^0 goes down.

Next, we discuss the impact of C_R on the EDC D_{eff}/D^0. One recognizes that the coefficient of restitution strongly influences the behavior of D_{eff}/D^0. While the EDC is a monotonously growing function for elastic reflection, the situation changes for $C_R < 1$. For $C_R = 0.5$, we find that D_{eff}/D^0 attains a minimum at moderate force strengths before it diverges like $D_{\text{eff}}/D^0 \propto f^{\varsigma_D}$ for $f \to \infty$. In the limit of perfectly inelastic collision, $C_R = 0$, the effective diffusion coefficient decays monotonically with f. The chaotic mechanism of ballistic collisions ($\gamma = 1$ and $f \gg 1$), resulting in the divergence of D_{eff}/D^0 for $C_R = 1$, is suppressed due to loss of kinetic energy at the top boundary. This leads to rectification of the particles' motion, cf. Fig. 6.12 (left). In the case of elastic scattering, the EDC grows monotonically with f like for $C_R = 1$, however, the attained values are smaller than the one for elastic reflection.

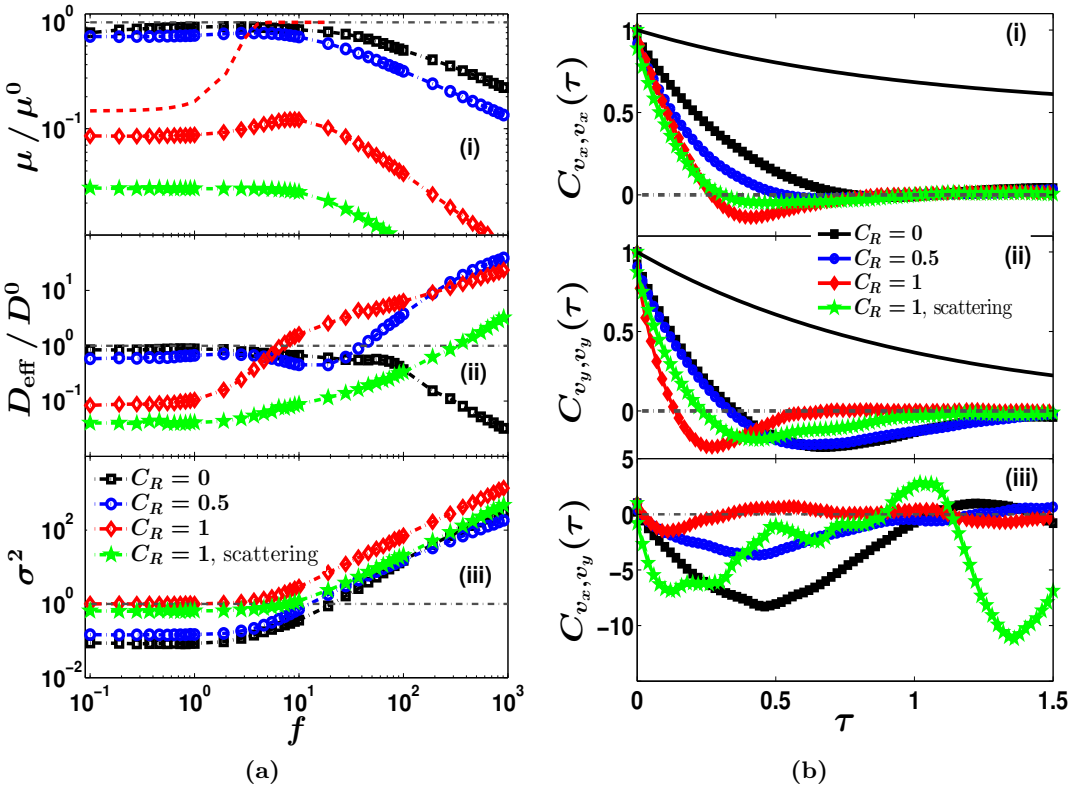

Figure 6.11.: Results of BD simulation of full dynamics, Eq. (6.1), in a sinusoidally modulated channel geometry with $\Delta\Omega = 0.1$, $\Delta\omega = 0.01$, and $\gamma = 1$. Left figure: In panel (i)-(iii), the force dependence of different dynamical characteristics of the system are depicted for $C_R = 0, 0.5$, and 1 and for elastic scattering. (i) Particle mobility μ/μ^0 (symbols) and numerical results for reduced dynamics, Eq. (6.11) (dashed line). (ii) The effective diffusion coefficient, $D_{\rm eff}/D^0$, versus f. (iii) The 2nd central moment $\sigma^2 = \langle v_y^2 \rangle - \langle v_y \rangle^2$ of v_y. Right figure: Normalized VACF $C_{v_x,v_x}(\tau)/C_{v_x,v_x}(0)$ (i), $C_{v_y,v_y}(\tau)/C_{v_y,v_y}(0)$ (ii), and normalized VCF $C_{v_x,v_y}(\tau)/C_{v_x,v_y}(0)$ (iii) for $C_R = 0, 0.5$, and 1 and for elastic scattering. Superimposed are the free VACFs, Eq. (6.30), by the solid line. The force strength is set to $f = 1$. In all panels, the horizontal dash-dotted lines indicate unity.

The two mean ingredients for the validity of the reduced description, Eq. (6.11), are (i) equipartition of the kinetic energy of v_y and (ii) vanishing correlation between v_x and v_y. In panel (iii) of Fig. 6.11 (a), we show the influence of f on 2nd central moment of v_y, $\sigma^2 = \langle v_y^2 \rangle - \langle v_y \rangle^2$, which indicates if equipartition holds. In addition, the impact of the coefficient of restitution on the normalized VACFs $C_{v_x,v_x}(\tau)/C_{v_x,v_x}(0)$, $C_{v_y,v_y}(\tau)/C_{v_y,v_y}(0)$, and the VCF $C_{v_x,v_y}(\tau)/C_{v_x,v_y}(0)$ are presented in Fig. 6.11 (b).

Comparing both elastic collision methods, we observe that $\sigma^2 \simeq 1$ for $f < f_c$ and diverges like $\sigma^2 \to \infty$ if f exceeds f_c. Thereby, the critical force strength f_c, beyond which equipartition is violated, becomes larger for elastic scattering. Concerning the correlation between the particle's velocity components, one notices that elastic scattering increases weakly the characteristic decay time of the VACFs $C_{v_x,v_x}(\tau)$ and $C_{v_y,v_y}(\tau)$. Nevertheless, the components still decorrelate faster compared to free motion (solid lines). Focusing on the VCF $C_{v_x,v_y}(\tau)$, we find that the velocity components remain correlated for any time difference τ and, in particular, elastic scattering enhances the correlation.

Due to the loss of kinetic energy during the collision of the particles with the channel boundary, Eq. (6.32), the fluctuation-dissipation relation and, consequently, equipartition of the kinetic energy of v_y are violated for $C_R \neq 1$. In particular, we find that the width of the velocity PDF $P(v_y)$ shrinks with decreasing coefficient of restitution C_R. Therefore, σ^2 attains values less than unity for weak forces, $f \ll 1$, see panel (iii) in Fig. 6.11 (a). With growing force magnitude, the width of $P(v_y)$, respectively, σ^2 grow and finally tend to infinity for $f \to \infty$. Remarkable, all graphs $\sigma^2(f)$ collapse to one unique curve on expressing the latter in units of its asymptotic value for $f \to 0$, viz., $\sigma^2(f)/\sigma^2(0)$ (not shown). Therefore, we conclude that the underlying mechanism leading to violation of equipartition for the transversal velocity v_y is solely determined by the length scales (channel parameters) and the viscous friction coefficient γ. Studying the impact of C_R on the VACFs, we recognize that the decay times grow with decreasing value of C_R, but nevertheless, the times are much shorter compared to the unconfined situation (solid lines). Additionally, one notices that VCF $C_{v_x,v_y}(\tau)$ differs from zero for all times τ regardless the value of C_R. Particularly, the correlation between v_x and v_y becomes amplified by reducing the coefficient of restitution C_R.

We conclude that additional sources of dissipation or randomness do not enhance the accuracy of the reduced dynamics, Eq. (6.11). Quite the contrary, due to the loss of kinetic energy as a consequence of inelastic particle-wall collision, $C_R \neq 1$, the equipartition presumption is not satisfied for any value of f. In the case of elastic scattering, the particles' direction of motion changes randomly during collisions with the top wall, resulting in a higher probability to move in opposite direction to the external force $\mathbf{f}$. Consequently, the particle mobility is reduced and thus the discrepancy grows. However, we find that the transport quality, which is measured by the Péclet number Pe (in units of its free value $Pe/f = (\mu/\mu^0)/(D_{\text{eff}}/D^0)$), grows with f for perfectly inelastic collision, $C_R = 0$. The attained values are larger than unity indicating that particle transport is directed. In compliance with Fig. 6.12 (left), perfectly inelastic collisions rectify the nearly ballistic (chaotic) particle motion appearing for weak damping and strong forces. For $C_R \neq 0$ as well as elastic scattering, the particle transport becomes more irregular with increasing force strength. Hence, the particle's response to external

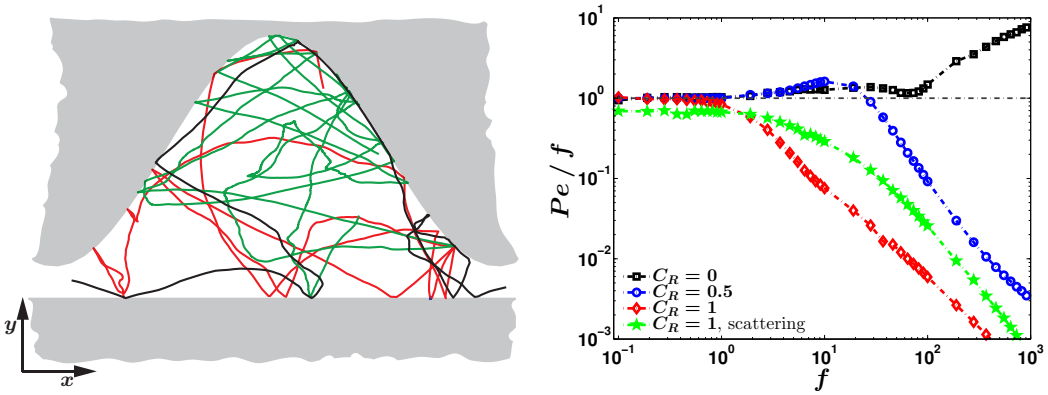

Figure 6.12.: Left: Exemplary particle trajectories for $C_R = 0$ (black), $C_R = 1$ (red), and elastic scattering (green); $\gamma = 1$ and $f = 1$. Right: Simulation results for Peclet number Pe versus external force magnitude f for $C_R = 0, 0.5$, and 1 and for elastic scattering. The remaining parameters are $\Delta\Omega = 0.1$, $\Delta\Omega = 0.01$, and $\gamma = 1$.

stimuli (μ/μ^0) decays, the EDC diverges like $D_{\text{eff}}/D^0 \propto f^{\varsigma_D}$, and the Péclet number Pe tends to zero with growing value of f, see Fig. 6.12 (right).

6.6. Summary

Let us summarize our findings. In this chapter, we investigated the impact of the viscous friction coefficient γ on biased Brownian motion of point-like particles in two-dimensional channels with periodically varying width. If the particle motion is spatially correlated on a length larger than bottleneck width, its dynamics becomes extremely sensitive to the finite viscosity of the surrounding solvent. In particular, we found that the particle mobility μ/μ^0 grows for small γ as a power of γ. Noteworthy, on expressing the viscous friction coefficient in units of the $\sqrt{f/\Delta\omega}$, all mobility curves tends to collapse on one unique curve regardless of the force strength. The latter demonstrate that the particle motion behaves as overdamped even for characteristic correlation times larger than the drift time, $\gamma^2\,\Delta\omega/f < 1$. Counterintuitively, this ratio becomes smaller with decreasing channel width and for stronger forces. Furthermore, the particle's response to the external force diminishes with its strength for finite value of γ. Solely, in the high friction limit, $\gamma \gg 1$, the particle mobility converges to the bulk value μ^0 for $f \to \infty$. In addition, the effective diffusion coefficient diverges as a power of f caused by ballistic collisions with the wall appearing for weak damping and strong forces.

Assuming that the time scales in transverse direction separate from the longitudinal one, adiabatic elimination of the transverse degrees of freedom results in a reduced description (Fick-Jacobs approach) for the x-coordinate involving the potential of mean force $A(x)$. This description is intimately connected with (i) equipartition of the kinetic energy of v_y and (ii) vanishing correlation between v_x and v_y. Comparing the results for the reduced dynamics with numerical results for the full problem, namely, biased particle transport through a 2D sinusoidally modulated channel, we showed that

the Fick-Jacobs description overestimates the mobility, although the accuracy of the approximation is sufficiently good for $\gamma \geq 5$ and weak forces $f < f_c$. There exists a characteristic force strength f_c beyond which the Fick-Jacobs approach fails. The force f_c gets smaller with decreasing friction. The effective description fails due to the violation of equipartition for the fast coordinate y and velocity v_y. The latter is caused by the transfer of the externally applied acceleration in x-direction to the transversal velocity component v_y during collisions with the boundaries, which were treated as elastic. Nevertheless that the equipartition condition is satisfied for $f < f_c$, we found a large discrepancy between the particle mobility of the full problem and the one of the reduced dynamics for $\gamma \lesssim 1$. We demonstrated that this deviation is caused by the non-vanishing correlation between the particle's velocity components.

Finally, we studied the influence of inelastic particle-wall collisions as well as elastic scattering on entropic particle transport. We showed that additional sources of dissipation or randomness do not enhance the accuracy of the reduced description. Quite the contrary, due to the loss of kinetic energy as a consequence of inelastic particle-wall collision, the equipartition presumption is not satisfied for any value of f. In the case of elastic scattering, the particles' direction of motion changes randomly during collisions with the top wall, resulting in a higher probability to move in opposite direction to the external force $\mathbf{f}$. Consequently, the particle mobility is reduced and thus the difference to the reduced dynamics grows. Notably, it turned out that perfectly inelastic collisions rectify the ballistic particle motion, resulting in a regular and directed transport for weak damping and strong forces.

7. Concluding remarks

In this thesis, we have addressed the problem of biased Brownian motion in spatially confined geometries which are ubiquitous in nature. The main attention has been directed towards the analysis of particle transport in confinements where entropic barriers play an important role. In the introduction, we have formulated two questions concerning the well-established Fick-Jacobs approach:

First, we asked whether there exists a methodology reproducing the Fick-Jacobs equation for weakly modulated geometries and, more importantly, leading to an extension towards extremely corrugated boundaries.

In chapter 3, we have presented a systematic treatment for biased particle transport by performing asymptotic perturbation analysis of the joint probability density function in terms of an expansion parameter specifying the corrugation of the channel walls. Exact solutions for the associated stationary Smoluchowski equation have been calculated for point-like Brownian particles moving in three-dimensional, axis-symmetric channel with periodically varying rectangular or circular cross-sections. In particular, we have demonstrated that the leading order of our developed series expansion is equivalent to the well-established Fick-Jacobs solution. Higher-order corrections to the joint probability density function become significant for extremely corrugated channel walls. Moreover, we have derived that the most important transport quantities like mean particle current, particle mobility, and the effective diffusion coefficient are determined by the product of their zeroth order result and the expectation value of a function – including the boundary corrugation – in the diffusion dominated regime. Remarkably, our analytic result can be calculated exactly for most smooth and discontinuous boundaries in contrast to the integrals appearing in the commonly used Lifson-Jackson formula. Moreover, it provides at least equally good or even better agreements with the numerical results.

Until now in the literature, the Fick-Jacobs approach has mainly been applied to conservative forces (scalar potentials) governing the overdamped dynamics of point-like Brownian particles. This led to our second question: "Under which conditions is a generalization of the Fick-Jacobs approach to more sophisticated situations including finite particle size, inertial effects, and more general forces feasible?"

For this purpose, based on our derived methodology we have generalized the Fick-Jacobs formalism to the most general external force field which can be decomposed into a curl-free (scalar potential) and a divergence-free component (vector potential) in chapter 4. Focusing on typical, weakly corrugated channel geometries, we have put forward an effective one-dimensional description involving the generalized potential of mean force. The latter comprises the commonly known "entropic" term in the presence of a constant

bias and a qualitatively novel contribution associated with the divergence-free force. To elucidate the intriguing features caused by divergence-free forces, we have applied our approach to the experimentally relevant situation where small Brownian objects are subject to both an external constant bias and to a pressure-driven flow. The analysis of particle transport, caused by the counteraction of the flow and the bias, has led to the intriguing finding that the mean particle current can vanish identically despite the presence of locally strong forces. This effect is accompanied by a significant suppression of diffusion, thus being robust against thermal fluctuations, and leads to the selective effect of strong particle accumulation – *hydrodynamically enforced entropic trapping*. The latter can be utilized to efficiently separate Brownian particles of the same size and it is inherently connected to the uneven shape of the channel. Noteworthy, the generalized Fick-Jacobs approach provides a powerful tool to calculate the transport quantities even for such complicated problems and it is in excellent agreement with the numerical results. Although the presented methodology admits the situation of a driven solvent, we expect that similar effects can be found in a resting solvent with non-vanishing divergence-free forces.

Beside the opportunity to separate Brownian particles of the same size, a main challenge in basic research is also to obtain pure single-size suspensions by filtering wanted from unwanted material. The particle size impacts numerous physical properties like the mass, the viscous friction coefficient, the accessible space or, equivalently, the entropic barriers within the channel. Additionally, it determines the strength of various forces exerted on the particles, e.g., external stimuli, hydrodynamic particle-particle and particle-wall interactions. In chapter 5, we have verified the simplifications made in our preceding theoretical considerations for their applicability in experiments. In particular, limits for the ratio of particle size to pore size and the mean distance between particles have been identified. Both demonstrate that a dilute particle concentration is essential. Additionally, we have validated that the transport quantities of extended, spherical objects are well described by the Fick-Jacobs approach within these limits. Interestingly, due to the nonlinear dependence of the entropic barriers' height on the object size, we have found a resonance-like behavior of the particles' terminal speeds on their diameter for extremely corrugated channels and weak forces. Such a sensitive dependence offers the possibility to separate Brownian objects of different size.

In chapter 6, we have studied the impact of the viscous friction coefficient on the particle dynamics to gain deeper insight into the key physical assumption behind the Fick-Jacobs approach. The existence of a hierarchy of relaxation times, governed by the geometry of the channel and by the viscous friction, guarantees the separation of time scales and the equipartition of energy. Both are necessary conditions to apply the Fick-Jacobs approach. Supposing further a vanishing correlation between the particle's velocity components, we have demonstrated that the expression for the potential of mean force does not depend on the friction coefficient. Comparisons of numerical results for biased particle transport with analytic estimates have shown that the reduced description is accurate for moderate up to strong damping and for weak forces. In particular, there exists an upper bound for the force magnitude beyond which the Fick-Jacobs approach fails even in narrow, weakly modulated channels. This force strength grows with increasing friction and tends to infinity for infinite strong damping (Smoluchowski approximation). The origin of the failure of the Fick-Jacobs description

is the violation of equipartition for the transversal coordinate and velocity. The latter is caused by the transfer of the externally applied acceleration into the transversal direction during particles' collisions with the boundaries. In particular, for weak damping we have found that our reduced description fails even for weak forces, nevertheless that equipartition holds, due to non-vanishing correlation between the particle's velocity components. Finally, we have studied the impact of the boundary conditions on the particle transport. We have shown that contrary to the case of ideal elastic collision, perfectly inelastic particle-wall collisions rectify the almost ballistic particle motion, resulting in a regular and directed transport for weak damping and strong forces.

In summary, this work shows how the well-established Fick-Jacobs approach can be extended to strongly corrugated channels and sophisticated external force fields, and, as well, how physical properties like particle size and viscous friction coefficient can be incorporated. Besides a number of analytic results derived for the particle mobility and the effective diffusion coefficient, we have gained a deeper insight into the key physical assumption behind this reduced energetic description, namely, separation of time scales, equipartition of energy, and vanishing velocity correlation. It would be gratifying if this work inspires experimentalists and theoreticians for further studies. For instance, an extension to other types of stochastic forces, e.g., colored noise [Radtke and Schimansky-Geier, 2012] or non-Gaussian noise [Wang et al., 2012], or to "active" matter [Romanczuk and Schimansky-Geier, 2011; Romanczuk et al., 2012], like motile cells [Church et al., 2009; Di Carlo et al., 2007] or artificial self-propelled particles [Paxton et al., 2004], would be worthwhile. Likewise, the incorporation of particle-particle interactions [Gallardo et al., 2012; Zeng et al., 2011] and irregularities in the channel structure [Neusius et al., 2009; Rols et al., 2008], as they are present in porous media, are very challenging tasks.

Appendices

A. Numerical methods

In this appendix, we present the numerical integration algorithms used in this thesis in detail. Basically two different methods were used to solve stochastic different equations [Kloeden and Platen, 1999], viz., Brownian dynamics (BD) simulation and finite element method (FEM).

Overdamped Brownian dynamics simulation

As a starting point, we consider the dimensionless Langevin equation

$$\dot{\mathbf{q}}(t) = \mathbf{f}(\mathbf{q}, t) + \boldsymbol{\xi}(t), \tag{A.1}$$

where $\mathbf{f}(\mathbf{q}, t)$ comprises all deterministic forces acting on the particle at position $\mathbf{q} = (x, y, z)^T$ and time t except for the hard-wall interactions. $\boldsymbol{\xi}(t)$ is Gaussian white noise whose components have zero mean $\langle\, \xi_i(t) \,\rangle$ with correllation $\langle\, \xi_i(t)\xi_j(s) \,\rangle = 2\,\delta_{i,j}\,\delta\,(t-s)$, i, j are x, y, or z, representing the thermal fluctuating forces. To numerically solve Eq. (A.1), we may discretize it according to the Euler algorithm [Kloeden and Platen, 1999], yielding

$$\mathbf{q}_{t+dt} = \mathbf{q}_t + \mathbf{f}(\mathbf{q}_t, t)\,dt + \sqrt{2\,dt}\,\mathbf{G}_t, \tag{A.2}$$

as an approximation for the displacement of the particle from $\mathbf{q}_t$ to $\mathbf{q}_{t+dt}$ during the time interval dt. In Eq. (A.2), each component of $\mathbf{G}_t$ is a Gaussian random number of zero mean and unit variance. In the simulations these Gaussian random numbers are calculated by the Polar-method [Kloeden and Platen, 1999] using uniformly distributed random numbers. These numbers are generated by the Mersenne Twister algorithm MT19937-64 [Matsumoto and Nishimura, 1998].

Each discretization step in the Euler algorithm Eq. (A.2) represents a Monte-Carlo step weighted by the transition PDF

$$p(\mathbf{q}_{t+dt}, t+dt; \mathbf{q}_t, t) = \frac{1}{\sqrt{4\pi\,dt}^3} \exp\left(-\frac{(\mathbf{q}_{t+dt} - \mathbf{q}_t - \mathbf{f}\,dt)^2}{4\,dt}\right), \tag{A.3}$$

for finding the particle at position $\mathbf{q}_{t+dt}$ after a time interval dt when it initially was located at position $\mathbf{q}_t$, provided the deterministic force $\mathbf{f}(\mathbf{q}_t, t)$ is constant in space and time. This algorithm works well for small enough time steps so that $\mathbf{f}$ does not vary significantly during dt and over the typical step size.

However, the particle wall-interaction is not included yet. In case a collision with a hard wall occurs and an unphysical configuration $\mathbf{q}_{t+dt}$ is produced by Eq. (A.2), i.e., the particle is placed beyond the channel wall, the component of the particle displacement $\mathbf{q}_{t+dt} - \mathbf{q}_t$ parallel to the wall remains unchanged while the component

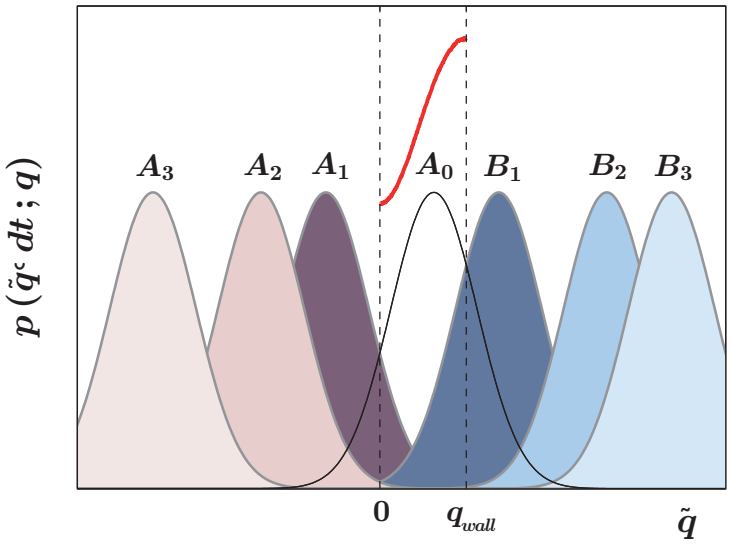

Figure A.1.: Illustration of the reflection approach used in our Brownian dynamics simulations. The solid line represents the transition PDF without walls Eq. (A.5). In addition, the first terms of the infinite series of Gaussian distribution centered at A_n and B_n are illustrated. Calculating the complete sum results in the red curve which represents the correct transition PDF $p(\tilde{q}, dt; q)$.

perpendicular to the wall has to be corrected. The exact final position $\mathbf{q}^*_{t+dt}$ is obtained by the forbidden position $\mathbf{q}_{t+dt}$ as

$$\mathbf{q}^*_{t+dt} = \mathbf{q}_t + [(\mathbf{q}_{t+dt} - \mathbf{q}_t) \cdot \mathbf{t}]\,\mathbf{t} + (q - \tilde{q})\,\mathbf{n}, \tag{A.4}$$

where $\mathbf{t}$ is the unit tangential vector and $\mathbf{n}$ is the unit normal vector on the hard surface that points in opposite direction to the location of the particle center $\mathbf{q}_t$ [Behringer and Eichhorn, 2011]. Further, q denotes the distance of the particle from the wall at time t and $\tilde{q}$ represents a random displacement. The one-dimensional transition probability $p(\tilde{q}, dt; q)$ for a particle starting at distance q at time $t = 0$ and reaching $\tilde{q}$ at dt is determined by the Smoluchowski equation $\partial_{dt}\, p + \partial_{\tilde{q}}(\mathbf{f} \cdot \mathbf{n}\, p - \partial_{\tilde{q}}\, p) = \delta(\tilde{q} - q)$. Furthermore, $p(\tilde{q}, dt; q)$ equals zero if $\tilde{q} \leq 0$ caused by the impenetrability of the hard wall and the transition PDF has to obey the no-flux boundary condition $(\mathbf{f} \cdot \mathbf{n}\, p - \partial_{\tilde{q}}\, p)|_{\tilde{q}=0} = 0$. A solution for the transition PDF can be found analytically [von Smoluchowski, 1916], however, it is quite difficult to implement the latter numerically.

Otherwise, $p(\tilde{q}, dt; q)$ can be evaluated numerically by reflecting unphysical displacements at the wall, i.e., $\tilde{q} \to -\tilde{q}$. The underlying idea for the reflection approach is illustrated in Fig. A.1. If $\tilde{q} > 0$, the transition PDF is given by Gaussian distribution with mean $q + \mathbf{f} \cdot \mathbf{n}\, dt$ and variance $2\, dt$

$$p(\tilde{q}, dt; q) = \frac{1}{\sqrt{4\pi\, dt}} \exp\left(-\frac{(\tilde{q} - q - \mathbf{f} \cdot \mathbf{n}\, dt)^2}{4\, dt}\right). \tag{A.5}$$

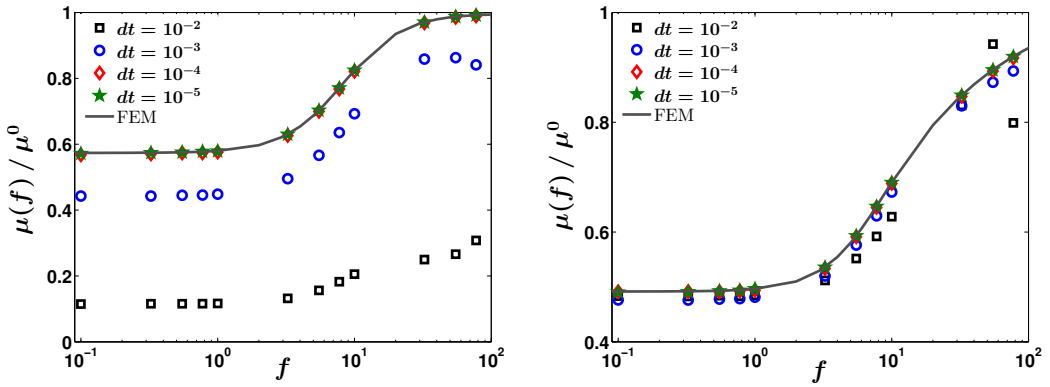

(a) $\Delta\Omega = 0.1$, $\Delta\omega = 0.01$ **(b)** $\Delta\Omega = 1$, $\Delta\omega = 0.1$

Figure A.2.: Impact of numerical time step dt on the results for the particle mobility $\mu(f)/\mu^0$ (markers) for weakly corrugated $\Delta\Omega = 0.1$ (left) and moderate modulated channels $\Delta\Omega = 1$ (right) is presented. The channel aspect ratio is kept fixed $\delta = 0.1$. Additionally, we depict the numerical result obtained by finite element method (solid line).

In the case of unphysical displacements, we reflect the tail of the transition PDF, Eq. (A.5), which contains all these unphysical displacements, from the forbidden region to the "physical" one. This is equivalent to add a second Gaussian distribution centered at $-q - \mathbf{f} \cdot \mathbf{n}\, dt$ to Eq. (A.5). In the case of two walls, the first located at $q = 0$ and the second at q_{wall}, the transition PDF $p(\tilde{q}, dt; q)$ is given by an infinite series of Gaussian distribution centered at A_n and B_n, respectively. The mean values A_n and B_n are determined by the recursion formula: $A_0 = B_0 = q + \mathbf{f} \cdot \mathbf{n}\, dt$, $A_n = -B_{n-1}$, and $B_n = 2\, q_{\text{wall}} - A_{n-1}$, for $n \geq 1$. Additionally, the conditions $p(0, dt; q) = 0$ and $p(q_{\text{wall}}, dt; q) = 0$ have to be included in the numerics by hand. For this procedure to yield a decent approximation to the solution of Eq. (A.1), it is required that the shape of the channel wall does not vary significantly over typical particle displacements in addition to the standard assumption of small variations in $\mathbf{f}$ during typical integration steps.

For this reason, the Langevin equation Eq. (A.1) was numerically integrated by Euler's method [Kloeden and Platen, 1999] with a position and force dependent time step $\Delta t = \min\left(10^{-4}, 0.01/\|\mathbf{f}\|, W(x)^2/100\right)$, where $W(x)$ reprents the local width at position x. A further decrease of the time step did not cause a noticeable change of the numerical results. This fact is presented in depth in Fig. A.2. Averages were performed over an ensemble of $N = 3 \cdot 10^4$ initially equilibrated trajectories which were integrated for not less than 10^7 time steps. Additionally, we also numerically integrated Eq. (A.1) by use of a Heun integration scheme [Mannella, 2000] and found no noticeable change of the numerical results for identical time steps (not explicitly shown).

The numerical error for the mean particle velocity $\langle \dot{x} \rangle$ can be estimated as follows. In the overdamped limit, Eq. (A.1), the particle's velocity is ill-defined. The set of final velocities v_i can only be calculated from the particle's final positions via

$v_i = x_i(t_{\text{simu}})/t_{\text{simu}}$, $i \in \{1, N\}$, where N is the ensemble size. Thus, the mean particle velocity is given by

$$\langle \dot{x} \rangle = \frac{1}{N} \sum_{i=1}^{N} v_i = \lim_{t \to t_{\text{simu}}} \frac{\langle x(t) \rangle}{t}. \tag{A.6}$$

The experimental standard deviation

$$\sigma_{\langle \dot{x} \rangle} = \sqrt{\frac{1}{N-1} \sum_{i=1}^{N} (v_i - \langle \dot{x} \rangle)^2}$$

is connected with the effective diffusion coefficient D_{eff}

$$D_{\text{eff}} = \frac{1}{2\,N\,t_{\text{simu}}} \sum_{i=1}^{N} (x_i - \langle x \rangle)^2\,, \tag{A.7}$$

via

$$\sigma_{\langle \dot{x} \rangle} = \sqrt{\frac{2\,N\,D_{\text{eff}}}{(N-1)\,t_{\text{simu}}}}. \tag{A.8}$$

The numerical uncertainties (errors) are determined by

$$u_{\langle \dot{x} \rangle} = \sqrt{\frac{2\,D_{\text{eff}}}{(N-1)\,t_{\text{simu}}}}, \quad \text{and} \quad u_\mu = \frac{1}{f} \sqrt{\frac{2\,D_{\text{eff}}(f)}{(N-1)\,t_{\text{simu}}}}. \tag{A.9}$$

They are negligible for large ensemble size $N \simeq 3 \cdot 10^4$, sufficient long simulation time t_{simu}, and non-diverging effective diffusivity.

Finite element method

Alternatively, the main transport quantities like the mean particle velocity and the effective diffusion coefficient were computed by finite element method [Hughes, 2000; Zienkiewicz et al., 2005]. The first step to calculate these quantities entails calculating the stationary joint PDF $P(\mathbf{q})$ whose evolution is governed by the stationary Smoluchowski equation

$$0 = \boldsymbol{\nabla} \cdot \mathbf{J}\,(\mathbf{q}) = \boldsymbol{\nabla} \cdot (\mathbf{f}\,P\,(\mathbf{q}) - \boldsymbol{\nabla} P\,(\mathbf{q}))\,. \tag{A.10}$$

By multiplying the latter with the auxiliary function $h(\mathbf{q})$ and integrating over the unit-cell area $\mathrm{d}A$, one gets

$$0 = \int \mathrm{d}A\, h(\mathbf{q}) \nabla \cdot (\mathbf{f} P(\mathbf{q})) - \int \mathrm{d}A\, h(\mathbf{q}) \Delta P(\mathbf{q}). \tag{A.11}$$

Using first Green's identity leads to

$$= \int \mathrm{d}A\, h\boldsymbol{\nabla}\cdot(\mathbf{f}P) - \int\limits_{\omega_\pm} \mathrm{d}s\, h\ (\boldsymbol{\nabla}P)\cdot\mathbf{n} + \int \mathrm{d}A\,(\boldsymbol{\nabla}h\cdot\boldsymbol{\nabla}P)\,. \tag{A.12}$$

Considering the boundary condition $\mathbf{J}\cdot\mathbf{n}=0$, finally, we derive

$$0 = \int \mathrm{d}A\, h\boldsymbol{\nabla}\cdot(\mathbf{f}P) + \int \mathrm{d}A\,(\boldsymbol{\nabla}h\cdot\boldsymbol{\nabla}P) - \int\limits_{\omega_\pm} \mathrm{d}s\, h\, P\,\mathbf{f}\cdot\mathbf{n}. \tag{A.13}$$

The corresponding code in FreeFem++[Pironneau et al., 2012] for biased Brownian motion in a two dimensional channel ($x-y$ plane) explicitly reads

```
1  // solve the Smoluchowski equation
2  solve FPE(p,h,solver=UMFPACK,eps=1.0e-10) =
3          int2d(Tu)(h*dxfx*p+h*fx*dx(p)+dx(p)*dx(h))
4          +int2d(Tu)(h*dyfy*p+h*fy*dy(p)+dy(p)*dy(h))
5          -int1d(Tu,2)(p*h*(N.x*fx+N.y*fy))                    //bc
6          +int2d(Tu)(q*h)                                      // source
7  ;
8
9  // normalization
10 real norm=int2d(Th)(p);
11 pnorm=p/norm;
```

The mean particle current is calculated by integrating the probability current $\mathbf{J}(\mathbf{q})$ over one channel's unit-cell, cf. Eq. (2.17),

```
12 int2d(Th)(fx*pnorm-dx(pnorm));   // current calculation
```

The second step involves the numerical calculation of the so-called $B(\mathbf{q})$-field Eq. (2.20) [Brenner, 1980; Brenner and Edwards, 1993] governed by the following convection-diffusion equation

$$\boldsymbol{\nabla}\cdot\left(P(\mathbf{q})\ \boldsymbol{\nabla}B(\mathbf{q})\right) - \left(\mathbf{J}(\mathbf{q})\cdot\boldsymbol{\nabla}\right)B(\mathbf{q}) = P(\mathbf{q})\ \langle\,\dot{x}\,\rangle\,. \tag{A.14}$$

The auxiliary function $b = B + x$ is periodic in transport direction $b(\mathbf{q}+\mathbf{e}_x) = b(\mathbf{q})$, yielding

$$P\triangle b - P\,\mathbf{f}\cdot\boldsymbol{\nabla}b + 2\,\boldsymbol{\nabla}P\cdot\boldsymbol{\nabla}b = P\ (\langle\,\dot{x}\,\rangle - \mathbf{f}\cdot\mathbf{e}_x) + 2\partial_x P. \tag{A.15}$$

Furthermore, the b-field obeys the no-flux boundary conditions

$$\boldsymbol{\nabla}b(\mathbf{q})\cdot\mathbf{n} - \mathbf{e}_x\cdot\mathbf{n} = 0\,, \quad \forall\mathbf{q}\in\text{channel wall}. \tag{A.16}$$

Multiplying the partial equation Eq. (A.15) with the auxiliary function $h(\mathbf{q})$, integrating the latter over the unit-cell area $\mathrm{d}A$, and considering the boundary condition,

finally, one gets

$$\int \mathrm{d}A\,[h\,(\boldsymbol{\nabla}P)\cdot(\boldsymbol{\nabla}b) - P\,(\boldsymbol{\nabla}h)\cdot(\boldsymbol{\nabla}b) - h\,P\,\mathbf{f}\cdot\boldsymbol{\nabla}b] = \int \mathrm{d}A\,h\,[P\,\langle\,\dot{x}\,\rangle - P\,\mathbf{f}\cdot\mathbf{e}_x + 2\partial_x P] - \int_{\omega_\pm} \mathrm{d}s\,h\,P\,\mathbf{e}_x\cdot\mathbf{n}. \tag{A.17}$$

```
13 solve bfield(b,h,solver=UMFPACK,eps=1.0e-10) =
14       int2d(TB)((h*dx(pnorm)-pnorm*dx(h)-h*pnorm*fx)*dx(b))
15      +int2d(TB)((h*dy(pnorm)-pnorm*dy(h)-h*pnorm*fy)*dy(b))
16      +int1d(TB,2)(pnorm*h*N.x) // bc
17      -int2d(TB)(h*(pnorm*strom-pnorm*fx+2*dx(pnorm)));
```

Finally, the effective diffusion coefficient $D_{\mathrm{eff}}(f)/D^0$ is obtained by subsequently evaluating the unit-cell quadrature Eq. (2.23)

```
18 deff=1+int2d(TB)(pnorm*(dx(b)*dx(b)-2*dx(b)+dy(b)*dy(b)));
```

The FEM code can easily be extended to 3D [Pironneau et al., 2012].

The numerical errors in the finite element method depend mostly on the mesh discretization of inner unit cell domain into a set of discrete sub-domains (triangles). For each parameter value, the number of triangles, respectively, the number of vortices was set large enough so that the output was independent of it.

Underdamped Brownian dynamics simulation

In what follows, we discuss how the particle-wall interaction is implemented in our simulations for the case of arbitrary friction coefficient γ. The corresponding Langevin equation reads

$$\dot{\mathbf{v}} + \gamma\,\mathbf{v} = \mathbf{f}(\mathbf{v},\mathbf{q},t) + \sqrt{2\gamma}\,\boldsymbol{\xi}(t). \tag{A.18}$$

To numerically solve Eq. (A.18), we may discretize it according to the Euler algorithm [Kloeden and Platen, 1999], yielding

$$\mathbf{q}_{t+dt} = \mathbf{v}_t(\mathbf{q}_t)\,dt, \tag{A.19a}$$

$$\mathbf{v}_{t+dt} = \mathbf{v}_t(\mathbf{q}_t) - \gamma\,\mathbf{v}_t(\mathbf{q}_t)\,dt + \mathbf{f}(\mathbf{v}_t,\mathbf{q}_t,t)\,dt + \sqrt{2\gamma\,dt}\,\mathbf{G}_t, \tag{A.19b}$$

as an approximation for the displacement of the particle's velocity and position from $\mathbf{v}_t$ to $\mathbf{v}_{t+dt}$, respectively, $\mathbf{q}_t$ to $\mathbf{q}_{t+dt}$ during the time interval dt. This Euler step works well for small enough time steps so that both $\mathbf{v}$ and $\mathbf{f}$ do not vary significantly during dt and over the typical step size. All integration steps that are performed according to Eqs. (A.19) indeed produce valid trajectories, as long as the particle's trajectory does not cross the channel wall (unphysical configuration).

Once an unphysical configuration is encountered, the particle-wall interaction has to be taken into account. Basically, the overall particle velocity has to be split into two perpendicular velocities: one tangent to the common normal surfaces of the wall at the point of contact, $\mathbf{v}^t = (\mathbf{v}\cdot\mathbf{t})\,\mathbf{t}$, and the other along the line of collision, $\mathbf{v}^n = (\mathbf{v}\cdot\mathbf{n})\,\mathbf{n}$.

Since the collision only imparts force along the line of collision, the tangential velocity does not change; yielding $\mathbf{v}^{t\prime} = \mathbf{v}^{t}$. The symbol $\prime$ denotes the velocity component after the collision. The collision of the particle with the wall was treated either elastically or inelastically. These two totally different behaviors can be controlled via the coefficient of restitution C_R. The latter represents the ratio of the normal velocity component after collision to the one before the collision, $C_R = \|\mathbf{v}^{n\prime}\|/\|\mathbf{v}^{n}\|$. Thereby, $C_R = 1$ corresponds to ideal elastic collision, i.e., conversation of momentum and energy during the collision process is supposed, whereas $C_R = 0$ represents perfectly inelastic collision, $\mathbf{v}^{n\prime} = \mathbf{0}$.

In detail, the following individual steps were executed in every Euler step during the simulation

1. Calculation of the boundary crossing point $\mathbf{q}_{\text{cross}}$
2. Evaluation of associated crossing time τ_{cross} which the trajectory needs to reach $\mathbf{q}_{\text{cross}}$ when it starts at $\mathbf{q}_t$ at time t, viz., $\tau_{\text{cross}} = \left((\mathbf{q}_{\text{cross}} - \mathbf{q}_t) \cdot \mathbf{e}_x\right) / (\mathbf{v}_{t+dt} \cdot \mathbf{e}_x)$ or $\tau_{\text{cross}} = \left((\mathbf{q}_{\text{cross}} - \mathbf{q}_t) \cdot \mathbf{e}_y\right) / (\mathbf{v}_{t+dt} \cdot \mathbf{e}_y)$
3. Correct final velocity $\mathbf{v}'_{t+dt}$

$$\mathbf{v}'_{t+dt} = \mathbf{v}_{t+dt} - (1 + C_R)\ (\mathbf{v}_{t+dt} \cdot \mathbf{n})\, \mathbf{n} \tag{A.20}$$

4. Correct final position $\mathbf{q}'_{t+dt}$

$$\mathbf{q}'_{t+dt} = \mathbf{q}_{\text{cross}} + \mathbf{v}'_{t+dt}\, (dt - \tau_{\text{cross}}) \tag{A.21}$$

Note that we assume that the particle's velocity instantaneously changes from $\mathbf{v}_t$ to $\mathbf{v}_{t+dt}$ at time t. We suppose that this algorithm works well for small enough time steps so that both the wall shape and $\mathbf{f}$ do not vary significantly during dt and over the typical step size. For this reason the Langevin equation Eq. (A.18) was numerically integrated with a position and velocity dependent time step

$$\Delta t = \min\left(10^{-5}, 0.01/(\mathbf{v}_t \cdot \mathbf{e}_x), W(x)/(100\, \mathbf{v}_t \cdot \mathbf{e}_y), \gamma\, W(x)^2/100\right).$$

In the underdamped limit, averages were also performed over an ensemble of $3 \cdot 10^4$ initially equilibrated trajectories which were integrated for not less than 10^7 time steps.

In contrast to the overdamped limit, the particle's velocity $\mathbf{v}_i$ is well-defined at any time for arbitrary viscous friction coefficient γ. Consequently, the mean particle velocity in channel's longitudinal direction reads $\langle\, v_x \,\rangle = \sum_{i=1}^{N} v_{x,i}/N$ and the numerical uncertainties (errors) are determined by $u_{v_x} = \sqrt{\sigma^2/(N\,(N-1))}$, respectively, $u_\mu = u_{v_x}/f$. Both quantities are sufficiently small for large ensemble size $N \simeq 3 \cdot 10^4$ and non-diverging second central moment $\sigma^2 = \langle\, v_x^2 \,\rangle - \langle\, v_x \,\rangle^2$.

We emphasize that due to the higher dimensionality of the underdamped particle dynamics in a two-dimensional channel geometry (4 degrees of freedom) the problem cannot be treated by FreeFem++ which is limited to 3 degrees of freedom.

B. Derivation of the generalized Fick-Jacobs equation

For particle dynamics decribed by

$$\dot{\mathbf{q}}(t) = -\boldsymbol{\nabla}\,\Phi(\mathbf{q}) + \boldsymbol{\nabla}\times\boldsymbol{\Psi}(\mathbf{q}) + \sqrt{2}\,\boldsymbol{\xi}(t), \tag{B.1}$$

the stationary joint PDF $P(\mathbf{q})$ following Eq. (B.1) is governed by the Smoluchowski equation [Risken, 1989]

$$0 = \boldsymbol{\nabla}\cdot\mathbf{J}\,(\mathbf{q}) = \boldsymbol{\nabla}\cdot\{[-\boldsymbol{\nabla}\,\Phi(\mathbf{q}) + \boldsymbol{\nabla}\times\boldsymbol{\Psi}(\mathbf{q})]\;P\,(\mathbf{q}) - \boldsymbol{\nabla}\,P\,(\mathbf{q})\}\,. \tag{B.2}$$

Caused by the impenetrability of the channel walls the probability flux obeys the no-flux boundary condition at the walls, $\mathbf{J}\,(\mathbf{q})\cdot\mathbf{n} = 0$. For 3D planar channel geometry the outward-pointing normal vectors are $\mathbf{n} = \left(\mp\omega'_{\pm}(x), \pm 1, 0\right)^T$ at the side-walls and $\mathbf{n} = (0, 0, \pm 1)^T$ at the top and bottom boundary, respectively. The prime denotes the derivative with respect to x.

We next measure, for the case of finite corrugation $\varepsilon \neq 0$, the transverse coordinate $y \to \varepsilon\, y$, the boundary functions $\omega_{\pm}(x) \to \varepsilon\, h_{\pm}(x)$, and $\boldsymbol{\Psi} \to (\varepsilon\,\Psi_x, \Psi_y, \varepsilon\,\Psi_z)^T$ in units of ε. Consequently, the gradient $\boldsymbol{\nabla} \to (\partial_x, \varepsilon^{-1}\partial_y, \partial_z)^T$ and the Laplace operator $\triangle \to (\partial_x^2 + \varepsilon^{-2}\partial_y^2 + \partial_z^2)$ change. Further, we expand the joint PDF $P(\mathbf{q}) = P_0(\mathbf{q}) + \varepsilon^2\, P_1(\mathbf{q}) + O(\varepsilon^4)$, the scalar potential $\Phi(\mathbf{q}) = \Phi_0(\mathbf{q}) + \varepsilon^2\,\Phi_1(\mathbf{q}) + O(\varepsilon^4)$, and each component of $\Psi_i(\mathbf{q}) = \Psi_i^0(\mathbf{q}) + O(\varepsilon^2)$, for $i = x, y$ or z, in the a series in even orders of ε. Substituting this ansatz into Eq. (B.2), yields

$$\begin{aligned} 0 = &-\partial_y\left[e^{-\Phi_0}\partial_y\left(e^{\Phi_0}\,P_0\right)\right] - \varepsilon^2\left\{\partial_y\left[\partial_y\Phi_1\,P_0 + \partial_y\Phi_0\,P_1 + \partial_y P_1\right] + \partial_x\left[e^{-\Phi_0}\partial_x\left(e^{\Phi_0}\,P_0\right)\right]\right. \\ &\left.+\partial_z\left[e^{-\Phi_0}\partial_z\left(e^{\Phi_0}\,P_0\right)\right] - (\boldsymbol{\nabla}\times\boldsymbol{\Psi}_0)\cdot\boldsymbol{\nabla}P_0\right\} + O(\varepsilon^4). \end{aligned} \tag{B.3}$$

Furthermore, no-flux bcs change to

$$\begin{aligned} \text{at } y = h_-, h_+ :\; 0 = &\mp e^{-\Phi_0}\partial_y\left(e^{\Phi_0}\,P_0\right) \mp \varepsilon^2\left\{\partial_y\Phi_1\,P_0 + \partial_y\Phi_0\,P_1 + \partial_y P_1\right. \\ &\left.-h'_{\pm}(x)e^{-\Phi_0}\partial_x\left(e^{\Phi_0}\,P_0\right) + h'_{\pm}(x)\left(\boldsymbol{\nabla}\times\boldsymbol{\Psi}_0\right)_x\,P_0 - \left(\boldsymbol{\nabla}\times\boldsymbol{\Psi}_0\right)_y\,P_0\right\} + O(\varepsilon^4), \end{aligned} \tag{B.4a}$$

$$\begin{aligned} \text{at } z = 0, \Delta H :0 = &\mp e^{-\Phi_0}\partial_z\left(e^{\Phi_0}\,P_0\right) \pm \left(\boldsymbol{\nabla}\times\boldsymbol{\Psi}_0\right)_z\,P_0 \mp \varepsilon^2\left\{\partial_z\Phi_1\,P_0 + \partial_z\Phi_0\,P_1\right. \\ &\left.+\partial_z P_1 - \left(\boldsymbol{\nabla}\times\boldsymbol{\Psi}_1\right)_z\,P_0 - \left(\boldsymbol{\nabla}\times\boldsymbol{\Psi}_0\right)_z\,P_1\right\} + O(\varepsilon^4). \end{aligned} \tag{B.4b}$$

From the leading order terms (ε^0) in Eqs. (B.3) and (B.4), immediately follows that $P_0(\mathbf{q}) = g(x,z)e^{-\Phi_0(\mathbf{q})}$, where $g(x,z)$ is an unknown function which has to be deter-

mined from the second order $O(\varepsilon^2)$ of Eq. (B.3). Integrating $O(\varepsilon^2)$ over the local cross-section $Q(x) = \Delta H\,(h_+(x) - h_-(x))$, using

$$\begin{aligned}\int_{h_-(x)}^{h_+(x)} \mathrm{d}y \int_0^{\Delta H} \mathrm{d}z\ (\boldsymbol{\nabla}\times\boldsymbol{\Psi}_0)\cdot\boldsymbol{\nabla}P_0 = \partial_x \int_{h_-(x)}^{h_+(x)} \mathrm{d}y \int_0^{\Delta H} \mathrm{d}z\ (\boldsymbol{\nabla}\times\boldsymbol{\Psi}_0)_x\ P_0 \\ - h'_+(x)\,(\boldsymbol{\nabla}\times\boldsymbol{\Psi}_0)_x\ P_0\Big|_{y=h_+} + h'_-(x)\,(\boldsymbol{\nabla}\times\boldsymbol{\Psi}_0)_x\ P_0\Big|_{y=h_-} \\ + \int_0^{\Delta H} \mathrm{d}z\ (\boldsymbol{\nabla}\times\boldsymbol{\Psi}_0)_y\ P_0\Big|_{y=h_-}^{y=h_+} + \int_{h_-(x)}^{h_+(x)} \mathrm{d}y\ (\boldsymbol{\nabla}\times\boldsymbol{\Psi}_0)_z\ P_0\Big|_{z=0}^{z=\Delta H},\end{aligned} \tag{B.5}$$

and taking account of the no-flux bcs, Eq. (B.4b), we get

$$0 = \partial_x J_0^x(x) = \partial_x \int_{h_-(x)}^{h_+(x)} \mathrm{d}y \int_0^{\Delta H} \mathrm{d}z\ \left[e^{-\Phi_0}\partial_x g + (\boldsymbol{\nabla}\times\boldsymbol{\Psi}_0)_x\, g\, e^{-\Phi_0}\right]. \tag{B.6}$$

In what follows, we suppose that the z-component of convergence-free force field vanishes identically at the top and bottom wall, i.e., $(\boldsymbol{\nabla}\times\boldsymbol{\Psi}_0)_z = 0$ at $z = 0$ and $z = \Delta H$. According to Eq. (B.4), the unknown function $g(x, z)$ must be independent of z and thus Eq. (B.6) simplifies to

$$J_0^x = e^{-A(x)}\, g'(x) + g(x)\, e^{-A(x)}\, \chi(x), \tag{B.7}$$

with effective entropic potential $A(x)$, cf. Eq. (2.35), and substitute

$$\chi(x) = \int_{h_-(x)}^{h_+(x)} \mathrm{d}y \int_0^{\Delta H} \mathrm{d}z\ (\boldsymbol{\nabla}\times\boldsymbol{\Psi}_0)_x\ e^{-\Phi_0(\mathbf{q})+A(x)}. \tag{B.8}$$

Solving the differential equation for $g(x)$ yields

$$P_0(\mathbf{q}) = \left[C_0 e^{-\Phi_0(\mathbf{q})} - J_x^0 \int_0^x \mathrm{d}x'\, e^{\mathcal{F}(x)}\right] e^{-\Phi_0(\mathbf{q})+\chi(x)}, \tag{B.9}$$

where $\mathcal{F}(x)$ is the potential of mean force in longitudinal channel direction

$$\begin{aligned}\mathcal{F}(x) = -\ln\left[\int_{h_-(x)}^{h_+(x)} \mathrm{d}y \int_0^{\Delta H} \mathrm{d}z\ e^{-\Phi_0(\mathbf{q})}\right] \\ - \int_0^x \mathrm{d}x' \int_{h_-(x')}^{h_+(x')} \mathrm{d}y \int_0^{\Delta H} \mathrm{d}z\ (\boldsymbol{\nabla}\times\boldsymbol{\Psi}_\mathbf{0})_x\ P_{\mathrm{eq}}(y, z|x').\end{aligned} \tag{B.10}$$

Here $P_{\mathrm{eq}}(y,z|x)$ represents the equilibrium PDF of y and z, conditioned on x, given by $P_{\mathrm{eq}}(y,z|x) = \exp(-\Phi_0(\mathbf{q}) + A(x))$.

The joint PDF has to satisfy the periodicity requirement $P(x+m,y,z) = P(x,y,z)$, $\forall m \in \mathbb{Z}$. Assuming that (i) the scalar potential scales like $\Phi(\mathbf{q}) \sim -f\, x^{\beta}$ with $\beta = \{0,1\}$ and (ii) $(\boldsymbol{\nabla} \times \boldsymbol{\Psi})_x$ is periodic in x with unit period, one gets

$$\begin{aligned} P_0(x+m,y,z) = & \left[C_0 - J_0^x \sum_{n=0}^{m+1} \left(e^{\Delta\mathcal{F}}\right)^n \int_0^1 \mathrm{d}x\, e^{\mathcal{F}(x)} - \int_0^x \mathrm{d}x'\, e^{\mathcal{F}(x')} \right] e^{-m\,\Delta\mathcal{F}} e^{-\Phi_0(\mathbf{q})+\chi(x)} \\ & \equiv P_0(x,y,z). \end{aligned}$$

In the case that $\mathcal{F}(x)$ is periodic in x, i.e, $\Delta\mathcal{F} = \mathcal{F}(x+1) - \mathcal{F}(x) = 0$, the solution Eq. (B.9) obeys the periodicity requirement if either the probability current vanishes, $J_x^0 = 0$, or $\int_0^1 \mathrm{d}x\, \exp(\mathcal{F}(x)) = 0$. The second condition is only feasible for $\mathcal{F}(x) = -\infty$ which is an unphysical situation. From the first condition $J_x^0 = 0$ immediately follows that divergence-free force has to equal zero for all values of x, i.e., $(\boldsymbol{\nabla} \times \boldsymbol{\Psi})_x = 0$. Consequently, $\Delta\Phi$ must vanish and therefore the stationary joint PDF is constant, $P_0(\mathbf{q}) = const.$ Then the marginal PDF, cf. Eq. (2.28), scales with the local channel cross-section

$$p_0(x) \sim \Delta H\, (h_+(x) - h_-(x))\,. \tag{B.11}$$

In the opposite limit, $\Delta\mathcal{F} \neq 0$, the periodicity requirement is fulfilled only for $C_0 = J_x^0 \int_0^1 \mathrm{d}x\, \exp(\mathcal{F}(x))/(1-\exp(\Delta\mathcal{F}))$ and we finally obtain [Risken, 1989]

$$p_0(x) = \frac{e^{-\mathcal{F}(x)} \int_x^{x+1} \mathrm{d}x'\, e^{\mathcal{F}(x)}}{\int_0^1 \mathrm{d}x\, e^{\mathcal{F}(x)} \int_x^{x+1} \mathrm{d}x'\, e^{\mathcal{F}(x')}}, \tag{B.12}$$

whereby the stationary marginal PDF obeys the normalization condition $\int_0^1 p(x)\mathrm{d}x = 1$. If $\beta > 1$ or the longitudinal coordinate x is multiplicative connected to the transverse coordinates, a closed periodic solution for the joint PDF cannot be found [Risken, 1989].

The kinetic equation for the time-dependent marginal PDF $p_0(x,t)$ can be gathered from its steady state solution, Eq. (B.12), resulting in the *generalized* Fick-Jacobs equation

$$\partial_t p_0(x,t) = \partial_x \left[\frac{\mathrm{d}\,\mathcal{F}(x)}{\mathrm{d}\,x}\, p_0(x,t) \right] + \partial_x^2 p_0(x,t). \tag{B.13}$$

C. Poiseuille flow in shape-perturbed channels

Here, we present the derivation of the leading order solution for the fluid's flow field through a three-dimensional, planar channel geometry with periodically varying cross-section $Q(x)$. Unit-cells with constant rectangular cross-section are often called *Hele-Shaw* cells and it is perhaps a surprising fact that no closed-form analytic solution is known to the Poiseuille-flow problem. The solution can only be represented by a Fourier sum [Bruus, 2008; Gondret et al., 1997].

The time and spatial evolution of the fluid velocity is governed by the Navier-Stokes equation (in dimensionless units)

$$Re\ \{\partial_t \mathbf{u}(\mathbf{q},t) + (\mathbf{u}\cdot\boldsymbol{\nabla})\ \mathbf{u}(\mathbf{q},t)\} = -\boldsymbol{\nabla}\mathcal{P}(\mathbf{q},t) + \triangle\mathbf{u}(\mathbf{q},t)\,, \tag{C.1}$$

where $\mathbf{u} = (u^x, u^y, u^z)^T$ denotes the solvent flow field, $\mathcal{P}(\mathbf{q},t)$ corresponds to the local pressure, and Re is the Reynolds number. For most micro-fluidic devices the Reynolds number is small $Re < 1$. If the pressure drop along one unit-cell is dominated by viscous losses $\triangle\mathbf{u}(\mathbf{q},t)$, the solvent flow is laminar [Gravesen et al., 1993]. Furthermore, a low Reynolds number $Re < 1$ is essential to safely disregard many forces exert by the fluid on a spherical particle, for details see Sect. 4.2. Therefore, the left hand side in Eqs. (C.1) can be disregarded, which leaves us with the Stokes' equation, respectively, the so-called "creeping flow" equation [Landau and Lifschitz, 1991]:

$$0 = -\boldsymbol{\nabla}\mathcal{P}(\mathbf{q},t) + \triangle\mathbf{u}(\mathbf{q},t)\,. \tag{C.2}$$

Since the particle's motion is bounded by two parallel plane walls located at $z = 0$ and $z = \Delta H$, the local pressure does not depend on the z-coordinate $\mathcal{P}(x,y,t)$. From the no-slip bc, $\mathbf{u}(\mathbf{q}) = \mathbf{0}\,, \forall\,\mathbf{q} \in$ wall, immediately follows $u_z(\mathbf{q}) = 0$. In addition, we highlight that the time dependence of the velocity field is merely parametric within the Stokes' equation, Eq. (C.2). Once a steady state solution $\mathbf{u}(\mathbf{q})$ has been determined for the stationary pressure field $\mathcal{P}(\mathbf{q})$, the solution $\mathbf{u}(\mathbf{q},t)$ at any time t is simply given by the product of the stationary solution $\mathbf{u}(\mathbf{q})$ times the time dependence of the pressure field [Kettner et al., 2000]. Thus, it is sufficient to focus on the steady state solution.

We begin by expanding all functions in the problem as Fourier series [Fourier, 1807] along the transverse z direction. To ensure the fulfillment of the no-slip bc, $\mathbf{u}(x,y,0) = \mathbf{u}(x,y,\Delta H) = 0$, we use only terms proportional to $\sin(n\pi z/\Delta H)\,, \forall n \in \mathbb{N}$. The Fourier expansion of any constant yields

$$1 = \frac{4}{\pi}\sum_{n=0}^{\infty}\frac{1}{2n+1}\,\sin\left((2n+1)\pi\frac{z}{\Delta H}\right), \tag{C.3}$$

a series containing only odd integers. The Fourier series for the flow components reads

$$u^x(x,y,z) = \sum_{n=1}^{\infty} f_n(x,y)\, \sin\left(n\pi \frac{z}{\Delta H}\right), \tag{C.4a}$$

$$u^y(x,y,z) = \sum_{n=1}^{\infty} g_n(x,y)\, \sin\left(n\pi \frac{z}{\Delta H}\right). \tag{C.4b}$$

Inserting these series into Eq. (C.2) and integrating the latter with regard to z leads to

$$0 = \triangle_{2\mathrm{D}}\, f_{2n+1}(x,y) - \frac{4}{\pi(2n+1)} \partial_x \mathcal{P}(x,y) - \frac{(2n+1)^2\,\pi^2}{\Delta H^2}\, f_{2n+1}(x,y), \tag{C.5a}$$

$$0 = \triangle_{2\mathrm{D}}\, g_{2n+1}(x,y) - \frac{4}{\pi(2n+1)} \partial_y \mathcal{P}(x,y) - \frac{(2n+1)^2\,\pi^2}{\Delta H^2}\, g_{2n+1}(x,y), \tag{C.5b}$$

where $\triangle_{2\mathrm{D}} = \partial_x^2 + \partial_y^2$. Any solution to the problem must satisfy that for all values of n, the n-th coefficient in the local pressure has to be equal to the n-th coefficient in the flow velocities terms, Eqs. (C.5). Consequently all even terms vanish identically $f_{2n} = g_{2n} = 0$.

In analogy to the derivative of the generalized FJ equation, cf. App. B, we measure all transverse quantities in units of expansion parameter ε, i.e., $y \to \varepsilon\, y$ and $\omega_\pm(x) \to \varepsilon\, h_\pm(x)$. Then, the series expansion for Fourier components and local pressure in ε read

$$f_m(x,y) = f_m^{(0)} + \varepsilon\, f_m^{(1)} + \ldots = \sum_{n=0}^{\infty} \varepsilon^n f_m^{(n)}(x,y), \tag{C.6a}$$

$$g_m(x,y) = \varepsilon\, g_m^{(0)} + \varepsilon^2\, g_m^{(1)} + \ldots = \sum_{n=0}^{\infty} \varepsilon^{n+1} g_m^{(n)}(x,y), \tag{C.6b}$$

$$\mathcal{P}(x,y) = \frac{1}{\varepsilon^2}\mathcal{P}_0 + \frac{1}{\varepsilon}\,\mathcal{P}_1 + \ldots = \sum_{n=0}^{\infty} \varepsilon^{n-2} \mathcal{P}_n(x,y). \tag{C.6c}$$

The leading orders in ε for the three quantities are determined by the known Poiseuille flow solution which is the exact solution for the Stokes' equation, $R_e \ll 1$, in a straight channel $\varepsilon = 0$. Substituting Eqs. (C.6) into Eqs. (C.5), we get

$$0 = -\frac{4}{\pi\, m} \partial_x \mathcal{P}_0(x,y) + \partial_y^2 f_m^{(0)}(x,y) - m^2\,\pi^2 \left(\frac{\varepsilon}{\Delta H}\right)^2 f_m^{(0)}(x,y) + O(\varepsilon), \tag{C.7a}$$

$$0 = -\frac{4}{\pi\, m}\frac{1}{\varepsilon} \partial_y \mathcal{P}_0(x,y) + O(\varepsilon), \tag{C.7b}$$

for any odd integer m. While the third term in Eq. (C.7a) is negligible for high channels, $\Delta H \gg \varepsilon$, this term becomes important if the gap between the flat walls is asymptotically small, $\Delta H \ll 1$ – *Hele-Shaw flow*. On the contrary, the counterpart in Eq. (C.7b) scales linearly with ε even for asymptotically small channel height and thus can safely be disregarded.

Additionally to the Stokes' equation, the Fourier components for the flow velocities have to obey the continuity equation

$$0 = \boldsymbol{\nabla} \cdot \mathbf{u} = \sum_{n=0}^{\infty} \varepsilon^n \left\{ \partial_x f_m^{(n)}(x,y) + \partial_y g_m^{(n)}(x,y) \right\}, \tag{C.8}$$

the no-slip bcs at the channel walls, $f_m^{(n)}(x, h_\pm(x)) = g_m^{(n)}(x, h_\pm(x)) = 0$, $\forall n \in \mathbb{N}$, and the periodicity requirement, $f_m^{(n)}(x+k,y) = f_m^{(n)}(x,y)$ and $g_m^{(n)}(x+k,y) = g_m^{(n)}(x,y)$, $\forall k \in \mathbb{Z} \wedge n \in \mathbb{N}$.

From Eq. (C.7b), one immediately sees that the pressure depends only on the x-coordinate in leading order. We obtain that the general solution of Eq. (C.7a) attains the form

$$f_m^{(0)}(x,y) = A_m \sinh(c_m \varepsilon y) + B_m \cosh(c_m \varepsilon y) - \frac{4}{\pi\, m\, c_m^2 \varepsilon^2} \partial_x \mathcal{P}_0(x), \tag{C.9}$$

with substitute $c_m = m\pi / \Delta H$. The coefficients A_m and B_m have to be determined by the no-slip bc, $f_m(x, h_\pm(x)) = 0$, which leads to the leading order solution for the Poiseuille flow in a channel with periodically varying rectangular cross-section $Q(x)$

$$\begin{aligned} u_0^x(\mathbf{q}) = -\frac{4\,\Delta H^2}{\pi^3} \partial_x \mathcal{P}_0(x) \sum_{n=0}^{\infty} \Bigg[1 - \frac{\sinh\left(c_{2n+1}\left(\omega_+(x) - y\right)\right)}{\sinh\left(c_{2n+1} W(x)\right)} \\ - \frac{\sinh\left(c_{2n+1}\left(y - \omega_-(x)\right)\right)}{\sinh\left(c_{2n+1} W(x)\right)} \Bigg] \frac{\sin\left(c_{2n+1} z\right)}{(2n+1)^3}, \end{aligned} \tag{C.10}$$

where $W(x) = \omega_+(x) - \omega_-(x)$ is the local width. In order to enhance the readability in the following, we scaled the transverse quantities back. The so far unknown solution for the local pressure $\mathcal{P}_0(x)$ is derived from the no-slip bcs for $u_0^y(\mathbf{q})$ giving rise to

$$\mathcal{P}_0(x) = \mathcal{P}^0 + \frac{\Delta \mathcal{P}}{\langle\, \chi(x)^{-1} \,\rangle_x} \int_0^x \mathrm{d}x'\; \chi(x')^{-1}, \tag{C.11}$$

where

$$\chi(x) = \sum_{n=0}^{\infty} \frac{c_{2n+1} W(x) \sinh\left(c_{2n+1} W(x)\right) + 2\left(1 - \cosh\left(c_{2n+1} W(x)\right)\right)}{(2n+1)^4 \sinh\left(c_{2n+1} W(x)\right)}. \tag{C.12}$$

The drop of pressure along a unit-cell is denoted by $\Delta\mathcal{P} = \mathcal{P}(x+1,y) - \mathcal{P}(x,y)$ and $\mathcal{P}^0$ corresponds to a constant offset which can be set to zero.

We derive that the leading order solutions for the longitudinal flow component u_0^x and the local pressure $\mathcal{P}_0$ are both given by an infinite sum of hyperbolic sine and cosine functions. The length scale over which u_0^x varies in x and y-direction is the local width $W(x)$, the channel height ΔH being involved through the ratio $W(x)/\Delta H$. In Figs. C.1 and C.2 we depict the simulation results for a laminar flow through a 3D channel with sinusoidally varying cross-section, Eq. (C.2), using FEM. We find that our analytic expression for the longitudinal flow component, Eq. (C.10), agrees very well

with the numerics for weakly modulated channels, cf. Fig. C.1 ($\varepsilon = 0.1$). Although, the leading order results tends to overestimate the numerics with growing channel corrugation, see Fig. C.2 ($\varepsilon = 0.4$), the compliance is notably well at the widest part of the channel. For reflection symmetric cross-sections, $\omega_{\pm}(x) = \pm\omega(x)$, Eq. (C.10) resembles Eq. (9) in [Lauga et al., 2004]. There the authors derived the leading order solution via lubrication theory [Reynolds, 1886] using the channel height as expansion coefficient, $\Delta H \ll 1$. In the limit of an non-modulated cross-section, $W(x) = \Delta\Omega$, Eqs. (C.10) and (C.11) give the Poisseuille flow in a rectangular channel with plane walls at $y = \pm\Delta\Omega/2$ and $z = 0, \Delta H$ [Bruus, 2008], viz., $\mathcal{P}(x) = \Delta\mathcal{P}\,x$, $u^y(\mathbf{q}) = 0$, and

$$u^x(\mathbf{q}) = -\frac{4\,\Delta H^2 \Delta\mathcal{P}}{\pi^3} \sum_{n=0}^{\infty} \left[1 - \frac{\cosh\left((2n+1)\pi\frac{y}{\Delta H}\right)}{\cosh\left((2n+1)\pi\frac{\Delta\Omega}{2\Delta H}\right)}\right] \frac{\sin\left((2n+1)\pi\frac{z}{\Delta H}\right)}{(2n+1)^3}.$$

For any modulated cross-section, one recognizes that the successive terms of the sum for u_0^x decrease with $1/(2n+1)^2$ and the terms in Eq. (C.12) lessen even more rapidly, roughly as $1/(2n+1)^4$. Consequently, it is sufficient to consider only the first terms of each sum. For most aspect ratios $\Delta H/\Delta\Omega$ and $\Delta H/\Delta\omega$, respectively, we find that the first two terms, $n = \{0, 1\}$, agrees quite well with the numerics; dashed lines in Figs. C.1 and C.2.

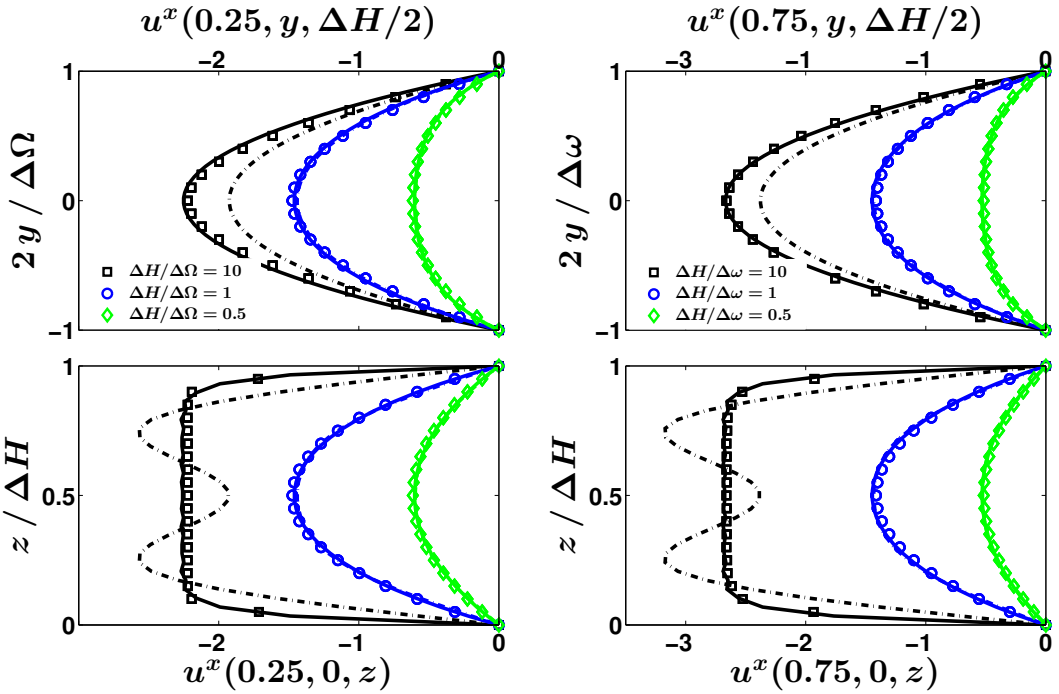

Figure C.1.: Profiles of the longitudinal flow component u^x in a 3D channel with sinusoidally modulated boundary, $\omega_\pm(x) = \pm\left[\Delta\Omega + \Delta\omega + (\Delta\Omega - \Delta\omega)\sin(2\pi x)\right]/4$, and constant height ΔH, see Fig. 3.1. The profiles in the $y-z$ plane were numerically evaluated by FEM (markers) for different ratios of channel height to local width: $\Delta H/\Delta\Omega$ at $x_{\text{pos}} = 0.25$ (left column) and $\Delta H/\Delta\omega$ at $x_{\text{pos}} = 0.75$ (right column). The lines represents the analytic estimate, Eq. (C.10), by calculating the sum either for the first 2 terms (dashed lines) or for the first 10 terms (solid lines). For several parameter values the dashed lines may are hidden by the associated solid lines. The remaining parameter values are $\Delta\Omega = 0.5$, $\Delta\omega = 0.4$, and $\Delta\mathcal{P} = 100$.

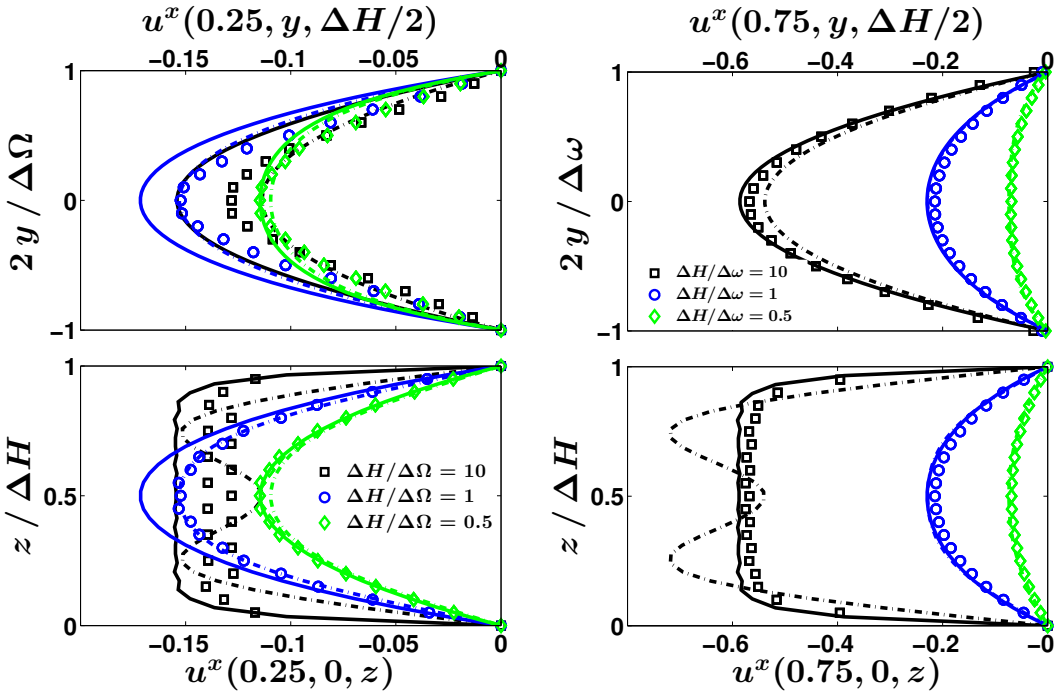

Figure C.2.: Profiles of the longitudinal flow component u^x in a 3D channel with sinusoidally modulated boundary, $\omega_\pm(x) = \pm\left[\Delta\Omega + \Delta\omega + (\Delta\Omega - \Delta\omega)\sin(2\pi x)\right]/4$, and constant height ΔH, see Fig. 3.1. The profiles in the $y-z$ plane were numerically evaluated by FEM (markers) for different ratios of channel height to local width: $\Delta H/\Delta\Omega$ at $x_{\text{pos}} = 0.25$ (left column) and $\Delta H/\Delta\omega$ at $x_{\text{pos}} = 0.75$ (right column). The lines represents the analytic estimate, Eq. (C.10), by calculating the sum either for the first 2 terms (dashed lines) or for the first 10 terms (solid lines). For several parameter values the dashed lines may are hidden by the associated solid lines. The remaining parameter values are $\Delta\Omega = 0.5$, $\Delta\omega = 0.1$, and $\Delta\mathcal{P} = 100$.

Infinitely high channel

For microfluidics devices the aspect ratio of height to width can often be so large that the channel is well approximated by an infinite parallel-plate configuration in z-direction, $\Delta H \gg \Delta\Omega$. By rotation, this situation can always be realized in experiments, i.e., $y \to z$ and $z \to y$. In the limit of infinite channel height, the velocity profile for u^x is flat in z except near the walls, see square markers in the bottom row of Figs. C.1 and C.2. Then the situation is quasi two-dimensional. Expanding Eqs. (C.10) and (C.11) in a Taylor series in $1/\Delta H$, one gets

$$u_0^x(x,y) \simeq -\frac{\mathcal{P}_0'(x)}{2}\,\frac{4}{\pi}\,(\omega_+(x)-y)\,(y-\omega_-(x)) + O\left(\Delta H^{-2}\right). \tag{C.13a}$$

Using the continuity equation Eq. (C.8), the leading order for the flow velocity in y-direction reads

$$u_0^y(x,y) \simeq \frac{1}{12}\partial_x\left[\mathcal{P}_0'(x)\,(y-\omega_-(x))^2\,(3\omega_+(x)-\omega_-(x)-2y)\right] + O\left(\Delta H^{-2}\right). \tag{C.13b}$$

The prime represents the derivative with respect to x. The solution for the local pressure, Eq. (C.11), reduces to

$$\mathcal{P}_0(x,y) \simeq \mathcal{P}_0 + \Delta\mathcal{P}\,\frac{\int_0^x \mathrm{d}x'\,W(x')^{-3}}{\langle\, W(x)^{-3}\,\rangle_x}. \tag{C.14}$$

As for every two-dimensional flow of incompressible fluid, the Stokes equation turns into the biharmonic equation $\boldsymbol{\nabla}^4\Psi_0(x,y)=0$ for the zeroth order stream function Ψ_0 for which $u_0^x = \partial_y\,\Psi_0$ and $u_0^y = -\partial_x\,\Psi_0$. From Eqs. (C.13) follows

$$\Psi_0(x,y) = -\frac{\Delta p}{12}\,\frac{(y-\omega_-(x))^2\,(3\,\omega_+(x)-\omega_-(x)-2y)}{W(x)^3\,\langle\, W(x)^{-3}\,\rangle_x}. \tag{C.15}$$

Nomenclature

Abbreviations

1D	one-dimensional	, page 9
2D	two-dimensional	, page 22
3D	three-dimensional	, page 16
bc(s)	boundary condition(s)	, page 13
BD	Brownian dynamics	, page 46
EDC	effective diffusion coefficient	, page 15
EDL	electric double layer	, page 71
EOM	equation of motion	, page 9
FEM	finite element method	, page 44
FJ	Fick-Jacobs	, page 18
HEET	hydrodynamically enforced entropic trapping	, page 85
MFPT	mean first passage time	, page 24
MSD	mean square displacement	, page 12
NSE	Navier-Stokes equation	, page 77
PDF	probability density function	, page 13
VACF	velocity auto-correlation function	, page 117
VCF	velocity correlation function	, page 116

Functions

${}_2F_1(\cdot)$	first hypergeometric function	, page 66

Symbols and Variables

α	force exponent $\mathbf{f} \propto d_p^{\alpha}$	, page 89
β	force orientation angle measured from the x-axis	, page 71
$\triangle$	Laplace operator	, page 77
$\triangle^2$	biharmonic operator	, page 78
$\Delta\mathcal{P}$	change of pressure along one channel unit cell	, page 79
ΔH	height of planar channel geometry	, page 16
δ	aspect ratio of the channel geometry $\delta = \Delta\omega/\Delta\Omega$	, page 42
$\Delta\Omega$	maximum width of the channel	, page 28
$\Delta\omega$	minimum width of the channel	, page 28
ε	dimensionless expansion parameter	, page 28
η	dynamic viscosity	, page 9
γ	viscous friction coefficient	, page 9
$\boldsymbol{\nabla}_{\mathbf{q}}$	gradient	, page 10
$\boldsymbol{\Psi}(\mathbf{q})$	vector potential	, page 74

κ_w	particle-wall interaction strength	, page 20
Λ	ratio of velocity correlation time to diffusion time	, page 91
λ_D	Debye length	, page 72
$\langle\cdot\rangle$	ensemble average	, page 10
$\langle\cdot\rangle_x$	geometrical average over one channel period	, page 25
$\langle\cdot\rangle_{x,y}$	geometrical average over local width and channel period	, page 32
$\langle\dot{\mathbf{q}}\rangle$	mean particle current vector	, page 14
$\mathbb{D}$	dispersion tensor	, page 12
$\mathbb{D}^{\text{eff}}$	effective dispersion tensor	, page 15
$\mathbb{M}$	mobility tensor	, page 11
$\mathbb{M}^{\text{eff}}$	effective mobility tensor	, page 14
$\mathbb{M}^{\text{hyd}}$	hydrodynamic mobility tensor	, page 98
$\mathcal{F}(x)$	potential of mean force for energetic and vector potentials	, page 75
$\mathcal{P}(\mathbf{q},t)$	local pressure field	, page 77
$\mathfrak{L}_0$	unperturbed steady state Fokker-Planck operator	, page 28
$\mathfrak{L}_1$	perturbed steady state Fokker-Planck operator	, page 28
$\max(a,b)$	maximum value of a or b	, page 22
μ	particle mobility	, page 14
μ^0	free particle mobility	, page 11
$\mathbb{N}^+$	set of all natural numbers excluding zero, $\mathbb{N}^+ = \mathbb{N} \setminus \{0\}$	, page 32
$\|\mathbf{q}\|$	Euclidean norm of vector $\mathbf{q}$	, page 15
$\omega_{\text{eff}}(x)$	effective boundary function for extended particles	, page 90
$\omega_{\pm}(x)$	upper (+) and lower (-) boundary function	, page 16
$\Phi(\mathbf{q})$	scalar potential	, page 18
ρ_f	density of the solvent	, page 9
ρ_p	density of the particle	, page 9
tr[ ]	trace	, page 12
$\mathbf{b}$	periodic $\mathbf{B}$-field	, page 15
$\varnothing$	diameter	, page 2
$\mathbf{B}$	$\mathbf{B}$-field	, page 15
$\mathbf{F}$	external force vector	, page 9
$\mathbf{f}$	dimensionless external force vector	, page 15
$\mathbf{J}(\mathbf{q},t)$	probability current	, page 13
$\mathbf{n}$	outward-pointing normal vector	, page 13
$\mathbf{q}$	local particle position vector	, page 12
$\mathbf{R}_n$	lattice-point position vector	, page 12
$\mathbf{u}(\mathbf{q},t)$	solvent flow field vector	, page 76
$\mathbf{v}$	particle velocity vector	, page 9
ζ	zeta potential	, page 72
$A(x)$	effective entropic potential or potential of mean force	, page 19
$C(x)$	center line of the channel $C(x) = (\omega_+(x) + \omega_-(x))/2$	, page 36
C_R	coefficient of restitution	, page 119
$C_{v_i,v_j}(\tau)$	velocity correlation function between v_i and v_j at time τ	, page 116
$D(x,f)$	spatially dependent diffusion coefficient	, page 22
D^0	free diffusion constant	, page 12
D_{eff}	effective diffusion coefficient	, page 15

d_p	diameter of particle	, page 9
f	magnitude of external force $f = \|\mathbf{f}\|$	, page 16
$h_\pm(x)$	dimensionless upper (+) and lower (-) boundary function	, page 30
k_B	Boltzmann constant	, page 10
L	period of channel unit cell	, page 12
l_k	Kuhn length	, page 89
m	mass of particle	, page 9
m^*	effective mass of particle	, page 10
N_k	number of Kuhn segments	, page 89
$P(\mathbf{q}, t)$	joint probability density function	, page 13
$p(x, t)$	marginal probability density function	, page 17
$P_{\mathrm{st}}(\mathbf{q})$	stationary joint probability density function	, page 14
Pe	Péclet number	, page 56
$Q(x)$	area of local cross-section	, page 12
$R(x)$	local tube radius	, page 16
R_g	radius of gyration	, page 90
Re	Reynolds number	, page 77
T	temperature	, page 10
t	time	, page 9
t_{corr}	velocity correlation time	, page 10
$W(x)$	local channel width $W(x) = \omega_+(x) - \omega_-(x)$	, page 16
$\boldsymbol{\xi}$	Gaussian white noise	, page 9

Bibliography

B.-q. Ai and L.-g. Liu. Current in a three-dimensional periodic tube with unbiased forces. *Phys. Rev. E*, 74(5):051114, 2006. doi: 10.1103/PhysRevE.74.051114.

B. Alberts, A. Johnson, J. Lewis, M. Raff, K. Roberts, and P. Walter. *Molecular Biology of the Cell*. Garland Science, New York, 4th edition, 2002. ISBN 0-8153-4072-9.

J. L. Anderson. Effect of nonuniform zeta potential on particle movement in electric fields. *J. Colloid Interface Sci.*, 105(1):45–54, 1985. doi: 10.1016/0021-9797(85)90345-5.

R. Aris. On the dispersion of a solute in a fluid flowing through a tube. *Phil. Trans. R. Soc. Lond. A*, 235(1200):67–77, 1956. doi: 10.1098/rspa.1956.0065.

V. Arnold. Proof of a A. N. Kolmogorov theorem on conservation of conditionally periodic motions under small perturbations of the Hamiltonian function. *Uspeki Mat. Nank.*, 18:13–40, 1963.

S. Arrhenius. Über die Dissoziationswärme und den Einfluss der Temperatur auf den Dissoziationsgrad der Elektrolyte. *Z. Phys. Chem. (Leipzig)*, 4:226, 1889.

A. Barone and G. Paternò. *Physics and Applications of the Josephson Effect*. Wiley, New York, 1982. ISBN 9780471014690.

M. Z. Bazant and T. M. Squires. Induced-charge electrokinetic phenomena: Theory and microfluidic applications. *Phys. Rev. Lett.*, 92(6):066101, 2004. doi: 10.1103/PhysRevLett.92.066101.

M. Z. Bazant and T. M. Squires. Induced-charge electrokinetic phenomena. *Curr. Opin. Colloid In.*, 15(3):203–213, 2010. doi: 10.1016/j.cocis.2010.01.003.

F. F. Becker, X. B. Wang, Y. Huang, R. Pethig, J. Vykoukal, and P. R. C. Gascoyne. Separation of human breast cancer cells from blood by differential dielectric affinity. *Proc. Nat. Ac. Sc. U.S.A*, 92(3):860, 1995. doi: 10.1073/pnas.92.3.860.

R. Becker. *Theorie der Wärme*. Springer, Berlin, 3rd edition, 1985. ISBN 3540153837.

E. Beerdsen, D. Dubbeldam, and B. Smit. Molecular understanding of diffusion in confinement. *Phys. Rev. Lett.*, 95(16):164505, 2005. doi: 10.1103/PhysRevLett.95.164505.

E. Beerdsen, D. Dubbeldam, and B. Smit. Understanding diffusion in nanoporous materials. *Phys. Rev. Lett.*, 96(4):044501, 2006. doi: 10.1103/PhysRevLett.96.044501.

H. Behringer and R. Eichhorn. Hard-wall interactions in soft matter systems: Exact numerical treatment. *Phys. Rev. E*, 83(6):065701, 2011. doi: 10.1103/PhysRevE.83.065701.

J. M. Bennett and L. Mattsson. *Introduction to surface roughness and scattering*. Optical Society of America, Washington, D.C., 1989. ISBN 9781557521088.

A. M. Berezhkovskii and S. M. Bezrukov. Optimizing Transport of Metabolites through Large Channels: Molecular Sieves with and without Binding. *Biophys. J.*, 88(3):L17–L19, 2005. doi: 10.1529/biophysj.104.057588.

A. M. Berezhkovskii and S. M. Bezrukov. Counting Translocations of Strongly Repelling Particles through Single Channels: Fluctuation Theorem for Membrane Transport. *Phys. Rev. Lett.*, 100(3):038104, 2008. doi: 10.1103/PhysRevLett.100.038104.

A. M. Berezhkovskii and L. Dagdug. Biased diffusion in tubes formed by spherical compartments. *J. Chem. Phys.*, 133(13):134102, 2010. doi: 10.1063/1.3489375.

A. M. Berezhkovskii and A. Szabo. Time scale separation leads to position-dependent diffusion along a slow coordinate. *J. Chem. Phys.*, 135(7):074108, 2011. doi: 10.1063/1.3626215.

A. M. Berezhkovskii, M. A. Pustovoit, and S. M. Bezrukov. Diffusion in a tube of varying cross section: Numerical study of reduction to effective one-dimensional description. *J. Chem. Phys.*, 126(13):134706, 2007. doi: 10.1063/1.2719193.

A. M. Berezhkovskii, M. A. Pustovoit, and S. M. Bezrukov. Entropic effects in channel-facilitated transport: Interparticle interactions break the flux symmetry. *Phys. Rev. E*, 80(2):020904, 2009. doi: 10.1103/PhysRevE.80.020904.

A. M. Berezhkovskii, L. Dagdug, Y. A. Makhnovskii, and V. Y. Zitserman. Communications: Drift and diffusion in a tube of periodically varying diameter. Driving force induced intermittency. *J. Chem. Phys.*, 132(22):221104, 2010. doi: 10.1063/1.3451115.

L. Boltzmann. *Vorlesungen über Gastheorie*. J.A. Barth, Leipzig, 1896.

M. Borromeo and F. Marchesoni. Backward-to-Forward Jump Rates on a Tilted Periodic Substrate. *Phys. Rev. Lett.*, 84(2):203–206, 2000. doi: 10.1103/PhysRevLett.84.203.

M. Borromeo and F. Marchesoni. Particle transport in a two-dimensional septate channel. *Chem. Phys.*, 375(2):536–539, 2010. doi: 10.1016/j.chemphys.2010.03.022.

M. Borromeo, G. Costantini, and F. Marchesoni. Critical hysteresis in a tilted washboard potential. *Phys. Rev. Lett.*, 82(14):2820–2823, 1999. doi: 10.1103/PhysRevLett.82.2820.

R. M. Bradley. Diffusion in a two-dimensional channel with curved midline and varying width: Reduction to an effective one-dimensional description. *Phys. Rev. E*, 80(6):061142, 2009. doi: 10.1103/PhysRevE.80.061142.

A. Brask, J. Kutter, and H. Bruus. Long-term stable electroosmotic pump with ion exchange membranes. *Lab Chip*, 5(7):730–738, 2005. doi: 10.1039/B503626G.

H. Brenner. Dispersion resulting from flow through spatially periodic porous media. *Phil. Trans. R. Soc. Lond. A*, 297(1430):81–133, 1980. doi: 10.1098/rsta.1980.0205.

H. Brenner and D. A. Edwards. *Macrotransport Processes*. Butterworth-Heinemann, Boston, 1993. ISBN 0750693320.

N. Brilliantov and T. Pöschel. Granular gases with impact-velocity-dependent restitution coefficient. In *Granular Gases*, volume 564 of *Lecture Notes in Physics*, pages 100–124. Springer Berlin Heidelberg, 2001. ISBN 978-3-540-41458-2. doi: 10.1007/3-540-44506-4_5.

R. Brown. XXVII. A brief account of microscopical observations made in the months of June, July and August, 1827, on the particles contained in the pollen of plants; and on the general existence of active molecules in organic and inorganic bodies. *Phil. Mag.*, 4:161–173, 1828.

H. Bruus. *Theoretical Microfluidics*. Oxford Master Series in Condensed Matter Physics. Oxford University Press, 2008. ISBN 9780199235094.

L. Bunimovich and Y. Sinai. Statistical properties of Lorentz gas with periodic configuration of scatterers. *Comm. Math. Phys.*, 78(4):479–497, 1981. doi: 10.1007/BF02046760.

L. A. Bunimovich. On ergodic properties of some billiards. *Funct. Anal. Appl.*, 8:254, 1974.

P. Burada, P. Hänggi, F. Marchesoni, G. Schmid, and P. Talkner. Diffusion in confined geometries. *ChemPhysChem*, 10(1):45–54, 2009. doi: 10.1002/cphc.200800526.

P. S. Burada. *Entropic transport in confined media*. PhD thesis, Universität Augsburg, Germany, 2008.

P. S. Burada and G. Schmid. Steering the potential barriers: Entropic to energetic. *Phys. Rev. E*, 82(5):051128, 2010. doi: 10.1103/PhysRevE.82.051128.

P. S. Burada, G. Schmid, D. Reguera, J. M. Rubí, and P. Hänggi. Biased diffusion in confined media: Test of the Fick-Jacobs approximation and validity criteria. *Phys. Rev. E*, 75(5):051111, 2007. doi: 10.1103/PhysRevE.75.051111.

P. S. Burada, G. Schmid, D. Reguera, M. H. Vainstein, J. M. Rubí, and P. Hänggi. Entropic Stochastic Resonance. *Phys. Rev. Lett.*, 101(13):130602, 2008a. doi: 10.1103/PhysRevLett.101.130602.

P. S. Burada, G. Schmid, P. Talkner, P. Hänggi, D. Reguera, and J. M. Rubí. Entropic particle transport in periodic channels. *BioSystems*, 93(1):16–22, 2008b. doi: 10.1016/j.biosystems.2008.03.006.

M. Büttiker. Transport as a consequence of state-dependent diffusion. *Z. Phys. B*, 68 (2):161–167, 1987. doi: 10.1007/BF01304221.

H. B. Callen and T. A. Welton. Irreversibility and Generalized Noise. *Phys. Rev.*, 83 (1):34–40, 1951. doi: 10.1103/PhysRev.83.34.

F. Cecconi, D. del Castillo-Negrete, M. Falcioni, and A. Vulpiani. The origin of diffusion: The case of non-chaotic systems. *Physica D*, 180(3-4):129–139, 2003. doi: 10.1016/S0167-2789(03)00051-4.

K.-L. Cheng, Y.-J. Sheng, and H.-K. Tsao. Brownian escape and force-driven transport through entropic barriers: Particle size effect. *J. Chem. Phys.*, 129(18):184901, 2008. doi: 10.1063/1.3009621.

C.-F. Chou, O. Bakajin, S. W. P. Turner, T. A. J. Duke, S. S. Chan, E. C. Cox, H. G. Craighead, and R. H. Austin. Sorting by diffusion: An asymmetric obstacle course for continuous molecular separation. *Proc. Nat. Ac. Sc. U.S.A*, 96(24):13762–13765, 1999. doi: 10.1073/pnas.96.24.13762.

C. Church, J. Zhu, G. Wang, T.-R. J. Tzeng, and X. Xuan. Electrokinetic focusing and filtration of cells in a serpentine microchannel. *Biomicrofluidics*, 3(4):044109, 2009. doi: 10.1063/1.3267098.

A. E. Cohen and W. E. Moerner. Suppressing Brownian motion of individual biomolecules in solution. *Proc. Nat. Ac. Sc. U.S.A*, 103(12):4362–4365, 2006. doi: 10.1073/pnas.0509976103.

A. Corma. From microporous to mesoporous molecular sieve materials and their use in catalysis. *Chem. Rev.*, 97(6):2373–2420, 1997. doi: 10.1021/cr960406n.

G. Costantini and F. Marchesoni. Threshold diffusion in a tilted washboard potential. *Europhys. Lett.*, 48(5):491, 1999. doi: 10.1209/epl/i1999-00510-7.

L. Dagdug and I. Pineda. Projection of two-dimensional diffusion in a curved midline and narrow varying width channel onto the longitudinal dimension. *J. Chem. Phys.*, 137(2):024107, 2012. doi: 10.1063/1.4733394.

L. Dagdug, M.-V. Vazquez, A. M. Berezhkovskii, and S. M. Bezrukov. Unbiased diffusion in tubes with corrugated walls. *J. Chem. Phys.*, 133(3):034707, 2010. doi: 10.1063/1.3431756.

L. Dagdug, A. M. Berezhkovskii, Y. A. Makhnovskii, V. Y. Zitserman, and S. M. Bezrukov. Communication: Turnover behavior of effective mobility in a tube with periodic entropy potential. *J. Chem. Phys.*, 134(10):101102, 2011. doi: 10.1063/1.3561680.

L. Dagdug, M.-V. Vazquez, A. M. Berezhkovskii, V. Y. Zitserman, and S. M. Bezrukov. Diffusion in the presence of cylindrical obstacles arranged in a square lattice analyzed with generalized Fick-Jacobs equation. *J. Chem. Phys.*, 136(20):204106, 2012. doi: 10.1063/1.4720385.

Y. Daghighi and D. Li. Induced-charge electrokinetic phenomena. *Microfluid. Nanofluid.*, 9(4):593–611, 2010. doi: 10.1007/s10404-010-0607-2.

C. Dekker. Solid-state nanopores. *Nature Nanotech.*, 2:209–215, 2007. doi: 10.1038/nnano.2007.27.

D. Di Carlo, D. Irimia, R. G. Tompkins, and M. Toner. Continuous inertial focusing, ordering, and separation of particles in microchannels. *Proc. Nat. Ac. Sc. U.S.A*, 104 (48):18892–18897, 2007. doi: 10.1073/pnas.0704958104.

P. S. Dittrich and A. Manz. Lab-on-a-chip: Microfluidics in drug discovery. *Nat. Rev. Drug. Discov.*, 5(3):210–218, 2006. doi: 10.1038/nrd1985.

M. Doi. *Introduction to Polymer Physics*. Clarendon Press, Oxford, 1996. ISBN 9780198517894.

K. D. Dorfman. DNA electrophoresis in microfabricated devices. *Rev. Mod. Phys.*, 82 (4):2903–2947, 2010. doi: 10.1103/RevModPhys.82.2903.

T. Duke and R. Austin. Microfabricated Sieve for the Continuous Sorting of Macromolecules. *Phys. Rev. Lett.*, 80(7):1552–1555, 1998. doi: 10.1103/PhysRevLett.80.1552.

S. Dukhin. Electrokinetic phenomena of the second kind and their applications. *Adv. Colloid Interface Sci.*, 35:173–196, 1991. doi: 10.1016/0001-8686(91)80022-C.

S. S. Dukhin and V. N. Shilov. Theory of the static polarization of the diffuse part of the thin double layer of spherical particles. *Colloid J. USSR*, 31:564–570, 1969.

W. Ebeling and I. M. Sokolov. *Statistical Thermodynamics and Stochastic Theory of Nonequilibrium Systems*. World Scientific, Singapore, 2005. ISBN 9810213824.

J. C. T. Eijkel and A. van den Berg. Nanofluidics: what is it and what can we expect from it? *Microfluid. Nanofluid.*, 1(3):249–267, 2005. doi: 10.1007/s10404-004-0012-9.

A. Einstein. Über die von der molekularkinetischen Theorie der Wärme geforderte Bewegung von in ruhenden Flüssigkeiten suspendierten Teilchen. *Ann. Physik*, 322 (8):549–560, 1905. doi: 10.1002/andp.19053220806.

A. Einstein. Eine neue Bestimmung der Moleküldimensionen. *Ann. Physik*, 324(2): 289–306, 1906. doi: 10.1002/andp.19063240204.

L. D. Favro. Theory of the Rotational Brownian Motion of a Free Rigid Body. *Phys. Rev.*, 119(1):53–62, 1960. doi: 10.1103/PhysRev.119.53.

O. H. Faxen. Der Widerstand gegen die Bewegung einer starren Kugel in einer zähen Flüssigkeit, die zwischen zwei parallelen ebenen Wänden eingeschlossen ist. *Ann. Phys. (Leipzig)*, 373(10):89–119, 1922. doi: 10.1002/andp.19223731003.

E. Fermi. On the Origin of the Cosmic Radiation. *Phys. Rev.*, 75(8):1169–1174, 1949. doi: 10.1103/PhysRev.75.1169.

A. Fick. Über Diffusion. *Ann. Phys.*, 94:59–86, 1855. doi: 10.1002/andp.18551700105.

M. Firnkes, D. Pedone, J. Knezevic, M. Döblinger, and U. Rant. Electrically facilitated translocations of proteins through silicon nitride nanopores: Conjoint and competitive action of diffusion, electrophoresis, and electroosmosis. *Nano Lett.*, 10 (6):2162–2167, 2010. doi: 10.1021/nl100861c.

P. Flory. Thermodynamics of High Polymer Solutions. *J. Chem. Phys.*, 10(1):51–61, 1942. doi: 10.1063/1.1723621.

J. Fourier. Mémoire sur la propagation de la chaleur dans les corps solides. *Nouveau bulletin des sciences par la société philomathique de Paris*, 1807.

J. A. Freund and L. Schimansky-Geier. Diffusion in discrete ratchets. *Phys. Rev. E*, 60(2):1304–1309, 1999. doi: 10.1103/PhysRevE.60.1304.

E. Frey and K. Kroy. Brownian motion: a paradigm of soft matter and biological physics. *Ann. Phys.*, 14(1-3):20–50, 2005. doi: 10.1002/andp.200410132.

A. Gallardo, S. Grandner, N. G. Almarza, and S. H. L. Klapp. Theory of repulsive charged colloids in slit-pores. *J. Chem. Phys.*, 137(1):014702, 2012. doi: 10.1063/1.4730923.

P. R. C. Gascoyne and J. Vykoukal. Particle separation by dielectrophoresis. *Electrophoresis*, 23(13):1973–1983, 2002. doi: 10.1002/1522-2683(200207)23:13<1973::AID-ELPS1973>3.0.CO;2-1.

P. R. C. Gascoyne, X. Wang, Y. Huang, and F. Becker. Dielectrophoretic separation of cancer cells from blood. *IEEE T. Ind. Appl.*, 33(3):670–678, 1997. doi: 10.1109/28.585856.

P. Gaspard and F. Baras. Chaotic scattering and diffusion in the Lorentz gas. *Phys. Rev. E*, 51(6):5332–5352, 1995. doi: 10.1103/PhysRevE.51.5332.

P. Gaspard, M. E. Briggs, M. K. Francis, J. V. Sengers, R. W. Gammon, J. R. Dorfman, and R. V. Calabrese. Experimental evidence for microscopic chaos. *Nature*, 394 (6696):026103, 1998. doi: 10.1038/29721.

P. K. Ghosh, P. Hänggi, F. Marchesoni, S. Martens, F. Nori, L. Schimansky-Geier, and G. Schmid. Driven Brownian transport through arrays of symmetric obstacles. *Phys. Rev. E*, 85(1):011101, 2012a. doi: 10.1103/PhysRevE.85.011101.

P. K. Ghosh, P. Hänggi, F. Marchesoni, F. Nori, and G. Schmid. Detectable inertial effects on Brownian transport through narrow pores. *Europhys. Lett.*, 98(5):50002, 2012b. doi: 10.1209/0295-5075/98/50002.

P. K. Ghosh, P. Hänggi, F. Marchesoni, F. Nori, and G. Schmid. Brownian transport in corrugated channels with inertia. *Phys. Rev. E*, 86(2):021112, 2012c. doi: 10.1103/PhysRevE.86.021112.

P. Gondret, N. Rakotomalala, M. Rabaud, D. Salin, and P. Watzky. Viscous parallel flows in finite aspect ratio Hele-Shaw cell: Analytical and numerical results. *Phys. Fluids*, 9:1841–1843, 1997. doi: 10.1063/1.869301.

P. Gravesen, J. Branebjerg, and O. Jensen. Microfluidics - a review. *J. Micromech. Microeng.*, 3:168, 1993. doi: 10.1088/0960-1317/3/4/002.

I. V. Grigoriev, Y. A. Makhnovskii, A. M. Berezhkovskii, and V. Y. Zitserman. Kinetics of escape through a small hole. *J. Chem. Phys.*, 116(22):9574–9577, 2002. doi: 10.1063/1.1475756.

A. Groisman and S. R. Quake. A microfluidic rectifier: Anisotropic flow resistance at low Reynolds numbers. *Phys. Rev. Lett.*, 92(9):094501, 2004. doi: 10.1103/PhysRevLett.92.094501.

K. Hahn, J. Kärger, and V. Kukla. Single-file diffusion observation. *Phys. Rev. Lett.*, 76(15):2762–2765, 1996. doi: 10.1103/PhysRevLett.76.2762.

P. Hall and D. Papageorgiou. The onset of chaos in a class of Navier-Stokes solutions. *J. Fluid Mech.*, 393(1):59–87, 1999. doi: 10.1017/S0022112099005364.

P. Hänggi and F. Marchesoni. Introduction: 100 years of Brownian motion. *Chaos*, 15 (2):026101, 2005. doi: 10.1063/1.1895505.

P. Hänggi and F. Marchesoni. Artificial Brownian motors: Controlling transport on the nanoscale. *Rev. Mod. Phys.*, 81(1):387, 2009. doi: 10.1103/RevModPhys.81.387.

P. Hänggi, P. Talkner, and M. Borkovec. Reaction-rate theory: Fifty years after Kramers. *Rev. Mod. Phys.*, 62(2):251–341, 1990. doi: 10.1103/RevModPhys.62.251.

P. Hänggi, F. Marchesoni, and F. Nori. Brownian motors. *Ann. Phys.*, 14(1-3):51–70, 2005. doi: 10.1002/andp.200410121.

J. Happel and H. Brenner. *Low Reynolds number hydrodynamics: with special applications to particulate media*. Prentice-Hall, Inc., Engelwood Cliffs, N. J., 1965. ISBN 9789024728770.

T. Harayama, R. Klages, and P. Gaspard. Deterministic diffusion in flower-shaped billiards. *Phys. Rev. E*, 66(2):026211, 2002. doi: 10.1103/PhysRevE.66.026211.

S. Harris. Steady, one-dimensional Brownian motion with an absorbing boundary. *J. Chem. Phys.*, 75(6):3103–3106, 1981. doi: 10.1063/1.442406.

R. Harrison, P. Todd, S. Rudge, and D. Petrides. *Bioseparations Science and Engineering*. Oxford University Press, USA, 2002. ISBN 9780195123401.

D. Hennig, L. Schimansky-Geier, and P. Hänggi. Directed transport of an inertial particle in a washboard potential induced by delayed feedback. *Phys. Rev. E*, 79(4): 041117, 2009. doi: 10.1103/PhysRevE.79.041117.

W. Hess and R. Klein. Particle separation by dielectrophoresis. *Adv. Phys.*, 32(2): 173–283, 1983. doi: 10.1080/00018738300101551.

B. Hille. *Ion Channels of Excitable Membranes*. Sinauer Associates, 3rd edition, 2001. ISBN 0878933212.

E. J. Hinch. Application of the Langevin equation to fluid suspensions. *J. Fluid Mech.*, 72(03):499–511, 1975. doi: 10.1017/S0022112075003102.

D. A. Hoagland and R. K. Prud'Homme. Taylor-aris dispersion arising from flow in a sinusoidal tube. *AIChE Journal*, 31(2):236–244, 1985. doi: 10.1002/aic.690310210.

S. Howorka and Z. Siwy. Nanopore analytics: sensing of single molecules. *Chem. Soc. Rev.*, 38:2360, 2009. doi: 10.1039/B813796J.

X. Hu, P. H. Bessette, J. Qian, C. D. Meinhart, P. S. Daugherty, and H. T. Soh. Marker-specific sorting of rare cells using dielectrophoresis. *Proc. Nat. Ac. Sc. U.S.A*, 102 (44):15757–15761, 2005. doi: 10.1073/pnas.0507719102.

L. Huang, J. Tegenfeldt, J. Kraeft, J. Sturm, R. Austin, and E. Cox. A DNA prism for high-speed continuous fractionation of large DNA molecules. *Nat. Biotechnol.*, 20(10):1048–1051, 2002. doi: 10.1038/nbt733.

R. Huang, I. Chavez, K. M. Taute, B. Lukić, S. Jeney, M. G. Raizen, and E.-L. Florin. Direct observation of the full transition from ballistic to diffusive Brownian motion in a liquid. *Nat. Phys.*, 7(7):576–580, 2011. doi: 10.1038/nphys1953.

T. Hughes. *The finite element method: linear static and dynamic finite element analysis*. Dover Civil and Mechanical Engineering Series. Dover Publications, 2000. ISBN 9780486411811.

J. Ingen-Housz. Bemerkungen über den Gebrauch des Vergrösserungsglases. *Verm. Schriften Physisch-Medicinischen Inhalts*, 1784.

J. N. Israelachvili. *Intermolecular and Surface Forces*. Academic Press. Elsevier Science & Technology, 2011. ISBN 9780123919274.

M. Jacobs. *Diffusion Processes*. Springer, New York, 2 edition, 1967. ISBN 9783540038825.

G. G. Joseph, R. Zenit, M. L. Hunt, and A. M. Rosenwinkel. Particle–wall collisions in a viscous fluid. *J. Fluid Mech.*, 433:329–346, 2001. doi: 10.1017/S0022112001003470.

P. Joseph and P. Tabeling. Direct measurement of the apparent slip length. *Phys. Rev. E*, 71(3):035303, 2005. doi: 10.1103/PhysRevE.71.035303.

T. Jovanovic-Talisman, J. Tetenbaum-Novatt, A. S. McKenney, A. Zilman, R. Peters, M. P. Rout, and B. T. Chait. Artificial nanopores that mimic the transport selectivity of the nuclear pore complex. *Nature*, 457:1023 – 1027, 2009. doi: 10.1038/nature07600.

A. J. Kainz and U. M. Titulaer. The analytic structure of the stationary kinetic boundary layer for Brownian particles near an absorbing wall. *J. Phys. A: Math. Gen.*, 24(19):4677–4695, 1991. doi: 10.1088/0305-4470/24/19/027.

P. Kalinay. Mapping of forced diffusion in quasi-one-dimensional systems. *Phys. Rev. E*, 80(3):031106, 2009. doi: 10.1103/PhysRevE.80.031106.

P. Kalinay and J. K. Percus. Corrections to the Fick-Jacobs equation. *Phys. Rev. E*, 74(4):041203, 2006. doi: 10.1103/PhysRevE.74.041203.

P. Kalinay and J. K. Percus. Approximations of the generalized Fick-Jacobs equation. *Phys. Rev. E*, 78(2):021103–021117, 2008. doi: 10.1103/PhysRevE.78.021103.

P. Kalinay and J. K. Percus. Mapping of diffusion in a channel with abrupt change of diameter. *Phys. Rev. E*, 82(3):031143, 2010. doi: 10.1103/PhysRevE.82.031143.

Y. Kang and D. Li. Electrokinetic motion of particles and cells in microchannels. *Microfluid. Nanofluid.*, 6(4):431–460, 2009. doi: 10.1007/s10404-009-0408-7.

Y. Kang, D. Li, S. A. Kalams, and J. E. Eid. DC-Dielectrophoretic separation of biological cells by size. *Biomed. Microdevices*, 10(2):243–249, 2008. doi: 10.1007/s10544-007-9130-y.

J. Kärger. Diffusion Measurements by NMR Techniques. In *Adsorption and Diffusion*, volume 7 of *Molecular Sieves*, pages 85–133. Springer-Verlag, Berlin - Heidelberg, 2008. doi: 10.1007/3829_2007_019.

J. Kärger and D. M. Ruthven. *Diffusion in zeolites and other microporous solids*. Willey & Sons, New York, 1992. ISBN 0-471-50907-8.

G. Karniadakis and G. Triantafyllou. Three-dimensional dynamics and transition to turbulence in the wake of bluff objects. *J. Fluid Mech.*, 238(1):1–30, 1992. doi: 10.1017/S0022112092001617.

F. J. Keil, R. Krishna, and M.-O. Coppens. Modeling of diffusion in zeolites. *Rev. Chem. Eng.*, 16(2):71–197, 2000. doi: 10.1515/REVCE.2000.16.2.71.

C. Kettner, P. Reimann, P. Hänggi, and F. Müller. Drift ratchet. *Phys. Rev. E*, 61(1): 312–323, 2000. doi: 10.1103/PhysRevE.61.312.

U. F. Keyser, B. N. Koeleman, S. van Dorp, D. Krapf, R. M. M. Smeets, S. G. Lemay, N. H. Dekker, and C. Dekker. Direct force measurements on DNA in a solid-state nanopore. *Nature Phys.*, 2:473–477, 2006. doi: 10.1038/nphys344.

P. K. Kitanidis and B. B. Dykaar. Stokes Flow in a Slowly Varying Two-Dimensional Periodic Pore. *Transport Porous Med.*, 26(1):89–98, 1997. doi: 10.1023/A:1006575028391.

R. Klages. *Deterministic diffusion in one-dimensional chaotic dynamical systems*. Wissenschaft und Technik Verlag, Berlin, 1996. ISBN 3-928943-49-9.

R. Klages. Transitions from deterministic to stochastic diffusion. *Europhys. Lett.*, 57 (6):796, 2002. doi: 10.1209/epl/i2002-00581-4.

P. Kloeden and E. Platen. *Numerical Solutions of Stoachstic Differential Equations*. Springer, Berlin, 4 edition, 1999. ISBN 3540540628.

I. D. Kosińska, I. Goychuk, M. Kostur, G. Schmid, and P. Hänggi. Rectification in synthetic conical nanopores: A one-dimensional Poisson-Nernst-Planck model. *Phys. Rev. E*, 77(3):031131, 2008. doi: 10.1103/PhysRevE.77.031131.

V. V. Kozlov and D. V. Treshchëv. Billiards, a Genetic Introduction to the Dynamics of Systems with Impacts. *Trans. Math. Monog.*, 89, 1991.

H. A. Kramers. Brownian motion in a field of force and the diffusion model of chemical reactions. *Physica (Utrecht)*, 7(4):284, 1940. doi: 10.1016/S0031-8914(40)90098-2.

R. Kubo. Statistical-Mechanical Theory of Irreversible Processes. I. General Theory and Simple Applications to Magnetic and Conduction Problems. *J. Phys. Soc. Jpn.*, 12(6):570–586, 1957. doi: 10.1143/JPSJ.12.570.

W. Kuhn. Über die Gestalt fadenförmiger Moleküle in Lösungen. *Colloid Polym. Sci.*, 68(1):2–15, 1934. doi: 10.1007/BF01451681.

N. Laachi, M. Kenward, E. Yariv, and K. D. Dorfman. Force-driven transport through periodic entropy barriers. *Europhys. Lett.*, 80(5):50009, 2007. doi: 10.1209/0295-5075/80/50009.

L. Landau and E. Lifschitz. *Hydrodynamik*. Verlag Harri Deutsch GmbH, 1991. ISBN 978-3-8171-1331-6.

P. Langevin. Sur la théorie du mouvement brownien. *C. R. Acad. Sci. (Paris)*, 146: 530–533, 1908.

E. Lauga, A. D. Stroock, and H. A. Stone. Three-dimensional flows in slowly varying planar geometries. *Phys. Fluids*, 16(8):3051–3062, 2004. doi: 10.1063/1.1760105.

T. Li, S. Kheifets, D. Medellin, and M. G. Raizen. Measurement of the Instantaneous Velocity of a Brownian Particle. *Science*, 328(5986):1673–1675, 2010. doi: 10.1126/science.1189403.

S. Lifson and J. L. Jackson. On the self-diffusion of ions in a polyelectrolyte solution. *J. Chem. Phys.*, 36(9):2410–2414, 1962. doi: 10.1063/1.1732899.

B. Lindner and L. Schimansky-Geier. Noise-Induced Transport with Low Randomness. *Phys. Rev. Lett.*, 89(23):230602–230605, 2002. doi: 10.1103/PhysRevLett.89.230602.

B. Lindner, M. Kostur, and L. Schimansky-Geier. Optimal diffusive transport in a tilted periodic potential. *Fluct. Noise Lett.*, 01(01):R25–R39, 2001. doi: 10.1142/S0219477501000056.

B. Lindner, J. García-Ojalvo, A. Neiman, and L. Schimansky-Geier. Effects of noise in excitable systems. *Phys. Rep.*, 392(6):321 – 424, 2004. doi: 10.1016/j.physrep.2003.10.015.

M. MacDonald, G. Spalding, and K. Dholakia. Microfluidic sorting in an optical lattice. *Nature*, 426(6965):421, 2003.

J. Machta. Power law decay of correlations in a billiard problem. *J. Stat. Phys.*, 32(3): 555–564, 1983. doi: 10.1007/BF01008956.

J. Machta and R. Zwanzig. Diffusion in a Periodic Lorentz Gas. *Phys. Rev. Lett.*, 50 (25):1959–1962, 1983. doi: 10.1103/PhysRevLett.50.1959.

L. Machura, M. Kostur, P. Talkner, J. Łuczka, and P. Hänggi. Absolute Negative Mobility Induced by Thermal Equilibrium Fluctuations. *Phys. Rev. Lett.*, 98(4): 040601, 2007. doi: 10.1103/PhysRevLett.98.040601.

Y. Makhnovskii, A. M. Berezhkovskii, and V. Y. Zitserman. Diffusion in a tube of alternating diameter. *Chem. Phys*, 370(1):238, 2010. doi: 10.1016/j.chemphys.2010.04.012.

R. Mannella. A gentle introduction to the integration of stochastic differential equations. In *Stochastic Processes in Physics, Chemistry, and Biology*, volume 557 of *Lecture Notes in Physics*, pages 353–364. Springer Berlin Heidelberg, 2000. ISBN 9783540410744. doi: 10.1007/3-540-45396-2_32.

F. Marchesoni and S. Savel'ev. Rectification currents in two-dimensional artificial channels. *Phys. Rev. E*, 80(1):011120, 2009. doi: 10.1103/PhysRevE.80.011120.

C. Marquet, A. Buguin, L. Talini, and P. Silberzan. Rectified Motion of Colloids in Asymmetrically Structured Channels. *Phys. Rev. Lett.*, 88(16):168301–168304, 2002. doi: 10.1103/PhysRevLett.88.168301.

S. Martens, G. Schmid, L. Schimansky-Geier, and P. Hänggi. Entropic particle transport: Higher-order corrections to the Fick-Jacobs diffusion equation. *Phys. Rev. E*, 83(5):051135, 2011a. doi: 10.1103/PhysRevE.83.051135.

S. Martens, G. Schmid, L. Schimansky-Geier, and P. Hänggi. Biased Brownian motion in extremely corrugated tubes. *Chaos*, 21(4):047518, 2011b. doi: 10.1063/1.3658621.

S. Martens, I. M. Sokolov, and L. Schimansky-Geier. Communication: Impact of inertia on biased Brownian transport in confined geometries. *J. Chem. Phys.*, 136(11): 111102, 2012a. doi: 10.1063/1.3696002.

S. Martens, A. V. Straube, G. Schmid, L. Schimansky-Geier, and P. Hänggi. Hydrodynamically enforced entropic trapping of Brownian particles. *Phys. Rev. Lett.*, in press, 2012b.

F. Martin, R. Walczak, A. Boiarski, M. Cohen, T. West, C. Cosentino, and M. Ferrari. Tailoring width of microfabricated nanochannels to solute size can be used to control diffusion kinetics. *J. Controll. Release*, 102(1):123–133, 2005. doi: 10.1016/j.jconrel.2004.09.024.

K. Mathwig, F. Müller, and U. Gösele. Particle transport in asymmetrically modulated pores. *New J. Phys.*, 13(3):033038, 2011. doi: 10.1088/1367-2630/13/3/033038.

M. Matsumoto and T. Nishimura. Mersenne twister: a 623-dimensionally equidistributed uniform pseudo-random number generator. *ACM Trans. Model. Comput. Simul.*, 8(1):3–30, 1998. doi: 10.1145/272991.272995.

S. Matysiak, A. Montesi, M. Pasquali, A. B. Kolomeisky, and C. Clementi. Dynamics of Polymer Translocation through Nanopores: Theory meets Experiment. *Phys. Rev. Lett.*, 96(11):118103, 2006. doi: 10.1103/PhysRevLett.96.118103.

M. R. Maxey. On the Advection of Spherical and Non-Spherical Particles in a Non-Uniform Flow. *Phil. Trans. R. Soc. Lond. A*, 333(1631):289–307, 1990. doi: 10.1098/rsta.1990.0162.

M. R. Maxey and J. J. Riley. Equation of motion for a small rigid sphere in a nonuniform flow. *Phys. Fluids*, 26(4):883–889, 1983. doi: 10.1063/1.864230.

A. Meller, L. Nivon, and D. Branton. Voltage-Driven DNA Translocations through a Nanopore. *Phys. Rev. Lett.*, 86(15):3435–3438, 2001. doi: 10.1103/PhysRevLett.86.3435.

N. A. Mishchuk, T. Heldal, T. Volden, J. Auerswald, and H. Knapp. Micropump based on electroosmosis of the second kind. *Electrophoresis*, 30(20):3499–3506, 2009. doi: 10.1002/elps.200900271.

N. A. Mortensen, F. Okkels, and H. Bruus. Reexamination of Hagen-Poiseuille flow: Shape dependence of the hydraulic resistance in microchannels. *Phys. Rev. E*, 71(5): 057301, 2005. doi: 10.1103/PhysRevE.71.057301.

M. Muthukumar. Translocation of a confined polymer through a hole. *Phys. Rev. Lett.*, 86(14):3188–3191, 2001. doi: 10.1103/PhysRevLett.86.3188.

J. Nagel, D. Speer, T. Gaber, A. Sterck, R. Eichhorn, P. Reimann, K. Ilin, M. Siegel, D. Koelle, and R. Kleiner. Observation of Negative Absolute Resistance in a Josephson Junction. *Phys. Rev. Lett.*, 100(21):217001, 2008. doi: 10.1103/PhysRevLett.100.217001.

T. Neusius, I. M. Sokolov, and J. C. Smith. Subdiffusion in time-averaged, confined random walks. *Phys. Rev. E*, 80(1):011109, 2009. doi: 10.1103/PhysRevE.80.011109.

T. Odijk. The statistics and dynamics of confined or entangled stiff polymers. *Macromolecules*, 16(8):1340–1344, 1983. doi: 10.1021/ma00242a015.

M. S. N. Oliveira, M. A. Alves, F. Pinho, and G. McKinley. Viscous flow through microfabricated hyperbolic contractions. *Exp. Fluids*, 43(2):437–451, 2007. doi: 10.1007/s00348-007-0306-2.

M. S. N. Oliveira, L. E. Rodd, G. McKinley, and M. A. Alves. Simulations of extensional flow in microrheometric devices. *Microfluid. Nanofluid.*, 5(6):809–826, 2008. doi: 10.1007/s10404-008-0277-5.

C. W. Oseen. Über die Stokes'sche Formel, und über eine verwandte Aufgabe in der Hydrodynamik. *Arkiv för matematik, astronomi och fysik*, vi:29, 1910.

N. Pamme and C. Wilhelm. Continuous sorting of magnetic cells via on-chip free-flow magnetophoresis. *Lab Chip*, 6(8):974–980, 2006. doi: 10.1039/b604542a.

A. Parashar, R. Lycke, J. A. Carr, and S. Pandey. Amplitude-modulated sinusoidal microchannels for observing adaptability in C. elegans locomotion. *Biomicrofluidics*, 5(2):024112, 2011. doi: 10.1063/1.3604391.

M. Patriarca, P. Szelestey, and E. Heinsalu. Brownian model of dissociated dislocations. *Acta Phys. Pol. B*, 36(5):1745, 2005.

W. F. Paxton, K. C. Kistler, C. C. Olmeda, A. Sen, S. K. St. Angelo, Y. Cao, T. E. Mallouk, P. E. Lammert, and V. H. Crespi. Catalytic nanomotors: Autonomous movement of striped Nanorods. *J. Amer. Chem. Soc.*, 126(41):13424–13431, 2004. doi: 10.1021/ja047697z.

J. C. E. Péclet. Sur la determination des coefficients de conductibilite des metaux par la chaleur. *Ann. Chim. Phys.*, 3:107, 1841.

D. Pedone, M. Langecker, G. Abstreiter, and U. Rant. A Pore-Cavity-Pore Device to Trap and Investigate Single Nanoparticles and DNA Molecules in a Femtoliter Compartment: Confined Diffusion and Narrow Escape. *Nano Lett.*, 11(4):1561–1567, 2011. doi: 10.1021/nl104359c.

J. B. Perrin. Mouvement brownien et réalité moléculaire. *Ann. Chim. Phys. 8ième série*, 18:5–114, 1909.

F. Petersson, L. Aberg, A.-M. Sward-Nilsson, and T. Laurell. Free flow acoustophoresis: Microfluidic-based mode of particle and cell separation. *Anal. Chem.*, 79(14):5117–5123, 2007. doi: 10.1021/ac070444e.

O. Pironneau, F. Hecht, and J. Morice. FreeFEM++, 2012. URL `http://www.freefem.org`.

S. B. Pope and E. S. C. Ching. Stationary probability density functions: An exact result. *Phys. Fluids A*, 5(7):1529–1531, 1993. doi: 10.1063/1.858830.

E. M. Purcell. Life at low reynolds number. *Am. J. Phys*, 45:3–11, 1977. doi: 10.1119/1.10903.

K. Pyragas. Continuous control of chaos by self-controlling feedback. *Phys. Lett. A*, 170(6):421–428, 1992. doi: 10.1016/0375-9601(92)90745-8.

P. K. Radtke and L. Schimansky-Geier. Directed transport of confined Brownian particles with torque. *Phys. Rev. E*, 85(5):051110, 2012. doi: 10.1103/PhysRevE.85.051110.

D. Reguera and J. M. Rubí. Kinetic equations for diffusion in the presence of entropic barriers. *Phys. Rev. E*, 64(6):061106–061113, 2001. doi: 10.1103/PhysRevE.64.061106.

D. Reguera, G. Schmid, P. S. Burada, J. M. Rubí, P. Reimann, and P. Hänggi. Entropic transport: Kinetics, scaling, and control mechanisms. *Phys. Rev. Lett.*, 96 (13):130603, 2006. doi: 10.1103/PhysRevLett.96.130603.

D. Reguera, A. Luque, P. S. Burada, G. Schmid, J. M. Rubí, and P. Hänggi. Entropic splitter for particle separation. *Phys. Rev. Lett.*, 108(2):020604, 2012. doi: 10.1103/PhysRevLett.108.020604.

P. Reimann. Brownian motors: noisy transport far from equilibrium. *Phys. Rep.*, 361 (2-4):57–265, 2002. doi: 10.1016/S0370-1573(01)00081-3.

P. Reimann, C. van den Broeck, H. Linke, P. Hänggi, J. M. Rubí, and A. Pérez-Madrid. Giant acceleration of free diffusion by use of tilted periodic potentials. *Phys. Rev. Lett.*, 87(1):010602, 2001. doi: 10.1103/PhysRevLett.87.010602.

P. Reimann, C. van den Broeck, H. Linke, P. Hänggi, J. M. Rubí, and A. Pérez-Madrid. Diffusion in tilted periodic potentials: Enhancement, universality, and scaling. *Phys. Rev. E*, 65(3):031104, 2002. doi: 10.1103/PhysRevE.65.031104.

O. Reynolds. On the theory of lubrication and its application to Mr. Beauchamp tower's experiments, including an experimental determination of the viscosity of olive oil. *Philos. T. R. Soc. Lond.*, 177:157–234, 1886. doi: 10.1098/rstl.1886.0005.

W. Riefler, G. Schmid, P. S. Burada, and P. Hänggi. Entropic transport of finite size particles. *J. Phys. Condens. Matter*, 22(45):454109–454115, 2010. doi: 10.1088/0953-8984/22/45/454109.

H. Risken. *The Fokker-Planck Equation*. Springer, Berlin, 2nd edition, 1989. ISBN 3540504982.

S. Rols, J. Cambedouzou, M. Chorro, H. Schober, V. Agafonov, P. Launois, V. Davydov, A. V. Rakhmanina, H. Kataura, and J.-L. Sauvajol. How Confinement Affects the Dynamics of C_{60} in Carbon Nanopeapods. *Phys. Rev. Lett.*, 101(6):065507, 2008. doi: 10.1103/PhysRevLett.101.065507.

P. Romanczuk and L. Schimansky-Geier. Brownian Motion with Active Fluctuations. *Phys. Rev. Lett.*, 106(23):230601, 2011. doi: 10.1103/PhysRevLett.106.230601.

P. Romanczuk, F. Müller, and L. Schimansky-Geier. Quasideterministic transport of Brownian particles in an oscillating periodic potential. *Phys. Rev. E*, 81(6):061120, 2010. doi: 10.1103/PhysRevE.81.061120.

P. Romanczuk, M. Bär, W. Ebeling, B. Lindner, and L. Schimansky-Geier. Active Brownian particles. *Eur. Phys. J. - Spec. Top.*, 202(1):1–162, 2012. doi: 10.1140/epjst.

D. A. Rose. Some aspects of the hydrodynamic dispersion of solutes in porous materials. *J. Soil Sci.*, 24(3):284–295, 1973. doi: 10.1111/j.1365-2389.1973.tb00766.x.

S. Roy, R. Raju, H. F. Chuang, B. A. Cruden, and M. Meyyappan. Modeling gas flow through microchannels and nanopores. *J. Appl. Phys.*, 93(8):4870–4879, 2003. doi: 10.1063/1.1559936.

S. Rüdiger and L. Schimansky-Geier. Dynamics of excitable elements with time-delayed coupling. *J. Theor. Bio.*, 259(1):96 – 100, 2009. doi: 10.1016/j.jtbi.2009.01.030.

P. G. Saffman. The lift on a small sphere in a slow shear flow. *J. Fluid Mech.*, 22(2): 385–400, 1965. doi: 10.1017/S0022112065000824.

M. Schindler, P. Talkner, M. Kostur, and P. Hänggi. Accumulating particles at the boundaries of a laminar flow. *Physica A*, 385(1):46–58, 2007. doi: 10.1016/j.physa.2007.06.030.

J. V. Selinger and U. M. Titulaer. The kinetic boundary layer for the Klein-Kramers equation. A new numerical approach. *J. Stat. Phys.*, 36(3-4):293–319, 1984. doi: 10.1007/BF01010986.

Y. G. Sinai. Dynamical systems with elastic reflections: Ergodic properties of dispersing billiards. *Russ. Math. Surveys Dokl. Acad. Sci. USSR*, 25:137, 1970.

Z. Siwy and A. Fulinski. A nanodevice for rectification and pumping ions. *Am. J. Phys.*, 72(5):567–574, 2004. doi: 10.1119/1.1648328.

Z. Siwy, I. D. Kosińska, A. Fuliński, and C. R. Martin. Asymmetric Diffusion through Synthetic Nanopores. *Phys. Rev. Lett.*, 94(4):048102, 2005. doi: 10.1103/PhysRevLett.94.048102.

J. L. Skinner and P. G. Wolynes. Derivation of Smoluchowski equations with corrections for Fokker-Planck and BGK collision models. *Physica A*, 96(3):561–572, 1979. doi: 10.1016/0378-4371(79)90013-X.

G. W. Slater, H. L. Guo, and G. I. Nixon. Bidirectional Transport of Polyelectrolytes Using Self-Modulating Entropic Ratchets. *Phys. Rev. Lett.*, 78(6):1170–1173, 1997. doi: 10.1103/PhysRevLett.78.1170.

G. W. Slater, S. Guillouzic, M. Gauthier, J.-F. Mercier, M. Kenward, L. C. McCormick, and F. Tessier. Theory of DNA electrophoresis. *Electrophoresis*, 23(22-23):3791–3816, 2002. doi: 10.1002/elps.200290002.

D. Smith, T. Perkins, and S. Chu. Dynamical Scaling of DNA Diffusion Coefficients. *Macromolecules*, 29(4):1372–1373, 1996. doi: 10.1021/ma951455p.

I. M. Sokolov. Statistical mechanics of entropic forces: disassembling a toy. *Eur. Phys. J.*, 31(6):1353–1367, 2010. doi: 10.1088/0143-0807/31/6/005.

M. Sommerfeld. Modelling of particle-wall collisions in confined gas-particle flows. *Int. J. Multiphase Flow*, 18(6):905–926, 1992. doi: 10.1016/0301-9322(92)90067-Q.

L. Song, M. R. Hobaugh, C. Shustak, S. Cheley, H. Bayley, and J. E. Gouaux. Structure of staphylococcal α-hemolysin, a heptameric transmembrane pore. *Science*, 274 (5294):1859–1865, 1996. doi: 10.1126/science.274.5294.1859.

G. Soni, T. M. Squires, and C. D. Meinhart. Nonlinear phenomena in induced-charge electroosmosis. *Proceedings of IMECE2007, ASME international mechanical engineering congress and exposition, Seattle, Washington, USA*, 2007.

T. M. Squires and M. Z. Bazant. Induced-charge electro-osmosis. *J. Fluid Mech.*, 509: 217–252, 2004. doi: 10.1017/S0022112004009309.

T. M. Squires and M. Z. Bazant. Breaking symmetries in induced-charge electro-osmosis and electrophoresis. *J. Fluid Mech.*, 560:65–101, 2006. doi: 10.1017/S0022112006000371.

T. M. Squires and S. R. Quake. Microfluidics: Fluid physics at the nanoliter scale. *Rev. Mod. Phys.*, 77(3):977–1026, 2005. doi: 10.1103/RevModPhys.77.977.

V. Srinivasan, V. Pamula, and R. Fair. An integrated digital microfluidic lab-on-a-chip for clinical diagnostics on human physiological fluids. *Lab Chip*, 4(4):310–315, 2004.

R. L. Stratonovich. Oscillator synchronization in the presence of noise. *Radiotekh. Elektron. (Moscow)*, 3:497, 1958.

A. V. Straube. Small-scale particle advection, manipulation and mixing: beyond the hydrodynamic scale. *J. Phys. Condens. Matter*, 23(18):184122, 2011.

W. Sutherland. LXXV. A dynamical theory of diffusion for non-electrolytes and the molecular mass of albumin. *Phil. Mag.*, 9:781–785, 1905.

M. Sven and F. Müller. Asymmetric pores in a silicon membrane acting as massively parallel brownian ratchets. *Nature*, 424(6944):53–57, 2003. doi: 10.1038/nature01736.

A. Szabo, K. Schulten, and Z. Schulten. First passage time approach to diffusion controlled reactions. *J. Chem. Phys.*, 72(8):4350–4357, 1980. doi: 10.1063/1.439715.

G. Taylor. Dispersion of soluble matter in solvent flowing slowly through a tube. *Phil. Trans. R. Soc. Lond. A*, 219(1137):186–203, 1953. doi: 10.1098/rspa.1953.0139.

M. Teubner. The motion of charged colloidal particles in electric fields. *J. Chem. Phys.*, 76(11):5564–5573, 1982. doi: 10.1063/1.442861.

V. I. Tikhonov. The effect of noise on phase-locked oscillator operation. *Avtom. Telemekh.*, 20:1188–1196, 1959.

V. I. Tikhonov. Phase-lock automatic frequency control operation in the presence of noise. *Avtom. Telemekh.*, 21:301–309, 1960.

U. M. Titulaer. A systematic solution procedure for the Fokker-Planck equation of a Brownian particle in the high-friction case. *Physica A*, 91:321–344, 1978. doi: 10.1016/0378-4371(78)90182-6.

J. H. van't Hoff. *Etudes de dynamiques chimiques*. F. Muller and Co., Amsterdam, 1884.

A. S. Verkman. Solute and macromolecule diffusion in cellular aqueous compartments. *Trends Biochem.*, 27(1):27 – 33, 2002. doi: 10.1016/S0968-0004(01)02003-5.

V. Vladimirsky and Y. A. Terletzky. Hydrodynamical theory of translational Brownian motion. *Zh. Eksp. Teor. Fiz.*, 15:258–263, 1945.

J. Voldman. Electrical forces for microscale cell manipulation. *Annu. Rev. Biomed. Eng.*, 8:425–454, 2006. doi: 10.1146/annurev.bioeng.8.061505.095739.

W. D. Volkmuth and R. H. Austin. DNA electrophoresis in microlithographic arrays. *Nature*, 358(6387):600, 1992.

M. von Smoluchowski. Zur kinetischen Theorie der Brown'schen Molekularbewegung und der Suspensionen. *Ann. Phys.*, 326(14):756–780, 1906. doi: 10.1002/andp.19063261405.

M. von Smoluchowski. Über die Brown'sche Molekularbewegung unter Einwirkung äußerer Kräfte und deren Zusammenhang mit der verallgemeinerten Diffusionsgleichung. *Ann. Phys.*, 353(24):1103–1112, 1915. doi: 10.1002/andp.19163532408.

M. von Smoluchowski. Drei Vorträge über Diffusion, Brown'sche Bewegung und Koagulation von Kolloidteilchen. *Phys. Z.*, 17:557–585, 1916.

J. von Stamm, U. Gerdts, T. Buzug, and G. Pfister. Symmetry breaking and period doubling on a torus in the VLF regime in Taylor-Couette flow. *Phys. Rev. E*, 54(5): 4938–4957, 1996. doi: 10.1103/PhysRevE.54.4938.

B. Wang, J. Kuo, S. C. Bae, and S. Granick. When Brownian diffusion is not Gaussian. *Nat. Mater.*, 11(6):481–485, 2012. doi: 10.1038/nmat3308.

X. Wang and G. Drazer. Transport properties of Brownian particles confined to a narrow channel by a periodic potential. *Phys. Fluids*, 21(10):102002, 2009. doi: 10.1063/1.3226100.

X. Wang and G. Drazer. Transport of Brownian particles confined to a weakly corrugated channel. *Phys. Fluids*, 22(12):122004, 2010. doi: 10.1063/1.3527546.

Q. Wei, C. Bechinger, and P. Leiderer. Single-file diffusion of colloids in one-dimensional channels. *Science*, 287(5453):625–627, 2000. doi: 10.1126/science.287.5453.625.

D. A. Weitz, D. J. Pine, P. N. Pusey, and R. J. A. Tough. Nondiffusive Brownian motion studied by diffusing-wave spectroscopy. *Phys. Rev. Lett.*, 63(16):1747–1750, 1989. doi: 10.1103/PhysRevLett.63.1747.

G. Wilemski. On the derivation of Smoluchowski equations with corrections in the classical theory of Brownian motion. *J. Stat. Phys.*, 14(2):153–169, 1976. doi: 10.1007/BF01011764.

R.-J. Yang, H.-H. Hou, Y.-N. Wang, C.-H. Lin, and L.-M. Fu. A hydrodynamic focusing microchannel based on micro-weir shear lift force. *Biomicrofluidics*, 6(3):034110, 2012. doi: 10.1063/1.4739073.

E. Yariv and K. D. Dorfman. Electrophoretic transport through channels of periodically varying cross section. *Phys. Fluids*, 19(3):037101, 2007. doi: 10.1063/1.2710894.

E. Yariv, H. Brenner, and S. Kim. Curvature-induced dispersion in electro-osmotic serpentine flows. *SIAM J. Appl. Math.*, 64(4):1099–1124, 2004. doi: 10.1137/S003613990342284X.

Y. Zeng, S. Grandner, C. L. P. Oliveira, A. F. Thunemann, O. Paris, J. S. Pedersen, S. H. L. Klapp, and R. von Klitzing. Effect of particle size and Debye length on order parameters of colloidal silica suspensions under confinement. *Soft Matter*, 7 (22):10899–10909, 2011. doi: 10.1039/C1SM05971H.

C. Zhao and C. Yang. Advances in electrokinetics and their applications in micro/nano fluidics. *Microfluid. Nanofluid.*, 13(2):179–203, 2012. doi: 10.1007/s10404-012-0971-1.

H.-X. Zhou and R. Zwanzig. A rate process with an entropy barrier. *J. Chem. Phys.*, 94(9):6147–6152, 1991. doi: 10.1063/1.460427.

H. X. Zhou, G. N. Rivas, and A. P. Minton. Macromolecular Crowding and Confinement: Biochemical, Biophysical, and Potential Physiological Consequences. *Annu. Rev. Biophys.*, 37:375 – 397, 2008. doi: 10.1146/annurev.biophys.37.032807.125817.

O. Zienkiewicz, R. Taylor, and J. Zhu. *The Finite Element Method: Its Basis And Fundamentals*. Elsevier Butterworth-Heinemann, 2005. ISBN 9780750663205.

R. Zwanzig. Diffusion past an entropy barrier. *J. Phys. Chem.*, 96(10):3926–3930, 1992. doi: 10.1021/j100189a004.

List of Figures

List of Tables

List of publications

9. **S. Martens**, A. V. Straube, G. Schmid, L. Schimansky-Geier, and P. Hänggi
Hydrodynamically enforced entropic trapping of Brownian particles
Physical Review Letters, *in press*.

8. **S. Martens**, I. M. Sokolov, and L. Schimansky-Geier
Impact of inertia on biased Brownian transport in confined geometries
Communication: Journal of Cheminal Physics 136, 111102 [2012], doi: 10.1103/PhysRevE.85.011101

7. P. K. Ghosh, P. Hänggi, F. Marchesoni, **S. Martens**, F. Nori, L. Schimansky-Geier, and G. Schmid
Driven Brownian transport through arrays of symmetric obstacles
Physical Review E 85, 011101 [2012], doi: 10.1103/PhysRevE.85.011101

6. **S. Martens**, G. Schmid, L. Schimansky-Geier, and P. Hänggi
Biased Brownian motion in extreme corrugated tubes
Chaos 21, 047518 [2011], doi: 10.1063/1.3658621

5. **S. Martens**, G. Schmid, L. Schimansky-Geier, and P. Hänggi
Entropic particle transport: higher order corrections to the Fick-Jacobs diffusion equation Physical Review E 83, 051135 [2011], doi: 10.1103/PhysRevE.83.051135

4. **S. Martens**, D. Hennig, S. Fugmann, and L. Schimansky-Geier
Resonancelike phenomena in the mobility of a chain of nonlinear coupled oscillators in a two-dimensional periodic potential
Physical Review E 78, 041121 [2008], doi: 10.1103/PhysRevE.78.041121

3. S. Fugmann, D. Hennig, **S. Martens**, and L. Schimansky-Geier
Deterministic escape of a dimer over an anharmonic potential barrier
Physica D 237, 3179 [2008], doi: 10.1016/j.physd.2008.08.008

2. D. Hennig, **S. Martens**, and S. Fugmann
Transition between locked and running states for dimer motion induced by periodic external driving
Physical Review E 78, 011104 [2008], doi: 10.1103/Phys-RevE.78.011104

1. *Thermally activated escape dynamics of coupled nonlinear oscillator chains in a 2D periodic potential*
Diplom thesis submitted at Humboldt-Universität zu Berlin, Germany, in 2007

Danksagung

Ich möchte an dieser Stelle die Gelegenheit nutzen und all jenen danken, die mich während meines Physikstudiums und der anschließenden Arbeit am Institut für Physik begleitet und unterstützt haben.

Zuallererst gilt mein herzlicher Dank meinem Betreuer Prof. Schimansky-Geier, der nicht nur mein Interesse an Stochastischen Prozessen und der Biophysik geweckt hat, sondern mir auch seit 6 Jahren die Möglichkeit gibt in seiner Arbeitsgruppe zu arbeiten. Mit seiner Unterstützung und seinen vielen Anregungen hat er sehr zum erfolgreichen Gelingen dieser Arbeit beigetragen.

Ich danke ihm auch für seinen engen Kontakt zu Prof. Hänggi, welcher mich in das faszierende Problem des entropischen Transports eingeführt hat. Seine Begeisterung für die Wissenschaft und die zahlreichen Diskussionen haben mich stets inspiriert und gefordert.

Besonders möchte ich mich bei Gerhard dafür bedanken, dass er sich trotz der Entfernung stets die Zeit nahm, um zu helfen und meine Fragen zu beantworten. Die vielen Diskussionen und das zahlreiche Korrekturlesen haben nicht nur zu gemeinsamen Publikationen geführt, sondern vor allem diese Arbeit sehr verbessert. Ich danke Arthur für die intensive Zusammenarbeit und seiner Unterstützung bei Fragen zur Hydrodynamik. Ich hoffe, dass wir weitere interessante Probleme zusammen lösen werden.

An dieser Stelle möchte ich mich bei den beiden Arbeitsgruppen für die äußerst freundliche und entspannte Arbeitsatmosphäre bedanken. Besonders die Kaffeepausen und die Gespräche haben jeden Tag bereichert.

Ich danke Simon und Pawel für viele lustige Gespräche und die zahlreichen erkenntnisreichen Diskussionen in den letzten Jahren. Im Speziellen möchte ich Paul, Bernard, beiden Christians, Martin, Felix und Justus für das Korrekturlesen meiner Arbeit danken. Insbesondere Justus war in den letzten (kritischen) Monaten ein angenehmer und stets lustiger Zimmergenosse, der jederzeit einen guten Titelvorschlag parat hat. Ich danke ebenfalls Fr. Rosengarten für ihre Hilfe bei allen anfallenden Problemen und ihren hilfreichen Lebensweisheiten.

Ein ganz spezieller Dank geht an meine Eltern dafür, dass sie mich während des gesamten Studiums immer moralisch und auch finanziell unterstützt haben. Auch wenn ihnen die letzten 10 Jahre bestimmt ewig vorgekommen sind, haben sie nie gefragt: “Wann bist du endlich fertig?” Danke!

Vom ganzem Herzen danke ich der wundervollsten Frau, meiner Verlobten Yasmin. Ihr unerschütterliches Vertrauen gab mir stets die nötige Kraft. Sie baute mich auf und trieb mich an, wenn ich es brauchte. Ich danke ihr vom ganzen Herzen für ihre Rücksicht und ihr Verständnis.

Meiner Familie und meinen Freunden möchte ich nur sagen: Danke für Euer Verständnis! Jetzt habt ihr mich wieder.

Abschließend danke ich der Volkswagen Stiftung und dem Steuerzahler für die jahrelange finanzielle Unterstützung.

Selbständigkeitserklärung

Ich erkläre, dass ich die vorliegende Arbeit selbständig und nur unter Verwendung der angegebenen Literatur und Hilfsmittel angefertigt habe.

Berlin, den 13.11.2012

(Steffen Martens)